DOCTOR OF SCIENCES

Symmetry breaking and Turing patterns on networks and higher-order structures
Nonlinear beasts and where to find them

Muolo, Riccardo

Award date:
2023

Awarding institution:
University of Namur

Université de Namur

Faculty of Sciences

Department of Mathematics & naXys - Namur Institute for Complex Systems

Funded by FNRS & Walloon Region - FRIA-FNRS PhD fellowship, Grant FC 33443

Symmetry breaking and Turing patterns on networks and higher-order structures
NONLINEAR BEASTS AND WHERE TO FIND THEM

Thesis presented by
Riccardo Muolo
for the title of
Doctor of Science

Composition of the Jury:

Ginestra BIANCONI, *Queen Mary University of London, UK*
Timoteo CARLETTI, *Université de Namur, Belgium* (Promoter)
Francesca DI PATTI, *Università di Perugia, Italy*
Mattia FRASCA, *Università di Catania, Italy*
Anne-Sophie LIBERT, *Université de Namur, Belgium* (President of the Jury)
Hiroya NAKAO, *Tokyo Institute of Technology, Japan*

Cover design: ©Presses universitaires de Namur

Rue Grandgagnage 19,
B-5000 Namur (Belgium)
pun@unamur.be - www.pun.be

Registration of copyright: D/2023/1881/7
ISBN: 978-2-39029-169-5
Printed in Belgium.

University of Namur
Faculty of Science
rue de Bruxelles, 61, 5000 Namur (Belgique)

Symmetry breaking and Turing patterns
on networks and higher-order structures
NONLINEAR BEASTS
AND WHERE TO FIND THEM

by Riccardo Muolo

Abstract: In the 50s, Alan Turing introduced and described a pattern-formation mechanism involving two interacting chemical species driven by diffusion. Since then, Turing patterns have been found in chemical, biological and even quantum systems, just to mention a few. In 2010, the theory was then extended to networked systems, opening a new framework with great potential. In this thesis we study the emergence of Turing patterns on networks and their generalizations; moreover, we establish a bridge with the theory of synchronization by emphasizing the similarities existing between the two frameworks. We then show how the network formalism is versatile and well-suited to study the emergence of new forms of Turing-like patterns, which would not be possible to obtain in its original framework, and how to better understand their phenomenological characterization. In the second part of the work, we further extend the theory to the new and exciting framework of many-body and high-order interactions. Instead of a network, the support is given by high-order structures such as hypergraphs and simplicial complexes. Stressing again the analogy between the synchronization framework and the Turing one, we develop a theory of Turing patterns on hypergraphs by extending an elegant and powerful formalism developed from synchronization. Finally, by using the mathematical tools of algebraic topology, we study diffusion-driven instabilities for topological signals defined on simplicial complexes.

Brisure de symétrie et motifs de Turing
sur réseaux et structures d'ordre supérieur
NONLINEAR BEASTS
AND WHERE TO FIND THEM

par Riccardo Muolo

Résumé: Dans les années 50, Alan Turing a introduit et étudié un mécanisme pour expliquer la formation de motifs basé sur la présence de deux espèces chimiques en interaction, en s'appuyant sur la diffusion. Depuis lors, des motifs de Turing ont été découverts dans des systèmes chimiques, biologiques et même quantiques, pour n'en citer que quelques-uns. En 2010, la théorie a ensuite été étendue aux systèmes en réseau, ouvrant ainsi un nouveau cadre avec un très grand potentiel. Dans cette thèse, nous étudions l'émergence des motifs de Turing sur les réseaux et leurs généralisations; en outre, nous établissons un pont avec la théorie de la synchronisation en mettant en évidence les similitudes qui existent les deux cadres. Nous montrons ensuite pourquoi le cadre des réseaux est polyvalent et bien adapté à l'étude de l'émergence de nouveaux motifs similaires à ceux de Turing, qu'ils seraient impossibles à obtenir dans le cadre d'origine, et comment mieux comprendre leur caractérisation phénoménologique. Dans le deuxième partie de ce travail, nous développons davantage la théorie au nouveau et passionnant cadre des interactions à plusieurs corps et d'ordre supérieur. Au lieu d'un réseau, le support est donné par des structures d'ordre supérieur, telles que des hypergraphes et des complexes simpliciaux. Insistant davantage sur l'analogie entre la synchronisation et celui de l'instabilité de Turing, nous développons une théorie des motifs de Turing sur les hypergraphes en adaptant un élégant et puissant formalisme développé pour la synchronisation. Enfin, en utilisant les outils mathématiques de la topologie algébrique, nous étudions les instabilités basées sur la diffusion pour les signaux topologiques sur des complexes simpliciaux.

Ph.D. thesis in Applied Mathematics
Date: 20/04/2023
Department of Mathematics, naXys Research Institute
Promoter: Professor Timoteo CARLETTI

In 1952 Alan Turing was prosecuted for his homosexuality,
which was illegal in the UK.
More than 70 years later, despite some progress,
members of the LGTBQ+ community worldwide
still face discrimination, bullying and violence.
This work is dedicated to all those who are fighting for equality.

Contents

Introduction

" Chaos is merely order waiting to be deciphered"
José Saramago

Recurrently in nature, we witness processes of self-organization, resulting from the interactions among many elementary units [1]. From the synchronous firing of fireflies in the rain forest [2], to the flocking of birds in the sky of southern European cities at sunset [3], we are continuously stunned by the harmony and mesmerizing beauty of these phenomena. The observation of such behaviors in natural and engineered systems has triggered the curiosity of scientists, who have tried to prove theoretically and experimentally the spontaneous emergence of order in controlled environments. One of the most popular theories accounting for such diversity was proposed by the British mathematician Alan Turing (1912-1954) in a seminal paper of 1952 [4]. The mechanism proposed by Turing relies on diffusion: in fact, the latter is the factor promoting the formation of patterns, which is astonishing given its usual role in homogenization processes. In a nutshell, the model consists of two (chemical) species lying in a homogeneous stable state, meaning that their concentrations do not vary in time nor throughout the spatial domain. We proceed by applying an external perturbation to the system, which has to be spatially inhomogeneous. Such *symmetry breaking* activates the diffusion, because now the concentrations are not homogeneous and their gradient is non-zero. Under certain conditions, which can be found analytically, the state becomes unstable and this amplification of the perturbation in the linear regime, called also *Turing* or *diffusion-driven instability*, drives the system away from the homogeneous equilibrium. When the nonlinearities of the model become relevant, the system settles onto a new stable state, which is spatially inhomogeneous and what we call a *Turing pattern*. Turing himself admitted that in nature there are never homogeneous states, but systems rather move from pattern to pattern. However, already the fact that it is mathematically possible to prove the emergence of inhomogeneous states is remarkable and for this reason Turing's original paper is, to this day, one of the milestones in the study of self-organization. This spontaneous emergence of spatial structures is strongly counterintuitive, especially given that diffusion is normally associated to homogeneization, rather than inhomogeneization. Consequently, Turing theory was neglected by the chemical and, especially, the biological community. The interest on the theory sparked in the

70s, thanks to the work of Gierer and Meinhardt, who described Turing's mechanism as an activator and an inhibitor species undergoing diffusion-driven instability [5]. All these features were already present in Turing original work, but Gierer and Meinhardt's reinterpretation allowed for a better understanding and a wider diffusion, especially in the chemical and biological communities. Nonetheless, to obtain experimentally Turing patterns proved to be a difficult task, and they were obtained only half a century later [6, 7]. The main limitation is the difference in the diffusion coefficients' magnitude required by the theory for the instability to develop, namely the inhibitor has to diffuse much faster than the activator, which is difficult to reproduce experimentally. Then, we find ourselves surrounded by patterns, we have an elegant theory accounting for such diversity, but we cannot experimentally match the observations. Paraphrasing Fermi's paradox on extraterrestrial life, where are all the Turing patterns? Such discrepancy motivated a part of the research carried out on Turing instability. In fact, Turing's original setting consists of two species[(1)], with no external effects, no noise, on a smooth domain, etc. Scholars have tried to add realistic assumptions, e.g., by increasing the number of species [9], by adding noise [10], and so on, to observe whether it was easier to obtain patterns or not. In most cases the answer is affirmative: realistic assumptions relax the conditions for patterns formation, which means that Turing theory is a good theory, epistemologically speaking. One issue that arises is whether patterns obtained in different settings can still be named Turing patterns; throughout this work we will argument that this is not an issue and that, yes, they are Turing patterns.

The framework in which this thesis is developed is that of discrete support and it is schematized in Figure I.1. Instead of studying diffusion on a continuous domain, hence dealing with partial differential equations (PDEs), as in Turing's original framework[(2)], our manifold will be a discrete structure, being a network or a higher-order one. We will, in fact, consider n identical units $\vec{x}_i$, whose dynamics are given by a nonlinear function $\vec{f}(\vec{x}_i)$. Each of those units is isolated and can be thought as lying in the space of nodes (blue in the Figure). Moreover, they are coupled with one another through the network's links (red). As we will see in the second part of the thesis, not all interactions are pairwise and some systems exhibit higher-order (many-body) interactions, which can be modeled through hyperedges (orange). The resulting dynamical equations will then be ordinary differential equations (ODEs), since the space is identified by the nodes. Note that, in the schematization of Figure I.1, the dynamics take place only within the nodes, while links and hyperedges model the way in which the elementary units are coupled. We can consider the nodes as well-mixed environments, where no spatial inhomogeneities are present and, hence, mean field equations describe the local system's behavior, i.e., inside each node. Thinking in the framework of Turing instability, when the concentrations in every node are all equal, then neither a "spatial" gradient, i.e., across the nodes, is present nor diffusion (interaction) takes place between the nodes. To have n isolated systems is equivalent to deal with n copies of the same

[(1)] Actually, Turing discussed also the setting of three interacting species and he concluded that this allowed for oscillatory patterns, but did not develop the mathematics, which was dealt with by other researchers in later years [8].

[(2)] Turing's original framework consisted of a lattice ring [4]. The latter is a continuous support, but, to be precise, a theory of Turing patterns for PDEs was developed later [11].

basic system, the units being identical. We can now proceed as above and perturb inhomogeneously such stable state, hence activating the interactions between the nodes, which can lead to the formation of Turing patterns. Each single node's dynamics can still be approximated by a well-mixed environment, while the differences in concentrations, i.e., the patterns, are between different nodes. In Chapter 7, we will show that this framework can be extended: in fact, thanks to the tools of algebraic topology, we can study a diffusion-driven instability mechanism also for topological signals, i.e., variables defined not only on nodes, but also on links and hyperedges. The dynamical equation of the figure, as well as pairwise and higher-order structures, will be discussed more in details in the following pages.

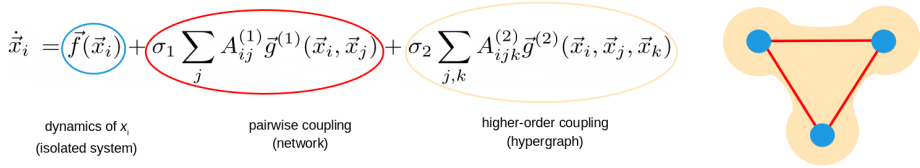

Figure I.1: From the left, the typical form of the dynamical equations for an ensemble of coupled elementary units. Such units have their own dynamical equation (blue) and interact in a pairwise fashion (red) and higher-order one (orange). On the right, we represent such interactions: the (isolated) units lie in the nodes (blue), the pairwise coupling is modeled by the links (red) and many-body interactions by the hyperedges (orange).

The thesis is organized in two parts: one regarding pairwise interactions and the other one devoted to the study of higher-order structures. Each part has its own introduction, Chapters 1 and 5 respectively, followed by three and two papers respectively. Each paper, Chapters 2, 3, 4, 6 and 7, is preceded by a short introduction, summarizing the main results and putting them in context with the rest of the thesis. Moreover, Chapters 2 and 4 are followed by a short comment, which clarifies some points discussed in the papers. It was our choice to leave the papers in their original form, with the exception of some editing and minor changes, which have been made for sake of uniformity, mainly for what concerns notation and orthography.
Chapter 1 introduces Turing theory on networks and discusses a broadening of the Turing framework, which will then be developed in the following three chapters. In Chapter 2, we extend the theory for oscillatory systems by considering non-normal networks as their support and showing that the homogeneous state is much more fragile in such cases; then, in Chapter 3, we consider networked systems when an upper bound on the signal propagation is present, and revisit the emergence of Turing patterns. Chapter 4 goes further beyond the Turing framework, as a Turing-like instability is studied for systems where no diffusion takes place. The second part is about higher-order interactions, which are introduced in Chapter 5. Chapter 6 develops a theory of Turing patterns for systems with many-body interactions, while, in Chapter 7, we consider topological signals on higher-order structures. In the Conclusions, some open questions and future perspectives will be discussed. The thesis is concluded with the summary of other relevant results obtained throughout this PhD, which go beyond the Turing theory and did not fit in the narrative.

Besides proposing the work done by the candidate, the main goal of this thesis is twofold: firstly, to revisit Turing theory on networks through the formalism of synchronization dynamics, proving that the former, at all effects, belongs to Dynamics on Networks; then, to further extend the boundaries of what are normally considered as Turing patterns, by showing that Turing-like patterns emerge even when the framework seems, in principle, far from the original Turing one. Whilst the first part, regarding pairwise interactions, deals with a well developed framework, as Turing patterns on networks have been thoroughly studied over the past decade, the papers in the second part are among the firsts of their kind and, thus, have a more didactic and fundamental structure.

The work of this thesis has been carried out at Université de Namur and the Namur Institute for Complex Systems (naXys) from January 1st 2020 up to the day of the defense and funded by the Fond National de la Recherche Scientifique, FNRS, and the region Wallonia through a FRIA PhD Grant FC 33443. Some parts of the work have been developed in collaboration with other international research groups. A first visit (10 days, Jan 2020) to the MACSI at University of Limerick (Ireland) in the group of Professor James Gleeson was funded by the Erasmus+ and partly led to Chapter 2. A second shorter visit (1 week, Jan 2022) was funded by the Bridge Grant of the Young Researchers of the Complex Systems Society (yrCSS) and inspired a work that is currently in preparation (see Conclusions and perspectives in Part III). The Erasmus+ also funded a visit (2 weeks, May 2022) to the group of Professor Mattia Frasca at Università di Catania (Italy), which partly led to Chapter 6 and to a work that is not part of the main thesis (see Summary of other coauthored papers in Part III). Moreover, such collaboration is still ongoing and other joint projects are currently discussed. Through the FRIA fundings, a short visit at Università degli Studi di Firenze (Italy) in the group of Professor Duccio Fanelli (1 week, June 2022) was important in the finalization of Chapter 7. The Royal Academy of Arts and Sciences of Belgium and additional funding from the FNRS (Mobility Out Grant) allowed for a long visit (2 months, Sep-Nov 2022) in the group of Professor Stefanella Boatto at the Mathematical Institute of Universidade Federal do Rio de Janeiro (Brazil), which resulted in a work that is currently being finalized and is thus not part of the thesis (see Conclusions and perspectives in Part III). Moreover, the FRIA funding allowed for a short visit (1 week, Nov 2022) to the group of Professor Juan Ignacio Perotti at Universidad Nacional de Córdoba (Argentina), inspiring a work that is still ongoing (see Conclusions and perspectives in Part III). Moreover, before joining naXys, first as a Teaching Assistant in September 2019, then as a FRIA PhD Student from January 2020, I was for a year a PhD Student of Systems Biology at VU Amsterdam (The Netherlands) within the Marie Curie ITN SynCrop, funded by the EU through the Horizon 2020 program. The research carried out in that year resulted in a paper published in a biology journal and, thus, far from the work of this thesis (see Summary of other coauthored papers in Part III).

Publications part of this thesis

- R. Muolo, T. Carletti, J.P. Gleeson & M. Asllani, *Synchronization dynamics in non-normal networks: the trade-off for optimality*, Entropy, Volume 23(1), 36, Pages 1-12 (2021) - **Chapter 2**
- T. Carletti & R. Muolo, *Finite propagation enhances Turing patterns in reaction-diffusion networked systems*, Journal of Physics: Complexity, Volume 2(4), 045004 (2021) - **Chapter 3**
- T. Carletti & R. Muolo, *Non-reciprocal interactions enhance heterogeneity*, Chaos, Solitons & Fractals, Volume 164, 112638 (2022) - **Chapter 4**
- R. Muolo, L. Gallo, V. Latora, M. Frasca & T. Carletti, *Turing patterns in systems with high-order interactions*, Chaos, Solitons & Fractals, Volume 166, 112912 (2023) - **Chapter 6**
- L. Giambagli, M.L. Calmon, R. Muolo, T. Carletti & G. Bianconi, *Diffusion-driven instability of topological signals coupled by the Dirac operator*, Physical Review E, Volume 106, 064314 (2022) - **Chapter 7**

Part I

Pairwise interactions

Chapter 1

Beyond the Turing mechanism: new frontiers of pattern formation on networks

The most wide-spread interpretation of Turing's original framework consists of two interacting species and it is mainly based on two pillars: the presence of a homogeneous stable fixed point and the successive activation of diffusion which provokes the instability. Alternatively, diffusion can be thought as always present and the distinction is made between homogeneous perturbations, which do not disrupt the stable state, and inhomogeneous ones, which yield instability. The two interpretations are equivalent and both consist of a symmetry breaking mechanism. However, over the years, such theory has been extended and many different settings have been studied [12]. Turing patterns have been found adding a differential flow, i.e., a drift, meaning that the diffusion is anisotropic due to a transport term [13, 14], noise, i.e., a source of constant perturbation endogenous to the system [10], cross-diffusion, i.e., the diffusion of a species has an effect on the variation of the other one and vice versa [15], an upper bound to the signal propagation, i.e., the equations become hyperbolic due to an inertia in the propagation [16] (and see Chapter 3), just to make a few examples. Moreover, recent findings have shown theoretical and experimental evidence of Turing patterns in quantum [17] and nanoscale systems [18]. We can extend the Turing framework in another direction, by considering three or more interacting species: in this case the system can exhibit oscillatory patterns, which are not allowed in the classical Turing setting [9, 19]. Such phenomenon, already discussed by Turing in his original paper, is found in the literature as wave instability [20, 8], despite the fact that diffusion is again the key factor. Interestingly, in some cases considered within the framework of Turing instability, e.g., when a differential flow is present, patterns can be oscillatory, but are called Turing patterns (or drift-induced Turing patterns). The hyperbolic case is even more peculiar: in fact, patterns that are solely due to the inertia in the propagation of the signal are called wave patterns, because it was thought that they are always oscillatory, and patterns due

to diffusion are called Turing patterns even when the stability of the homogeneous state is lost before the diffusion is active [16, 21, 22]. We will show that these interpretations are not correct in Chapter 3. There seem to be already a few inconsistencies in the nomenclature and characterization of Turing patterns, which in the network framework, as we will see in the next pages, become even more manifest. The question we try to answer in this Chapter is the following: when can we call an instability leading to the formation of patterns "Turing Instability"? Of course, the answer depends on the interpretation of the Turing mechanism and, in the end, it is more important to understand the phenomenon we are dealing with, rather than its name. We, however, believe that a reflection in such sense is necessary, given the confusion and the arbitrariness of the definitions used in the literature.
Before proceeding in the analysis, we would like to add one more thing. All the variations of Turing's original framework consist in getting closer to the experimental setting in order to fill the gap between theory and observations: nature is noisy, the signal does not propagate at infinite speed, etc. In almost every case[(1)] the system becomes unstable for a larger range of parameters, hence the formation of patterns is enhanced. In our opinion, the fact that, by adding more realistic hypotheses, the theory improves is a good indication of its epistemological value.

In the next section we will go through the basics of Turing theory on networks, showing how certain kinds of topologies enhance the formation of patterns. Then we will highlight the analogy between the Turing framework and the synchronization one, showing that the former can be revisited with the formalism of the latter, hence introducing Chapter 2. Successively, we will focus on oscillatory patterns, which do not coincide with what are called "wave" patterns in the literature, and show the incongruence of such nomenclature, focusing in particular on the case of hyperbolic reaction-diffusion systems, which are the subject of Chapter 3. Lastly, we will present a mechanism qualitatively very similar to the Turing one and show that it can yield patterns even in systems where no diffusion takes place. The latter will be further examined in Chapter 4, ending the part of this thesis focused on pairwise interactions.

1.1 Turing theory on networks: from lattices to non-normal structures

Our framework for this first part is the network one, i.e., the "manifold" where our dynamics take place is discrete. To use the word manifold may seem audacious, but, as we will see in the second part (Chapters 5-7), thanks to topology, we can appreciate a much deeper connection between continuous and discrete space. Let us leave the latter for a discussion further in the thesis and consider, for the moment, the case networks. The dynamical processes we will be interested in take place in the nodes, while links mediate the interactions between the latter. Without links we would have n isolated systems, but as soon as we "switch them on" our system becomes a whole and the interactions

[(1)] An interesting exception is the case of time-varying networks [23], in which the presence of a dynamic support leads to a shrinking of the instability region [24]. Such case will not be examined throughout this thesis.

among the nodes may yield a different and much richer dynamics than the decoupled case.

Turing theory was studied on discrete support first by Othmer and Scriven in two pioneering works in which they zoomed into Turing's continuum to consider actual cells where the reactions were taking place, connected in various lattices configurations [25, 26]. Othmer and Scriven's vision was certainly ahead of time, as network theory would become popular only thirty years later, with the works of Albert and Barabasi [27], Newman [28], Strogatz [29], Pastor-Satorras and Vespignani [30], to name a few. For this reason, the works on lattices are still anchored to the duality continuum-discrete. In fact, Othmer and Scriven's approach is a development of the discretization already present in Turing's original paper. The first work where Turing theory is studied using the modern tools of Network Science is due to Nakao and Mikhailov [31], in a milestone paper which opened the way to a new line of research. All successive works on Turing patterns on networks owed their main implant to such paper and this thesis is no exception. The key idea of Nakao and Mikhailov's work is the main pillar of everything discussed in this thesis and will be found in every Chapter, except for Chapter 5. However, being so important, let us see, in a nutshell, in what it consists through the key points. We start from the equations describing an isolated system of two species u and v, given by the following nonlinear equations

$$\begin{cases} \dot{u}(t) = f(u(t), v(t)) \\ \dot{v}(t) = g(u(t), v(t)) \end{cases} \tag{1.1.1}$$

and assume that there exists a stable equilibrium point (u^*, v^*), solution of the isolated system. We then proceed by coupling through a network n interacting copies of the above system. As we have discussed, diffusion plays a key role in Turing's mechanism. On networks, the role of diffusion is filled by the Discrete Laplacian, a matrix whose entries are given by $L_{ij} = A_{ij} - k_i \delta_{ij}$, with A_{ij} entries of the adjacency matrix $\mathbf{A}$ and k_i node degree. Such Laplacian, also called *combinatorial* Laplacian [32], provides the way in which the units are coupled[(2)]. The diffusion is then proportional to a constant D, which is specific for each species and is called *diffusion coefficient*. The form of reaction-diffusion equations hence is

$$\begin{cases} \dot{u}_i = f(u_i, v_i) + D_u \sum_{j=1}^{n} L_{ij} u_j \\ \dot{v}_i = g(u_i, v_i) + D_v \sum_{j=1}^{n} L_{ij} v_j \end{cases} \qquad \forall i = 1, 2, \ldots, n \tag{1.1.2}$$

The units being identical, (u^*, v^*) is also a solution of the coupled system. Hence, these equations can be linearized around the the equilibrium point (u^*, v^*), for every

[(2)] We will see in Chapter 3 a different definition of the combinatorial Laplacian, which is obtained from the *incidence matrix*. The two definitions are equivalent, although the latter allows us to generalize to higher orders of interactions, as we will show in Chapters 5 and 7.

node i, giving

$$\begin{cases} \delta\dot{u}_i = f_u\delta u_i + f_v\delta v_i + D_u\sum_{j=1}^{n} L_{ij}\delta u_j \\ \delta\dot{v}_i = g_u\delta u_i + g_v\delta v_i + D_v\sum_{j=1}^{n} L_{ij}\delta v_j \end{cases} \tag{1.1.3}$$

where $\delta u_i = u_i - u^*$, $\delta v_i = v_i - v^*$ are the inhomogeneous perturbations and f_u the derivative of function f with respect to variable u computed on the fixed point (analogously for the others). By defining $\vec{\zeta} = (\delta u_1, \ldots, \delta u_n, \delta v_1, \ldots, \delta v_n)^\top$, we can rewrite the latter in compact form, we obtain

$$\dot{\vec{\zeta}} = (\mathbb{I}_n \otimes \mathbf{J}_0 + \mathbf{L} \otimes \mathbb{D})\,\vec{\zeta} \tag{1.1.4}$$

where $\mathbb{D} = \begin{pmatrix} D_u & 0 \\ 0 & D_v \end{pmatrix}$, $\mathbf{J}_0 = \begin{pmatrix} f_u & f_v \\ g_u & g_v \end{pmatrix}$ is the Jacobian matrix of the isolated system and $\otimes$ is the Kronecker product. Equation (1.1.4) determines the evolution of the perturbation: the system will relax back to the homogeneous equilibrium or exponentially escape toward another attraction point depending whether the largest real part of the spectrum of the $2n \times 2n$ matrix $\mathbb{I}_n \otimes \mathbf{J}_0 + \mathbf{L} \otimes \mathbb{D}$ is positive or negative. However, the basis arbitrarily chosen is not ideal to study the evolution of the perturbation, as the (potential) instability modes are not decoupled. The ingenious idea of Nakao and Mikhailov, previously used by Turing himself in the case of continuous support, was to expand the perturbation on the basis of the Laplacian's eigenvectors, which are orthonormal the network being symmetric. In the new basis, the $2n \times 2n$ system is decomposed onto n 2×2 systems. For $\alpha = 1, \ldots, n$, we obtain then

$$\dot{\vec{\xi}}_\alpha = \left[\mathbf{J}_0 + \Lambda^{(\alpha)}\mathbb{D}\right]\vec{\xi}_\alpha = \mathbf{J}_\alpha\vec{\xi}_\alpha \tag{1.1.5}$$

where $\vec{\xi}_\alpha = \begin{pmatrix} \hat{u}_\alpha \\ \hat{v}_\alpha \end{pmatrix}$ is the perturbation in the new basis and $\Lambda^{(\alpha)}$ is the α-th eigenvalue of $\mathbf{L}$, which is either zero or negative. By analyzing the stability of matrix $\mathbf{J}_\alpha$, one can find the conditions for the emergence of patterns. Note that, the support (i.e., the operator's spectrum) being discrete, there will always be finite size effects: in fact, while the continuous counterpart obtained by studying the stability as a function of a continuous parameter in place of the discrete $\Lambda^{(\alpha)}$ may be unstable, it can happen that the interval of values yielding instability does not contain any discrete instability mode.

Another interesting fact about the above analysis, which could be noticed also from Equations (1.1.2), is that the difficulty of the problem does not change with the topology. On continuous support there is a notable difference between studying the problem on a $1D$-lattice or on a Rienmannian surface [33]: the structure of Equations (1.1.5) remains the same, but the Laplacian operator changes. In our framework, instead, the diffusion operator is a matrix, whose eigenvectors are easily computable independently of the network[3], and the numerical problem to be solved remains an ODE one. This is

[3] This is not true anymore for the case of multiplex [34, 35] and multilayer networks [36], where computing the spectrum of the Laplacian requires a perturbative approach. However, the statement in the text is true for any *network*, hence excluding multilayer structures.

particularly interesting, considering that some network topologies do not have a trivial embedding, or even no embedding at all [37] and the power of this approach becomes manifest when studying directed [38] and non-normal [39] topologies. In fact, while on continuous support one would have to deal with a drift term to account for the privileged direction of diffusion [40], the expansion of the perturbation on the Laplacian's eigenbasis can be generalized even when such basis is not orthonormal or generalized eigenvectors are needed, cases which will be discussed in the next Chapter and, thoroughly, in Chapter 4, Section 4.6.

Let us conclude with a comment. It is sometimes said that physics mainly breaks down to two things: a linearization and a change of basis. Nakao and Mikhailov's elegant solution of the Turing problem on networks is a remarkable example of this.

1.2 Synchronization dynamics from the Turing perspective

It is common to see Turing pattern formation within the realm of physical chemistry or partial differential equations. However, the problem can be reformulated within the framework of Dynamics on Networks and we will show in this section its analogy to the formalism used of synchronization dynamics [41, 42]. The study of synchronization dynamics is a vast field and many different frameworks and models are investigated. The most common is certainly the Kuramoto model [43], where the oscillators are in general not identical. Instead, we will focus our attention on a different approach to synchronization, namely that developed by Pecora and Carroll in a seminal paper that opened a new line of research [44]. Scholars of such field are accustomed to study systems of identical units coupled through a network. Before proceeding any further, we need to make an important clarification: a homogeneous (global synchronous) solution exists because we are considering *n identical* units, condition that is not generically matched in the Kuramoto framework, where, in fact, there is no homogeneous solution. For every unit $\vec{x}_i$, which can have a chaotic or periodic dynamics[(4)], the equation describing the system takes the following form

$$\dot{\vec{x}}_i = \vec{f}(\vec{x}_i) + \sigma \sum_{j=1}^{n} A_{ij} \vec{g}(\vec{x}_j, \vec{x}_i) \tag{1.2.1}$$

where n is the number of interacting units (i.e., nodes of the network), $\vec{x} \in \mathbb{R}^l$ is the dynamical variable, $\vec{f}$ a nonlinear vectorial function describing the dynamics of the decoupled system, σ the coupling strength and $\vec{g}$ a vectorial function describing the coupling between the units through the network topology. The latter needs to be non-invasive, i.e., $\vec{g}(\vec{x},\vec{x}) = 0$, which guarantees the existence of the global synchronous solution $\vec{x}_1 = ... = \vec{x}_n \equiv \vec{x}^*(t)$ [44][(5)]. In general, the coupling is also diffusive-like,

[(4)] The following discussion was originally developed for chaotic oscillators, but it remains valid also for periodic ones.

[(5)] Especially in the literature on synchronization, the synchronous solution is indicated with $\vec{x}^s$, rather than $\vec{x}^*$. Let us also remark that the synchronous solution can be time-dependent or -independent; in the next pages we will not always explicit the dependence on time when cleared by the context.

i.e., $\vec{g}(\vec{x}_j,\vec{x}_i) = \vec{h}(\vec{x}_j) - \vec{h}(\vec{x}_i)$, meaning that it can be linearly approximated by a Fickean diffusive process[6]. Also in this case, the interest is to study if and how the coupling affects the dynamics of the isolated system. In particular, in such framework the main research question is whether all the interacting units will follow the same trajectories, i.e., they will be globally synchronized following $\vec{x}^*(t)$, or a perturbation will disrupt the collective motion. The stability of the synchronous solution can be studied through the Master Stability Function (MSF), a powerful numerical tool developed by Pecora and Carroll in the aforementioned paper [44]. The procedure will be detailed in Chapters 2 and 5, but let us go through the key points, so to show the similarities between this framework and the Turing on network's one. In a nutshell, the synchronous solution is perturbed and the maximum Lyapunov exponent is computed as a function of a continuous coupling parameter. The equation for the perturbation linearized about the synchronous solution is

$$\dot{\vec{\zeta}} = \left(\mathbb{I}_n \otimes \mathbf{J}_f + \mathbf{L} \otimes \mathbf{J}_h\right) \vec{\zeta} \tag{1.2.2}$$

where now the perturbation vector $\vec{\zeta}$ has dimension nl and the $l \times l$ matrices $\mathbf{J}_f$ and $\mathbf{J}_h$ are the Jacobian of functions $\vec{f}$ and $\vec{h}$ respectively. Let us point out that the Jacobian matrices are computed on the synchronous solution, hence they will be, in general, time-dependent. The network Laplacian appears due to the hypothesis of diffusive-like coupling[7]. In order to decouple the modes, we need to perform a change of basis and, from the above $ln \times ln$ system, get n $l \times l$ ones. If we transform through the basis of eigenvectors of the matrix $\mathbf{L}$, Equation (1.2.2) becomes for each mode α

$$\dot{\vec{\xi}}_\alpha = \left[\mathbf{J}_f + \Lambda^{(\alpha)}\mathbf{J}_h\right] \vec{\xi}_\alpha = \mathbf{J}_\alpha \vec{\xi}_\alpha \tag{1.2.3}$$

where again $\Lambda^{(\alpha)}$ is the α-th eigenvalue of $\mathbf{L}$. The first mode, associated to the 0 eigenvalue, is the perturbation parallel to the synchronized solution, i.e., the equation for the isolated systems. All the other modes are orthogonal to the synchronization manifold and the computation of the MSF reveals if one of them drives the system away from the synchronous state.

If all that sounds familiar, it is because the procedure and the philosophy behind it is similar to what we have shown in the previous section to compute the dispersion relation in the context of Turing patterns. The key difference between the two frameworks is that, when studying Turing patterns, the coupling needs to change the stability of the fixed point (from stable to unstable) to yield an interesting dynamics [46]. Taken that into account, one can consider the homogeneous fixed point as the synchronous solution, $\vec{x}^* \in \mathbb{R}^2$, i.e., a two species system, $\mathbf{J}_h$ the diagonal matrix of the diffusion coefficients and the dispersion relation as the maximum Lyapunov exponent as a function

[6] The hypothesis of diffusive-like coupling function, besides simplifying the problem, allows to develop an elegant and powerful formalism [45], that we will use in Chapter 6 to develop Turing theory for systems with higher-order interactions.

[7] In Pecora and Carroll's original work, the coupling matrix was not exactly the Laplacian, but a very close relative. The above discussion bears the same philosophy of the original work, but it is presented in a revisited formulation.

of the coupling, i.e., the MSF, to recover exactly the equation of the previous section, i.e., Equation (1.1.4). There is another caveat in this analogy. The dispersion relation has a physical meaning, i.e., it relates to the wave-number of the perturbation driving the system away from the equilibrium, besides the stability properties, while the MSF merely indicates the latter. We can say that the dispersion relation is *a* MSF, but *not all* MSFs are dispersion relations.
When the isolated system has a stable fixed point, i.e., a negative Lyapunov exponent, we talk about dispersion relation, when it has a stable limit cycle, i.e., zero Lyapunov exponent[(8)], we talk about Floquet multipliers and when it has a strange attractor, i.e, positive Lyapunov exponent, we talk about Lyapunov exponent. *Mutatis mutandis*, the analysis is very similar and in the end the objective is to study the stability of the whole system, i.e., the n interacting units, as a function of the coupling. In the case of fixed point the MSF can be computed analytically, while for the other cases, the linearized system being non-autonomous, we need to resort to numerical simulations, as discussed in details in Chapter 2. Nonetheless, there is a notable exception, the Stuart-Landau models, that is also the normal form of the Hopf-Andronov bifurcation [48], for which the Jacobian of the system computed on the limit cycle is constant and the MSF can be computed analytically; such model will be discussed in Chapter 4.

After what we have shown in this section, we can conclude that the techniques applied to investigate the emergence of Turing patterns are analogous to those used to study the stability of the synchronous states for coupled oscillators on networks. Given that the community of synchronization is larger than that of Turing patterns on networks, it may seem at first that the latter may benefit more from such connection, as all the insights and techniques developed in the former framework can be transported in the new context. It is indeed the case of the work presented in Chapter 6, where we have adapted an elegant formalism developed in the context of synchronization dynamics to Turing theory. However, also the study of Turing patterns on networks can very well contribute to the study of synchronization by looking at the problem from a different perspective[(9)]. This is the case of the work presented in the next Chapter, where, thanks to a theory which was developed for Turing patterns, we have been able to give a contribution in the field of synchronization by proving that a certain kind of networks is not optimal for synchronization, in contrast to what it was thought before.

1.3 Inertia-driven and other oscillatory patterns

In Chapter 3 we study the emergence of patterns when the signal propagation is finite, the latter being a necessary assumption when the reaction-diffusion process takes place on a large domain. Leaving a formal derivation for later in the thesis, the reaction-diffusion equations take the following form

[(8)] A zero Lyapunov exponent, on the other hand, does not imply that the isolated system has a stable limit cycle, since also centers and quasi-periodic dynamics yield a zero Lyapunov exponent [47].

[(9)] Let us remember that, while the reformulation of Turing theory on network is rather new, it carries decades of insights developed experimentally and theoretically on continuous support.

$$\begin{cases} \dot{u}_i + \tau_u \ddot{u}_i = f(u_i, v_i) + D_u \sum_{j=1}^{n} L_{ij} u_j \\ \\ \dot{v}_i + \tau_v \ddot{v}_i = g(u_i, v_i) + D_v \sum_{j=1}^{n} L_{ij} v_j \end{cases} \tag{1.3.1}$$

where now τ_u and τ_v are the inertial times in the propagation of species u and v respectively[(10)]. On continuum support, such equations are called hyperbolic, because that is the kind of PDEs we would obtain, in contrast with the "classic" parabolic reaction-diffusion equations. The emergence of Turing patterns for hyperbolic reaction-diffusion equations has been studied for equal [16] and different [21] inertial times, but never on networks, and that is what we did [49], which is the subject of Chapter 3.
Moreover, studying Turing instability for hyperbolic systems on discrete support allowed us to reinterpret the kinds of patterns we observed. In fact, a class of patterns emerges, which is solely due to the inertia in the signal propagation, and they are called *wave patterns* in the literature. Such nomenclature is rather peculiar, mainly because this kind of patterns are also stationary and then because the physical reason for their existence is the inertia in the signal propagation, while classical wave patterns emerge because of the interactions of three (or more) reacting and diffusing species [8]. It is true, as rightly pointed out in [22], that a necessary condition for the emergence of oscillation is a third time derivative, which makes the two frameworks mathematically similar, however the physical reason is intrinsically different. Because of that we renamed this kinds of patterns *inertia-driven*.

In mathematics and physics there is often an opposition to renaming phenomena, which is in our opinion correct. In fact, we should always try to understand if what we are observing has already been observed in different circumstances and try to find common patterns rather than differentiate our results from what is already known. Science is full of examples of "name changing", which later mislead the attribution of the discovery. One of the most notable cases in nonlinear science regards Chimera States, which where first discovered by Kaneko in the late 80s in maps [50], Cerdeira and collaborators in Josephson junctions [51], Kuramoto, Nakao and Battogtokh in systems of non-locally coupled oscillators (Ginzburg-Landau systems, Rössler oscillators, logistic maps) [52, 53, 54, 55, 56] and identical phase oscillators [57], but were then renamed "Chimeras" by Strogatz and Abrams citing only the last of the previous references [58]. Nevertheless, we would like to stress the fact that the case of *inertia-driven patterns* is different, as we are not only renaming, but reinterpreting the phenomenon. The name *wave patterns* is misleading because such patterns are not always oscillatory, but can also be stationary, independently of the imaginary part of the unstable modes. Additionally, they are solely caused by the inertia in the signal propagation, as much as classical Turing patterns are caused by the diffusion. In analogy with diffusion-driven, we believe that inertia-driven is the most correct form to address such patterns. Moreover, in the context of hyperbolic reaction-diffusion system, the inertial times may cause a

[(10)] The finite propagation velocity for the species will thus be $V = \sqrt{D/\tau}$.

loss of stability of the homogeneous stable state, hence diffusion-driven patterns are no longer due to a Turing instability, as we would lose the main feature of homogeneous stable equilibrium. Surprisingly, in the literature these patterns are considered Turing patterns and the fact there is no stable homogeneous equilibrium is ignored [16, 21, 22]. In our work we show that whether the instability is a Turing instability or not depends on the values of the inertial times.
The case for which the homogeneous stable equilibrium loses its stability is sometimes called Hopf instability or Turing-Hopf instability, even though sometimes also an instability leading to oscillatory patterns is called in such a way [59, 60]. We do not believe that this characterization makes sense in the context of networks. In fact, the loss of stability of the fixed point may result in stable limit cycle, hence every node would oscillate on the same attractor and the global system would still be in a homogeneous stable state. As previously shown, such homogeneous stable state can undergo a Turing-like bifurcation and become unstable due to diffusion. Hence, when the homogeneous equilibrium is no longer stable, we are not dealing with a Turing-like instability. It is also interesting to note, as it will be shown in the next Chapter, that, despite a non-zero imaginary part of the dispersion relation (or MSF, in this context), the patterns can be stationary. The problem of pattern prediction remains an open problem and we cannot know *a priori* whether the observed patterns will be stationary or oscillatory, but we need to resort to numerical simulations to have an answer.

1.4 Systems without diffusion and non-reciprocal interactions

We have learned that diffusion is the essence of the Turing-instability. But then also noise, a differential flow or certain network topologies can drive the instability together with diffusion. In some cases, instability is purely due to the inertia in the signal propagation. We are slowly moving away from Turing original framework, but from a network perspective its philosophy still holds: n isolated systems lie in a homogeneous stable state, that is disrupted by an inhomogeneous perturbation. One could ask: can we avoid diffusion *tout court* and still observe patterns?
There are indeed many systems where no diffusion takes place but which exhibit patterns, for instance photosentive chemical reactions, where the reactants interacts via emission of photons without any displacement of particles [61, 62, 63]. Interactions without diffusion are often called *non-local* interactions and have been studied in chemical [64] and ecological [65] systems. The mechanism of instability is intrinsically different from the Turing one, despite some similarities, i.e., the homogeneous stable state is disrupted by an inhomogeneous perturbation. However, let us consider the network framework, with n isolated units interacting with each other without diffusion. Let us start by the equations for the isolated units, i.e., the local interactions

$$\begin{cases} \dot{u}_i = f(u_i, v_i) \\ \dot{v}_i = g(u_i, v_i) \end{cases} \quad \forall i = 1, \dots, n \tag{1.4.1}$$

If we now assume that the species in node i can interact non-locally with species in the adjacent nodes, we can represent the long-range interactions in the following way

$$\begin{cases} \dot{u}_i = \dfrac{1}{k_i}\displaystyle\sum_{j=1}^{n} A_{ij} F(u_i, v_i, u_j, v_j) \\ \\ \dot{v}_i = \dfrac{1}{k_i}\displaystyle\sum_{j=1}^{n} A_{ij} G(u_i, v_i, u_j, v_j) \end{cases} \tag{1.4.2}$$

where the nonlinear function F (resp. G) is such that $F(u_i, v_i, u_i, v_i) = f(u_i, v_i)$, meaning that, when the non-local interactions are inactive, we recover the local dynamics. If we now define the matrix

$$\mathscr{L}_{ij} = \frac{A_{ij}}{k_i} - \delta_{ij}$$

and write for variable u (resp. v)

$$\dot{u}_i = \frac{1}{k_i}\sum_{j=1}^{n} A_{ij} F(u_i, v_i, u_j, v_j) + f(u_i, v_i) - f(u_i, v_i)$$

we obtain

$$\begin{cases} \dot{u}_i = f(u_i, v_i) + \displaystyle\sum_{j=1}^{n} \mathscr{L}_{ij} F(u_i, v_i, u_j, v_j) \\ \dot{v}_i = g(u_i, v_i) + \displaystyle\sum_{j=1}^{n} \mathscr{L}_{ij} G(u_i, v_i, u_j, v_j) \end{cases} \tag{1.4.3}$$

which is, indeed, similar to the reaction-diffusion system (1.1.2), even though no diffusion takes place. The matrix $\mathscr{L}$ is called *reactive* or *consensus* Laplacian and has analogous properties to the diffusion (combinatorial) one. The intuition leading to such form of the equations describing non-local interactions was made by Cencetti and collaborators [66], who showed that one can obtain a Turing-like mechanism of pattern formation with purely reactive interactions. Such non-local interactions are sometimes called *long-range* interactions, which may be misleading. In fact, long-range interactions are usually referred to interactions due to nodes which are not directly connected with each other, but still affect the dynamics [67]. In this context, we will consider long-range interactions as non-local interactions, stressing the fact that the elementary units interact with each other without any displacement of particles.

Moreover, interactions are in general non-reciprocal, meaning that the underlying network is asymmetric[(11)]. The effects of non-reciprocal interactions has been thoroughly studied in the framework of Turing patterns [38, 40], population dynamics [68] and, recently, phase transitions [69], just to mention a few examples, and in all cases it seems that non-reciprocity greatly enhances the possibility and variety of observed patterns. In Chapter 4, we will study the case of non-reciprocal non-local interactions

[(11)]More than asymmetric, real-world networks are non-normal, as shown in [39]. The effects of non-normality will be discussed in Chapter 2.

and, in particular, focus on the effects of such asymmetry in the formation of patterns, showing more in general that, indeed, patterns emerge more easily in such a context. We will also show that the analysis performed to study the stability of the system after an inhomogeneous perturbation of the homogeneous stable state closely resembles that shown at the beginning of this Chapter for reaction-diffusion systems, hence justifying the inclusion of such framework in the Turing one.

1.5 Discussion

Answering the question at the beginning of this Chapter, we gave, of course, a subjective version of the story, which is based on the work done and is strongly influenced by the received training and the researchers with whom we had the luck to collaborate. Far from a definitive word, our is more an exercise to bring out the absurdity of a strict characterization, which ignores not only multiple contradictions but also clear evidence, so that as a community interested in Turing patterns we can move forward, away from obsolete classifications. We have seen that what it is called Turing patterns is rather arbitrary and that we should not be strict in the nomenclature. Either we call Turing patterns only the patterns due to the original Turing mechanism (two species and diffusion-driven) and exclude the rest, or we acknowledge that all patterns shown in the previous pages are undeniably inspired by Turing's work. We could call Turing patterns the patterns due to the original Turing mechanism and call all the rest Turing-like patterns. To add clarity, we could add the driver of the instability, in order to distinguish them among each other, and so call them drift-Turing patterns, wave-Turing patterns or inertia-Turing patterns as we did in one of our works [49] (Chapter 3).

As discussed in the previous paragraphs, in the following three chapters we will find three different settings in which patterns emerge, none of which is close to the classical Turing setting. But there is absolutely no doubt that they are inspired by Turing original idea, to which they have a huge intellectual debt. All these works are Turing paper's great-great grand-children, and this stands also for those within the framework of higher-order interactions, which will come in the second part of this thesis. All the patterns found in the next pages deserve, in our opinion, to bear Turing's name.

Chapter 2

Synchronization dynamics on non-normal networks: the trade-off for optimality

The framework of Turing instability on networks is connected to that of synchronization, even though at first sight they may appear far. In fact, we can consider n systems of 2 species in a limit cycle regime and couple them through a network, to then observe either the disruption of the homogeneous synchronized solution due to diffusion or the system going asymptotically back to the latter state [46]. As we have seen in Chapter 1, the two frameworks are related, so what is valid in one should stand also in the other. We knew that when the homogeneous stable state is a fixed point, a linear stability analysis might fail in predicting the instability if the system is on top of a non-normal network, as it has been shown in previous studies [70, 71]. The research question driving the development of the following paper was whether an analogous mechanism could be observed in the framework of synchronization.
This question was answered positively and it stimulated a discussion in the community [72, 73] whether certain networks are optimal for synchronization or not. First of all, let us stress that what we intend with "optimal for synchronization" slightly differs from the one given in [74], and this could have been the source of some misunderstanding. Secondly, the latter authors refer to the *synchronizability* of the network and their theoretical study is correct, namely the system synchronizes provided the initial perturbation is sufficiently small. On the other hand our approach focused on the difference of sizes the perturbations can have, once the underlying network is non-normal or not. Indeed, we numerically showed that the *optimal* networks presented in [74] are strongly non-normal and, hence, although they may seem a good choice to enhance synchronization, their homogeneous (synchronized) state is weak against finite perturbations; stated differently, the basin of attraction of the synchronous manifold can be very small and thus "invisible" to finite perturbations. With those *caveats*, we can affirm thus that our nu-

merical results are solid and, in fact, they have been criticized but without being proven wrong. Eventually, two independent groups replicated and corroborated our numerical results [75, 76]: non-normal networks make the synchronized solution weaker with respect to finite perturbations and stability can be lost even when a linear stability analysis predicts otherwise. All this is in agreement with the known results on non-normal matrices and operators [39, 77]. Moreover, in [75] it is proven that, among all the non-normal networks, only star-networks are actually optimal for synchronization. This is clear, because one node affects all other and only *ad hoc* perturbations can drive the system away from the equilibrium. The interested reader may follow the whole story, starting with [78] (i.e., this very Chapter), then the comment [72], the reply [73] and the final word [75, 76]. The busy reader, after this Chapter, may go directly to [75].
Working on the paper below was extremely interesting and educational, because we put on the "hat" of Turing pattern formation to enter the world of synchronization and looked at things from a different perspective. It was fascinating how we could give a contribution to a field, in principle, not too close. Nonetheless, there are still many open questions on non-normality and its effects on the dynamics and this topic is just starting to be investigated. Some of these points will be discussed at the end of the Chapter, in Section 2.5.

R. Muolo, T. Carletti, J.P. Gleeson & M. Asllani. Entropy 23 (1), 36 (2021) [78]

Abstract

Synchronization is an important behavior that characterizes many natural and human made systems composed by several interacting units. It can be found in a broad spectrum of applications, ranging from neuroscience to power-grids, to mention a few. Such systems synchronize because of the complex set of coupling they exhibit, the latter being modeled by complex networks. The dynamical behavior of the system and the topology of the underlying network are strongly intertwined, raising the question of the optimal architecture that makes synchronization robust. The Master Stability Function (MSF) has been proposed and extensively studied as a generic framework to tackle synchronization problems. Using this method, it has been shown that for a class of models, synchronization in strongly directed networks is robust to external perturbations. In this paper, our approach is to transform the non-autonomous system of coupled oscillators into an autonomous one, showing that previous results are model-independent. Recent findings indicate that many real-world networks are strongly directed, being potential candidates for optimal synchronization. Inspired by the fact that highly directed networks are also strongly non-normal, in this work, we address the matter of non-normality by pointing out that standard techniques, such as the MSF, may fail in predicting the stability of synchronized behavior. These results lead to a trade-off between non-normality and directedness that should be properly considered when designing an optimal network, enhancing the robustness of synchronization.

2.1 Introduction

Systems in nature are often constituted by a large number of small parts that continuously interact with each other [79, 41]. Although it might be possible to accurately know the dynamics that characterize each of the individual constituents, it is, in general, nontrivial to figure out the collective behavior of the systems as a whole resulting from the individual/local interactions. A relevant example is provided by a system composed by an ensemble of coupled non-linear oscillators, that behave at unison driven by the non-local interaction, then the system is said to be synchronized [80, 41]. Synchronization has been extensively studied in network science as a paradigm of dynamical processes on a complex network, mainly due to the essential role of the coupling topology in the collective dynamics [79]. Its generic formulation allowed researchers to use it to model several applications, ranging from biology, e.g., neurons firing in synchrony, to engineering, e.g., power grids [42]. The ubiquity of synchronization in many natural or artificial systems has naturally raised questions about the stability and robustness of synchronized states [81, 82, 83, 74]. In their seminal work, Pecora and Caroll [44] introduced a method known as Master Stability Function (MSF) to help understand the role that the topology of interactions has on system stability. Assuming a diffusive-like coupling among the oscillators, the MSF relates the stability of the synchronous state to the nontrivial spectrum of the (network) Laplace matrix; in particular, it has been proven that the latter should lie in the region where the Lyapunov exponent that characterizes the MSF takes negative values [41, 84]. For a family of models (e.g., Rössler, Lorenz, etc.) whose stable part of the MSF has a continuous interval where the (real part of the) Laplacian's eigenvalues can lie, it has been proven that they maximize their stability once the coupling network satisfies particular structural properties. Such optimal networks should be directed spanning trees and without loops [83, 74]. These networks have the peculiarity of possessing a degenerate spectrum of the Laplacian matrix and laying in the stability domain provided by the Master Stability Function. The Laplacian degeneracy is also often associated with a real spectrum or with considerably low imaginary parts compared to the real ones [85, 77].

The vast interest in complex networks in recent years has also provided an abundance of data on empirical networked systems that initiated a large study of their structural properties [86]. From this perspective, it has been recently shown that many real networks are strongly directed, namely they possess a high asymmetry adjacency matrix [39]. Most of these networks present a highly hierarchical, almost-DAG (Directed Acyclic Graph) structure. This property potentially makes the real networks suitable candidates for optimally synchronized dynamical systems defined on top of them. Another aspect which is unavoidably associated with the high asymmetry of real networks, is their non-normality [39], namely their adjacency matrix $\mathbf{A}$ satisfies the condition $\mathbf{A}\mathbf{A}^T \neq \mathbf{A}^T\mathbf{A}$ [77]. The non-normality can be critical for the dynamics of networked systems [87, 39, 70, 88, 89, 90]. In fact, in the non-normal dynamics regime a finite perturbation about a stable state can undergo a transient instability [77] which because of the non-linearities could never be reabsorbed [87, 39]. The effect of non-normality in dynamical systems has been studied in several contexts, such as hydrodynamics [91], ecosystems stability [92], pattern formation [93], chemical reactions [94], etc. However, it is only recently that the ubiquity of non-normal networks and the related dy-

namics have been put to the fore [87, 39, 70, 88, 89, 90]. In this paper, we will elaborate on these lines showing the impact of non-normality on the stability of a synchronous state. We first show that a strongly non-normal network has, in general, a spectrum very close to a real one and that this in principle should imply a larger domain of parameters for which stability occurs, for systems with a generic shaped MSF. For illustration purposes, we will consider the Brusselator model [95, 96], a two-species system with a discontinuous interval of stability in the MSF representation. We will also examine the limiting cases of our analysis to two simple network models [40], namely a (normal) bidirected circulant network and a (non-normal) chain, both with tunable edge weights in such a way to allow a continuous adjustment respectively of the directedness and non-normality.

The MSF relies on the computation of the Lyapunov exponent, and thus in the case of time-dependent systems, it does not possess the full predictability power it has in the autonomous case (fixed point in/stability). For this reason, we will use a homogenization method, whose validity is limited to a specific region of the model parameters, allowing us to transform the linearized periodic case problem into a time-independent one [97]. This way, we remap our problem to an identical one studied in the context of pattern formation in directed networks where spectral techniques provide significant insight [38, 40]. Such an approach allows us on one side to assess the quantitative evaluation of the role of the imaginary part of the Laplacian's spectrum in the stability problem. On the other it permits the use of numerical methods, such as the pseudo-spectrum [77] in the study of the non-normal dynamics. To the best of our knowledge, this is the first attempt to use such techniques in the framework of time-varying systems, being the theory of non-normal dynamical systems limited so far to autonomous systems [77]. As expected, the non-normality plays against the stability of the synchronized ensemble of oscillators. Furthermore, a high non-normality translates to a high spectral degeneracy, which brings to a large pseudo-spectrum, indicating a high sensibility toward the instability. Clearly, the directionality and the non-normality stand on two parallel tracks regarding the stability of synchronized states and their robustness. As a conclusion of our work, we show that the most optimal design should be looked at as a trade-off between a high and low directionality/non-normality. Such choice should depend either on the magnitude of perturbation or the ratio directed vs. non-normal of the network structure.

2.2 Optimal synchronization: Directed vs. Non-normal networks

We consider a network constituted of n nodes (e.g., the idealized representation of a cell), and we assume a metapopulation framework, where the species dynamics inside each node is described by the *Brusselator* model, a portmanteau term for Brussels and oscillator. It has been initially introduced by Prigogine & Nicolis to capture the autocatalytic oscillation [95] phenomenon, resulting from a Hopf bifurcation curve in the parameter plane. This will be the framework we will consider in the following, neglecting thus the fixed point regime. Species can migrate across nodes with a diffusion-like

mechanism. In formulae, this model translates to a reaction-diffusion set of equations:

$$\begin{cases} \dot{u}_i = 1-(b+1)u_i + cu_i^2 v_i + D_u \sum_{j=1}^{n} L_{ij} u_j \\ \dot{v}_i = bu_i - cu_i^2 v_i + D_v \sum_{j=1}^{n} L_{ij} v_j \end{cases} \qquad \forall i = 1,\dots,n \tag{2.2.1}$$

where u_i and v_i indicate the concentration of the two species per node, D_u, D_v are their corresponding diffusion coefficients, and b, c are the model parameters. The coupling is represented by the matrix $\mathbf{A}$, whose non-negative entries A_{ij} represent the strength of the edge pointing from node j to node i. The entries of the Laplacian matrix $\mathbf{L}$ are given by $L_{ij} = A_{ij} - k_i^{in}\delta_{ij}$ where $k_i^{in} = \sum_j A_{ij}$ stands for the in-coming degree of node i, i.e. the number of all the entering edges into node i. We want to emphasize here that many other coupling operators are also possible; nevertheless, most of them will reduce at the linear level to a Laplacian involving the differences of the observable among coupled nodes [41], i.e., $\sum_{j=1}^{n} L_{ij}x_j = \sum_{j=1}^{n} A_{ij}(x_j - x_i)$. This form ensures that the coupling is in action only when the observable assume different values in two coupled nodes.

The reason for choosing such a model, as mentioned earlier, is mainly due to the discontinuous interval of the stability domain provided by the MSF of the problem (as it can be noticed in the inset of Figure 2.3 *a*)). To proceed with the stability analysis, we first need to identify the homogeneous periodic solution, $\vec{u}^*(t)$ and $\vec{v}^*(t)$, hereby called the *synchronized manifold* (or *synchronous solution*) and then to linearize the system around this. Let us introduce the perturbations for the i-th node by δu_i and δv_i, then the linearized equations describing their evolution are given by:

$$\begin{aligned} \delta\dot{u}_i &= \left[f_u \delta_{ij} + D_u \sum_{j=1}^{n} L_{ij} \right] \delta u_j + f_v \delta v_i \\ \delta\dot{v}_i &= g_u \delta u_i + \left[g_v \delta_{ij} + D_v \sum_{j=1}^{n} L_{ij} \right] \delta v_j \\ &\quad \forall i = 1,\dots,n \end{aligned} \tag{2.2.2}$$

where the partial derivatives are given by $f_u = -(b+1) + 2cu^*(t)v^*(t)$, $f_v = cu^*(t)^2$, $g_u = b - 2cu^*(t)v^*(t)$, and $g_v = cu^*(t)^2$. Notice that the partial derivatives of the reaction part are evaluated on the synchronized manifold. This translates into a time-dependent Jacobian matrix due to the periodicity of the solutions and thus to a non-autonomous linear system.

To make a step forward let us introduce the following compact notation; let $\vec{\zeta} = (\delta u_1,\dots,\delta u_n,\delta v_1,\dots,\delta v_n)^{\mathrm{T}}$ be the $2n$-dimensional perturbation vector, $\mathbb{D}$ the diagonal diffusion coefficients matrix and $\mathbf{J}(t)$ the time-dependent Jacobian matrix, hence Equation (2.2.2) can be rewritten as

$$\dot{\vec{\zeta}} = (\mathbb{I}_n \otimes \mathbf{J}(t) + \mathbf{L} \otimes \mathbb{D})\,\vec{\zeta}\,, \tag{2.2.3}$$

where $\otimes$ is the coordinate-wise multiplication operator. Then, we proceed by diagonalizing the linearized system using the basis of eigenvectors of the network Laplace

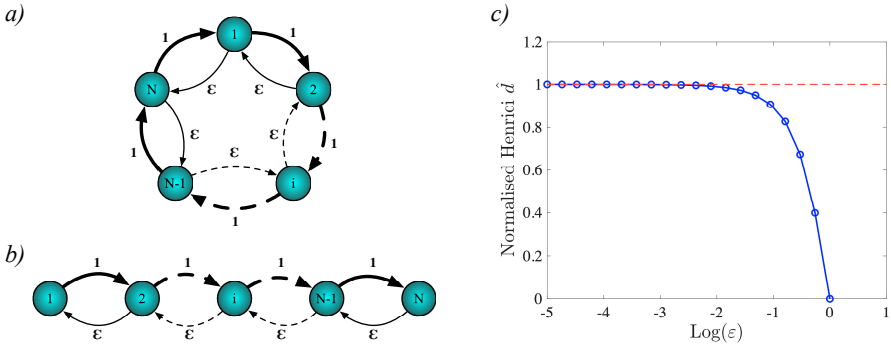

Figure 2.1: The network toy models for the case of a normal bidirectional circulant network, panel a), and a non-normal bidirectional chain, panel b). c) Normalized Henrici's departure from non-normality as a function of tuning parameter ε for the non-normal model. We observe that starting from 0, the network is symmetric, and the non-normality increases as the weight of the reciprocal edges decreases, taking the maximal value of non-normality in the limit when $\varepsilon = 0$. In this case, the Laplacian's spectrum is degenerate.

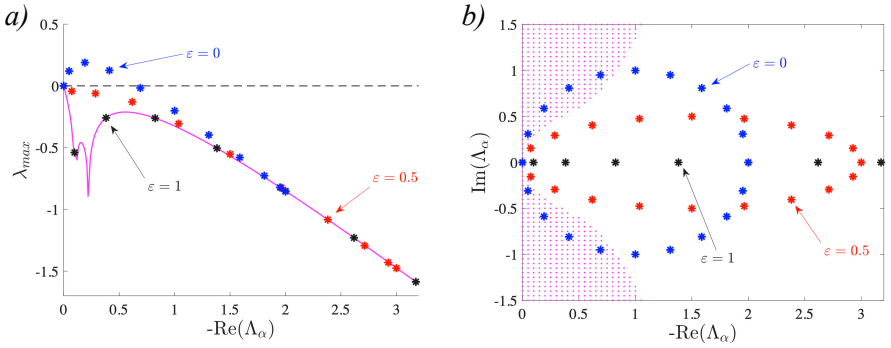

Figure 2.2: a) MSF for the Brusselator model with $b = 2.5$, $c = 1$ (limit cycle regime), $D_u = 0.7$, $D_v = 5$ on a circulant network of 20 nodes; $\Lambda^{(\alpha)}$ indicates the the Laplacian's eigenvalues, of which we plot only the real part. In this setting the system should remain stable after a perturbation: in fact, when the network is symmetric ($\varepsilon = 1$), the discrete MSF (black dots) lies on the continuous one (magenta line); however, when we introduce an asymmetry in the topology as ε decreases (red and blue dots), the MSF reaches the instability region, and the system loses synchronization. b) The equivalent representation in the complex domain where the instability region is shaded magenta and the discrete Laplacian's spectrum is denoted by the symbols. For the network topology with at least one eigenvalue that lies in the instability region, the synchronized state is lost.

operator $\mathbf{L}$. Notice that this is not always possible because the Laplacian matrix of directed networks might not have linearly independent eigenvectors. We will assume such a basis to exist for the time being, and we will consider such an issue again when discussing the non-normal case. Denoting by $\vec{\xi}$ the transformed perturbations vector, Equation (2.2.3) becomes

$$\dot{\vec{\xi}} = (\mathbb{I}_n \otimes \mathbf{J}(t) + \mathbf{\Lambda} \otimes \mathbb{D})\,\vec{\xi} \tag{2.2.4}$$

where $\mathbf{\Lambda}$ denotes the diagonal matrix of the Laplacian's eigenvalues. The largest Lya-

punov exponent of Equation (2.2.4), known in the literature as the Master Stability Function [44, 84, 41, 79], is thus a function of the eigenvalues $\mathbf{\Lambda}$. Let us stress that the study of the stability of a general non-autonomous system is normally not possible through the classical spectral analysis, and one has therefore to resort to the MSF.

Before proceeding in the quest for the optimal network topological features that minimize the MSF, we will introduce two simple network models, shown in Figure 2.1, for which we can tune the directionality and the non-normality acting on a single parameter. In the first case, Figure 2.1 a), we consider a bidirectional circulant network, i.e., a network whose adjacency matrix is circulant [98], made by two types of links, one of weight 1 forming a clockwise ring and the other winding a counterclockwise ring of tunable weights ε. The latter can vary in the interval $\varepsilon \in [0,1]$ exploring in this way the possible topologies from a fully symmetric case when $\varepsilon = 1$, to a totally mono-directed network when $\varepsilon = 0$. Since such a network is circulant, the adjacency matrix will be normal, a property that is inherited by the Laplace operator. On the contrary, if we remove two reciprocal links, respectively, of weights 1 and ε, we obtain instead a non-normal network, as depicted in Figure 2.1 b). In this case, the adjacency matrix is non-normal [77], a feature also reflected on the Laplacian matrix. Even in this case, we can tune the non-normality by varying the ε parameter in the unitary interval as for the previous case, this can be appreciated from the results shown in Figure 2.1 c) where we report the normalized Henrici index, a well-known proxy of non-normality, as a function of ε. The main advantage of using the above network models is the existence of a basis of eigenvectors for the Laplacian matrix. In the first network model, this is due to the normality of the graph Laplacian, while in the second one it is because of the tridiagonal form of the coupling operator[(1)]. This property is essential for the applicability of the MSF analysis, which otherwise requires some *caveats* [74].

2.2.1 The case of normal directed networks

We start by considering the bidirected circular network and studying the linear stability of the synchronized state using the MSF analysis. The results shown in Figure 2.2 a), indicate that the network topology increasingly contrasts the stability of the synchronous manifold when the directionality increases. In fact, when the MSF computed for the directed network is compared to the symmetric case used as reference line (the continuous magenta curve), we can always observe larger values, which moreover increase as ε decreases (for the same fixed Laplacian's eigenvalue). Because of the circulant property of the Laplace matrix, its spectrum can be explicitly computed [40] $\Lambda^{(\alpha)} = 1+\varepsilon+(1+\varepsilon)\cos(2\alpha\pi/n)+i(1-\varepsilon)\sin(2\alpha\pi/n)$. One can easily notice that, for $\varepsilon = 0$, the spectrum distributes uniformly onto the unitary circle centered at $(1,0)$ as also shown in Figure 2.2 b) in blue stars. On the other side, when $\varepsilon = 1$, the network turns symmetric, making the spectrum real. The MSF formalism ultimately relies on the maximum Lyapunov exponent, which, despite having proven its validity in ruling out the chaotic behavior of dynamical system [80], remains grounded on numerical methods. To improve our analytical understanding of the problem, we proceed by transforming Equation (2.2.4) into an autonomous one, allowing in this way to deploy

[(1)]This follows from the fact that every tridiagonal matrix is similar to a symmetric one. However, the set of eigenvectors is not the same; they are linearly independent in both cases

the spectral analysis tools. This method is part of the broader set of homogenization methods that aim at averaging a time-dependent system to obtain a time-independent one [97]. Such methods have been found useful also for the stability analysis of synchronized states [99, 46]. The resulting autonomous version of the MSF is sometimes referred to as the dispersion relation [93]. The mathematical validity of the proposed approximation is grounded on the Magnus series expansion truncated at the first order [46]; hence, the set of model parameters for which we expect a good agreement with the original model corresponds to the case when higher-order terms are negligible. For more details, the interested reader should consult [46]. In formula, it translates to

$$\mathbf{J}(t) \longrightarrow \langle \mathbf{J} \rangle_T = \frac{1}{T} \int_0^T \mathbf{J}(\tau) d\tau \tag{2.2.5}$$

Remarkably, as shown in Figure 2.3, this approximation yields qualitative results in excellent agreement with the original model for a specific range of parameters. An alternative to this approach is to apply a perturbative expansion near the bifurcation point, obtaining this way the time-independent Ginzburg-Landau normal form [100]. However, the effectiveness of the latter method is exclusively limited to parameters values very close to the stability threshold. In this sense, our approach is more general, both from allowing a larger set of parameters where the method remains valid, and at the same time, it is independent of the choice of the model compared to previous works [48]. The passage to an autonomous system is also essential in explaining the effect of the imaginary part of the Laplacian's eigenvalues in the newly obtained stability function, the dispersion relation. It has been rigorously shown in [38, 40] that the dispersion relation increases proportional to the magnitude of the imaginary part of the spectrum. We already observed similar results for the case of the MSF presented in Figure 2.2. We can in this way conclude that the averaging method sheds light on the role of the directed topology in the destabilization of a synchronized regime.

2.2.2 The case of non-normal directed networks

The analysis performed in the previous section has been based on the study of the linearized system, in some cases, however, such analysis is not sufficient to understand the outcome of the nonlinear system. In Figure 2.4 we consider again the MSF computed for the directed chain previously introduced (panel *b*) of Figure 2.1). From Figure 2.4 *b*) one might naively conclude that the system will synchronize, since the MSF is non-positive for all values of $\mathscr{R}(\Lambda^{(\alpha)})$. Moreover, the spectrum is completely real (see panel *b*)) and thus there cannot be any contribution from the imaginary part of the spectrum. However, a direct inspection of the orbit behavior (panel *c*)) clearly shows that the system does not synchronize. Once the system is defined on a symmetric support, the synchronized behavior is recovered (panel *d*)).

This diversity of behavior is related to the non-normal property of the considered network, indeed it has been recently proven that such structural property can strongly alter the asymptotic behavior of networked systems [101]. A finite perturbation about a stable equilibrium goes through a transient amplification (see Figure 2.4 *d*)) proportional to the level of non-normality before it is eventually reabsorbed in the linear approximation [77], while in the full non-linear system the finite perturbation could

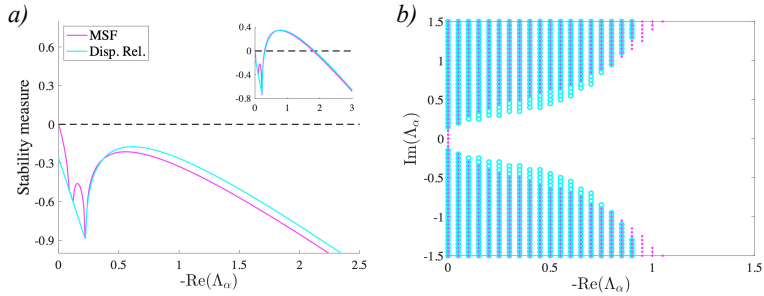

Figure 2.3: *a*) The comparison of the MSF and dispersion relation for the Brusselator with model parameters $b = 3, c = 1.8, D_u = 0.7, D_v = 5$. We depict in magenta the MSF of the system in a limit cycle regime and cyan the dispersion relation of the averaged autonomous system. Inset: Similar comparison for a set of parameters where the instability occurs. Notice also the lack of continuity of the stability interval of eigenvalues. *b*) The same representation in the complex domain. We see that for the chosen values of the parameters, the two approaches give an excellent agreement in predicting the instability interval.

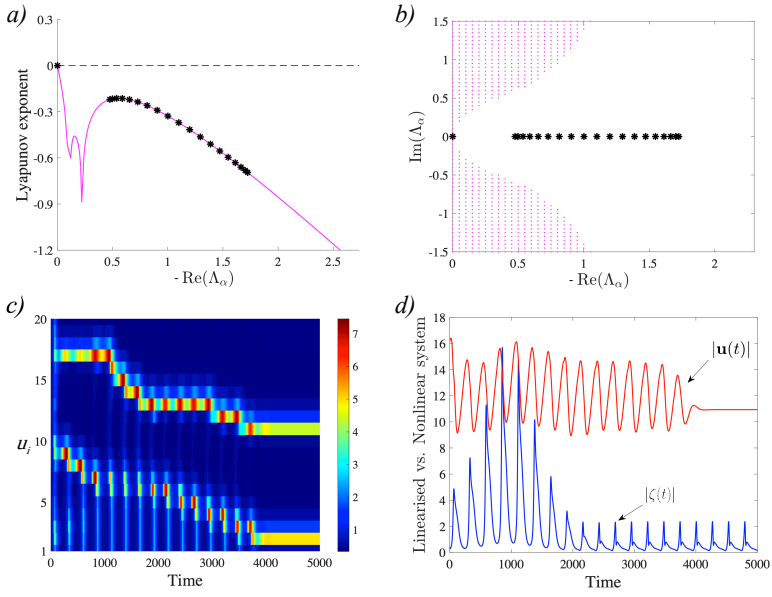

Figure 2.4: Desynchronization in a non-normal network. The parameters for the Brusselator model are as follows: $b = 2.5$, $c = 1$, $D_u = 0.7$, $D_v = 5$ on the (directed chain) non-normal network of 20 nodes with $\varepsilon = 0.1$ of Figure 2.1 *b*). As it can be observed from panels *a*) and *b*), respectively, for the MSF and the stability region, the set of parameters is such that the MSF is neatly stable. Nevertheless, the instability occurs as shown by the pattern evolution in panel *c*) at odd with the outcome that would have been expected from the symmetrized version. Such a result is strong evidence of the role of the network non-normality in the nonlinear dynamics of the system under investigation. The mechanism that drives the instability in the non-normal linearized regime manifests in the transition growth of the perturbations vector $\vec{\zeta}(t)$ eq. (2.2.3), the blue curve in panel *d*), before the system relaxes to the oscillatory state of the equilibrium. Such growth might transform in a permanent instability for the nonlinear system $\vec{u}(t) = [u(t), v(t)]$, red curve.

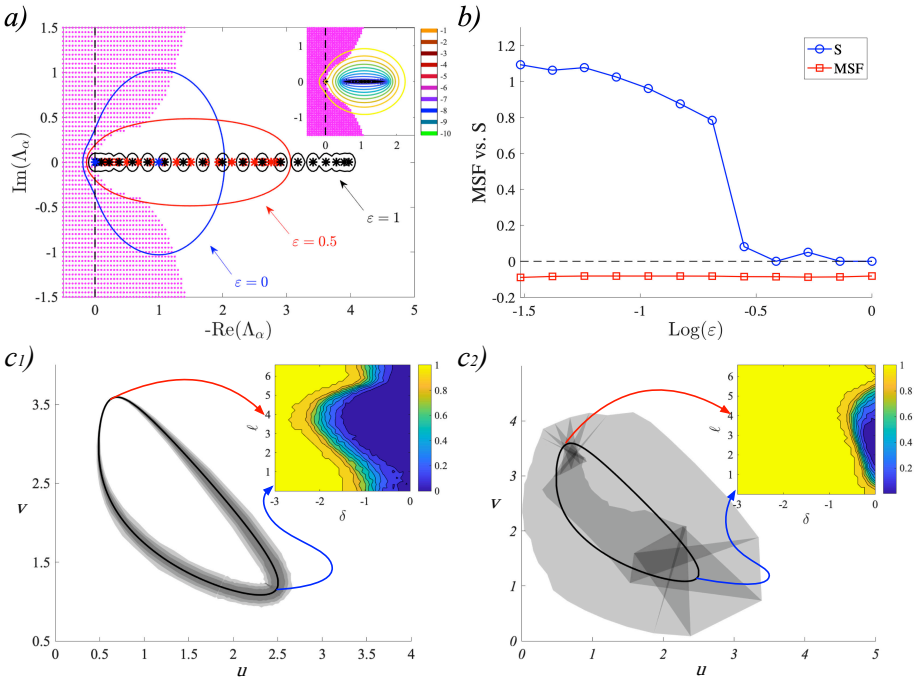

Figure 2.5: *a*) The pseudo-spectral description of the stability of the directed chain of 20 nodes for the Brusselator model with $b = 2.5$, $c = 1.12$, $D_u = 0.7$, $D_v = 5$, and an initial condition perturbation of the average magnitude $\delta = 0.1$. We show the pseudo-spectra for three different values of the control parameter ε for the chain network, emphasizing the considerably large difference between the pseudo-spectra regions and the spectrum of the Laplacian matrix. Inset: the pseudo-spectra for many other values of the perturbation magnitude δ for the chain with $\varepsilon = 0.1$. Notice that although the eigenvalues do not lie inside the instability region due to the lack of an imaginary part, the pseudo-spectra might do. *b*) The comparison between the expected outcome as predicted from the MSF and the actual outcome as measured by the standard deviation of the desynchronized pattern. The stability basin (shaded gray) projected onto the limit cycle plane for the non-normal case, panel c_1) and the symmetrized (normal) one, panel c_2), calculated over 300 different initial conditions (of the same averaged magnitude) and a perturbation whose maximum magnitude varies from 10^{-3} to 1. Inset: In the y-axis we plot the points of limit cycle we perturb and in the x-axis the magnitude of the perturbation; the colormap gives the fraction of orbits that conserve the synchronized regime. It can be clearly noticed that the attraction basin for the non-normal network is strongly reduced, though not at the same amount compared to where the perturbation occurs.

persist indefinitely. Up to now, this analysis has been limited to the case of autonomous systems; in this paper for the first time we extend it to the periodic time-dependent case making use of the homogenization process. This explains the permanent instability, shown in Figure 2.4, causing the loss of stability for the synchronized state.

The non-normal dynamics study cannot be straightforwardly tackled with the analytical methods of the local stability, mostly because the instability occurs in a highly nonlinear regime. Such condition requires a global analysis that can be obtained using the numerical technique based on a spectral perturbation concept known as the pseudo-spectrum. For a given matrix $\mathbf{A}$ the latter is defined as $\sigma(\mathbf{A}_\delta) = \sigma(\mathbf{A}+\mathbf{E})$, for all $||\mathbf{E}|| \leq \delta$ where $\sigma(\cdot)$ represents the spectrum and $||\cdot||$ a given norm. The package

EigTool [102] allows us to compute and draw in the complex plane the level curves of the pseudo-spectrum for a given value of ε. Although the pseudo-spectrum is not sufficient to fully explain the system behavior, it is certainly of great utility in estimating the role of non-normality in the dynamical outcomes. In particular, in panel b) of Figure 2.5 we report level curves of the pseudo-spectrum for three different values of the parameter ε representing the reciprocal links of the directed chain. Notice that by increasing the non-normality of the toy network, the pseudo-spectrum will also increase the chances of intersection with the instability region. In panel b) of Figure 2.5, we have shown a comparison between a proxy of the presence of a synchronized state, i.e. the standard deviation[(2)] of the asymptotic orbit behavior S and the MSF demonstrating a clear different behavior. For all the considered values of ε, the MSF is always negative suggesting a stable synchronized state, on the other hand S becomes positive and large for small enough ε, testifying a loss of synchronization. The dependence on the different values of the initial conditions is further shown in panels c_1) and c_2). As expected, the instability is more probable for both larger values of non-normality and magnitude of the initial conditions. In particular, it can be observed that the synchronization basin of attraction is strongly reduced for the non-normal network compared to the normal one, and moreover its width varies along the limit cycle, implying that desynchronization will depend also on the point at which the perturbation starts.

2.3 Conclusions

In this paper, we have studied the quest for the optimal conditions ensuring the stability of synchronization dynamics in directed networks. Such conditions determine the design of a networked system that makes the synchronization regime as robust as possible. Previous results have proven that a strictly directed topology is necessary for the synchronized state's robustness. Based on the well-known Master Stability Function, it has been shown that directed tree-like networks are optimal for models with a discontinuous interval of the Laplacian's spectrum in the stability range of MSF. Here, we have extended such results proving that they are generally independent of the dynamic model. Using an averaging procedure, we transformed the problem from a time-dependent (non-autonomous) to a time-invariant (autonomous) one. This method allows to prove that networks whose Laplacian matrix exhibits a spectrum that lacks an imaginary part are the most optimal. In general, the loss of synchronization increases with the magnitude of the imaginary part of the spectrum. Secondly, recent findings have shown that real-world networks present strong directed traits, resulting in a strong non-normality. This latter feature can play a very important role in the linear dynamics influencing the local stability of the synchronized state through a strong transient amplification of the perturbations. We have extended the idea of non-normal dynamics to the case of non-autonomous synchronization dynamics, revealing how network non-normality can drive the system to instability, thus increasing the understanding of

[(2)]For a given species, e.g., u, the standard deviation at a given time t is $S(t) = \sqrt{\frac{1}{n-1}\sum_{i=1}^{n}(u_i(t) - \hat{u}(t))^2}$, where n is the number of nodes and $\hat{u}(t) = \frac{1}{n}\sum_{i=1}^{n} u_i(t)$. We can observe that such quantity is 0 if the system is synchronized, i.e., $u_i(t) = \hat{u}(t)\ \forall t$, while a value different from 0 indicates that not every node has the same concentration at any given time.

synchronization in complex networks. We have also numerically quantified the effect of non-normality in driving the instability through the pseudo-spectrum technique. In conclusion, we have analytically and numerically demonstrated that there is no compelling recipe for optimal network architecture in order to conserve the synchronized state, but rather a trade-off between the network directedness and its non-normality. We are aware that the interesting outcomes of the interaction of structural non-normality networks with the fascinating synchronization phenomenon require deeper and further investigation (e.g. synchronization basin). In this sense, with this work we aim to initiate a new direction of research of the synchronization problem.

2.4 SM 1: Another example of non-normal network

In this Section, we extend our results of the main text to a family of random networks with a tunable level of non-normality and systematically study the loss of synchronization in relation to the control parameter. We initially start with an (unweighted) directed Erdős-Rényi random graph [103] with a fixed number of nodes N and a probability p_0 of having a directed edge from node i to node j. Notice that such Erdős-Rényi networks, being directed, will be automatically non-normal, and their non-normality will depend on the density of the edges and the eventual hierarchy of the network structure [39]. Our primary step for generating random networks with tunable non-normality is to increase the network directionality, more precisely we remove entries form the lower triangular part of the adjacency matrix; this corresponds to the removal of links at random with probability p. The latter will be our control parameter. As can be observed from Figure 2.6, panel a), the non-normality of the network, measured with the normalized Henrici index, monotonically increases for increasing values of the control parameter p.

To emphasize the consequence of the increasing non-normality in the stability of the synchronized regime, we systematically investigate the behavior of the system of coupled Brusselator oscillators[(3)]. As shown in Figure 2.6, the fraction of simulations for which the system does not synchronize when the random network becomes more non-normal increases (red curve), compared to the symmetrized counterpart (green curve) where synchronization is always achieved. This is thus the same qualitative result and prediction presented in the main text for the two simple networks. Furthermore, for values of the control parameter $p \gtrsim 0.75$, the networks' Laplace spectrum becomes degenerate, and the Master Stability Function approach cannot be used in its simplified form due to the lack of an eigenvector basis. Nevertheless, the fraction of cases where the system desynchronizes keeps increasing as in the case of non-degenerate spectra.

As a conclusion, we can state that the results we have shown in this paper are valid more generally, beyond the model used for the generation of the synthetic networks and directly related to the amount of the non-normality of the underlying networked structure.

[(3)] Notice that the set of parameters, in this case, is far from the region where the averaging method presented in the main text is valid.

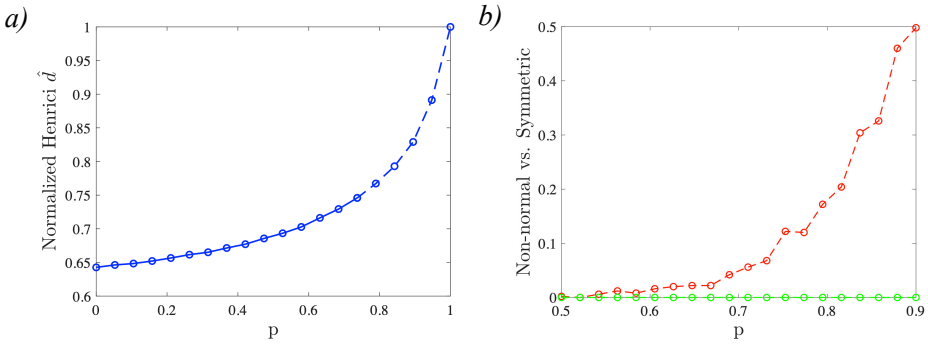

Figure 2.6: *a*) The normalized Henrici departure from non-normality $\hat{d}$ vs. the control parameter p averaged over 500 independent realizations of networks generated with the algorithm described in the text for 50 nodes, and $p_0 = 0.2$. We can observe that the non-normality of the ensemble of networks increases with the control parameter. For a given threshold of the control parameter p, the networks become degenerate (depicted in dashed line). *b*) The fraction of the outcomes of integrating the Brusselator model when the synchronization is lost averaged over 500 different initial conditions (red curve). The parameters are $b = 5$, $c = 1.6$, $D_u = 0.6$ and $D_v = 4.5$, and the networks generated as in the left panel. For comparison, we have also shown the outcomes of the symmetrized network (green curve), where the synchronization is conserved in any case.

2.5 On the basin of attraction and non-normality

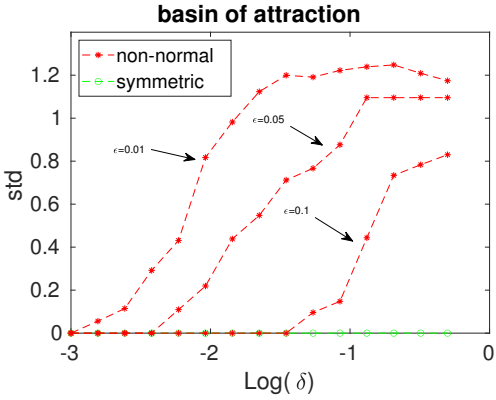

Figure 2.7: Attraction basin of the homogeneous (synchronous) state as a function of the perturbation δ for different non-normal networks. We use the standard deviation (std) as a proxy for synchronization, i.e., when std$= 0$ the system is synchronized. We can see that, while on a symmetric network (green dots) we always achieve synchronization (i.e., the attraction basin of the homogeneous state is large), on a non-normal network, finite perturbations destroy the synchronized state, meaning that the attraction basin has shrunk. Moreover, we can observe that such shrinking increases with the non-normality, given by the parameter ϵ (the smaller the parameter, the larger the non-normality). The networks are as in Figure 2.1b and the model parameters as in Figure 2.5.

This section was not part of the original paper, but was added to further discuss the relation between non-normality and the shrinking of the attraction basin.

In the above Chapter, we conducted a numerical study proving that the homogeneous (synchronous) state of a system is significantly weakened, i.e., its attraction basin is strongly reduced, by increasing the non-normality of the network, consistently with previous results [39, 70, 87, 91]. Nonetheless, there are many open questions, especially regarding the basin of attraction and its relation with the non-normality. Some of the cited works, such as [70, 75], included a part concerning the attraction basin, showing that it shrinks when the network is non-normal. In the above Chapter, we also discuss such property in Figure 2.5. We hereby add a supplementary Figure 2.7, to better explain our results. From the latter figure, we can clearly appreciate that the basin of attraction shrinks as the non-normality of the network increases. All the cited results are universal with respect to the considered model (as long as they admit a homogeneous stable state), but they are restricted to particular choice of non-normal network. Except for directed star-network, for which it is obvious that the attraction basin does not shrink, we do not have a general theory relating some non-normality measure with the robustness of the attraction basin. Hence, it would be compelling to conduct a comprehensive study of the attraction basins for different kinds of non-normal networks, of the kind that has been carried out in [104] for symmetric networks, comparing different network features with the minimal perturbation capable of driving the system away from the equilibrium.
Unrelated to the attraction basin issue, another interesting study which could be conducted is to relate the non-normality of the network to the synchronizability properties of Kuramoto oscillators. The formalism behind the study of synchronization in the Kuramoto model is different from the one above, mainly because in general there is no homogeneous state (the oscillators not being identical), hence we would not have a shrinking of the attraction basin of the synchronized state. Nonetheless, it would be instructive to vary the non-normality of a network of Kuramoto oscillators as the one in Figure 2.1b and observe the effect on their synchronization. One important *caveat* would concern the coupling strength: in fact, in the Kuramoto model, the coupling strength is crucial in the phase-transition from asynchrony to synchrony and, when varying the non-normality by lowering the strength of the return links as in Figure 2.1b, we would lower the global coupling strength.

Chapter 3

Finite propagation enhances Turing patterns in reaction–diffusion networked systems

The classic diffusion equation relies on the assumption of infinite propagation of the signal, which works very well only for small domains. Following the analysis of Cattaneo [105], reaction-diffusion equations subject to an upper bound on the propagation become hyperbolic, i.e., there is a second time derivative term accounting for the relaxation time, adding in the picture a coefficient representing the inertia in the propagation. Since the Turing mechanism has been applied also in the case of large domains, e.g., in ecosystems [106], it would be interesting to study which are the effects of imposing an upper bound to the propagation. Of course, we were not the first ones to ask this question and the aforementioned problem was studied on continuous support for the case of equal inertial times for both species [16].

Hence, we started by studying the case for different inertial times and by realizing that the networked structure allowed for different interpretations of the patterns. First of all, the classical Turing region shrinks due to the inertial times, responsible of disrupting the homogeneous stable state, which becomes an inhomogeneous oscillatory solution. This happens also in the case of equal inertial time, but on continuous support it is more difficult to notice, as every oscillatory aspatial solution is called Hopf instability. However, we have seen that on networks there exist homogeneous oscillatory solutions, i.e., when all units oscillate with same frequency and phase about a limit cycle. This case is different, because the state is inhomogeneous even before a spatially inhomogeneous perturbation, hence it is not a Turing-like instability. Moreover, we noticed that, when the support is a network, the classical distinction between Turing and wave instability becomes inadequate as we may have oscillatory patterns even with unstable

modes without imaginary part and also the opposite case where stationary patterns are found while conditions would suggest oscillations. Until now, the prediction of patterns remains an open question. In fact, we cannot know *a priori* whether a pattern will be stationary or oscillatory from a linear stability analysis, but we need to resort to numerical simulations.

T. Carletti & R. Muolo. Journal of Physics: Complexity 2 (4), 045004 (2021) [49]
This article is open access.

Abstract

We hereby develop the theory of Turing instability for reaction-diffusion systems defined on complex networks assuming finite propagation. Extending to networked systems the framework introduced by Cattaneo in the 40's, we remove the unphysical assumption of infinite propagation velocity holding for reaction-diffusion systems, thus allowing to propose a novel view on the fine tuning issue and on existing experiments. We analytically prove that Turing instability, stationary or wave-like, emerges for a much broader set of conditions, e.g., once the activator diffuses faster than the inhibitor or even in the case of inhibitor-inhibitor systems, overcoming thus the classical Turing framework. Analytical results are compared to direct simulations made on the FitzHugh-Nagumo model, extended to the relativistic reaction-diffusion framework with a complex network as substrate for the dynamics.

3.1 Introduction

A blossoming of regular spatio-temporal patterns can be observed in nature. These are the signature of self-organized processes where ordered structures emerge from disordered ones [107, 108]. Very often, the interaction among the microscopic units, by which the system is made of, can be modeled by means of reaction-diffusion equations that describe the deterministic evolution of the concentrations both in time and space, the latter being a regular substrate [108] or a discrete one, e.g., a complex network [109]. Spatially homogeneous equilibria of a reaction-diffusion system may undergo a symmetry breaking instability, when subjected to a heterogeneous perturbation, eventually driving the system toward a patchy, i.e., spatially heterogeneous, stationary or oscillatory solution, as firstly explained by Alan Turing [4] in the 50's and corroborated experimentally almost four decades later [6, 7, 110]. Nowadays, applications of the Turing instability phenomenon go well beyond the original framework of the morphogenesis or chemical reaction systems and it stands for a pillar to explain self-organization in nature [111, 29, 112]. The conditions for the emergence of Turing patterns have been elegantly grounded on the interplay between slow diffusing activators and fast diffusing inhibitors [5]; indeed this determines a local feedback, short range production of

a given species, which should be, at the same time, inhibited at long ranges. Starting from these premises, scholars have been able to extend the original Turing mechanism to non-autonomous systems, e.g., evolving domains [113, 33] or time dependent diffusion and reaction rates [114], as well as discrete substrates, e.g., lattices [26] or complex networks [31], and their generalization, e.g., directed networks [38], multiplex networks [34] and recently to time varying networks [115, 116]. The interested reader can consult the recent review [12] for a modern perspective on Turing instability.

As previously observed, at the root of Turing instability there is a reaction-diffusion process which is thus grounded on a (nonlinear) "heat equation", namely a parabolic partial differential equation (PDE) with a nonlinear source term. The latter PDE is characterized by an infinite fast propagation of the initial datum along the supporting medium and, thus, it can accurately model the physical phenomenon only in cases of very large diffusivity, $D \gg 1$. To overcome this drawback, scholars have considered more realistic frameworks. In particular Cattaneo proposed in 1948 to modify the constitutive equation (Fick's first law) by including a relaxation term with some given characteristic inertial time, $\tau > 0$. Operating in this framework, Fick's second law returns a modified diffusion equation allowing also for a second derivative with respect to time [105, 117, 118, 119]. The resulting equation is nowadays known in the literature as the Cattaneo equation as well as the telegraph equation, the damped nonlinear Klein-Gordon equations or the relativistic heat equation, depending on the research field and on the feature one is interested to emphasize [120]. In any case, its main characteristic is to exhibit a finite propagation velocity, $V = \sqrt{D/\tau}$, and moreover in the limit of arbitrarily small relaxation time, $\tau \to 0$, one recovers Fick's second law and thus a parabolic reaction-diffusion model with an infinite propagation velocity. Our focus being the role of the finite propagation, we will hereby name such framework finite-velocity as done in [121] or sometimes *relativistic heat equation* although no Lorentz phenomena are at play, to recall the existence of a maximal allowed velocity as for the speed of light in relativity theory; we thus operated a different choice with respect to [16, 21], where the name "hyperbolic reaction-diffusion equations" has been preferred.

The aim of this paper is to study the conditions for the onset of Turing instability, being them stationary or oscillatory patterns, for a reaction-diffusion system defined on top of a *complex network* and modified according to the *Cattaneo recipe*, to allow for a finite propagation velocity (Section 3.1). We thus consider two different species populating a network composed by n nodes. When species happen to share the same node, they interact via nonlinear functions $f(u_i, v_i)$ and $g(u_i, v_i)$, being u_i and v_i the species concentrations at the i-th node. On the other hand, they can diffuse across the available network links. The local currents, i.e., associated to each links, are assumed to satisfy a modified constitutive equation, Fick's first law, that includes a relaxation term with a given *inertial time*. Hence, the continuity equation, Fick's second law, allows to derive a modified local diffusion term, i.e., defined on the node. The latter, together with the reaction part, determines the hyperbolic reaction-diffusion system defined on top of a complex network, we will hereby be interested in.

Our work extends to the network case, the study presented in [16], realized under the simplifying hypothesis of equal inertial times for the two species, namely $\tau_u = \tau_v$, and assuming a continuous substrate. Indeed, we hereby assume generic inertial times for each species, $\tau_u \neq \tau_v$. Let observe that our results established for a discrete sub-

strate, can be straightforwardly extended to the continuous case and thus they complete the work done in [16] to allow for different inertial times. This setting has been recently studied in [21] in the framework of hyperbolic reaction-diffusion models with cross-diffusion defined on a continuous substrate. Differently from our approach of directly adapting the Cattaneo idea to the current flowing on each network link, the authors of [21] have used Extended Thermodynamics [122]; the resulting characteristic polynomial (see below) we obtained is different from the one given in [21] and it allows us to draw several interesting conclusions.

The Turing mechanism relies on the assumption of the existence of a stable homogeneous equilibrium that looses its stability once subjected to spatially heterogeneous perturbations, in presence of a diffusive term; for this reason, such process is also known as *diffusion-driven instability*. The system can then exhibit stationary spatially heterogeneous solutions as well as time oscillatory ones. The same mechanism can be proven to hold true in the new proposed framework of the hyperbolic reaction-diffusion systems defined on top of a complex network (Section 3.1). The dispersion relation, which ultimately signals the onset of the instability, is a function of the discrete spectrum of the Laplace matrix, namely the diffusion operator associated to the underlying network. Let us mention that cross-diffusion is excluded. The dispersion relation is obtained from the roots of the fourth order characteristic polynomial. To progress with the analytical understanding of the problem, we resort to the Routh-Hurwitz stability criterion [123, 124, 125], allowing to prove the (in)stability feature of a real coefficients polynomial. Let us observe that this criterion is a widely used tool in dynamical systems and control theory (see, e.g., [119]).

We have shown that the use of the inertial times strongly enlarges the parameter region for which Turing instability and Turing-waves can emerge, even beyond the classical Turing conditions of fast inhibitor and slow activator. For generic values of the inertial times, $\tau_u \neq \tau_v$, we have proven that Turing patterns can set up with a *fast activator* and *slow inhibitor*, with species exhibiting the *same diffusion coefficients* and even with an *inhibitor-inhibitor* system. As in these cases classical Turing instability cannot develop and being the latter solely due to the presence of the inertial times, we propose to call them *inertia-driven instability*, that can result into stationary or wave-like phenomena. Of course, the proposed framework allows to prove the existence of Turing instability also for an inhibitor diffusing faster than the activator, as for the non-relativistic framework.

In the particular case where both species have the same inertial time, we have shown that the stability of the homogeneous solution is conditional to the inertial time; indeed there exists a threshold, $\tau_{\max}$, beyond which the homogeneous equilibrium turns out to be unstable. The system exhibits thus patterns but they cannot be associated to Turing instability, even if they are indistinguishable from the latter. Moreover, the threshold $\tau_{\max}$ depends on the model parameters and there are combinations of the latter for which it is arbitrary large; stated differently, for such parameters the homogeneous equilibrium is always stable (with respect to the inertial time).

The theoretical framework hereby proposed has been complemented with a dedicated numerical analysis of the FitzHugh-Nagumo model [126, 127, 128] (see Section 3.4), that is a nonlinear system often used as paradigm for the study of the emergence of Turing patterns [129, 130, 131, 132] as well as for synchronization phenom-

ena [133, 134]. The FitzHugh-Nagumo model has thus been extended to the framework of hyperbolic reaction-diffusion networked systems. We have numerically found stationary patterns as well as synchronized oscillatory ones. We have also found new interesting solutions for which the dispersion relation has limited predictive power; indeed, we showed the existence of two sets of model parameters associated to similar dispersion relations, for which the unstable modes have a nontrivial complex component, but in one case the solution oscillates in time whereas in the second it converges to a stationary pattern.

The proposed framework tackles thus the issue of infinite propagation velocity for networked reaction-diffusion systems, and it is general enough to account for novel interesting results, strengthening the importance of self-organization in nonlinear networked system. In particular the possibility to prove the emergence of Turing patterns, the latter being stationary or wave-like, in the case of activator diffusing faster than the inhibitor but also in the case of inhibitor-inhibitor systems, could provide new insights into the fine tuning problem [135, 12] and propose a novel view on experimental results.

3.2 Reaction-diffusion system with finite propagation on networks

The aim of this section is to extend Cattaneo's idea to a discrete substrate, i.e., to deal with a networked system. We will briefly show how to modify networked reaction-diffusion systems in order to allow for a finite velocity of propagation.

Let us thus consider a network made of n nodes and connected by a collection of m undirected links allowing for pairwise exchanges among nodes. Such structure can be encoded into the $n \times m$ *incidence matrix*, $\mathbf{B}$. Let $e = (i, j)$ be the link connecting nodes i and j, then $B_{ie} = -1$, $B_{je} = 1$ and $B_{\ell e} = 0$ for all $\ell \neq i, j$. From this matrix we can build the *Laplace matrix*, $\mathbf{L} = -\mathbf{B}\mathbf{B}^\top$, where $^\top$ denotes the matrix transpose[1]. The *Laplace matrix* is symmetric by construction and thus it admits a set of orthonormal eigenvectors, $\vec{\varphi}^{(\alpha)}$, and real non-positive[2] eigenvalues $\Lambda^{(\alpha)}$, for $\alpha = 1, \ldots, n$. By construction $\sum_j L_{ij} = 0$, hence the largest eigenvalue is $\Lambda^{(1)} = 0$ associated to the eigenvector $\vec{\varphi}^{(1)} = (1, \ldots, 1)^\top / \sqrt{n}$. The diagonal element $-L_{ii}$ defines the nodes degree, say k_i, namely the number of incidents links of the i-th node; hence we can rewrite $\mathbf{L} = \mathbf{A} - \mathbf{D}$, where $\mathbf{D} = \mathrm{diag}(k_1, \ldots, k_n)$ and $\mathbf{A}$ is the *adjacency matrix*, that is $A_{ij} = 1$ if and only if nodes i and j are connected, encoding thus the coupling network.

Let us now focus on the diffusion of a single species in the network, the generalization to more species being a direct extension. Let $\vec{u}(t) = (u_1(t), \ldots, u_n(t))^\top$ denote the state of the system at time t, where $u_i(t)$ is the density of the species in node i at time t. Let $e = (i, j)$ be a link in the network and let $\chi_e(t)$ be the current flowing through it at time t; then, borrowing the constitutive equation, namely Fick's first law, from the

[1] The definition of $\mathbf{B}$, and hence of $\mathbf{L}$ varies. For example, in [86] the incidence matrix is $n \times m$, hence $\mathbf{L} = -\mathbf{B}^\top\mathbf{B}$.

[2] The matrix $\mathbf{L}$ is negative-semidefinite. Indeed let $\vec{\varphi}^{(\alpha)}$ be any orthonormal eigenvector, then $(\vec{\varphi}^{(\alpha)}, \mathbf{L}\vec{\varphi}^{(\alpha)}) = \Lambda^{(\alpha)}$ and at the same time $(\vec{\varphi}^{(\alpha)}, \mathbf{L}\vec{\varphi}^{(\alpha)}) = -(\vec{\varphi}^{(\alpha)}, \mathbf{B}\mathbf{B}^\top\vec{\varphi}^{(\alpha)}) = -(\mathbf{B}^\top\vec{\varphi}^{(\alpha)}, \mathbf{B}^\top\vec{\varphi}^{(\alpha)}) = -||\mathbf{B}^\top\vec{\varphi}^{(\alpha)}||^2 \leq 0$.

continuous framework, we can state that

$$\chi_e(t) = -D_u \left[u_j(t) - u_i(t)\right] \equiv D_u \left[\mathbf{B}^\top \vec{u}(t)\right]_e \tag{3.2.1}$$

that is, the current is proportional to the difference of the densities in the nodes forming the link and flowing from higher concentrations to lower ones[(3)], being D_u the diffusion coefficient of species u. By defining the currents vector $\vec{\chi} = (\chi_{e_1}, \ldots, \chi_{e_m})^\top$, the continuity equation can be written as

$$\dot{u}_i(t) = -\left[\mathbf{B}\vec{\chi}(t)\right]_i \tag{3.2.2}$$

namely the variation of u_i is proportional to the sum of the currents entering and exiting from node i. The classical Fick's second law follows by combining the above equations

$$\dot{\vec{u}}(t) = -\mathbf{B}\vec{\chi} = -D_u \mathbf{B}\mathbf{B}^\top \vec{u} = D_u \mathbf{L}\vec{u} \tag{3.2.3}$$

where we can realize [26, 31] that $\mathbf{L}$ replaces the second order differential operator used in the continuous substrate case and thus the model given by (3.2.3) exhibits infinite propagation velocity.
To overcome this problem we modify, as Cattaneo did, the constitutive equation (3.2.1) by introducing a relaxation factor with some characteristic inertial time $\tau_u > 0$, namely

$$\chi_e(t) + \tau_u \dot{\chi}_e(t) = D_u \left[\mathbf{B}^\top \vec{u}(t)\right]_e \tag{3.2.4}$$

Combining this equation with the continuity equation (3.2.2) allows us to obtain

$$\begin{aligned} \dot{\vec{u}}(t) &= -\mathbf{B}\vec{\chi} = -\mathbf{B}\left[-\tau_u \dot{\vec{\chi}} + D_u \mathbf{B}^\top \vec{u}(t)\right] = \tau_u \mathbf{B}\dot{\vec{\chi}} - D_u \mathbf{B}\mathbf{B}^\top \vec{u}(t) \\ &= -\tau_u \ddot{\vec{u}} + D_u \mathbf{L}\vec{u}(t) \end{aligned} \tag{3.2.5}$$

eventually providing the generalized Cattaneo equation defined on networks

$$\dot{\vec{u}}(t) + \tau_u \ddot{\vec{u}}(t) = D_u \mathbf{L}\vec{u}(t) \tag{3.2.6}$$

The latter can be seen as a modification of the "heat equation" defined on network by the inclusion of a second order time derivative, returning thus a relativistic or hyperbolic heat equation.

Consider now two different species populating a network composed by n nodes and let us denote by u_i and v_i, $i = 1, \ldots, n$, their respective concentrations on node i. When species happen to share the same node, they interact via nonlinear functions $f(u_i, v_i)$ and $g(u_i, v_i)$. On the other hand, they can diffuse across the available network

[(3)] Let us observe that, despite the different sign in front of Equation (3.2.1), the latter is the analogous of Fick's first law in the continuous setting: the current flows from regions of higher concentration to regions of lower one. Indeed, once we fix the link "ordering" as $e = (i, j)$, then the current χ_e will be positive, i.e., respecting the link ordering if $u_i > u_j$, while the current will be negative, i.e., opposite to the link order if $u_i < u_j$.

links accordingly to the modified Cattaneo equation (3.2.6). The model can hence be mathematically expressed in the form

$$\begin{cases} \dot{u}_i + \tau_u \ddot{u}_i &= f(u_i, v_i) + D_u \sum_{j=1}^{n} L_{ij} u_j \\ & \qquad \forall i = 1, \dots, n \\ \dot{v}_i + \tau_v \ddot{v}_i &= g(u_i, v_i) + D_v \sum_{j=1}^{n} L_{ij} v_j \end{cases} \tag{3.2.7}$$

where $D_u > 0$ (resp. $D_v > 0$) is the diffusion coefficients of species u (resp. v) and $\tau_u > 0$ (resp. $\tau_v > 0$) the inertial time for species u (resp. v).

3.3 Turing instability in networked reaction-diffusion systems with finite propagation

The Turing mechanism is the result of a diffusion-driven instability, namely a homogeneous stable equilibrium of the reaction-diffusion system turns out to be unstable, with respect to inhomogeneous spatial perturbations, once the diffusion is at play. The aim of this section is to determine the conditions for such instability to develop in the relativistic, i.e., in presence of a maximal allowed velocity, reaction-diffusion systems defined on networks given by Equation (3.2.7).

Let us hence assume there exists a homogeneous solution of (3.2.7), that is $u_i(t) = u^*$ and $v_i(t) = v^*$ for all $i = 1, \dots, n$ and $t > 0$. Namely u^* and v^* should satisfy $f(u^*, v^*) = g(u^*, v^*) = 0$. Being the latter equilibrium solely determined by the reaction terms, it happens to be also an equilibrium for the non-relativistic system. Let us denote by $\delta u_i(t) = u_i(t) - u^*$ and $\delta v_i(t) = v_i(t) - v^*$ the perturbations from the homogeneous solution. In order to determine the time evolution of the latter, we use (3.2.7), keeping only the first order terms in the perturbation (the latter assumed to be small). We thus obtain

$$\begin{cases} \delta\dot{u}_i + \tau_u \delta\ddot{u}_i &= f_u \delta u_i + f_v \delta v_i + D_u \sum_{j=1}^{n} L_{ij} \delta u_j \\ & \qquad \forall i = 1, \dots, n \\ \delta\dot{v}_i + \tau_v \delta\ddot{v}_i &= g_u \delta u_i + g_v \delta v_i + D_v \sum_{j=1}^{n} L_{ij} \delta v_j \end{cases} \tag{3.3.1}$$

where we employed the fact that $\sum_j L_{ij} = 0$ to nullify the terms $\sum_j L_{ij} u^*$ and $\sum_j L_{ij} v^*$. Let us also stress that throughout the rest of the section the partial derivatives, i.e., $f_u \equiv \partial f / \partial u$ and similarly for the other ones, are evaluated at the homogeneous equilibrium (u^*, v^*).

To progress with the analytical understanding, we develop the perturbations on the eigenbasis of the Laplace matrix $\delta u_i(t) = \sum_\alpha \hat{u}_\alpha(t) \varphi_i^{(\alpha)}$ and $\delta v_i(t) = \sum_\alpha \hat{v}_\alpha(t) \varphi_i^{(\alpha)}$. Inserting the latter into Equation (3.3.1), we obtain the equation describing the evolution

of the modes $\hat{u}_\alpha(t)$ and $\hat{v}_\alpha(t)$

$$\begin{cases} \dfrac{d\hat{u}_\alpha}{dt}(t) + \tau_u \dfrac{d^2\hat{u}_\alpha}{dt^2}(t) &= f_u\hat{u}_\alpha(t) + f_v\hat{v}_\alpha(t) + D_u\Lambda^{(\alpha)}\hat{u}_\alpha(t) \\ & \qquad\qquad \forall i = 1,\dots,n \\ \dfrac{d\hat{v}_\alpha}{dt}(t) + \tau_v \dfrac{d^2\hat{v}_\alpha}{dt^2}(t) &= g_u\hat{u}_\alpha(t) + g_v\hat{v}_\alpha(t) + D_v\Lambda^{(\alpha)}\hat{v}_\alpha(t) \end{cases}$$

namely, we end up with n linear 2×2 systems instead of the initial $2n\times 2n$ one. We further hypothesize $\hat{u}_\alpha(t) \sim e^{\lambda_\alpha t}$ and $\hat{v}_\alpha(t) \sim e^{\lambda_\alpha t}$, and, to ensure the existence of a nontrivial solution, we eventually obtain that the linear growth rate λ_α should solve

$$\det \begin{pmatrix} \lambda_\alpha + \tau_u\lambda_\alpha^2 - f_u - \Lambda^{(\alpha)}D_u & -f_v \\ -g_u & \lambda_\alpha + \tau_v\lambda_\alpha^2 - g_v - \Lambda^{(\alpha)}D_v \end{pmatrix} = 0 \Leftrightarrow p_\alpha(\Lambda^{(\alpha)}) = 0 \tag{3.3.2}$$

where the fourth degree characteristic polynomial is defined by

$$p_\alpha(\lambda) = a\lambda^4 + b\lambda^3 + c_\alpha\lambda^2 + d_\alpha\lambda + e_\alpha \tag{3.3.3}$$

whose coefficients are given by

$$a = \tau_u\tau_v \quad , \quad b = (\tau_u + \tau_v) \tag{3.3.4}$$

$$c_\alpha = 1 - \tau_u g_v - \tau_v f_u - \Lambda^{(\alpha)}(\tau_u D_v + \tau_v D_u) \tag{3.3.5}$$

$$d_\alpha = -\mathrm{tr}(J_0) - \Lambda^{(\alpha)}(D_v + D_u) \tag{3.3.6}$$

$$e_\alpha = \det(J_0) + (D_v f_u + D_u g_v)\Lambda^{(\alpha)} + D_u D_v \left(\Lambda^{(\alpha)}\right)^2 \tag{3.3.7}$$

being $J_0 = \left(\begin{smallmatrix} f_u & f_v \\ g_u & g_v \end{smallmatrix}\right)$ the Jacobian of the sole reaction system without diffusive coupling, hence also named aspatial system, evaluated at the homogeneous equilibrium (u^*, v^*), $\mathrm{tr}(J_0) = f_u + g_v$ its trace and $\det(J_0) = f_u g_v - f_v g_u$ its determinant. The coefficients a and b are positive and do not depend on the index α.

Turing instability arises if the homogeneous equilibrium (u^*, v^*) is stable, namely if the four roots of the polynomial $p_1(\lambda)$ all have negative real part[(4)], while there exists at least one $\alpha > 1$ for which the polynomial $p_\alpha(\lambda)$ does admit at least one root with positive real part. The root with the largest real part seen as a function of $\Lambda^{(\alpha)}$ is called in the literature the *dispersion relation*, $\lambda_\alpha := \max_{i=1,\dots,4} \mathscr{R}\lambda_i(\Lambda^{(\alpha)})$. Turing instability is thus equivalent to require $\lambda_1 < 0$ and $\lambda_\alpha > 0$ for some $\alpha > 1$, hereby called critical roots. Indeed, because of the ansatz $\hat{u}_\alpha(t) \sim e^{\lambda_\alpha t}$ and $\hat{v}_\alpha(t) \sim e^{\lambda_\alpha t}$, the former implies an initial exponential divergence from the homogeneous equilibrium. In the following we will also use information about the imaginary part of λ_α, we thus define $\rho_\alpha := \max_{i=1,\dots,4}\{\mathscr{I}\lambda_i(\Lambda^{(\alpha)}) : \lambda_\alpha > 0\}$, i.e., the largest imaginary part of the critical roots. In case that the imaginary part of the critical root is non-zero, $\rho_\alpha \neq 0$, we are in presence of a Turing-wave instability, and the perturbation initially exhibits a combination of exponential growth and oscillating behavior. Eventually the nonlinearities of the model determine the final pattern, that could result to be stationary or wave-like one.

[(4)] Inspecting Equation (3.3.2) it is clear that the $\Lambda^{(1)} = 0$ eigenvalue represents the behavior of the aspatial system.

To prove the existence of Turing instability for the system (3.2.7) we shall rely on the Routh-Hurwitz criterion [123, 124, 125], providing necessary and sufficient conditions to prove that p_1 is stable[(5)] while p_α is unstable for some $\alpha > 1$

Remark (*Connection with the relativistic reaction-diffusion system defined on a continuous substrate*) As already remarked, the Laplace matrix $\mathbf{L}$ in Equation (3.2.7) takes the place of the second order differential operator $\nabla^2 = \sum_i \partial^2_{x_i}$. After linearizing the resulting PDE system about the homogeneous equilibrium, the use of the periodic boundary conditions and the Fourier series is equivalent to project the linear system onto the eigenfunctions of ∇^2, that is e^{ikx} (for $k \in \mathbb{Z}$, in the case of a 1 dimensional spatial domain), whose eigenvalues are $-k^2$. Proceeding in this way, one can determine a polynomial similar to the one given in (3.3.3), where we have to replace $\Lambda^{(\alpha)}$ by $-k^2$. However, let us observe that now the spectrum of $\mathbf{L}$ is discrete and thus the dispersion relation for the networked system will be "sampled" from the one holding in the continuous case (see red dots on the blue curves in the following figures representing the dispersion relations). This may introduce finite size effects, as the continuous support case is capable to exhibit Turing patterns, while the networked one cannot because the Laplace spectrum has a gap that exactly avoids the region of positive dispersion relation. To control for this phenomenon, one should be able to relate topological features of the network to the Laplace spectrum [136, 137].

3.3.1 Conditions for the stability of p_1

The aim of this section is to introduce the conditions for the linear stability of the homogeneous solution of (3.2.7). As already noticed, the coefficients $a = \tau_u \tau_v$ and $b = \tau_u + \tau_v$ are positive, hence the necessary and sufficient conditions (see SM 3.6) to ensure the stability of p_1 are given by:

$$1 - \tau_u g_v - \tau_v f_u > 0 \tag{3.3.8}$$

$$\mathrm{tr}(J_0) = f_u + g_v < 0 \tag{3.3.9}$$

$$\det(J_0) = f_u g_v - f_v g_u > 0 \tag{3.3.10}$$

$$(\tau_u + \tau_v)(1 - \tau_u g_v - \tau_v f_u) + \tau_u \tau_v \mathrm{tr}(J_0) > 0 \tag{3.3.11}$$

$$-\mathrm{tr}(J_0)\left[(\tau_u + \tau_v)(1 - \tau_u g_v - \tau_v f_u) + \tau_u \tau_v \mathrm{tr}(J_0)\right] + -(\tau_u + \tau_v)^2 \det(J_0) > 0 \tag{3.3.12}$$

Before proceeding with the analysis in the general setting, let us consider a special but relevant case, namely $\tau_u = \tau_v = \tau$. Assuming Equation (3.3.9) to hold true, then Equations (3.3.8) and (3.3.11) easily follow. Moreover, if $4\det(J_0) < (\mathrm{tr}(J_0))^2$, then Equation
(3.3.12) is always satisfied, while if $4\det(J_0) > (\mathrm{tr}(J_0))^2$, the following upper bound for τ is obtained to satisfy (3.3.12):

$$\tau < \tau_{\max} = \frac{-2\mathrm{tr}(J_0)}{[4\det(J_0) - (\mathrm{tr}(J_0))^2]} \tag{3.3.13}$$

[(5)]Let us recall that, borrowed from the theory of the linear stability of dynamical systems, a polynomial is (asymptotically) stable if and only if all its roots have negative real part, while a polynomial is said to be unstable if there exists at least one root with positive real part.

This last results will be important in the following, because it states that the stability of the homogeneous equilibrium depends on τ (see panel b) in Figure 3.1). More importantly, if τ is large enough, the system (3.2.7) exhibits patterns; they are *not emerging from a Turing mechanism* but instead from the *instability of the homogeneous equilibrium*. Let us observe that one cannot discriminate them with respect to Turing patterns by simple visual inspection.

3.3.2 Conditions for the instability of p_α

Using again the Routh-Hurwitz criterion we can prove the existence of (at least) an $\alpha > 1$ for which p_α is unstable conditioned on the stability of p_1.

Observe again that the coefficients a and b are positive. Moreover, by assuming Equations (3.3.8) and (3.3.9) to hold true and by recalling that $-\Lambda^{(\alpha)} > 0$ for all $\alpha > 1$, then $c_\alpha > 0$ and $d_\alpha > 0$ (see Equations (3.3.5) and (3.3.6)). In conclusion the unique coefficient of p_α that can be negative is e_α. Hence (see SM 3.6) the instability can arise if one of the following couples of conditions is verified:

$$\begin{cases} B := -(\tau_u+\tau_v)(D_u+D_v)(1-\tau_u g_v-\tau_v f_u)+ \\ \qquad +(\tau_u+\tau_v)\mathrm{tr}(J_0)(\tau_u D_v+\tau_v D_u)-2\mathrm{tr}(J_0)(D_u+D_v)\tau_u\tau_v+ \\ \qquad\qquad -(\tau_u+\tau_v)^2(D_v f_u+D_u g_v)>0 \qquad (3.3.14a) \\ \\ B^2-4(D_v\tau_u-D_u\tau_v)^2\Big[-\mathrm{tr}(J_0)(\tau_u+\tau_v)(1-\tau_u g_v-\tau_v f_u)+ \\ \qquad\qquad -\tau_u\tau_v(\mathrm{tr}(J_0))^2-(\tau_u+\tau_v)^2\det(J_0)\Big]>0 \qquad (3.3.14b) \end{cases}$$

or

$$\begin{cases} D_u g_v + D_v f_u > 0 & (3.3.15a) \\ (D_u g_v + D_v f_u)^2 - 4D_u D_v \det(J_0) > 0 & (3.3.15b) \end{cases}$$

Let us observe that Equations (3.3.15a) and (3.3.15b) do not depend on τ_u and τ_v and are indeed the same conditions one imposes to obtain the Turing instability in the classical, i.e., non-relativistic setting [31]. In particular, they require $D_v > D_u$. However, Equations (3.3.14a) and (3.3.14b) do not ask for such condition on the diffusivities, implying that the hypothesis of a finite propagation velocity allows to enlarge the parameter region for which Turing instability arises, in particular allowing for $D_v \leq D_u$.

Based on the above, one can conclude that if the patterns with positive inertial times are due to Equations (3.3.15a) and (3.3.15b), then they persist also in the non-relativistic limit, $\tau_u \to 0$ and $\tau_v \to 0$. On the other hand, if the instability has been initiated by conditions Equations (3.3.14a) and (3.3.14b), we can show (see SM 3.7) that, in the non-relativistic limit, the patterns fade out and disappear for positive and sufficiently small inertial times.

To start our analysis, let us thus consider the case $D_u = D_v = D$. As already observed Equation (3.3.15a) cannot be satisfied having by Equation (3.3.9) the fact that $\mathrm{tr}(J_0) < 0$, thus this cannot be a path toward Turing instability. On the other hand, let us reorganize terms and rewrite condition (3.3.14a) as follows

$$B|_{D_u=D_v=D} = -2D\left[\tau_u+\tau_v+(\tau_u^2-\tau_v^2)f_u+\tau_u(\tau_v-\tau_u)\mathrm{tr}(J_0)\right]$$

and observe that if $\tau_u \geq \tau_v$ then $B|_{D_u=D_v=D} < 0$. Indeed, $f_u > 0$, being u the activator species, and $\mathrm{tr}(J_0) < 0$ by the stability assumption on $p_1(\lambda)$; hence the term in brackets on the right-hand side is the sum of three positive terms, from which the claim follows. On the contrary, if $\tau_u < \tau_v$, then $B|_{D_u=D_v=D} > 0$ provided

$$-\mathrm{tr}(J_0) > \frac{\tau_u + \tau_v}{\tau_u(\tau_v - \tau_u)} - \frac{\tau_u + \tau_v}{\tau_u} f_u$$

Finally, condition (3.3.14b) no longer depends on D and can thus be verified by a suitable choice of the remaining parameters.

In conclusion, we can have Turing instability also in the case of equal diffusivites, $D_u = D_v$, provided the inhibitor has a larger inertial time than the activator, $\tau_v > \tau_u$.

Let us conclude this section by considering again the case $\tau_u = \tau_v = \tau$. Because of the previous analysis, we have to assume $D_u \neq D_v$, otherwise no Turing instability can develop. Then Equation (3.3.14a) simplifies into

$$B|_{\tau_u=\tau_v=\tau} = -2\tau\left[(D_u + D_v) + \tau(D_v - D_u)(f_u - g_v)\right]$$

Being v the inhibitor species we have $g_v < 0$, hence, if $D_v > D_u$, we can conclude that the term in brackets on the right-hand side is the sum of positive terms and thus $B|_{\tau_u=\tau_v=\tau} < 0$. On the other hand, if $D_v < D_u$, we can have $B|_{\tau_u=\tau_v=\tau} > 0$ provided that

$$\tau > \frac{D_u + D_v}{D_u - D_v} \frac{1}{f_u - g_v}$$

Finally, the remaining condition (3.3.14b) can be rewritten as

$$4\tau^2\left[(D_u + D_v)^2 + 2D_u D_v \mathrm{tr}(J_0) - 4\tau^2(D_v - D_u)^2 \det J_0\right] > 0$$

and a straightforward computation allows to show that it is satisfied if

$$\tau > \frac{D_u D_v \mathrm{tr}(J_0) + \sqrt{\left[D_u D_v \mathrm{tr}(J_0)\right]^2 + 4(D_v^2 - D_u^2)^2 \det(J_0)}}{4(D_v - D_u)^2 \det(J_0)}$$

Let us stress that in this setting, $D_v < D_u$, the conditions (3.3.15a) and (3.3.15b) cannot be satisfied, hence the emergence of Turing instability is solely due to the finite propagation velocity and imposes a lower bound on the inertial time. Before introducing the model we will use to present our results, let us emphasize two more relevant results. First, the proposed framework allows to prove the emergence of Turing instability also in an inhibitor-inhibitor system, that is $f_u < 0$ and $g_v < 0$; indeed, while Equation (3.3.15a) cannot hold true, Equations (3.3.14a) and (3.3.14b) can be satisfied for suitable choice of the parameters, as we will show below (see Figure 3.8 and the associated discussion). Second, inertia-driven Turing instability cannot manifest in suitable m-species linear kinetic models, as described in the following remark.

Remark (*Kinetic linear systems*) As shown in [138], an m-species non-relativistic kinetic system can be expressed as a polynomial differential equation assuming mass-action for the reaction rates; however, not all polynomials can be considered models of

chemical reactions [139] because of the possible presence of negative cross terms, i.e., the abundance of a species decreases in a process where it is not involved. The absence of negative cross effects in the case of first order kinetic differential systems, prevents the Turing instability [138]. We can prove a similar result to hold true in the relativistic framework, provided all the species have the same inertial time and the ratios of the diffusion coefficients divided by the inertial time are large enough (see SM 3.8).

3.4 The FitzHugh-Nagumo model

The aim of this section is to present an application of the theory hereby developed. For sake of definitiveness, we decided to use the FitzHugh-Nagumo model [126, 127, 128], but our results go beyond the chosen model. The FitzHugh-Nagumo model (for short *FHN*) is a paradigmatic nonlinear system already used in the literature to study the emergence of Turing patterns [129, 130, 131, 132] as well as synchronization phenomena [133, 134]. Let us observe that this model is not a kinetic one, since the $-v$ term appearing in the rate evolution for u, expresses a negative cross-effect [138], at the same time this supports our statement that Turing instability finds applications beyond the morphogenesis and chemical frameworks. Our choice relies also on the observation that such model has been conceived in the framework of neuroscience as a schematization of an electric impulse propagating through an axon. For this reason, we believe that it would make a suitable setting to account for a finite velocity propagation of signals and it could be interesting for future applications. The *FHN* model can be described by the system of ODEs

$$\begin{cases} \dot{u} &= \mu u - u^3 - v \\ \\ \dot{v} &= \gamma(u - \beta v) \end{cases} \tag{3.4.1}$$

where the parameters μ, γ and β are assumed to be positive. We will hereby focus on its behavior close to the fixed point $(u^*, v^*) = (0,0)$. The linear stability analysis ensures stability of the latter under the conditions $\mu < \gamma\beta$ and $\mu\beta < 1$ (see panel a) in Figure 3.1). Let us observe that, once such conditions are not met, the system undergoes a supercritical Hopf-Andronov bifurcation [47]: the equilibrium point becomes unstable giving birth to a limit cycle solution. In this study, we will limit ourselves to the former case, leaving the oscillating case for a future work.

Consider now n identical copies of the FitzHugh-Nagumo model (4.3.10) interacting with each other through a diffusive-like coupling and assume to work in the Cattaneo framework presented in Section 3.1. The resulting model can thus be written as

$$\begin{cases} \dot{u}_i + \tau_u \ddot{u}_i &= \mu u_i - u_i^3 - v_i + D_u \sum_{j=1}^{n} L_{ij} u_j \\ \\ & \qquad\qquad \forall i = 1, \dots n \\ \\ \dot{v}_i + \tau_v \ddot{v}_i &= \gamma(u_i - \beta v_i) + D_v \sum_{j=1}^{n} L_{ij} v_j \end{cases} \tag{3.4.2}$$

where D_u (resp. D_v) is the diffusion coefficients of species u (resp. v) and τ_u (resp. τ_v)

the inertial time for species u (resp. v). The matrix $\mathbf{L}$ is the Laplace matrix describing the diffusive coupling among the FitzHugh-Nagumo systems.

Remark (*About the network substrate*) The possible onset of Turing instability depends both on the dynamical system as well as the network substrate via the eigenvalues $\Lambda^{(\alpha)}$ of the associated Laplace matrix, $\mathbf{L}$. As previously stated, a discrete topology may affect the dynamics due to finite size effects. Because a comprehensive study of such impact on Turing instability goes beyond the scope of this paper and, for sake of definitiveness, we decided to use an Erdős-Rényi random graph [140] made of n nodes and each couple of nodes having a probability $p \in (0,1)$ to be linked. In the following, we fixed $n = 30$ and $p = 0.1$ and we also checked that the resulting network is connected.

In the rest of this Section we will present our analysis about the emergence of Turing instability in the relativistic *FHN* defined on networks (3.4.2). Let us start by determining the parameter region associated to a stable homogeneous equilibrium, $(u^*, v^*) = (0,0)$. Panel a) of Figure 3.1 represents the classical case where we assume an infinite propagation velocity, namely $\tau_u = \tau_v = 0$. The stability region (black) is delimited by the conditions $\mu < \gamma\beta$ (red line) and $\mu\beta < 1$ (yellow line). In panel b) we report the case of equal inertial times, $\tau_u = \tau_v = 1$; we can observe that the stability region (black and shades of gray) is contained in the previous one, being delimited by the same conditions and in addition by Equation (3.3.12) (blue line). As previously observed, the stability of the homogeneous solution depends on the value of $\tau_u = \tau_v = \tau$, meaning that the equilibrium loses its stability if the inertial time is too large, as shown by Equation (3.3.13). The gray shaded region in panel b) has thus been colored according to $\ln \tau_{\max}$: smaller values are associated to lighter shades of gray. On the contrary, in the black region any positive value of τ returns a stable homogeneous equilibrium (being $\tau_{\max} = \infty$). In the remaining panels of Figure 3.1 we considered different inertial times, $\tau_u = 5$ and $\tau_v = 1$ in panel c), and $\tau_u = 1$ and $\tau_v = 5$ in panel d). The stability region (black) is delimited by the same lines as before, with the exception of the case $\tau_u < \tau_v$, where an extra condition needs to be considered, i.e., Equation (3.3.11) (green line). We are now able to study the emergence of Turing instability under the assumption $\tau_u = \tau_v = \tau$. In panel a) of Figure 3.2 we report the region (black) in the parameter space allowing for classical Turing instability to arise for a choice of the diffusivities $D_u < D_v$. Such region is contained in the one associated to a stable homogeneous solution and it is now also bounded by the conditions $D_v f_u + D_u g_v = 0$ (dashed blue line) and $(D_u g_v + D_v f_u)^2 - 4 D_u D_v \det(J_0) = 0$ (dashed red line). The same values of the parameters are used in panel b), assuming now the inertial times to be positive, $\tau_u = \tau_v = 1$; the Turing region (black and shades of gray) is smaller, as it is also delimited by the condition Equation (3.3.12) (blue line). Once again, the shades of gray represent the values of $\ln \tau_{\max}$ to ensure the stability of the homogeneous solution (see Equation (3.3.13)). Finally, in panel c), we report the analysis of a setting for which classical Turing instability can never emerge because the inhibitor diffuses slower than the activator, $D_u = 2.2 > D_v = 0.2$. The instability being determined by the inertial time $\tau > 0$, we named it *inertia-driven instability*. The Turing region (black and shades of gray) is now delimited also by the condition Equation (3.3.14b), where again the shades of gray represent the values of $\ln \tau_{\max}$.

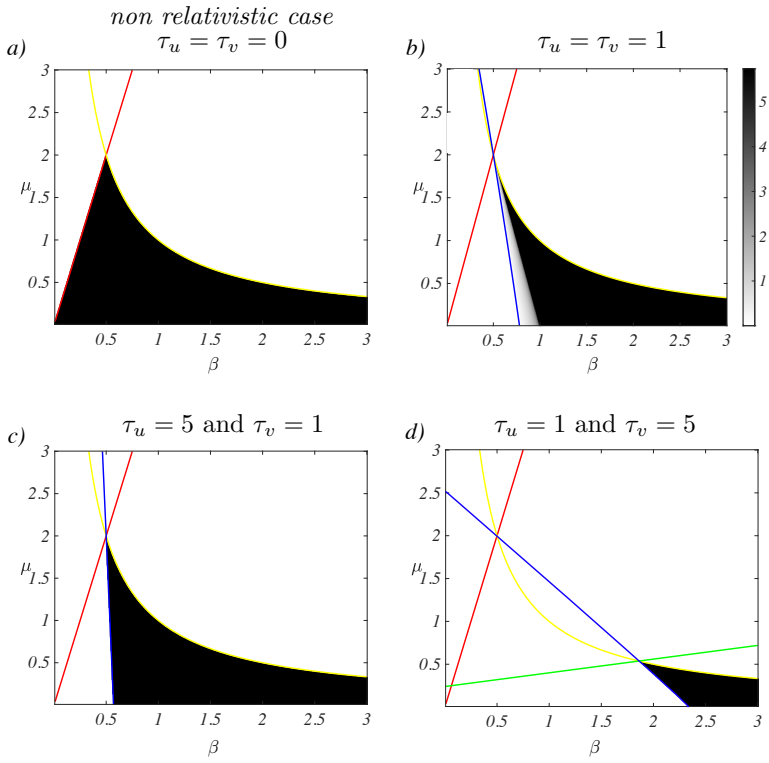

Figure 3.1: Parameter region associated to the stability of the homogeneous solution for the *FHN* model. For a fixed value of $\gamma = 4$, we study the stability of the homogeneous equilibrium $(u_i, v_i) = (0,0)$, $i = 1,\dots,n$, as a function of β and μ: the black regions denote stability while white ones instability. Panel a) corresponds to the classical setting, i.e., $\tau_u = \tau_v = 0$, the remaining panels are associated to positive values of the inertial times, $\tau_u = \tau_v = 1$ (panel b)), $\tau_u = 5$ and $\tau_v = 1$ (panel c)) and $\tau_u = 1$ and $\tau_v = 5$ (panel d)). In all the panels, the red line denotes the condition $\mathrm{tr}(J_0) = 0$, while $\det(J_0) = 0$ is represented by the yellow one; these two lines determine the boundary of the stability region in the classical setting. Such region is shrunk in the case of positive inertial times because of the additional constraints, Equation (3.3.11) (green line) and Equation (3.3.12) (blue one). The gray shaded region in panel b), colored according to $\ln \tau_{\max}$, is associated to a stability of the homogeneous equilibrium constrained to a bound on τ, see Equation (3.3.13), while in the black region any positive value of τ is admissible.

The impact of $\tau_{\max}$ can be appreciated in Figure 3.3, where we report for few generic sets of parameters the *dispersion relation*, λ_α, as a function of $\Lambda^{(\alpha)}$, the eigenvalues of the Laplace matrix, $\mathbf{L}$. In panel a), we show the dispersion relation for the choice $\tau_u = \tau_v = 1$ and $(\beta, \mu) = (0.8, 1.0)$, lying in the Turing instability region (yellow star in the panel c) of Figure 3.2). We can observe that the homogeneous equilibrium is stable (the dispersion relation is negative for $\Lambda^{(1)} = 0$), but it turns out to be unstable under heterogeneous perturbations (there exist $\alpha > 1$ (red dots) for which $\lambda_\alpha > 0$)

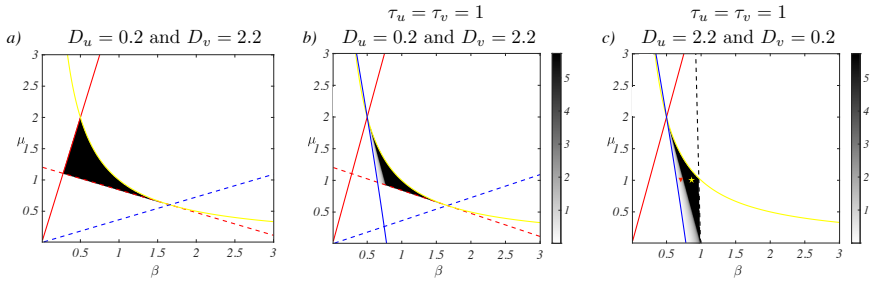

Figure 3.2: Parameter region associated to Turing instability for the *FHN* model, $\tau_u = \tau_v$. For a fixed value of $\gamma = 4$, we study the onset of Turing instability (black regions) close to the homogeneous equilibrium $(u_i, v_i) = (0,0)$, $i = 1, \dots, n$, as a function of β and μ. Panel a) corresponds to the classical setting, i.e., $\tau_u = \tau_v = 0$, the remaining panels are associated to positive values of the inertial times, $\tau_u = \tau_v = 1$. In panels a) and b), the diffusivities have been set equal to $D_u = 0.2$ and $D_v = 2.2$, namely the inhibitor diffuses faster than the activator. Panel c) present a completely new setting where Turing instability can develop even for a slower inhibitor, $D_u = 2.2$ and $D_v = 0.2$. In all the panels, the red line denotes the condition $\mathrm{tr}(J_0) = 0$, while $\det(J_0) = 0$ is represented by the yellow one. In panels a) and b), the dashed blue line represents the condition $D_v f_u + D_u g_v = 0$ (Equation (3.3.15a)), while the dashed red line the condition $(D_u g_v + D_v f_u)^2 - 4 D_u D_v \det(J_0) = 0$ (Equation (3.3.15b)). Together with the blue line in panel b) corresponding to Equation (3.3.12), these lines delimitate the parameter region allowing for Turing instability in the case $D_u < D_v$. In panel c), corresponding to $D_u > D_v$, a similar parameter region is bounded by the same blue line but also by the dashed black line, namely Equation (3.3.14b). The gray shaded region in panels b) and c), colored according to $\ln \tau_{\max}$, is associated to a stability of the homogeneous equilibrium constrained to a bound on τ, see Equation (3.3.13), while in the black region any positive value of τ is admissible.

and synchronized oscillatory patterns emerge (see inset where we report[(6)]), indeed, we are in presence of an oscillatory Turing instability because $\rho_\alpha > 0$ (data not shown). Panel b) ($\tau_u = \tau_v = 2.2$ and $(\beta, \mu) = (0.7, 1.0)$, red triangle in the panel c) of Figure 3.2) corresponds to a similar behavior, the parameters still being in the Turing region, but conditioned to the value of $\tau_{\max}$; the dispersion relation assumes positive values, but the homogeneous equilibrium is weakly stable, the dispersion relation is negative but very close to 0 for $\Lambda^{(1)} = 0$, being $\tau_u = \tau_v = 2.2$ close to $\tau_{\max} \sim 2.31$; again, an oscillating synchronous behavior is observed (inset). In panel c), we used the same parameters (β, μ), but we increased the inertial times beyond the critical values, $\tau_u = \tau_v = 3.5 > \tau_{\max}$, and indeed the homogeneous equilibrium is unstable, given that the dispersion relation is positive for $\Lambda^{(1)} = 0$. Again, synchronized oscillatory patterns emerge (inset), they are indistinguishable from the ones one can obtain from the setting presented in panels a) and b), but they are not the result of Turing instability.

[(6)]Throughout this work the numerical simulations have been performed using a 4-th order Runge-Kutta scheme implemented in Matlab [141] $u_i(t)$ vs. t; the code is available upon request to the corresponding author. The initial conditions have been realized by drawing uniformly random perturbations δ-close to the homogeneous equilibrium and the simulation time has been taken of the order of $-\log \delta / \max_\alpha \mathscr{R}\lambda_\alpha$. Indeed according to the ansatz $\hat{u}_\alpha \sim e^{\lambda_\alpha t}$ and $\hat{u}_\alpha \sim e^{\lambda_\alpha t}$, this is the time necessary to (possibly) increase the δ-perturbation up to a macroscopic size. In the rest of the work we set $\delta = 10^{-2}$, small enough to discriminate between the onset of the instability using a reasonable simulation time for the values of $\max_\alpha \mathscr{R}\lambda_\alpha$ we are dealing with.

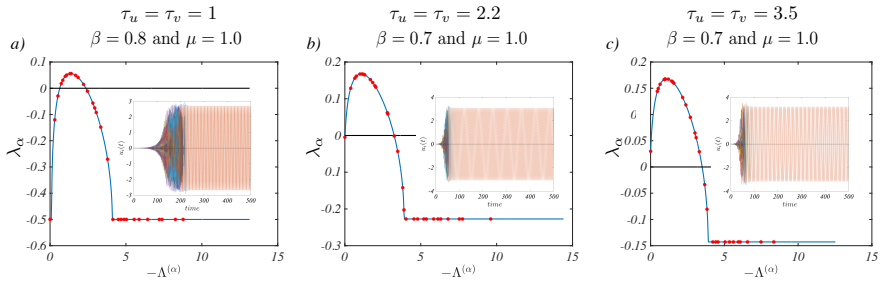

Figure 3.3: Dispersion relation and patterns for the *FHN* model, $\tau_u = \tau_v$. For fixed values of $\gamma = 4$, $D_u = 2.2$, $D_v = 0.2$ and two couples (β, μ) we show in the main panels the dispersion relation, λ_α as a function of $\Lambda^{(\alpha)}$. Panel a) corresponds to the choice $\tau_u = \tau_v = 1$ and $(\beta, \mu) = (0.8, 1.0)$ (yellow star in panel c) of Figure 3.2), lying the Turing instability region and indeed the dispersion relation assumes positive values (red dots lying on the positive part of the blue curve). The homogeneous equilibrium is stable (the dispersion relation is negative for $\Lambda^{(1)} = 0$), but it turns out to be unstable under heterogeneous perturbations and synchronized oscillatory patterns emerge (inset), indeed the critical root has positive imaginary part, $\rho_\alpha > 0$ (conditions (3.3.14a) and (3.3.14b) are satisfied). In panel b), we fix $\tau_u = \tau_v = 2.2$ and $(\beta, \mu) = (0.7, 1.0)$ (red triangle in panel c) of Figure 3.2), still in the Turing region but conditioned to the value of $\tau_{\max}$. The behavior is similar to the one reported in panel a), but now the homogeneous equilibrium is weakly stable, the dispersion relation is negative but very close to 0 for $\Lambda^{(1)} = 0$, indeed for these values of the parameters we have $\tau_{\max} \sim 2.31$. Again, an oscillatory behavior is obtained (inset) associated to $\rho_\alpha > 0$. In panel c), we used the same parameters (β, μ) but we increased $\tau_u = \tau_v = 3.5 > \tau_{\max}$ and indeed the homogeneous equilibrium is unstable, the dispersion relation is positive for $\Lambda^{(1)} = 0$. Again, synchronized oscillatory patterns emerge (inset), they are indistinguishable from the ones one could obtain with the parameters used in panels a) and b), but they are not the result of Turing instability.

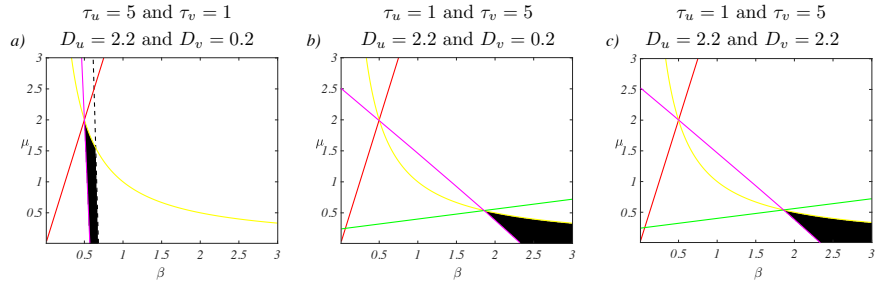

Figure 3.4: Parameter region associated to the inertia-driven instability for the *FHN* model. For a fixed value of $\gamma = 4$, we study the onset of Turing instability (black regions) close to the homogeneous equilibrium $(u_i, v_i) = (0,0)$, $i = 1, \ldots, n$, as a function of β and μ and driven by the inertial times, $\tau_u \neq \tau_v$. Indeed, we assume $D_u \geq D_v$, resulting in a setting where classical Turing instability cannot emerge. Panel a) corresponds to the setting, $\tau_u = 5$ and $\tau_v = 1$, $D_u = 2.2$ and $D_v = 0.2$. In panel b), we use the same diffusivities while the inertial times are exchanged, i.e., $\tau_u = 1$ and $\tau_v = 5$. Panel c) reports result for $D_u = D_v = 2.2$ and $\tau_u = 1$ and $\tau_v = 5$. In all the panels the red line denotes the condition $\mathrm{tr}(J_0) = 0$, while $\det(J_0) = 0$ is represented by the yellow one. The green line represents condition (3.3.11), while the magenta one represents condition (3.3.12); once present, the dashed black line stands for Equation (3.3.14b).

We can now consider the more general case of different inertial times and show the onset of Turing instability for a choice of the diffusivities that cannot allow for the classical Turing phenomenon, notably because the activator can diffuse faster than the inhibitor. For this reason, we hereby stress again that *inertia-driven instability* should be a suitable name for such phenomena. In Figure 3.4 we report the region (black) in the parameter space (β,μ) allowing for Turing instability under the assumptions $\tau_u \neq \tau_v$ and $D_u \geq D_v$. Such region is contained in the region associated to a stable homogeneous solution (see panels c) and d) of Figure 3.1) and delimited in addition by the conditions (3.3.11) (green line), (3.3.12) (magenta line) and (3.3.14b) (dashed black line). We can observe that, for all the choices of the inertial times and diffusion constants ($\tau_u = 5$, $\tau_v = 1$, $D_u = 2.2$ and $D_v = 0.2$ panel a), $\tau_u = 1$, $\tau_v = 5$, $D_u = 2.2$ and $D_v = 0.2$ panel b) and $\tau_u = 1$, $\tau_v = 5$, $D_u = D_v = 2.2$ panel c)), there are always parameters (β,μ) allowing Turing instability to occur. One can show that in all the presented cases we are dealing with a Turing oscillatory instability driven by the inertial times. We report in Figure 3.5 two generic dispersion relations for the latter settings. In both cases, we can appreciate the fact that the aspatial solution is stable, indeed $\lambda_1 < 0$, while there are $\alpha > 1$ (red dots) for which $\lambda_\alpha > 0$, testifying the instability of such equilibrium once subjected to heterogeneous perturbations and resulting into synchronized oscillatory patterns (see panels c) and f)) associated with a positive ρ_α (see panels b) and e)).

The bifurcation regions reported in Figure 3.6 correspond to a parameters setting for which Turing instability could emerge because the inhibitor diffuses faster than the activator, $D_v > D_u$, even without the presence of positive inertial times, indeed the conditions (3.3.15a) and (3.3.15b) are satisfied. However, the resulting patterns and dispersion relations (see Figure 3.7) are quite different in the relativistic case, $\tau_u > 0$ and $\tau_v > 0$. The top three panels refer to a generic point in the Turing region (see panel b) Figure 3.6), here $\gamma = 4$, $\beta = 0.9$, $\mu = 1.0$, $\tau_u = 1$, $\tau_v = 2$, $D_u = 0.2$ and $D_v = 2.2$; we can clearly appreciate that Turing instability is at play. Indeed, the aspatial equilibrium is stable, $\lambda_1 < 0$, and there are modes $\alpha > 1$ for which the dispersion relation is positive, $\lambda_\alpha > 0$ (panel a)); moreover, such unstable modes are real, being their imaginary part zero, $\rho_\alpha = 0$ (panel b)). One should thus expect the system to settle into stationary patterns, but that is not the case (panel c)): in fact, the solution departs from the homogeneous equilibrium and it spends a transient time (much longer that the initial period needed to depart from the equilibrium) oscillating with very small amplitudes around different values, only after this phase the amplitudes increase and a wave develops. Observe also that each node oscillates about a different average value, which is not the case in the oscillating patterns shown before. The bottom three panels correspond to a generic point still in the Turing region (see panel a) Figure 3.6), with $\gamma = 4$, $\beta = 0.7$, $\mu = 1.15$, $\tau_u = 5$, $\tau_v = 1$, $D_u = 0.2$ and $D_v = 2.2$ (conditions (3.3.15a) and (3.3.15b) hold true). The dispersion relation and its imaginary part behave similarly to the previous case, however now the solution diverging from the unstable homogeneous equilibrium settles onto a stationary heterogeneous equilibrium (panel f)), as one should expect from the classical, i.e., non-relativistic, Turing instability.

To the best of our knowledge, this is a remarkable phenomenon that should be taken into account in the problem of patterns prediction [142]. Indeed, since the seminal paper by Turing [4], scholars are aware of the existence of stationary Turing patterns, often

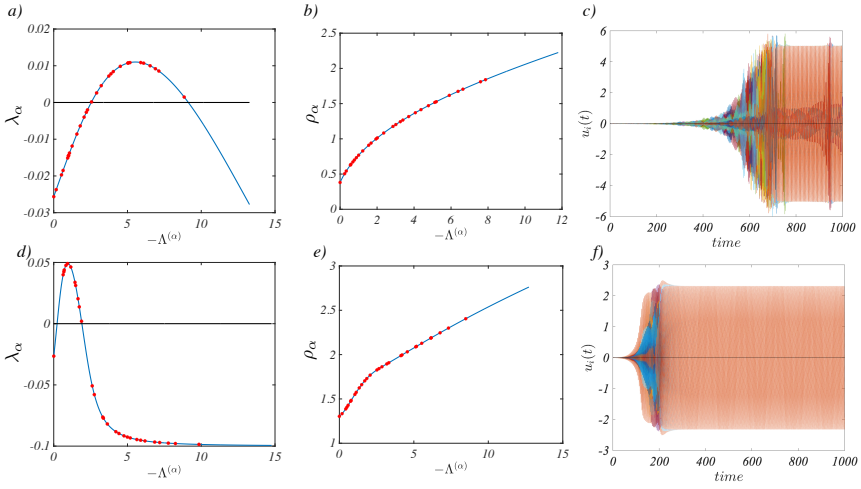

Figure 3.5: Dispersion relation and patterns for the *FHN* model in the case $\tau_u \neq \tau_v$. For a fixed value of $\gamma = 4$ and two couples (β, μ) and (τ_u, τ_v) we show the dispersion relation (panels a) and d)), λ_α as a function of $\Lambda^{(\alpha)}$, the imaginary part of the root with the largest real part, ρ_α (panels b) and e)), and the time evolution of the solutions $u_i(t)$ (panels c) and f)). The top three panels correspond to the choice $\tau_u = 5$ and $\tau_v = 1$, $(\beta, \mu) = (0.6, 1.0)$, and $D_u = 2.2$ and $D_v = 0.2$, lying the inertia-driven instability region (see panel a) Figure 3.4), indeed the conditions (3.3.14a) and (3.3.14b) hold true. The bottom three panels are associated to $\tau_u = 1$ and $\tau_v = 5$, $(\beta, \mu) = (2.5, 0.18)$ and with equal diffusivity $D_u = D_v = 2.2$; these values are still in the inertia-driven region (see panel c) Figure 3.4) and the conditions (3.3.14a) and (3.3.14b) are satisfied. In both cases the aspatial equilibrium is stable ($\lambda_1 < 0$), but it turns out to be unstable under heterogeneous perturbations and synchronized oscillatory patterns emerge. Being $\rho_\alpha > 0$, we are in presence of a Turing-wave instability driven by the inertial times.

associated to a real dispersion relation, and of oscillatory Turing patterns resulting from a Turing wave instability. The use of discrete substrates such as networks questioned this dichotomy and a rule of thumb seems to apply [40]: oscillatory patterns develop if the most unstable mode has a large imaginary part, $\rho_\alpha \gg \lambda_\alpha$. The last example goes in the opposite direction because here $\lambda_\alpha > \rho_\alpha = 0$ and the system can exhibit stationary patterns as well as waves, recalling that the final patterns are initiated by the linear behavior, but rather shaped by the nonlinear character of the system.

3.5 Discussion

In this work we have improved the Cattaneo framework of relativistic reaction-diffusion systems to allow for complex network substrates. We have thus analytically studied the conditions for the emergence of Turing instability, stationary or wave-like, for hyperbolic reaction-diffusion networked systems. The introduction of the inertial times removes the unphysical assumption of infinite propagation velocity and, more importantly, this new framework allows for Turing patterns to emerge also for parameter

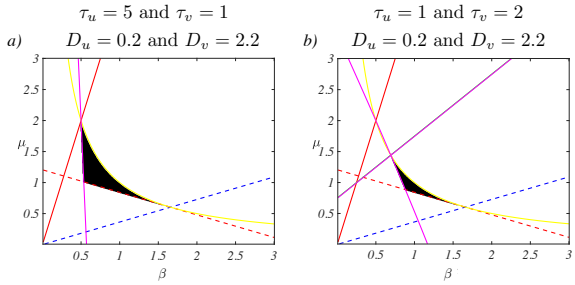

Figure 3.6: Parameter region associated to Turing instability for the *FHN* model, $D_u < D_v$. For a fixed value of $\gamma = 4$, we study the onset of Turing instability (black regions) close to the homogeneous equilibrium $(u_i, v_i) = (0,0)$, $i = 1,\dots,n$, as a function of β and μ and different choices of inertial times, τ_u and τ_v, and of the diffusivities, D_u and D_v, in a setting where classical Turing instability could emerge because $D_u < D_v$. Panel a) corresponds to the setting, $\tau_u = 5$ and $\tau_v = 1$, $D_u = 0.2$ and $D_v = 2.2$, while panel b) shows results with the same diffusivities but $\tau_u = 1$ and $\tau_v = 2$. In all the panels the red line denotes the condition $\mathrm{tr}(J_0) = 0$, while $\det(J_0) = 0$ is represented by the yellow one. The magenta line denotes the condition (3.3.12). The dashed blue line represents the condition $D_v f_u + D_u g_v = 0$ (Equation (3.3.15a)), while the dashed red line the condition $(D_u g_v + D_v f_u)^2 - 4 D_u D_v \det(J_0) = 0$ (Equation (3.3.15b)).

values for which classical, i.e., non-relativistic, Turing instability cannot arise, e.g., once the activator diffuses faster than the inhibitor or even in the case of *inhibitor-inhibitor* systems. To support the last claim, let us consider a generic quadratic Lotka - Volterra system [143, 144] involving two species, namely $f(u,v) = u(a_1 - b_1 u + c_1 v)$ and $g(u,v) = v(a_2 - b_2 v - c_2 u)$, where all the parameters are positive numbers, and let us consider its relativistic networked extension:

$$\begin{cases} \dot{u}_i + \tau_u \ddot{u}_i &= u_i(a_1 - b_1 u_i + c_1 v_i) + D_u \sum_{j=1}^{n} L_{ij} u_j \\ & \qquad \forall i = 1,\dots,n \\ \dot{v}_i + \tau_v \ddot{v}_i &= v_i(a_2 - b_2 v_i - c_2 u_i) + D_v \sum_{j=1}^{n} L_{ij} v_j \end{cases} \tag{3.5.1}$$

The homogeneous nontrivial equilibrium is $u^* = (c_1 a_2 + a_1 b_2)/(c_2 c_1 + b_2 b_1)$ and $v^* = (a_2 b_1 - c_2 a_1)/(c_2 c_1 + b_2 b_1)$, and one can easily show that $f_u = -b_1 u_0 < 0$ and $g_v = -b_2 v_0 < 0$, provided $u^* > 0$ and $v^* > 0$, as we will hereby assume; we are hence dealing with an inhibitor-inhibitor system. Contrary to the classical setting where Turing pattern are not allowed for, in the relativistic framework parameters can be chosen in such a way that the above system exhibits an inertia-driven instability resulting in an oscillatory behavior (see Figure 3.8). We have shown that the stability of the homogeneous solution is conditional to the inertial time common to both species. There exists a threshold, $\tau_{\max}$, that, if exceeded, returns an unstable homogeneous solution: the system exhibits patterns but they are not ascribed to a Turing instability; let us observe that the latter are indistinguishable from the ones emerging following the Turing mechanism. Interestingly enough, such threshold depends on the model parameters and it can become arbitrarily large for a specific range of the latter; in such case, the homoge-

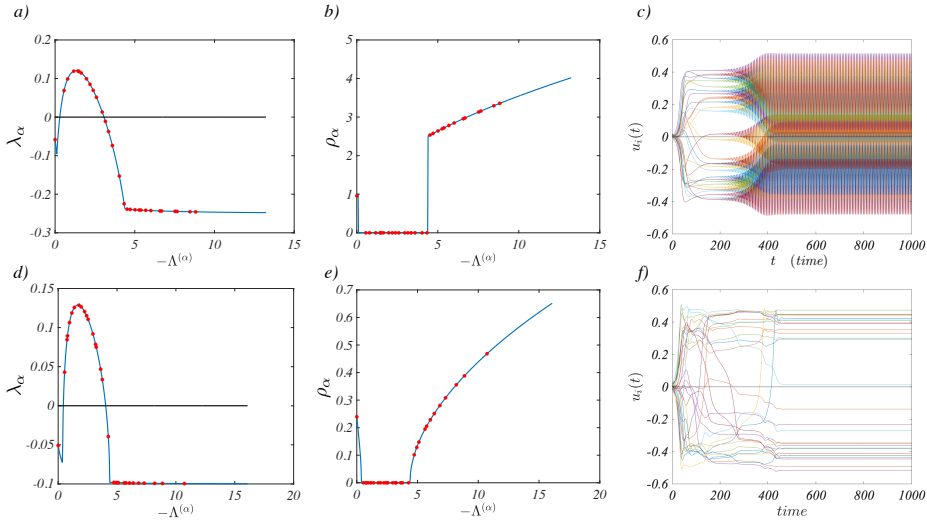

Figure 3.7: Dispersion relation and patterns for the *FHN* model, $\tau_u \neq \tau_v$. For a fixed value of $\gamma = 4$ and two couples (β, μ) and (τ_u, τ_v), we show the dispersion relation (panels a) and d)), λ_α as a function of $\Lambda^{(\alpha)}$, the imaginary part of the root with the largest real part, ρ_α (panels b) and e)), and the time evolution of the solutions $u_i(t)$ (panels c) and f)). The top three panels correspond to the choice $\tau_u = 1$, $\tau_v = 2$, $\beta = 0.9$, $\mu = 1.0$, $D_u = 0.2$ and $D_v = 2.2$, associated to Turing instability (see panel b) Figure 3.6); the conditions (3.3.15a) and (3.3.15b) hold true. In the bottom three panels, we invert the sizes of the inertial times, $\tau_u = 5$ and $\tau_v = 1$, and the remaining parameters are $(\beta, \mu) = (0.7, 1.15)$, $D_u = 0.2$ and $D_v = 2.2$, still in the Turing region (see panel a) Figure 3.6) and the conditions (3.3.15a) and (3.3.15b) are satisfied. In both cases the aspatial equilibrium is stable ($\lambda_1 < 0$), but it turns out to be unstable under heterogeneous perturbations and synchronized oscillatory patterns can emerge. Let us observe that ρ_α vanishes on an interval containing all the unstable modes, $-\Lambda^{(\alpha)}$, and it is positive elsewhere, i.e. in correspondence to decaying modes, the obtained instability possesses thus both the characteristic of a Turing instability and a Turing-wave. Indeed, the pattern associated to the first set of parameters (top panels) keeps oscillating after a transient time (panel c)) while the pattern resulting from the second set of parameters (bottom panels) settle onto a stationary solution (panel f)).

neous equilibrium is always stable (with respect to the inertial time). For generic values of the inertial times, $\tau_u \neq \tau_v$, we have proven that Turing instability can set up both for the inhibitor diffusing faster than the activator, $D_v > D_u$, as it occurs in the classical setting, but also in the complementary regime, i.e., $D_v \leq D_u$, which is forbidden in the absence of inertial time. Even more striking, Turing patterns can emerge also in the case of inhibitor-inhibitor systems. The framework we propose allows to relax the severe parameters conditions for the patterns onset and thus provide new insights into the fine tuning problem [135, 12]. Hence, existing experiments could also be read with this novel perspective and analyzed in the proposed framework.

We have complement our general analytical results with a numerical study of the FitzHugh-Nagumo model extended to the framework of hyperbolic reaction-diffusion

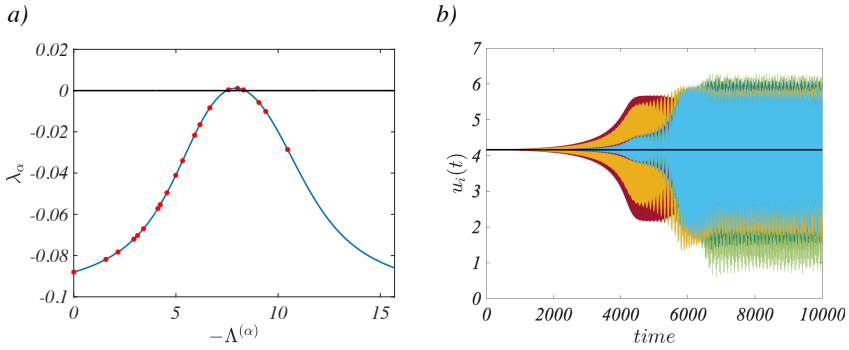

Figure 3.8: Dispersion relation and patterns for the *inhibitor - inhibitor* model. We show the dispersion relation (panel a)), λ_α as a function of $\Lambda^{(\alpha)}$, and the time evolution of the solutions $u_i(t)$ (panel b)) for the system (3.5.1), for the choice of parameters: $a_1 = 4$, $a_2 = 3$, $b_1 = 2$, $b_2 = 1$, $c_1 = 4.7$, $c_2 = 0.5$, $D_u = 0.1$, $D_v = 5.2$, $\tau_u = 1$ and $\tau_v = 5$. We can observe that the homogeneous equilibrium is stable ($\lambda_1 < 0$), but it turns out to be unstable under heterogeneous perturbations (red dots in the panel a)) and oscillatory patterns can emerge (panel b)). The imaginary part of the largest roots is positive (data not shown) and we are thus dealing with an inertia-driven wave-instability.

networked systems. We have found stationary patterns as well as synchronized oscillatory ones; we have also found an interesting class of solutions where the system spends a transient time into a stationary-like regime, but then it evolves into an oscillatory one. This example raises relevant questions about the prediction of the patterns following a Turing instability, which is, up to now, an open problem [142].

The investigation discussed in this paper could be further extended in several directions. Previous studies have shown that different kinds of networks, such as directed [38] or non-normal ones [39, 70], extend the conditions for the emergence of patterns and allow for a richer spectrum of instabilities. Moreover, it has been shown that an instability similar to the Turing mechanism can be obtained by perturbing a stable limit cycle [46] and that non-normal networks further enhance such instability [78]. Given the oscillatory behaviors of neurons [126, 127] and the non-normal nature of neural networks [39], an extension toward such direction would open the way to interesting new results and applications.

3.6 SM 1: The Routh-Hurwitz criterion

The Routh-Hurwitz criterion [123, 124, 125] is a well known tool of dynamical systems and control theory, allowing to prove the linear (in)stability of an equilibrium for a time invariant system[(7)]. Indeed, the latter relies on the spectral properties of the Jacobian matrix evaluated at the sought equilibrium, which ultimately accounts to determine the location in the complex plane of the roots of a suitable polynomial.

We hereby present the method using a fourth order polynomial, but it applies to any given order ones. Let thus $p(\lambda) = a\lambda^4 + b\lambda^3 + c\lambda^2 + d\lambda + e$ be a polynomial with real coefficients and assume $a > 0$; the Routh-Hurwitz criterion can be stated using the Hurwitz matrix associated to $p(\lambda)$ and then compute its leading principal minors or building the Routh-Hurwitz table and check the signs of the first column.

More precisely, a necessary condition, also known in the literature as Stodola criterion [145], for the roots of $p(\lambda)$ to have negative real part is that all the coefficients are positive:

$$a > 0, b > 0, c > 0, d > 0 \text{ and } e > 0 \tag{3.6.1}$$

while a sufficient condition is

$$a > 0, b > 0, bc - da > 0, d(bc - da) - eb^2 > 0 \text{ and } e > 0 \tag{3.6.2}$$

3.6.1 Application of the criterion to the stability of $p_1(\lambda)$

Let us now apply the Routh-Hurwitz criterion to determine the stability feature of the polynomial $p_1(\lambda)$ given by Equation (3.3.3), hereby rewritten

$$\begin{aligned} p_1(\lambda) &= a\lambda^4 + b\lambda^3 + c_1\lambda^2 + d_1\lambda + e_1 \\ &= \tau_u\tau_v\lambda^4 + (\tau_u + \tau_v)\lambda^3 + [1 - \tau_u g_v - \tau_v f_u]\lambda^2 + [-\mathrm{tr}(J_0)]\lambda + \det(J_0) \end{aligned}$$

Being the coefficients of $a = \tau_u\tau_v$ and $b = \tau_u + \tau_v$ positive, the Routh-Hurwitz criterion rewrites:

$$c_1 > 0, d_1 > 0, bc_1 - d_1 a > 0, d_1(bc_1 - d_1 a) - b^2 e_1 > 0 \text{ and } e_1 > 0$$

Replacing the definition of the coefficients in the above equation, we straightforwardly obtain the five conditions (3.3.8)–(3.3.12).

3.6.2 Application of the criterion to the stability of $p_\alpha(\lambda)$

Let us now study the instability character of $p_\alpha(\lambda)$, for some $\alpha > 1$ under the assumption of stability for $p_1(\lambda)$. We once again rely on the Routh-Hurwitz criterion. Let us thus rewrite

$$p_\alpha(\lambda) = a\lambda^4 + b\lambda^3 + c_\alpha\lambda^2 + d_\alpha\lambda + e_\alpha$$

where again $a = \tau_u\tau_v$, $b = \tau_u + \tau_v$ and

$$c_\alpha = 1 - \tau_u g_v - \tau_v f_u - \Lambda^{(\alpha)}(\tau_u D_v + \tau_v D_u) = c_1 - \Lambda^{(\alpha)}(\tau_u D_v + \tau_v D_u)$$

[(7)] To be more precise, the R-H criterion determines the position of the roots of a given polynomial in the complex plane. Then, it is applied to study the stability properties of linear systems.

$$\begin{aligned} d_\alpha &= -\mathrm{tr}(J_0) - \Lambda^{(\alpha)}(D_v + D_u) = d_1 - \Lambda^{(\alpha)}(D_v + D_u) \\ e_\alpha &= \det(J_0) + (D_v f_u + D_u g_v)\Lambda^{(\alpha)} + D_u D_v \left(\Lambda^{(\alpha)}\right)^2 \end{aligned}$$

and we emphasized the relation between the coefficients defined for $\alpha > 1$ and those for $\alpha = 1$.

As already observed, the coefficients a and b are positive. Moreover, because of the assumption on the stability of $p_1(\lambda)$, we also have $c_1 > 0$ and $d_1 > 0$. Finally, observing that $-\Lambda^{(\alpha)} \geq 0$ for all α we can conclude that

$$c_\alpha > 0 \text{ and } d_\alpha > 0 \quad \forall \alpha$$

The Routh-Hurwitz criterion ensures that $p_1(\lambda)$ is unstable if at least one of the following conditions is met

i) $bc_\alpha - d_\alpha a < 0$

ii) $d_\alpha(bd_\alpha - d_\alpha a) - b^2 e_\alpha < 0$

iii) $e_\alpha < 0$

Let us first show that condition i) is never met under the assumption of stability of $p_1(\lambda)$. From the definitions of the coefficients a, b, c_α and d_α we obtain

$$\begin{aligned} bc_\alpha - d_\alpha a &= (\tau_u + \tau_v)\left[c_1 - \Lambda^{(\alpha)}(\tau_u D_v + \tau_v D_u)\right] - \tau_u\tau_v\left[d_1 - \Lambda^{(\alpha)}(D_v + D_u)\right] \\ &= (\tau_u + \tau_v)c_1 - \tau_u\tau_v d_1 - \Lambda^{(\alpha)}\left[(\tau_u + \tau_v)(\tau_u D_v + \tau_v D_u) - \tau_u\tau_v(D_v + D_u)\right] \\ &= bc_1 - d_1 a - \Lambda^{(\alpha)}\left(\tau_u^2 D_v + \tau_v^2 D_u\right) \end{aligned}$$

We can now conclude that $bc_\alpha - d_\alpha a > 0$. Indeed, because of the stability of $p_1(\lambda)$, $bc_1 - d_1 a > 0$, and being $-\Lambda^{(\alpha)} > 0$ for all $\alpha > 1$, the claim easily follows.

Let us now consider condition ii) and look for the existence of $\alpha > 1$ such that

$$d_\alpha(bc_\alpha - d_\alpha a) - b^2 e_\alpha < 0$$

We firstly rewrite this equation by using the definition of the involved coefficients

$$\begin{aligned} \left(d_1 - \Lambda^{(\alpha)}(D_v + D_u)\right)\Big[(\tau_u + \tau_v)\left(c_1 - \Lambda^{(\alpha)}(\tau_u D_v + \tau_v D_u)\right) + \\ - \left(d_1 - \Lambda^{(\alpha)}(D_v + D_u)\right)\tau_u\tau_v)\Big] + \\ -(\tau_u + \tau_v)^2\left[\det(J_0) + (D_v f_u + D_u g_v)\Lambda^{(\alpha)} + D_u D_v\left(\Lambda^{(\alpha)}\right)^2\right] < 0 \end{aligned}$$

and then we reorganize the terms in the latter, to write it as a second order polynomial in the variable $\Lambda^{(\alpha)}$, hence

$$A\left(\Lambda^{(\alpha)}\right)^2 + B\Lambda^{(\alpha)} + C < 0$$

where, after some algebraic manipulation, we obtain

$$\begin{aligned} A &= (\tau_u D_v - \tau_v D_u)^2 \\ B &= -(\tau_u+\tau_v)(D_u+D_v)(1-\tau_u g_v - \tau_v f_u) + (\tau_u+\tau_v)\mathrm{tr}(J_0)(\tau_u D_v + \tau_v D_u) \\ &- 2\mathrm{tr}(J_0)(D_u+D_v)\tau_u\tau_v - (\tau_u+\tau_v)^2(D_v f_u + D_u g_v) \\ C &= d_1(bc_1 - ad_1) - b^2 e_1 \end{aligned}$$

The coefficient A is positive, as well as the coefficient C, under the assumption of stability for $p_1(\lambda)$. Then, the second order polynomial in $\Lambda^{(\alpha)}$ can exhibit negative values if and only if

$$B > 0 \text{ and } B^2 - 4AC > 0$$

that are exactly the conditions (3.3.14a) and (3.3.14b). Finally, an eigenvalue $\Lambda^{(\bar{\alpha})}$, $\bar{\alpha} > 1$, must exist such that

$$x_1 < \Lambda^{(\bar{\alpha})} < x_2$$

where x_1 and x_2 are the two real and negative roots of second order polynomial in $\Lambda^{(\alpha)}$.

Let us finally consider condition iii) and look for the existence of $\alpha > 1$ such that

$$e_\alpha = \det(J_0) + (D_v f_u + D_u g_v)\Lambda^{(\alpha)} + D_u D_v \left(\Lambda^{(\alpha)}\right)^2 < 0$$

This is a second order polynomial in the variable $\Lambda^{(\alpha)}$ whose leading coefficient, $D_u D_v$, is positive as well as the constant term, $\det(J_0)$, because of the stability of $p_1(\lambda)$. The polynomial can thus assume negative values if and only if

$$\begin{aligned} D_v f_u + D_u g_v &> 0 \\ (D_v f_u + D_u g_v)^2 - 4 D_u D_v \det(J_0) &> 0 \end{aligned}$$

namely, the conditions (3.3.15a) and (3.3.15b). Let us observe that the latter do not depend on τ_u and τ_v and indeed they are the classical conditions required for the Turing instability to arise [31]: an eigenvalue $\Lambda^{(\bar{\alpha})}$, $\bar{\alpha} > 1$, must exist such that

$$\eta_1 < \Lambda^{(\bar{\alpha})} < \eta_2$$

where η_1 and η_2 are the two real and negative roots of $e_\alpha = 0$.

3.7 SM 2: Non-relativistic limit of inertia-driven instability

In the main text, we have proven that a Turing instability sets up driven by the inertial times τ_u and τ_v if any couple of conditions Equations (3.3.14a) and (3.3.14b) or Equations (3.3.15a) and (3.3.15b) are satisfied. Let us observe that the latter do not depend on the inertial times and thus they can be satisfied for a suitable choice of the model parameters, also for $\tau_u = \tau_v = 0$. The same could not hold true for the former one, explicitly dependent on the inertial times. The aim of this section is thus to study the *non-relativistic limit* of the inertia-driven instability.

For sake of definitiveness, let us assume $\tau_v = \theta\tau_u$ for some $\theta > 0$, that is the inertial times approach zero with the same rate. The characteristic polynomial given by (3.3.3) can thus be rewritten as

$$p_\alpha(\lambda) = \theta\tau_u^2\lambda^4 + \tau_u(1+\theta)\lambda^3 + (1-\tau_u\hat{c}_\alpha)\lambda^2 + d_\alpha\lambda + e_\alpha \tag{3.7.1}$$

where we have used (3.3.4) to rewrite the coefficients of λ^4 and λ^3, and we have defined $\hat{c}_\alpha = g_v + \theta f_u + \Lambda^{(\alpha)}(D_v + \theta D_u)$ (see (3.3.5)). Let us observe that d_α and e_α do not depend on the inertial times (see (3.3.6) and (3.3.7)).

In the limit $\tau_u \to 0$ the latter results to be a singular polynomial, indeed its degree jumps from 4 once $\tau_u > 0$ to 2 for $\tau_u = 0$. Mathematically this means that two of the four roots of $p(\lambda)$ should diverge to infinity. By determining which ones and the followed path will allow to conclude about the non-relativistic limit of the inertia-driven instability.

Let us start by looking at the roots that remain in a bounded domain. To do this let us set[8] $\lambda = \lambda_0 + \tau_u\lambda_1 + \ldots$, impose $p(\lambda) = 0$ and by reordering the involved terms (see Equation (3.7.1)) according to the powers of τ_u, we eventually get

$$0 = p_\alpha(\lambda) = \lambda_0^2 + d_\alpha\lambda_0 + e_\alpha + \tau_u\left[(1+\theta)\lambda_0^3 + 2\lambda_0\lambda_1 - \hat{c}_\alpha\lambda_0 + d\lambda_1\right] + \mathscr{O}(\tau_u^2) \tag{3.7.2}$$

We can thus conclude that λ_0 is a solution of the second degree equation

$$\lambda_0^2 + d_\alpha\lambda_0 + e_\alpha = 0 \tag{3.7.3}$$

while λ_1 is obtained by solving

$$(1+\theta)\lambda_0^3 + 2\lambda_0\lambda_1 - \hat{c}_\alpha\lambda_0 + d\lambda_1 = 0 \tag{3.7.4}$$

In conclusion we get for the two roots

$$\lambda_\pm = \lambda_{0\pm} \pm \tau_u\frac{\hat{c}_\alpha - (1+\theta)\lambda_{0\pm}^2}{2\lambda_{0\pm} + d_\alpha} + \mathscr{O}(\tau_u^2) \tag{3.7.5}$$

where we denoted by $\lambda_{0\pm}$ the two roots of (3.7.3). Let us observe that the latter is the same second order equation one will obtain in the classical Turing framework; we have thus shown that in the non-relativistic limit two roots of the fourth degree characteristic polynomial $p(\lambda)$ converge to the roots of the second order polynomial one should deal with in the classical Turing case.

Let us now study the remaining two roots and determine their path toward infinity. As already stated, the characteristic polynomial is singular, one should thus resort to the *singular perturbation theory* [146]. Let us set $\lambda = \omega/\tau_u$ and evaluate $p_\alpha(\lambda)$ on $\lambda = \omega/\tau_u$, then we get

$$\begin{aligned} p_\alpha(\omega/\tau_u) &= \frac{\theta}{\tau_u^2}\omega^4 + \frac{1+\theta}{\tau_u^2}\omega^3 + \frac{1-\tau_u\hat{c}_\alpha}{\tau_u^2}\omega^2 + \frac{d_\alpha}{\tau_u}\omega + e_\alpha = \\ &= \frac{1}{\tau_u^2}\left[\theta\omega^4 + (1+\theta)\omega^3 + (1-\tau_u\hat{c}_\alpha)\omega^2 + d_\alpha\tau_u\omega + e_\alpha\tau_u^2\right] = \end{aligned}$$

[8] To lighten the notation, we will not explicitly write the dependence on $\Lambda^{(\alpha)}$; our results will thus hold for all $\alpha = 1, \ldots, n$.

$$= \frac{1}{\tau_u^2} q_\alpha(\omega) \tag{3.7.6}$$

where the fourth degree polynomial $q_\alpha(\omega)$ has been defined by the last equality. Let us observe that $p_\alpha(\lambda)$ vanishes if and only if $q_\alpha(\omega)$ does.

Let us now assume[9] $\omega = \omega_0 + \omega_1 \tau_u + \mathscr{O}(\tau_u^2)$, with $\omega_0 \neq 0$. By inserting the former into $q_\alpha(\omega)$ and by reordering the terms according to the powers of τ_u, we get

$$\begin{aligned} 0 = q_\alpha(\omega) &= \theta\omega_0^4 + (1+\theta)\omega_0^3 + \omega_0^2 + \\ &+ \tau_u \left[4\theta\omega_0^3\omega_1 + 3(1+\theta)\omega_0^2\omega_1 + 2\omega_0\omega_1 - \hat{c}_\alpha\omega_0^2 + d_\alpha\omega_0\right] + \\ &+ \mathscr{O}(\tau_u^2) \end{aligned} \tag{3.7.7}$$

Hence, $\omega_0 \neq 0$ solves the second degree equation

$$\theta\omega_0^2 + (1+\theta)\omega_0 + 1 = 0 \tag{3.7.8}$$

while ω_1 is obtained by solving

$$\omega_1 \left[4\theta\omega_0^2 + 3(1+\theta)\omega_0 + 2\right] = \hat{c}_\alpha\omega_0 - d_\alpha \tag{3.7.9}$$

In conclusion, if $\theta > 1$, we obtain

$$\lambda_+ = \frac{1}{\tau_u}\left[-\frac{1}{\theta} + \tau_u \frac{\hat{c}_\alpha + d_\alpha\theta}{\theta - 1} + \mathscr{O}(\tau_u^2)\right] \tag{3.7.10}$$

$$\lambda_- = \frac{1}{\tau_u}\left[-1 + \tau_u \frac{\hat{c}_\alpha + d_\alpha\theta}{1 - \theta} + \mathscr{O}(\tau_u^2)\right] \tag{3.7.11}$$

while, if $\theta < 1$, we obtain

$$\lambda_+ = \frac{1}{\tau_u}\left[-1 + \tau_u \frac{\hat{c}_\alpha + d_\alpha\theta}{1 - \theta} + \mathscr{O}(\tau_u^2)\right] \tag{3.7.12}$$

$$\lambda_- = \frac{1}{\tau_u}\left[-\frac{1}{\theta} + \tau_u \frac{\hat{c}_\alpha + d_\alpha\theta}{\theta - 1} + \mathscr{O}(\tau_u^2)\right] \tag{3.7.13}$$

In both cases we have that $\mathscr{R}\lambda_\pm \to -\infty$ in the limit $\tau_u \to 0$ and thus these two roots cannot modify the (un)stable character of the homogeneous equilibrium.

In conclusion, if τ_u and τ_v are positive and sufficiently small, then the onset of Turing instability is ruled out by the roots (3.7.5), i.e., those associated to the ones arising in the classical setting. Stated differently, if for $\tau_u > 0$ and $\tau_v > 0$, the instability can be initiated by conditions Equations (3.3.14a) and (3.3.14b), then by decreasing the inertial times the patterns fade out and disappear before reaching the limit and thus the transition is not abrupt.

In Figure 3.9 we report numerical results to complement the analytical findings described above. We selected two generic sets of parameter values $\gamma = 4.0$, $\beta = 0.6$, $\mu = 1.0$, $D_u = 2.2$ and $D_v = 0.2$ (left panel) and $\gamma = 4.0$, $\beta = 0.7$, $\mu = 1.15$, $D_u = 0.2$ and $D_v = 2.2$ (right panel), and we study the emergence of an inertia-driven instability as

[9] Let us stress once again that, to lighten the notation, we did not explicitly write the dependence on α.

a function of τ_u and τ_v. A black dot corresponds to the presence of the instability, while a white one to its absence. We can observe that the first set of parameters does not allow the onset of the instability for small enough values of the inertial times, indeed the black region, bounded below by condition (3.3.12) and above by condition (3.3.14b), does not intersect the axes $\tau_u = 0$ or $\tau_v = 0$. On the other hand the second set of parameters allows the existence of patterns for $\tau_0 = 0$ or $\tau_v = 0$, the black region (bounded above by condition (3.3.14b)) reaches the axes. This means that in this case also classical Turing patterns are allowed.

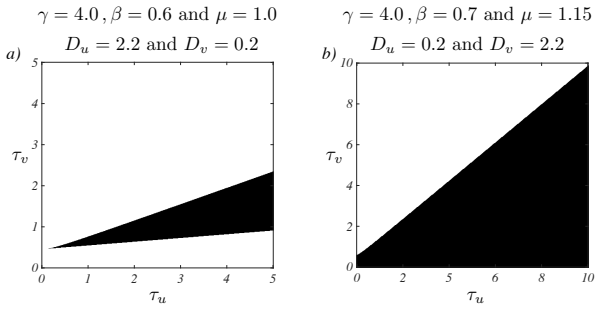

Figure 3.9: **Non-relativistic limit of inertia-driven instability for the *FHN* model.** For a fixed value of the model parameters γ, μ, β, D_u and D_v, we study the onset of inertia-driven instability (black regions) close to the homogeneous equilibrium $(u_i, v_i) = (0,0)$, $i = 1,\dots,n$, as a function of τ_u and τ_v. Panel a) corresponds to a setting where classical Turing instability cannot emerge, one can observe that the black region (bounded below by Equation (3.3.14b) and above by Equation (3.3.12)) does not touch the boundary $\tau_u = 0$ or $\tau_v = 0$. Panel b) refers to a choice of the parameters for which the classical Turing instability can emerge, indeed the black region (bounded above by Equation (3.3.12)) reaches the boundary $\tau_u = 0$ or $\tau_v = 0$.

3.8 SM 3: Existence of Turing instability in linear kinetic systems

Let us consider a linear kinetic system involving m chemical species interacting with each other "inside" the network nodes and allowed to diffuse across the available links under the constraint of finite propagation. Assuming the network to be composed by n nodes and to denote the concentration of the m species inside the i-th node by $\vec{x}_i = (x_1^{(i)}, \dots, x_m^{(i)})^\top \in \mathbb{R}_+^m$, then the main system (3.2.7) rewrites as

$$\frac{dx_j^{(i)}}{dt} + \tau_j \frac{d^2 x_j^{(i)}}{dt^2} = \sum_{l=1}^{m} a_{jl} x_l^{(i)} + D_j \sum_{k=1}^{n} L_{ik} x_j^{(k)} \tag{3.8.1}$$

$\forall i = 1,\dots,n$ and $\forall j = 1,\dots,m$, where $D_j > 0$ (resp. $\tau_j > 0$) is the diffusion coefficient (resp. the inertial time) for species $j = 1,\dots,m$; a_{jl} is the linear kinetic representing the action of species l on the j-th one and L_{ik} is the Laplacian matrix encoding the network links.

To handle this equation, we decompose $\vec{x}_i$ on the Laplacian's eigenbasis, namely $x_j^{(i)} = \sum_\alpha \hat{x}_j^\alpha \varphi_i^{(\alpha)}$, we insert the latter into Equation (3.8.1) and, making use of the orthonormality of the eigenvectors, we eventually obtain

$$\frac{d\hat{x}_j^\alpha}{dt} + \tau_j \frac{d^2\hat{x}_j^\alpha}{dt^2} = \sum_{l=1}^{m} a_{jl}\hat{x}_l^\alpha + D_j \Lambda^{(\alpha)} \hat{x}_j^\alpha \tag{3.8.2}$$

$\forall \alpha = 1,\dots,n$ and $\forall j = 1,\dots,m$.

The previous equation can be expressed in a compact form by introducing $\vec{\hat{x}}^\alpha = (\hat{x}_1^\alpha,\dots,\hat{x}_m^\alpha)^\top$, the matrix of the diffusive coefficients $\mathbf{D} = \mathrm{diag}(D_1,\dots,D_m)$, the inertial times matrix $\mathbf{T} = \mathrm{diag}(\tau_1,\dots,\tau_m)$, and the linear kinetic matrix $\mathbf{a}$

$$\frac{d^2\vec{\hat{x}}^\alpha}{dt^2} + \mathbf{T}^{-1}\frac{d\vec{\hat{x}}^\alpha}{dt} - \left(\mathbf{T}^{-1}\mathbf{a} + \Lambda^{(\alpha)}\mathbf{T}^{-1}\mathbf{D}\right)\vec{\hat{x}}^\alpha = 0 \quad \forall \alpha = 1,\dots n \tag{3.8.3}$$

Let us assume the matrix $\mathbf{A} := \mathbf{T}^{-1}\mathbf{a}$ to be diagonalizable, i.e., there exist an invertible matrix $\mathbf{P}$ such that $\mathbf{P}^{-1}\mathbf{A}\mathbf{P} = \mathrm{diag}(\kappa_1,\dots,\kappa_m)$. Hence, by defining $\vec{y} = \mathbf{P}^{-1}\vec{x}$, and recalling that $\Lambda^{(1)} = 0$, we can obtain from (3.8.3)

$$\frac{d^2\vec{\hat{y}}}{dt^2} + \mathbf{P}^{-1}\mathbf{T}^{-1}\mathbf{P}\frac{d\vec{\hat{y}}}{dt} - \mathrm{diag}(\kappa_1,\dots,\kappa_m)\vec{\hat{y}} = 0 \tag{3.8.4}$$

To make some analytical progress, let us assume all the inertial times to be equal, i.e., $\tau_j = \tau$ for all $j = 1,\dots,m$. We have thus to solve m second order linear ODEs with constant coefficients, depending each one on κ_j

$$\frac{d^2\hat{y}_j}{dt^2} + \frac{1}{\tau}\frac{d\hat{y}_j}{dt} - \kappa_j\hat{y}_j = 0 \quad \forall j = 1\dots,m \tag{3.8.5}$$

The associated characteristic polynomial is thus $\lambda^2 + \frac{1}{\tau}\lambda - \kappa_j = 0$, with roots $\lambda = -\frac{1}{2\tau} \pm \frac{1}{2\tau}\sqrt{1+4\tau^2\kappa_j}$. One can prove that if $\mathscr{R}\kappa_j < 0$ and $\tau|\mathscr{I}\kappa_j| < \sqrt{-\mathscr{R}\kappa_j}$ then $\mathscr{R}\lambda < 0$.

Assuming the linear kinetic does not admit cross inhibition terms, namely $a_{jl} \geq 0$ for all $j \neq l$, then we can conclude that the matrix $\mathbf{a}$ is non-negative and this implies that the matrix $\mathbf{A} = \mathbf{T}^{-1}\mathbf{a}$ is also non-negative, being $\mathbf{T}$ a diagonal matrix with positive entries on the diagonal. Let us define $\mathbf{C}^{(\alpha)} = -\Lambda^{(\alpha)}\mathbf{T}^{-1}\mathbf{D}$. Then, the latter is a diagonal matrix with non-negative elements on the diagonal, being $\Lambda^{(\alpha)} \leq 0$, $D_j > 0$ and $\tau > 0$. We can thus conclude invoking the following result proved in [138]: if $\mathbf{A}$ is stable, i.e., its spectral abscissa[10] is negative, then also $\mathbf{A} - \mathbf{C}$ is stable for all diagonal matrix $\mathbf{C}$ with non-negative diagonal terms. Indeed, assume $\mathbf{A} = \mathbf{T}^{-1}\mathbf{a}$ to be stable, i.e. $\max_j \mathscr{R}\kappa_j < 0$, and moreover assume to fix τ such that $\tau|\mathscr{I}\kappa_j| < \sqrt{-\mathscr{R}\kappa_j}$ holds true. Let us observe that, if $\mathbf{T}^{-1}\mathbf{a}$ has a real spectrum, the latter relation is always satisfied. This implies that the homogeneous solution for the aspatial system is also stable. The Turing instability emerges if one can find α such that Equation (3.8.3) admits an unstable solution.

[10] The spectral abscissa of a matrix $\mathbf{A}$ is defined as $\max(\mathscr{R}(\sigma(A)))$, i.e., it is the largest real part of its spectrum.

Let $\rho_j^{(\alpha)}$, $j = 1,\dots,m$, be the eigenvalues of $\mathbf{A} - \mathbf{C}^{(\alpha)} = \mathbf{T}^{-1}\mathbf{a} + \Lambda^{(\alpha)}\mathbf{T}^{-1}\mathbf{D}$. Then, the above quoted result [138] ensures that $\mathscr{R}\rho_j^{(\alpha)} < 0$ for all $j = 1,\dots,m$ and $\alpha = 1,\dots,n$. Because $\mathbf{T}^{-1}\mathbf{D}$ is a diagonal matrix, the diagonal elements of $\mathbf{A} - \mathbf{C}^{(\alpha)}$ are translated to the left, while the off-diagonal elements do not vary. Invoking the Geršgorin circle theorem [147], we can take the elements of $\mathbf{T}^{-1}\mathbf{D}$ sufficiently large, i.e., $D_j \gg 1$ or $\tau \ll 1$, such that $\tau|\mathscr{I}\rho_j^{(\alpha)}| < \sqrt{-\mathscr{R}\rho_j^{(\alpha)}}$ for all $j = 1,\dots,m$, $\alpha = 1,\dots,n$. We can thus conclude that the relation dispersion associated to Equation (3.8.3) is always negative and thus the Turing instability cannot develop. In conclusion, linear kinetic systems without cross inhibition and equal (small) inertial times, or large diffusion coefficients, cannot exhibit Turing instability in the relativistic framework. The necessity of the latter assumptions remains an open question that we believe goes beyond the scope of this work.

Chapter 4

Non-reciprocal interactions enhance heterogeneity

Diffusion is the main driver of the Turing mechanism, which is in fact also known as diffusion-driven instability. However, experimental evidence shows that pattern formation happens as well in systems without diffusion [148, 149]. It would be logical to think that it makes no sense to talk about Turing pattern formation when no diffusion takes place. But, as explained in Chapter 1, the Turing framework can be looked from different angles. If we consider as a main feature the fact that the equilibrium, i.e., the homogeneous stable state, is disrupted by any interaction with the surroundings, then, even when such interactions are non-diffusive, we can consider the phenomenon within the Turing paradigm. Of course, we cannot directly talk about Turing patterns, but the similarity with the Turing mechanism is, at least according to our vision, undeniable.

Pattern formation for systems without diffusion have been studied by Cencetti and collaborators [66], where it was shown that a system with local and non-local interactions could be rewritten in a form that resembles reaction-diffusion systems, even though no diffusion takes place. Let us remark that in the literature there are several Laplacian operators, each one used to model different phenomena; such point is discussed in Section 4.13, at the end of the Chapter. Pattern formation in systems with non-local interactions have been also studied on continuous support [150, 151, 152], however, it is important to notice that in these works non-local interactions are additional to diffusion. When the support is a complex network, we are able to obtain patterns even without diffusion, which makes the latter a natural embedding for this framework. The following paper extends the framework of [66], but with the difference that the non-local interactions are non-reciprocal. Besides extending the previous theory and corroborating it with several numerical examples, we also prove the important claim stating that non-reciprocal interactions *tout court* always enhance the loss of stability, hence they promote heterogeneity. It would be an important step to have an experimental proof of this statement and that was the motivation to start a project, currently ongoing, with our colleagues in Catania. In fact, for a previous work regarding

remote synchronization [153], they have developed an experimental set up of Stuart-Landau oscillators coupled through a normalized Laplacian, which is the same kind of coupling that we used for our theoretical study. In the coming weeks we will be able to test our theoretical predictions through their experimental apparatus and, hopefully, being able to further validate our theory.

T. Carletti & R. Muolo. Chaos, Solitons & Fractals 164, 112638 (2022) [154]
This article is not open access, but it is freely available as a pre-print.

Abstract

We study a process of pattern formation for a generic model of species anchored to the nodes of a network where local reactions take place, and that experience non-reciprocal non-local long-range interactions, encoded by the network directed links. By assuming the system to exhibit a stable homogeneous equilibrium whenever only local interactions are considered, we prove that such equilibrium can turn unstable once suitable non-reciprocal non-local long-range interactions are allowed for. Stated differently, we propose sufficient conditions allowing for patterns to emerge using a non-symmetric coupling, while initial perturbations about the homogeneous equilibrium always fade away assuming reciprocal coupling, namely the latter is stable. The instability, precursor of the emerging spatio-temporal patterns, can be traced back, via a linear stability analysis, to the complex spectrum of an interaction non-symmetric Laplace operator. The proposed theory is then applied to several paradigmatic dynamical models largely used in the literature to study the emergence of patterns or synchronization. Taken together, our results pave the way for the understanding of the many and heterogeneous patterns of complexity found in ecological, chemical or physical systems composed by interacting parts, once no diffusion takes place.

4.1 Introduction

We live in an interconnected world [86, 155] where complex patterns [109] spontaneously emerge from the intricate web of nonlinear interactions existing between the basic units by which the system under study is made of [107]. These emergent structures can be found in the synchronized activity of neurons, resulting from the exchange of electrochemical signals via synapses [42, 41], as well as the geometric visual hallucinations product of the retinocortical map linking the retina and the striate cortex [156, 157]. Such self-organized structures can also manifest in groups of fireflies that flash at unison, each one observing the behavior of their close neighbors [158]. Or they can materialize as the striped or spotted motifs on the skin of the zebrafish *Danio rerio*, due to the long-range interactions between melanophores and xantophores, without requiring diffusion nor any kind of cell motion [148, 149].

The latter phenomena, as well as many other ones modeled within a similar framework of local reactions and long-range interactions without displacement of the reacting

species, cannot be ascribed to a Turing instability [4], a widely used paradigm for pattern formation. Indeed the latter requires a diffusive process, whereas the common key factor linking the above examples is the immobility of the reacting species and the existence of a web of long-range interactions due to some signal propagation.

In this work, we set the theoretical basis for the understanding of self-organization in systems without diffusing species where asymmetric long-range interactions play a pivotal role. Network science [86, 155] provides a natural framework where to study such phenomena. Indeed, local interactions can be described by a dynamical system evolving on each node, that represents a portion of physical space, say a natural habitat or a chemical reactor, large enough to contain enough species to describe their evolution with a nonlinear ordinary differential equation. On the other hand, non-local long-range interactions can be modeled by links connecting the nodes of the network, allowing thus species anchored to each distinct node to communicate by exchanging some generic signals. Let us observe that our definition of local and long-range dynamics can differ from the one sometimes used in the literature, that considers local dynamics to be related to the in-node processes but also to the interactions with species sitting in nodes at distance one, i.e., first neighborhood, while long-range interactions are used to describe far away interacting nodes, i.e., distances larger than two. For this reason, in this work we name the latter process non-local long-range interaction; let us notice, however, that when it will be clear from the context, we will simply use long-range interactions. Let us finally stress that the latter do not involve displacement of the reacting species, for this reason the theory hereby developed applies to systems without diffusion. An interesting example is the web of chemical light-triggered reactions obtained by connecting reactors where the local concentration of chemicals, i.e., in each node, determines the amount of light to be put onto connected distant nodes, i.e., long-range interaction. Chemicals do not leave any nodes but they interact at distance [61, 62, 63].

In the aforementioned examples, the system converges to a homogeneous solution, being stationary or time varying, once only local interactions are taken into account, i.e., long-range ones are silenced, while heterogeneous solutions spontaneously emerge in presence of a suitable web of interactions among the units. Let us observe that the existence of an attracting homogeneous solution for the decoupled system is a natural and largely assumed working hypothesis, see for instance [4] in the framework of Turing instability or [44] for synchronization.

A preliminary result in this direction has been proposed in [159] with the assumption of reciprocal non-local interactions and treating the latter in a mean-field setting. There, authors have been able to prove that the stable homogeneous solution, existing once the long-range interactions have been silenced, can turn unstable by introducing a suitable symmetric non-local coupling and eventually lead to the emergence of a spatially (and temporally) dependent solution. The aim of the present work is to make one step forward by studying the general case of *non-reciprocal* interactions and their impact on the system outcome. Indeed, the interactions existing among the constituting units are often not symmetric; this is the case of plant-animal mutualistic networks [160, 68], the specific example of sheep and deer [161] or the case of olfactory receptor neurons in the Drosophila antenna [162], just to mention a few.

Anticipating our conclusion, we claim that the diversity and heterogeneity of patterns observed in nature, being associated to spatial or temporal non-homogeneous

states, is enhanced by non-reciprocal long-range interactions. The onset of the instability, precursor of the pattern, can be detected with a linear stability analysis, providing a condition on the complex spectrum of a non-symmetric consensus Laplacian operator resulting from the mean-field ansatz, as we will hereafter explain. The proposed framework is general enough to cover systems of any dimension $d \geq 2$ displaying a fixed-point or a limit cycle homogeneous solution, once we silence the long-range interactions, by proving the existence of a suitable non-reciprocal web of interactions driving the emergence of patterns while the latter can never exist in the case of symmetric support. To emphasize the relevance of the proposed theory to many and different research domains, we applied the developed theory to several paradigmatic models largely used in the literature to study the emergence of patterns or synchronization. In conclusion, the proposed mechanism provides the way for alternative routes to pattern formation, beyond the Turing one [4, 31], and to the emergence of desynchronized states [44], suitable for all phenomena where diffusion is not the main driver for the heterogeneity of the complex patterns seen in nature, opening thus new possibilities for modeling ecological, chemical and physical interacting systems, endowed with non-reciprocal couplings and without diffusing species.

4.2 The model

Let us consider a dynamical system composed by n identical units and assume the d-dimensional vector $\vec{x}_i(t) = (x_{i_1}(t), \dots, x_{i_d}(t))^\top$ to represent the state of the i-th copy, for $i = 1, \dots, n$. The isolated systems are described by an ordinary differential equation[(1)], resulting from the assumption of a "well stirred" distribution of species inside each node

$$\dot{\vec{x}}_i = \vec{F}(\vec{x}_i) \quad \forall i = 1, \dots, n \tag{4.2.1}$$

where $\vec{F}$ is a generic nonlinear function responsible for the local interactions, i.e., depending on the species anchored to the same node. Let us now allow each system to possess non-local interactions, i.e., the growth rate of the system anchored at node i is influenced by some nonlinear function of the amount of species in distant nodes. Moreover, we assume the latter to be described by

$$\dot{\vec{x}}_i = \frac{1}{k_i^{(in)}} \sum_{j=1}^{n} A_{ij} \vec{F}(\vec{x}_i, \vec{x}_j) \quad \forall i = 1, \dots, n \tag{4.2.2}$$

where A_{ij} is the (possibly weighted) non-symmetric adjacency matrix encoding the long-range interactions, i.e., $A_{ij} = 1$ if and only if node j influences node i. Let $k_i^{(in)} = \sum_j A_{ij}$ be the in-degree of node i and observe that we allow $A_{ii} = 1$, thus the in-degree takes into account also the possible self-loops. Finally, $\vec{F}(\vec{x}_i, \vec{x}_j)$ is a nonlinear function that describes the effect of the j-th system on the i-th one. Moreover, we require $\vec{F}(\vec{x}_i, \vec{x}_i) = \vec{F}(\vec{x}_i)$, namely the self-interaction is represented by the original nonlinear function $\vec{F}$ describing the evolution of the isolated systems. This is a natural

[(1)] Let us observe that the theory hereby developed could be straightforwardly adapted to the case of discrete time, where, i.e., the ODE is replaced with a finite differences system.

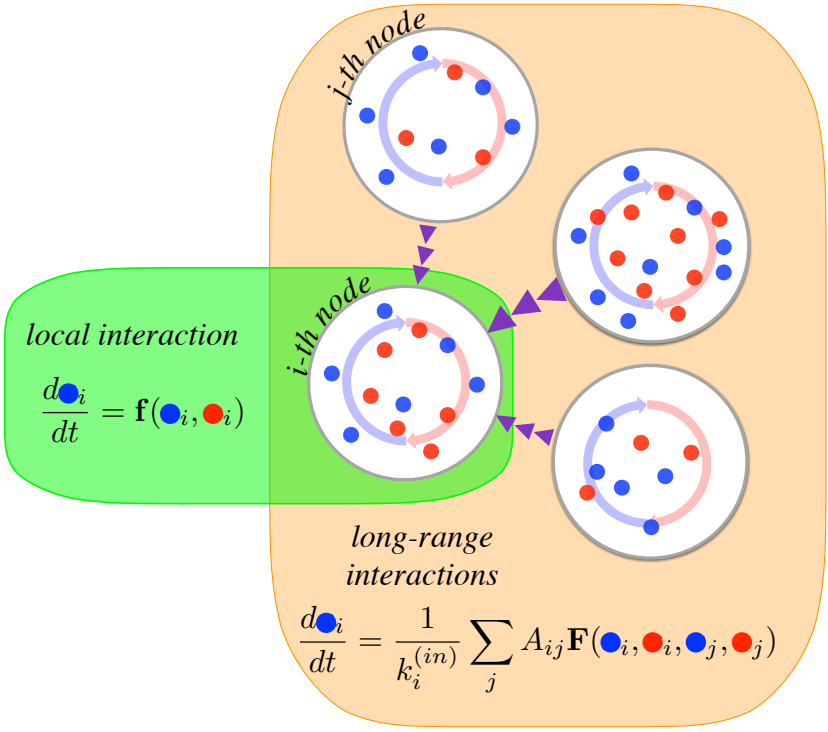

Figure 4.1: A schematic visual representation of the model (4.2.2). Nodes (large white circles) contain two species (blue and red dots). We then focus on the growth rate of the "blue" species in the i-th node, that results from two terms. The first one is the local reaction $\vec{F}$, represented by the light-blue and light-red curved arrows, involving only "blue" and "red" species indexed by i (green oval). The second contribution arises from the long-range interactions $\vec{F}$, represented as violet triangles pointing from each nearby node to the i-th one. The average of these terms impacts the growth rate of the "blue" species in node i (orange oval).

assumption allowing to recover the initial system (4.2.1) composed by isolated units, i.e., once we set $\mathbf{A} = \mathbf{I}_n$, the latter being the $n \times n$ identify matrix[(2)]. Let us observe that the right-hand side of (4.2.2) can be rewritten as the average of the interactions perceived by node i, $\langle \vec{F}(\vec{x}_i, \cdot) \rangle = \sum_j A_{ij} \vec{F}(\vec{x}_i, \vec{x}_j)/k_i^{(in)}$, hence describing the mean-field ansatz. Finally, let us stress that species cannot move across nodes: the long-range interactions are thus mediated by some generic signals, as we have proposed in the introduction and we will discuss in the following. The model (4.2.2) describes thus local interactions coupled with long-range ones without the need of diffusion. This is in contrast with the fundamental assumption of Turing instability [4, 31], where diffusion plays a key role, or in the synchronization based on diffusive-like couplings [44, 111] (see Figure 4.1 for a schematic representation of the proposed model).

[(2)]Let us observe that this condition has been already used in [159] and it is related to the one adopted in [45]

By defining the matrix

$$\mathscr{L}_{ij} = \frac{A_{ij}}{k_i^{(in)}} - \delta_{ij} \tag{4.2.3}$$

and using the property of the function $\vec{F}$, we can rewrite Equation (4.2.2) as

$$\dot{\vec{x}}_i = \vec{F}(\vec{x}_i) + \sum_{j=1}^{n} \mathscr{L}_{ij}\vec{F}(\vec{x}_i,\vec{x}_j) \quad \forall i = 1,\dots,n \tag{4.2.4}$$

Once the long-range interactions are silenced and each node interacts only with itself, then $\mathscr{L} = 0$ and thus Equation (4.2.4) reduces to Equation (4.2.1). Let us observe that, in the case of reciprocal interactions, the above defined matrix $\mathscr{L}$ corresponds to the *consensus Laplace* operator [163, 164, 165, 166], also named *reactive Laplace* matrix in [159], whose spectrum is real and non-positive. In the case under scrutiny, involving non-reciprocal interactions, the spectrum is generally complex but one can prove that $\Lambda^{(1)} = 0$ is still an eigenvalue associated to the uniform eigenvector $\vec{\varphi}^{(1)} \sim (1,\dots,1)^\top$. Moreover, the Geršgorin circle theorem [167] allows to prove that the real part of the spectrum of $\mathscr{L}$ is contained in the strip $[-2,0]$ in the complex plane, hence $\mathscr{L}$ is stable having all the eigenvalues with a negative real part, except for the one equal to 0. Observe that by using a symmetric network the eigenvalues are real and non-positive, even if the consensus Laplacian is not symmetric (see SM 4.5). Let us stress that the operator $\mathscr{L}$ results from the mean-field assumption and not from any kind of diffusive-like process as in the cases where the combinatorial Laplace operator arises because of Fick's law.

Let us assume $\vec{x}_i(t) = \vec{s}(t)$, $i = 1,\dots,n$, to be a solution of the initial system (4.2.1); then, because of the above hypothesis on $\vec{F}$ and of the definition of $k_i^{(in)}$, it is also a spatially-dependent, i.e., node-dependent, solution of Equation (4.2.4). To study the bifurcation of patchy solutions from the stable homogeneous one, $\vec{x}_i(t) = \vec{x}^*(t)$ for all i, we consider a node dependent perturbation about the latter solution, i.e., $\vec{\zeta}_i(t) = \vec{x}_i(t) - \vec{x}^*(t)$, whose evolution can be studied by inserting it into Equation (4.2.4) and then keeping only first order terms, assumed to be small enough. Hence we obtain for all $i = 1,\dots,n$

$$\dot{\vec{\zeta}}_i = [\mathbf{J}_1(\vec{x}^*(t)) + \mathbf{J}_2(\vec{x}^*(t))]\,\vec{\zeta}_i + \sum_{j=1}^{n} \mathscr{L}_{ij}\mathbf{J}_2(\vec{x}^*(t))\vec{\zeta}_j \tag{4.2.5}$$

where we have introduced the Jacobian matrices $\mathbf{J}_1(\vec{x}^*) = \partial_{\vec{x}_1}\vec{F}(\vec{x}_1,\vec{x}_2)|_{(\vec{x}^*,\vec{x}^*)}$, i.e., the derivatives are computed with respect to the first group of variables, and $\mathbf{J}_2(\vec{x}^*) = \partial_{\vec{x}_2}\vec{F}(\vec{x}_1,\vec{x}_2)|_{(\vec{x}^*,\vec{x}^*)}$, i.e., the derivatives are performed with respect to the second group of variables. In both cases the derivatives are evaluated on the reference solution $\vec{x}^*(t)$. The latter equation encodes n linear systems involving matrices with size $d \times d$. To progress with the analytical understanding, we assume the existence of an eigenbasis of right eigenvectors[3] $\vec{\varphi}^{(\alpha)}$, $\alpha = 1,\dots,n$for $\mathscr{L}$ and then, following the

[3]Let us observe that this hypothesis can be relaxed (see SM 4.6) and one could obtain similar results by invoking the Jordan block decomposition as done in [74] in the case of synchronization. For sake of definitiveness we preferred to present our results under this restrictive assumption, but allowing for straightforward analysis.

ideas pioneered by [4, 44], we project the former equation onto each eigendirection, i.e., $\vec{\zeta}_i = \sum_\alpha \vec{\xi}_\alpha \varphi_i^{(\alpha)}$, to eventually obtain (see SM 4.6)

$$\dot{\vec{\xi}}_\alpha = \left[\mathbf{J}(\vec{x}^*(t)) + \mathbf{J}_2(\vec{x}^*(t))\Lambda^{(\alpha)}\right]\vec{\xi}_\alpha \quad \forall \alpha = 1,\dots,n \tag{4.2.6}$$

where $\mathbf{J} = \mathbf{J}_1 + \mathbf{J}_2$ and $\Lambda^{(\alpha)}$ is the eigenvalue relative to the eigenvector $\vec{\varphi}^{(\alpha)}$. The above equation enables us to infer the (in)stability of the homogeneous solution, $\vec{x}^*(t)$, by studying the Master Stability Function [44, 168], namely the largest Lyapunov exponent of Equation (4.2.6).

To make one step further in the study of the problem, let us hypothesize that each isolated system converges to the same stationary point, i.e., the stable homogeneous solution is time-independent, $\vec{x}^*(t) = \vec{x}^*$. Hence Equation (4.2.6) rewrites for all $\alpha = 1,\dots,n$, as

$$\dot{\vec{\xi}}_\alpha = \left[\mathbf{J}(\vec{x}^*) + \mathbf{J}_2(\vec{x}^*)\Lambda^{(\alpha)}\right]\vec{\xi}_\alpha := \mathbf{J}^{(\alpha)}\vec{\xi}_\alpha \tag{4.2.7}$$

where the constant matrix $\mathbf{J}^{(\alpha)}$ has been defined by the latter equation. The homogeneous solution will prove unstable to spatially dependent perturbations if (at least) one eigenmode $\hat{\alpha}$ exists for which the largest real part of the eigenvalues, λ_i, of $\mathbf{J}^{(\hat{\alpha})}$ is positive, the latter being known in the literature with the name of *dispersion relation*, hereby denoted by $\lambda_\alpha = \max_{i=1,\dots,d} \mathscr{R}\lambda_i(\Lambda^{(\alpha)})$, where we emphasized the dependence of the latter on the spectrum of the Laplace matrix. Let us observe that the positivity of the dispersion relation initiates the instability but it does not determine the final outcome of the system. Convergence to other homogeneous solutions is possible if $\vec{F}$ possesses several zeros, namely if the system (4.2.1) exhibits multiple equilibria. However, this kind of solution can arise with lower probability with respect to a patchy one; indeed, assuming to act on a parameter in Equation (4.2.4), then a homogeneous zero of the latter generically bifurcates in an heterogeneous one.

4.3 Results

For sake of pedagogy and to be able to determine closed and manageable analytical formulae, let us assume the local systems to be 2 dimensional, i.e., $d = 2$ in Equation (4.2.1). Let us however emphasize that, as we will discuss later on, our results go beyond this simplified framework and we can indeed prove that non-reciprocal interactions can drive the emergence of heterogeneous patterns in any dimension $d \geq 2$, even when this is not possible using a symmetric coupling. Assuming thus $d = 2$, being the eigenvalues of $\mathbf{J}^{(\alpha)}$ the solutions of the second order equation

$$\lambda_i^2 - \mathrm{tr}\mathbf{J}^{(\alpha)}\lambda_i + \det\mathbf{J}^{(\alpha)} = 0 \tag{4.3.1}$$

we can adapt to the present case the analysis done in [38, 40] and express the condition for the onset of instability, i.e., $\lambda_{\hat{\alpha}} > 0$, as follows

$$\exists \hat{\alpha} > 1 \text{ st } (\mathscr{I}\Lambda^{(\hat{\alpha})})^2 S_2(\mathscr{R}\Lambda^{(\hat{\alpha})}) \leq -S_1(\mathscr{R}\Lambda^{(\hat{\alpha})}) \tag{4.3.2}$$

where $S_2(\kappa)$, resp. $S_1(\kappa)$, is a second, resp. fourth, degree polynomial in κ (see SM 4.6 for more details and the explicit form of S_1 and S_2 in terms of the model parameters).

To illustrate the potential of the theory let us consider several examples of dynamical systems largely used in the literature as paradigmatic models for synchronization or patterns emergence.

4.3.1 The Brusselator model

Let us consider the Brusselator model [95, 169], often invoked in the literature as a paradigmatic nonlinear reaction scheme for studying self-organized phenomena, synchronization [78], Turing patterns [31, 34, 36, 115, 40] and oscillation death [170, 171]. The key feature of the model is the presence of two species, reacting via a cubic nonlinearity

$$\begin{cases} \dot{u} &= 1-(b+1)u+cu^2v \\ \dot{v} &= bu-cu^2v \end{cases} \tag{4.3.3}$$

where $b>0$ and $c>0$ act as tunable model parameters. One can easily realize the existence of a unique equilibrium $u^*=1$ and $v^*=b/c$, that results stable if the Jacobian of the reaction part evaluated on the equilibrium, $\mathbf{J}_{\text{Bxl}}=\left(\begin{smallmatrix} b-1 & c \\ -b & -c \end{smallmatrix}\right)$, has a negative trace, $\text{tr}\mathbf{J}_{\text{Bxl}}=b-c<1$, and a positive determinant, $\det\mathbf{J}_{\text{Bxl}}=c>0$.

The model can be expressed in the framework presented in the previous section by setting $\vec{x}_i=(u_i,v_i)$ and $\vec{F}(\vec{x}_i)=(1-(b+1)u_i+cu_i^2v_i, bu_i-cu_i^2v_i)$, for $i=1,\dots,n$, to denote the n isolated systems. For sake of concreteness let us consider the coupling given by

$$\vec{F}(\vec{x}_i,\vec{x}_j)=(1-(b+1)u_i+cu_i^2v_i, bu_j-cu_i^2v_i)$$

where $\vec{x}_j=(u_j,v_j)$. Such function clearly satisfies the constraint $\vec{F}(\vec{x}_i,\vec{x}_i)=\vec{F}(\vec{x}_i)$, hence Equation (4.2.2) becomes (see SM 4.7)

$$\begin{cases} \dot{u}_i &= 1-(b+1)u_i+cu_i^2v_i \\ \dot{v}_i &= bu_i-cu_i^2v_i+b\displaystyle\sum_{j=1}^{n}\mathscr{L}_{ij}u_j \end{cases} \qquad \forall i=1,\dots,n \tag{4.3.4}$$

namely, a set of n Brusselator models (4.3.3) coupled via long-range connections in the second variable.

Given the above coupling we can explicitly compute the polynomials $S_1(\kappa)$ and $S_2(\kappa)$ as a function of the model parameters (see SM 4.7) and characterize the instability region defined by (4.3.2) as reported in panel a) of Figure 4.2, where we show in the complex plane $(\mathscr{R}\Lambda,\mathscr{I}\Lambda)$ the regions for which the instability condition is satisfied (gray), for a given set of parameters. Patterns emerge if there exists at least one eigenvalue $\Lambda^{(\hat{\alpha})}$ belonging to this region. For sake of simplicity, we hereby assume the non-reciprocal interactions to be described by a directed Erdős-Rényi network made of 50 nodes and the probability to create a directed link to be 0.05. The symmetric coupling is obtained by considering all the existing links to be reciprocal ones and, as already noticed, the eigenvalues are negative real numbers. In conclusion, if the model parameters shape an instability region that does not intersect the real negative axis (see panel a) in Figure 4.2), then only an asymmetric coupling can drive the instability and the ensuing (oscillatory) patterns (see panel b) in Figure 4.2), while this is impossible

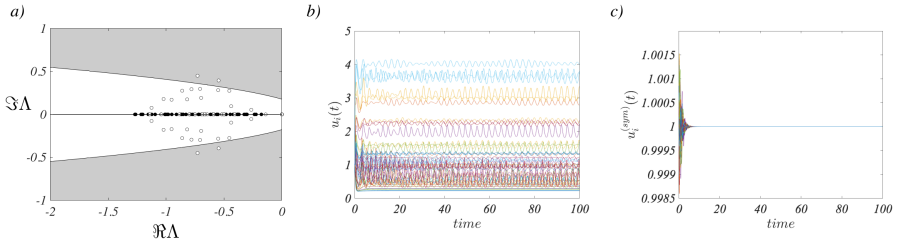

Figure 4.2: Instability region and patterns for the Brusselator model. In panel a), we report the region of the complex plane $(\mathscr{R}\Lambda, \mathscr{I}\Lambda)$ for which the instability condition is satisfied (gray). For the chosen parameters values ($b = 4.3$ and $c = 5.0$), we can observe that the instability region does not intersect the real axis and thus only a non-reciprocal coupling can exhibit complex eigenvalues (white dots), entering into the instability region and thus initiating the pattern as shown in panel b), where we report $u_i(t)$ vs. t starting from initial conditions close to the stable equilibrium, $u^* = 1$. Any symmetric coupling determines real eigenvalue (black dots in panel a)) that cannot give rise to the instability, as shown in panel c), where we report $u_i(t)$ vs. t starting from the same initial conditions used in panel b). The underlying coupling is obtained with a directed Erdős-Rényi network with $n = 50$ nodes and a probability for a directed link to exist between two nodes is $p = 0.05$.

for any web of reciprocal long-range interactions (see panel c) in Figure 4.2) and the system solution converges toward the homogeneous solution[(4)].

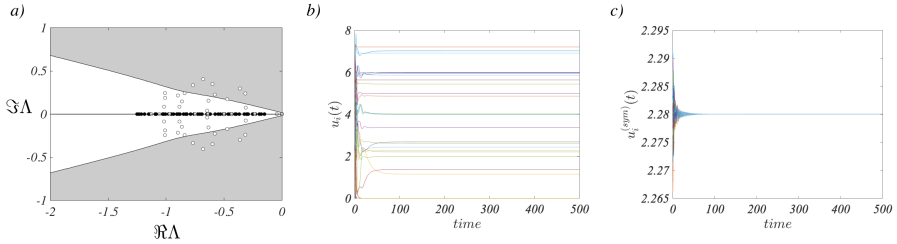

Figure 4.3: Instability region and patterns for the Mimura-Murray model. In panel a), we report the region of the complex plane $(\mathscr{R}\Lambda, \mathscr{I}\Lambda)$ for which the instability condition is satisfied (gray). For the chosen parameters values ($a = 35$, $b = 15$, $c = 20$ and $d = 2/5$), we can observe that the instability region does not intersect the real axis and thus only non-reciprocal coupling can exhibit complex eigenvalues (white dots) entering into the instability region and thus initiating the pattern as shown in panel b), where we report $u_i(t)$ vs. t starting from initial conditions close to the stable equilibrium, $u^* \sim 2.28$, $v^* \sim 3.20$. Any symmetric coupling determines real eigenvalues (black dots in panel a)) that cannot give rise to the instability, as shown in panel c), where we report $u_i(t)$ vs. t starting from the same initial conditions used in panel b). The underlying coupling is obtained with a directed Erdős-Rényi network with $n = 50$ nodes and a probability for a directed link to exist between two nodes is $p = 0.05$.

[(4)]Throughout the work, the numerical simulations have been performed by initializing the system δ-close to the homogeneous equilibrium by drawing uniformly random perturbations in $(-\delta, \delta)$. Then its time evolution has been numerically simulated using a 4-th order Runge-Kutta method over a time span of the order of $-\log\delta / \max_\alpha \lambda_\alpha$, namely sufficiently long to (possibly) increase the δ-perturbation up to a macroscopic size.

4.3.2 The Mimura-Murray model

The second model we consider is the Mimura-Murray system [172, 31, 46, 173]. It also involves two reacting species, that can be associated to prey and predator, whose densities denoted by u and v evolve via the nonlinear system of ODEs

$$\begin{cases} \dot{u} &= u\left(\dfrac{a+bu-u^2}{c}-v\right) \\ \dot{v} &= v(u-(1+dv)) \end{cases} \tag{4.3.5}$$

where a,b,c and d are positive parameters. The model possesses 6 equilibria, whose stability and positivity depend on the value of the chosen parameters. We here focus on the fixed point (u^*,v^*)

$$u^* = 1+\frac{bd-2d-c+\sqrt{\Delta}}{2d} \text{ and } v^* = \frac{bd-2d-c+\sqrt{\Delta}}{2d^2} \tag{4.3.6}$$

where

$$\Delta = (bd-2d-c)^2+4d^2(a+b-1)$$

and assume $a=35$, $b=15$, $c=20$ and $d=0.4$, which in turn implies $(u^*,v^*)\sim(2.28,3.20)$. The Jacobian matrix evaluated at the fixed point reads $\mathbf{J}_{\mathrm{MM}}\sim\left(\begin{smallmatrix}1.19 & -2.28\\ 3.20 & -1.28\end{smallmatrix}\right)$, hence, $\det\mathbf{J}_{\mathrm{MM}}>0$ and $\mathrm{tr}\mathbf{J}_{\mathrm{MM}}<0$ and the fixed point is a stable equilibrium.

Let us consider the following long-range coupling

$$\vec{F}(\vec{x}_i,\vec{x}_j) = \left(u_i\left(\frac{a+bu_j-u_i^2}{c}-v_j\right), v_i(u_j-(1+dv_i))\right)$$

where $\vec{x}_i=(u_i,v_i)$ and $\vec{x}_j=(u_j,v_j)$. Let us observe that the present coupling contains nonlinear terms in the variables u_iv_j and u_jv_i, while in the previous section we dealt with a linear term. Let $\vec{F}(\vec{x}_i)=\left(u_i\left(\frac{a+bu_i-u_i^2}{c}-v_i\right), v_i(u_i-(1+dv_i))\right)$, then $\vec{F}(\vec{x}_i,\vec{x}_i)=\vec{F}(\vec{x}_i)$, and we are thus in the framework of Equation (4.2.2) that now can be rewritten as (see SM 4.8)

$$\begin{cases} \dot{u}_i &= u_i\left(\dfrac{a+bu_i-u_i^2}{c}-v_i\right)+\dfrac{b}{c}u_i\displaystyle\sum_{j=1}^n\mathscr{L}_{ij}u_j-u_i\sum_{j=1}^n\mathscr{L}_{ij}v_j \\ \dot{v}_i &= v_i(u_i-(1+dv_i))+v_i\displaystyle\sum_{j=1}^n\mathscr{L}_{ij}u_j \end{cases} \quad \forall i=1,\dots,n \tag{4.3.7}$$

One can realize that we are dealing with n Mimura-Murray models (4.3.5) coupled via nonlinear long-range connections in both variables.

As explained in the SM 4.8, one can numerically determine the instability region by evaluating the polynomials $S_1(\kappa)$ and $S_2(\kappa)$ as a function of the model parameters (see panel a) of Figure 4.3). We can observe that the instability region does not intersect the negative real axis and thus only complex eigenvalues, associated to non-symmetric coupling can enter into such region. This is the case reported in panel a) of Figure 4.3 and confirmed by the time evolution of the density $u_i(t)$ (panel b) in the case of non symmetric long-range interactions and panel c) in the symmetric case). The non-reciprocal interactions are obtained with a directed Erdős-Rényi network made of 50 nodes and the probability to create a directed link to be 0.05.

4.3.3 The Volterra model

By remaining in the framework of ecological models, we consider an application dealing with a Volterra model [174] modified by the assumption of the presence of non-reciprocal interactions among animals. For sake of pedagogy, we hereby decided to present our results with a simplified and abstract model that describes the interactions of preys and predators in an ecological setting. Let us however observe that our theory could be applied as to include other phenomena, e.g., harvesting [175, 176]. The model we are interested in results thus to be described by:

$$\begin{cases} \dot{x} = -dx + c_1 xy \\ \dot{y} = ry - sy^2 - c_2 xy \end{cases} \tag{4.3.8}$$

Here x denotes the concentration of predators, while y stands for the preys, and all the parameters are assumed to be positive. The Volterra model (4.3.8) admits a nontrivial fixed point, $x^* = \frac{c_1 r - sd}{c_1 c_2}$, $y^* = \frac{d}{c_1}$, which is positive and stable, provided that $c_1 r - sd > 0$, condition hereby assumed to hold true.

Following the above presented scheme, let us now consider the long-range coupling

$$\vec{F}(\vec{x}_i, \vec{x}_j) = \left(-dx_i + ac_1 x_j y_i + (1-a)c_1 x_i y_j, ry_i - sy_i^2 - c_2 x_j y_i\right)$$

where $\vec{x}_i = (x_i, y_i)$ and $\vec{x}_j = (x_j, y_j)$. The parameter a belongs to $[0,1]$ and weights the contribution arising from the nonlinear terms $x_i y_j$ and $x_j y_i$; such term disappears in the local dynamics. Let $\vec{F}(\vec{x}_i) = \left(-dx_i + c_1 x_i y_i, ry_i - sy_i^2 - c_2 x_i y_i\right)$, then $\vec{F}(\vec{x}_i, \vec{x}_i) = \vec{F}(\vec{x}_i)$. In SM 4.9 we show that the main equation (4.2.2) can now be written as

$$\begin{cases} \dot{x}_i &= -dx_i + c_1 x_i y_i + ac_1 y_i \sum_{j=1}^{n} \mathscr{L}_{ij} x_j + (1-a)c_1 x_i \sum_{j=1}^{n} \mathscr{L}_{ij} y_j \\ \dot{y}_i &= ry_i - sy_i^2 - c_2 x_i y_i - c_2 y_i \sum_{j=1}^{n} \mathscr{L}_{ij} x_j \end{cases} \tag{4.3.9}$$

where we can recognize the n copies of the isolated Volterra system (4.3.8) and the coupling due to the long-range interactions.

We can thus compute the explicit form of the polynomials $S_1(\kappa)$ and $S_2(\kappa)$ as a function of the model parameters (see SM 4.9) and characterize the instability region defined by (4.3.2) as reported in Figure 4.4 where we show in the complex plane $(\mathscr{R}\Lambda, \mathscr{I}\Lambda)$ the regions for which the instability condition is satisfied (gray), for a given set of parameters. By using again a directed Erdős-Rényi network made of 50 nodes and the probability to create a directed link to be 0.5 to describe the non-reciprocal interactions, we can show the existence of eigenvalues $\Lambda^{(\hat{\alpha})}$ (white dots in panel a) of Figure 4.4) belonging to this region, associated thus to a patchy solution (panel b) of Figure 4.4). The symmetric coupling being associated to a real spectrum is unable to drive the system away from the homogeneous equilibrium (panel c) of Figure 4.4). Because of the peculiar shape of the instability region, one can have parameters values for which the instability region intersects the real axis (see Figure 4.7 in SM 4.9). In this case also a symmetric coupling can trigger the instability. From this example one can

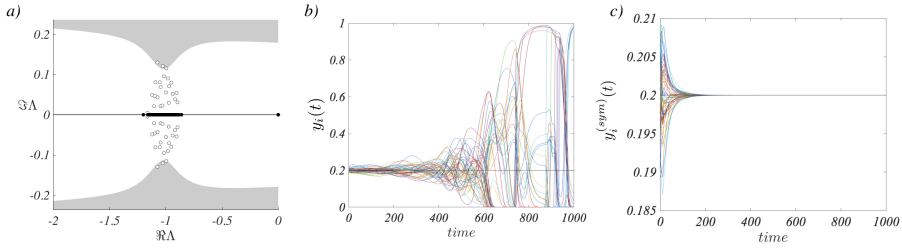

Figure 4.4: Instability region and patterns for the Volterra model. In panel a), we report the region of the complex plane $(\mathscr{R}\Lambda, \mathscr{I}\Lambda)$ for which the instability condition is satisfied (gray). For the chosen parameters values ($c_1 = 2$, $c_2 = 13$, $r = 1$, $s = 1$, $d = 0.4$ and $a = 0.05$), we can observe that the instability region does not intersect the real axis and thus only non-reciprocal coupling can exhibit complex eigenvalues (white dots) entering into the instability region and thus initiating the pattern as shown in panel b), where we report $y_i(t)$ vs. t starting from initial conditions close to the stable equilibrium. Any symmetric coupling determines real eigenvalue (black dots in panel a)) that cannot give rise to the instability as reported in the panel c), where we show $y_i(t)$ vs. t. The underlying coupling is a directed Erdős-Rényi network with $n = 50$ nodes and a probability for a directed link to exist between two nodes is $p = 0.5$.

draw a general conclusion: if the instability is possible by using symmetric long-range interactions, then the same holds true for non-reciprocal ones; on the other hand, patterns resulting from an instability due to non-symmetric interactions can never emerge if the long-range interactions reciprocate.

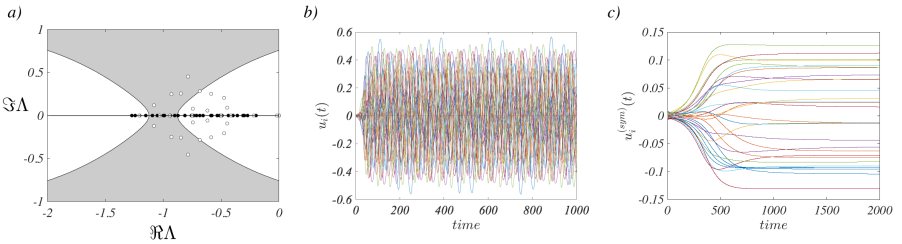

Figure 4.5: Instability region and patterns for the FitzHugh-Nagumo model. In panel a), we report the region of the complex plane $(\mathscr{R}\Lambda, \mathscr{I}\Lambda)$ for which the instability condition is satisfied (gray). For the chosen parameters values ($\alpha = 1.5$, $\beta = 0$, $\gamma = 2.5$ and $\mu = 0.01$), we can observe that the instability region intersects the real axis and thus both reciprocal (black dots) and non-reciprocal coupling (white dots) can exhibit eigenvalues entering into the instability region and thus initiating the pattern, as shown in panels b) and c) where we report $u_i(t)$ vs. t starting from initial conditions close to the stable equilibrium, $u^* = 0$ for the asymmetric coupling and the symmetric one. The underlying coupling is obtained with a directed Erdős-Rényi network with $n = 30$ nodes and a probability for a directed link to exist between two nodes is $p = 0.1$.

4.3.4 The FitzHugh-Nagumo model

The next system we consider is the FitzHugh-Nagumo model [126, 127, 128], a nonlinear system often used as paradigm for the study of the emergence of Turing patterns [129, 130, 131, 132, 131] as well as for synchronization phenomena [133, 134]. The model has been conceived in the framework of neuroscience as a schematization

of an electric impulse propagating through an axon. For this reason, we believe that it would make a suitable example for the long-range interactions we are describing in this work.

The FitzHugh-Nagumo model can be described by the system of ODEs

$$\begin{cases} \dot{u} &= \mu u - u^3 - v \\ \dot{v} &= \gamma(u - \beta v) \end{cases} \tag{4.3.10}$$

where the parameters μ, γ and β are assumed to be positive. We will hereby focus on its behavior close to the fixed point $(u^*, v^*) = (0,0)$. The linear stability analysis ensures stability of the latter under the conditions $\mu < \gamma\beta$ and $\mu\beta < 1$. Let us observe that, once such conditions are not met, the system undergoes a supercritical Hopf-Andronov bifurcation [47]: the equilibrium point becomes unstable giving birth to a stable limit cycle solution. In this study, we will limit ourselves to the former case, leaving the oscillating case for a future work. Let us also observe that this model is not a kinetic one, since the $-v$ term appearing in the rate evolution for u, expresses a negative cross-effect [138]; we can thus claim that pattern formation finds applications beyond morphogenesis and chemical frameworks.

By setting $\vec{x}_i = (u_i, v_i)$ and $\vec{F}(\vec{x}_i) = (\mu u_i - u_i^3 - v_i, \gamma(u_i - \beta v_i))$, we can expressed the model in the framework presented in the previous section by using the following coupling

$$\vec{F}(\vec{x}_i, \vec{x}_j) = (\mu u_i - u_i^3 - v_j, \gamma(u_j - v_i))$$

where $\vec{x}_j = (u_j, v_j)$, that clearly satisfies $\vec{F}(\vec{x}_i, \vec{x}_i) = \vec{F}(\vec{x}_i)$. The main equation (4.2.2) becomes (see SM 4.10)

$$\begin{cases} \dot{u}_i &= \mu u_i - u_i^3 - v_i - \sum_{j=1}^{n} \mathscr{L}_{ij} v_j \\ \dot{v}_i &= \gamma(u_i - \beta v_i) + \gamma \sum_{j=1}^{n} \mathscr{L}_{ij} u_j \end{cases} \quad \forall i = 1, \dots, n \tag{4.3.11}$$

namely a set of n FitzHugh-Nagumo models (4.3.10) coupled via long-range connections in both variables.

We can then compute the polynomials $S_1(\kappa)$ and $S_2(\kappa)$ (see SM 4.10) and determine the instability region (gray) as reported in panel a) of Figure 4.5. By using a directed Erdős-Rényi network made of 30 nodes and the probability to create a directed link to be 0.1 to encode the non-reciprocal interactions, we can show the existence of eigenvalues (white dots) lying in the instability region and thus allowing for the instability onset (panel b) of Figure 4.5). Let us observe that, because of the shape of the instability region, exhibiting a non-empty intersection with the negative real axis, there can also be symmetric couplings for which patterns do emerge (panel c) of Figure 4.5).

4.3.5 The Stuart-Landau model

As anticipated, the proposed method goes beyond the framework above presented dealing with stationary homogeneous solution, but can be extended to study systems exhibiting an oscillatory behavior, being the latter a regular or a chaotic one. To support

this claim, let us study for sake of definitiveness the Stuart-Landau system (SL) [177, 100], as a paradigmatic model of nonlinear oscillators. The complex amplitude w evolves thus in time according to

$$\dot{w} = \sigma w - \beta |w|^2 w \tag{4.3.12}$$

where $\sigma = \sigma_{\mathscr{R}} + i\sigma_{\mathscr{I}}$ and $\beta = \beta_{\mathscr{R}} + i\beta_{\mathscr{I}}$ are complex parameters, and we denote by $z_{\mathscr{R}}$ (resp. $z_{\mathscr{I}}$) the real (resp. imaginary) part of the complex number z. Let us observe that the SL determines the normal form for a generic system close to a supercritical Hopf-bifurcation, hence the results hereby presented are more general than the specific model explored. Let us thus consider a system made of n identical SL oscillators and set the parameters such that each isolated oscillator converges to the same limit cycle $w_{LC}(t) = \sqrt{\sigma_{\mathscr{R}}/\beta_{\mathscr{R}}}e^{i\omega t}$, $\omega = \sigma_{\mathscr{I}} - \beta_{\mathscr{I}}\sigma_{\mathscr{R}}/\beta_{\mathscr{R}}$. We are then interested in determining the conditions responsible for the persistence of this synchronous behavior once the SL oscillators are allowed to interact through non-reciprocal long-range interactions or, if on the contrary, an instability sets up and drives the whole system to a new (spatially possibly) heterogeneous state. Assume again the long-range interactions to be modeled through a mean field ansatz (4.2.2), for instance

$$\dot{w}_j = \frac{\sigma}{k_j^{(in)}} \sum_{\ell=1}^{n} A_{j\ell} w_\ell - \beta w_j |w_j|^2 = \sigma w_j - \beta w_j |w_j|^2 + \sigma \sum_{\ell=1}^{n} \mathscr{L}_{j\ell} w_\ell \tag{4.3.13}$$

where w_j is the complex state variable of the j-th SL system and $A_{j\ell}$ encodes the non-reciprocal coupling. Such system admits a homogeneous stable limit cycle solution if $\sigma_{\mathscr{R}} > 0$ and $\beta_{\mathscr{R}} > 0$. We can then show the existence of non-reciprocal couplings able to trigger the instability by destabilizing the limit cycle solution, eventually driving the system toward a new heterogeneous wavy solution.

Indeed, according to the theory hereby developed, we can always determine model parameters allowing for an instability region in the complex plane (see SM 4.11), that does not intersect the real axis; the spectrum of a reciprocal web of long-range interactions could thus never belong to the instability region (black dots in Figure 4.6) and any perturbation fades away. On the other hand, the complex spectrum associated to non-reciprocal couplings could intersect the instability region (white dots in Figure 4.6), driving thus the system toward the formation of patterns. We can thus state a claim similar to the ones made above, namely non-reciprocal long-range interactions can more easily drive the system toward a desynchronized state.

4.3.6 A sufficient condition for $d \geq 2$

As already anticipated, the $d = 2$ dimensional systems have been presented for sake of pedagogy, because they allow to obtain explicit and analytical conditions for the onset of heterogeneous solutions, where the role of the non-reciprocal links is clearly understood. We are now able to show that similar results hold true in any dimensions, $d \geq 2$, and for generic systems beyond the paradigmatic examples above presented. We will indeed prove that given a system built using reciprocal interactions for which the reference solution is stable and thus any small enough perturbation about it will fade away, then one can always find non-reciprocal interactions capable to destabilize the

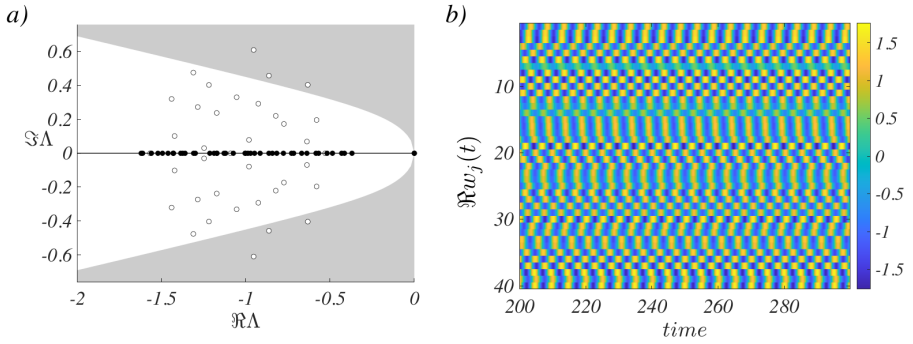

Figure 4.6: Instability region and patterns for the Stuart-Landau model. The region of instability in the complex plane $(\mathscr{R}\Lambda, \mathscr{I}\Lambda)$ is reported (gray) in panel a). We fixed the model parameters to the values $\sigma_{\mathscr{R}} = 1$, $\sigma_{\mathscr{I}} = 4.3$, $\beta_{\mathscr{R}} = 1$ and $\beta_{\mathscr{I}} = 1$, resulting into an instability region that does not intersect the real axis, thus only an asymmetric coupling (white dots) can have a complex spectrum entering the instability region and initiating a heterogeneous pattern as shown in panel b), where we report $\mathscr{R}w_j(t)$ vs. time. Any symmetric coupling determines real eigenvalue (black dots in panel a)) and thus it cannot initiate the instability, in consequence all the units synchronize (data not shown). The underlying coupling is a directed Erdős-Rényi network with $n = 40$ nodes and a probability for a directed link to exist between two nodes is $p = 0.08$.

reference solution, provided a condition on the model parameters holds true, and can thus drive the system toward a new heterogeneous asymptotic state.

The starting point is hence the general system given by (4.2.4) and Equation (4.2.7) obtained by linearizing the dynamics about the stationary reference solution, $\vec{x}^*$, and then by projecting onto the Laplace eigenbasis, $\vec{\varphi}^{(\alpha)}$, $\alpha = 1, \dots, n$. The characteristic polynomial, whose roots determine the stability feature of the reference solution, is now given by

$$p_d(\lambda) := (-1)^d \left[a_0 \lambda^d + a_1 \lambda^{d-1} + a_2 \lambda^{d-2} + \cdots + a_d \right] \tag{4.3.14}$$

where the coefficients a_j, $j = 1, \dots, d$, depend on the model parameters and on the eigenvalues $\Lambda^{(\alpha)}$. A straightforward computation allows to obtain for instance

$$a_0 = 1\,, \quad a_1 = -\mathrm{tr}\mathbf{J}^{(\alpha)} \quad \text{and} \quad a_d = \det \mathbf{J}^{(\alpha)}$$

with $\mathbf{J}^{(\alpha)} = \mathbf{J}(\vec{x}^*) + \mathbf{J}_2(\vec{x}^*)\Lambda^{(\alpha)}$; it is thus clear that Equation (4.3.1) is a particular case of the latter. A more cumbersome computation (see SM 4.12) allows to obtain an explicit formula for a_2 that will be needed in the following. In the general d-dimensional case, there are not explicit formulae for the roots of the polynomial p_d and, even if they exist, their use to understand the role of the model parameters and the impact of the eigenvalues $\Lambda^{(\alpha)}$ will be hopeless. We have thus to resort to a different approach based on the Routh-Hurwitz stability criterion [123, 124, 125], allowing to prove the (in)stability feature of a real coefficients polynomial. In particular, we will use the fact that a necessary condition to have a stable polynomial, i.e., a polynomial whose roots have negative real parts, is that all its coefficients exhibit the same sign, in the present case they should be positive being $a_0 = 1$.

Before proceeding any further, we observe that the coefficients a_j of the polynomial p_d are not (in general) real numbers, because of their dependence on the complex $\Lambda^{(\alpha)}$.

One cannot thus directly apply the above criterion. To overcome this issue, we introduce the polynomial $q(\lambda)$ of degree $2d$ given by

$$q(\lambda) := p_d(\lambda)\overline{p_d(\overline{\lambda})} = \lambda^{2d} + b_1\lambda^{2d-1} + b_2\lambda^{2d-2} + \cdots + b_{2d}$$

where $\overline{z}$ denotes the complex conjugate of the complex number z. One can prove (see SM 4.12) that the roots of this polynomial have the same real parts of the roots of p_d (counted twice) and moreover its coefficients become real numbers, whose expression can be related to the coefficients of p_d.

The proof of our statement proceeds thus as follows. Assume to have a system whose nodes interact through a symmetric ensemble of links and fix the model parameters in such a way that the reference solution $\vec{x}^*$ is stable, with respect to heterogeneous perturbations. Hence, for all $\alpha = 1,\dots,n$, all the roots λ_i, $i = 1,\dots,d$, of p_d have negative real parts and so do the ones of q. Invoking the necessary condition of the Routh-Hurwitz stability criterion, we can conclude that the coefficients of q are positive numbers whenever we set $\mathscr{I}\Lambda^{(\alpha)} = 0$, for all α, because the Laplacian's spectrum is real (see SM 4.5)

$$b_j|_{\mathscr{I}\Lambda^{(\alpha)}=0} > 0 \quad \forall j = 1,\dots,2d$$

We can then prove (we refer to SM 4.12 for more details) that if the model parameters satisfy the condition

$$\mathrm{tr}\mathbf{J}_2^2 < 0 \tag{4.3.15}$$

then we can always find a non-reciprocal coupling such that the imaginary part of the spectrum satisfies the condition

$$\exists\hat{\alpha} > 1 \text{ s.t. } \left(\mathscr{I}\Lambda^{(\hat{\alpha})}\right)^2 > \frac{\left(2\mathscr{R}a_2 + \left[\mathrm{tr}\mathbf{J}^{(\hat{\alpha})}\right]^2\right)\Big|_{\mathscr{I}\Lambda^{(\hat{\alpha})}=0}}{|\mathrm{tr}\mathbf{J}_2^2|} \tag{4.3.16}$$

ensuring that the coefficient b_2 is negative and thus the polynomial q is not stable. Hence, q admits at least one root, the one associated to $\hat{\alpha}$, whose real part is positive, and so does p_d. In conclusion, the reference solution $\vec{x}^*$ is unstable, any spatially inhomogeneous perturbation is amplified and the system moves away from the homogeneous solution. Let us observe that we can always build a web of non-reciprocal interactions satisfying the latter conditions, by using the ideas developed in [178] to generate asymmetric Laplacian matrices, and thus directed networks, that possess prescribed spectra.

4.4 Conclusion

In conclusion, we have proposed and analyzed a mechanism for pattern formation, being the latter stationary or time dependent, rooted on the presence of non-reciprocal long-range interactions, to show that self-organization can manifest without the presence of diffusion. Long-range non-reciprocal interactions, modeled with a mean-field scheme, return a consensus Laplace operator, whose complex spectrum sets the conditions for the instability and the ensuing spatial or temporal patterns. The intrinsic asymmetries within the system, described by non-reciprocal interactions, are the key factor

in the disruption of the homogeneous solution and thus the driver for the diversity of patterns of complexity one can observe in nature. The theory has been applied to several paradigmatic models used in the literature to study the emergence of patterns or synchronization. The proposed mechanism complements thus the Turing one [4, 31] and it is suitable for all phenomena where patterns emergence is not driven by a diffusive process, but immobile species interact through non-reciprocal long-range couplings.

4.5 SM 1: About the spectrum of the reactive Laplacian in case of reciprocal interactions.

Let us assume the network of interactions to be symmetric, $A_{ij} = A_{ji}$, for all i and j, and let us recall the definition of the reactive Laplacian $\mathscr{L}_{ij} = A_{ij}/k_i - \delta_{ij}$, where $k_i = \sum_j A_{ij}$, is the node degree. Let us introduce the symmetric Laplace matrix $\mathscr{L}^{sym}_{ij} = A_{ij}/\sqrt{k_i k_j} - \delta_{ij}$ and observe that its eigenvalues are real and negative but the null one. Let $\mathbf{D}$ be the diagonal matrix with the nodes degree on the diagonal, then

$$\mathscr{L} = \mathbf{D}^{-1}\mathbf{A} - \mathbf{I} = \mathbf{D}^{-1/2}\left[\mathbf{D}^{-1/2}\mathbf{A} - \mathbf{I}\right]\mathbf{D}^{1/2} = \mathbf{D}^{-1/2}\mathscr{L}^{sym}\mathbf{D}^{1/2}$$

Namely, $\mathscr{L}$ and $\mathscr{L}^{sym}$ are similar matrices and thus exhibit the same set of eigenvalues.

4.6 SM 2: Linear stability analysis

Let us consider the homogeneous reference solution $\vec{x}^*(t)$ and a spatially dependent perturbation about the latter, $\vec{x}_i(t) = \vec{x}^*(t) + \vec{\zeta}_i(t)$, then by inserting this information into Equation (4.2.2) (main text) and by retaining only the linear terms in $\vec{\zeta}_i$ we obtain

$$\begin{aligned}
\dot{\vec{\zeta}}_i = \dot{\vec{x}}_i - \dot{\vec{x}}* &= \frac{1}{k_i^{(in)}}\sum_{j=1}^{n} A_{ij}\vec{F}(\vec{x}^* + \vec{\zeta}_i, \vec{x}^* + \vec{\zeta}_j) - \vec{F}(\vec{x}^*) \\
&= \frac{1}{k_i^{(in)}}\sum_{j=1}^{n} A_{ij}\left(\sum_\ell \partial_{x_\ell^{(i)}}\vec{F}(\vec{x}^*,\vec{x}^*)\zeta_\ell^{(i)} + \sum_\ell \partial_{x_\ell^{(j)}}\vec{F}(\vec{x}^*,\vec{x}^*)\zeta_\ell^{(j)}\right) \\
&= \sum_\ell \partial_{x_\ell^{(i)}}\vec{F}(\vec{x}^*,\vec{x}^*)\zeta_\ell^{(i)} + \frac{1}{k_i^{(in)}}\sum_{j=1}^{n} A_{ij}\sum_\ell \partial_{x_\ell^{(j)}}\vec{F}(\vec{x}^*,\vec{x}^*)\zeta_\ell^{(j)} \\
&= \mathbf{J}_1\vec{\zeta}_i + \frac{1}{k_i^{(in)}}\sum_{j=1}^{n} A_{ij}\mathbf{J}_2\vec{\zeta}_j \quad \forall i = 1,\dots,n
\end{aligned}$$

where we recall that $\mathbf{J}_1 = \partial_{\vec{x}_1}\vec{F}(\vec{x}_1,\vec{x}_2)_{(\vec{x}^*,\vec{x}^*)}$ and $\mathbf{J}_2 = \partial_{\vec{x}_2}\vec{F}(\vec{x}_1,\vec{x}_2)_{(\vec{x}^*,\vec{x}^*)}$. By observing that $\vec{F}(\vec{x}) = \vec{F}(\vec{x},\vec{x})$, one can prove that $\partial_{\vec{x}}\vec{F} := \mathbf{J} = \mathbf{J}_1 + \mathbf{J}_2$. Hence, by slightly rewriting the previous equation, we obtain

$$\dot{\vec{\zeta}}_i(t) = \mathbf{J}_1\vec{\zeta}_i + \frac{1}{k_i^{(in)}}\sum_{j=1}^{n} A_{ij}\mathbf{J}_2\vec{\zeta}_j = \mathbf{J}_1\vec{\zeta}_i + \mathbf{J}_2\vec{\zeta}_i + \sum_{j=1}^{n}\left(\frac{A_{ij}}{k_i^{(in)}} - \delta_{ij}\right)\mathbf{J}_2\vec{\zeta}_j$$

$$
\begin{aligned}
&= (\mathbf{J}_1+\mathbf{J}_2)\,\vec{\zeta}_i + \sum_{j=1}^{n} \mathscr{L}_{ij}\mathbf{J}_2\vec{\zeta}_j \\
&= \mathbf{J}\vec{\zeta}_i + \sum_{j=1}^{n} \mathscr{L}_{ij}\mathbf{J}_2\vec{\zeta}_j
\end{aligned} \tag{4.6.1}
$$

where we used the matrix $\mathscr{L}$, given by Equation (4.2.3) (main text).

By introducing the $n\times d$ vector $\vec{\zeta} = ((\vec{\zeta}_1)^\top,\dots,(\vec{\zeta}_n)^\top)^\top$, we can eventually rewrite the latter equation in a compact form as

$$
\dot{\vec{\zeta}}(t) = [\mathbf{I}_n\otimes(\mathbf{J}_1+\mathbf{J}_2) + \mathscr{L}\otimes\mathbf{J}_2]\,\vec{\zeta} = [\mathbf{I}_n\otimes\mathbf{J} + \mathscr{L}\otimes\mathbf{J}_2]\,\vec{\zeta} \tag{4.6.2}
$$

where $\otimes$ denotes the Kronecker product of matrices. In this way, we emphasize the role of the Jacobian of the isolated system, $\mathbf{I}_n\otimes\mathbf{J}$, and the one for the coupling part, $\mathscr{L}\otimes\mathbf{J}_2$, that vanishes once we assume $\mathbf{A}=\mathbf{I}_n$.

Equation (4.6.1) is a linear system involving matrices with size $nd\times nd$. One can reduce the complexity of the latter by assuming the existence of an eigenbasis of $\mathscr{L}$, $\vec{\varphi}^{(\alpha)}$, $\alpha=1,\dots,n$, with associated eigenvalue $-2<\mathscr{R}\Lambda^{(\alpha)}\leq 0$. Then by rewriting $\vec{\zeta}_i=\sum_\beta \vec{\xi}_\beta\varphi_i^{(\beta)}$ and inserting the latter into (4.6.1) we obtain

$$
\begin{aligned}
\sum_\beta \dot{\vec{\xi}}_\beta\varphi_i^{(\beta)} &= \sum_\beta \mathbf{J}(\vec{x}^*(t))\vec{\xi}_\beta\varphi_i^{(\beta)} + \sum_{j=1}^{n}\sum_\beta \mathscr{L}_{ij}\mathbf{J}_2(\vec{x}^*(t))\vec{\xi}_\beta\varphi_j^{(\beta)} \\
&= \sum_\beta \mathbf{J}(\vec{x}^*(t))\vec{\xi}_\beta\varphi_i^{(\beta)} + \sum_\beta \Lambda^{(\beta)}\mathbf{J}_2(\vec{x}^*(t))\vec{\xi}_\beta\varphi_i^{(\beta)}
\end{aligned}
$$

By multiplying by the left eigenvectors $\psi_i^{(\alpha)}$ and summing over the index i, recall that $\sum_i \psi_i^{(\alpha)}\varphi_i^{(\beta)}=\delta_{\alpha\beta}$, we can obtain Equation (4.2.6) (main text), namely

$$
\dot{\vec{\xi}}_\alpha = \mathbf{J}(\vec{x}^*(t))\vec{\xi}_\alpha + \Lambda^{(\alpha)}\mathbf{J}_2(\vec{x}^*(t))\vec{\xi}_\alpha \quad \forall\alpha=1,\dots,n
$$

Assuming to deal with $d=2$ dimensional systems and with a stationary reference solution, i.e., $\vec{x}^*(t)=\vec{x}^*$ for all t, one can then realize that the eigenvalues of $\mathbf{J}^{(\alpha)}$, λ_i, are the solutions of the second order equation

$$
\lambda_i^2 - \mathrm{tr}\mathbf{J}^{(\alpha)}\lambda_i + \det\mathbf{J}^{(\alpha)} = 0 \quad \forall i=1,\dots,n
$$

Note that if, on the other hand, we were interested in studying $d>2$ dynamical systems, then we should consider roots of d-degree polynomial equations for which there is no general closed form solution and thus one has to recur to numerical simulations to determine the instability region or to other ideas, as we have shown in the main text and detailed in SM 4.12.

Back to the $d=2$ case, one can express the real part of the above roots as:

$$
\mathscr{R}\lambda_i = \frac{1}{2}\left(\mathscr{R}\mathrm{tr}\mathbf{J}^{(\alpha)} + \gamma\right)
$$

where

$$\gamma = \sqrt{\frac{A+\sqrt{A^2+B^2}}{2}}, A = \left(\mathscr{R}\mathrm{tr}\mathbf{J}^{(\alpha)}\right)^2 - \left(\mathscr{I}\mathrm{tr}\mathbf{J}^{(\alpha)}\right)^2 - 4\mathscr{R}\mathrm{det}\mathbf{J}^{(\alpha)}$$

and

$$B = 2\mathscr{R}\mathrm{tr}\mathbf{J}^{(\alpha)}\mathscr{I}\mathrm{tr}\mathbf{J}^{(\alpha)} - 4\mathscr{I}\mathrm{det}\mathbf{J}^{(\alpha)}$$

A straightforward but lengthy computation allows to rewrite the condition for instability Equation (4.3.2) (main text), in terms of two polynomials, S_2 of second degree and S_1 of fourth degree. More precisely, $S_2(\kappa) = c_{2,2}\kappa^2 + c_{2,1}\kappa + c_{2,0}$ with coefficients

$$\begin{aligned} c_{2,2} &= -\det\mathbf{J}_2(4\det\mathbf{J}_2 - (\mathrm{tr}\mathbf{J}_2)^2) \\ c_{2,1} &= -\Delta_1(4\det\mathbf{J}_2 - (\mathrm{tr}\mathbf{J}_2)^2) \\ c_{2,0} &= -\Delta_1^2 + \Delta_1\mathrm{tr}\mathbf{J}\mathrm{tr}\mathbf{J}_2 - \det\mathbf{J}_2\,(\mathrm{tr}\mathbf{J})^2 \end{aligned} \tag{4.6.3}$$

and $S_1(\kappa) = c_{1,4}\kappa^4 + c_{1,3}\kappa^3 + c_{1,2}\kappa^2 + c_{1,1}\kappa + c_{1,0}$ with coefficients

$$\begin{aligned} c_{1,4} &= \det\mathbf{J}_2\,(\mathrm{tr}\mathbf{J}_2)^2 \\ c_{1,3} &= \mathrm{tr}\mathbf{J}_2(\Delta_1\mathrm{tr}\mathbf{J}_2 + 2\det\mathbf{J}_2\mathrm{tr}\mathbf{J}) \\ c_{1,2} &= \det\mathbf{J}\,(\mathrm{tr}\mathbf{J}_2)^2 + 2\Delta_1\mathrm{tr}\mathbf{J}\mathrm{tr}\mathbf{J}_2 + \det\mathbf{J}_2\,(\mathrm{tr}\mathbf{J})^2 \\ c_{1,1} &= \mathrm{tr}\mathbf{J}(2\det\mathbf{J}\mathrm{tr}\mathbf{J}_2 + \Delta_1\mathrm{tr}\mathbf{J}) \\ c_{1,0} &= \det\mathbf{J}\,(\mathrm{tr}\mathbf{J})^2 \end{aligned} \tag{4.6.4}$$

where we introduced $\Delta_1 = J_{2,11}J_{22} - J_{2,12}J_{21} - J_{2,21}J_{12} + J_{2,22}J_{11}$.

Let us now consider the general case in which the existence of an eigenbasis of $\mathscr{L}$ is not guaranteed, namely the Laplace matrix is defective. We can then invoke the Jordan canonical form theorem to determine an invertible $n \times n$ matrix $\mathbf{P}$ such that

$$\mathbf{P}^{-1}\mathscr{L}\mathbf{P} = \mathbf{B} = \mathrm{diag}(\mathbf{B}_1, \ldots, \mathbf{B}_\ell)$$

where the $\mathbf{B}_j$ is the $m_j \times m_j$ Jordan block, $m_1 + \cdots + m_\ell = n$

$$\mathbf{B}_j = \begin{pmatrix} \Lambda^{(j)} & & & \\ 1 & \Lambda^{(j)} & & \\ & \ddots & \ddots & \\ & & 1 & \Lambda^{(j)} \end{pmatrix}$$

being $\Lambda^{(j)}$ the j-th eigenvalue of $\mathscr{L}$. Because $\Lambda^{(1)} = 0$ we also have $\mathbf{B}_1 = 0$.

Let us again consider Equation (4.6.2). By defining $\mathbf{Q} = \mathbf{P} \otimes \mathbf{I}_d$ and $\vec{\eta} = \mathbf{Q}^{-1}\vec{\zeta}$, we get

$$\dot{\vec{\eta}}(t) = \mathbf{Q}^{-1}\dot{\vec{\zeta}}(t) = (\mathbf{P}^{-1} \otimes \mathbf{I}_d)\,[\mathbf{I}_n \otimes \mathbf{J} + \mathscr{L} \otimes \mathbf{J}_2]\,(\mathbf{P} \otimes \mathbf{I}_d)\mathbf{Q}^{-1}\vec{\zeta} = [\mathbf{I}_n \otimes \mathbf{J} + \mathbf{B} \otimes \mathbf{J}_2]\,\vec{\eta} \tag{4.6.5}$$

The vector $\vec{\eta}$ inherits the Jordan decomposition, hence we can write $\vec{\eta} = ((\vec{\eta}_1)^\top, \dots, (\vec{\eta}_\ell)^\top)^\top$, where $\vec{\eta}_j$ is a $(d \times m_j)$-dimensional vector. Equation (4.6.5) can thus be rewritten as

$$\dot{\vec{\eta}}_1(t) = \begin{pmatrix} \mathbf{J} & & \\ & \ddots & \\ & & \mathbf{J} \end{pmatrix} \vec{\eta}_1 \,, \tag{4.6.6}$$

$$\dot{\vec{\eta}}_j(t) = \begin{pmatrix} \mathbf{J} & & \\ & \ddots & \\ & & \mathbf{J} \end{pmatrix} \vec{\eta}_j + \tag{4.6.7}$$

$$+ \begin{pmatrix} \Lambda^{(j)}\mathbf{J}_2 & & & \\ \mathbf{J}_2 & \Lambda^{(j)}\mathbf{J}_2 & & \\ & \ddots & \ddots & \\ & & \mathbf{J}_2 & \Lambda^{(j)}\mathbf{J}_2 \end{pmatrix} \vec{\eta}_j \quad \forall j = 2, \dots, \ell$$

The first Equation (4.6.6) returns again the stability condition for the isolated systems, which is a working assumption for the developed framework. Let us now consider the generic Equation (4.6.8) and by writing $\vec{\eta}_j = ((\vec{\eta}_{j1})^\top, \dots, (\vec{\eta}_{jm_j})^\top)^\top$, where $\vec{\eta}_{j_i} \in \mathbf{R}^d$ for all $i = 1, \dots, m_j$, we get

$$\dot{\vec{\eta}}_{j1j}(t) = \mathbf{J}\vec{\eta}_{j1} + \Lambda^{(j)}\mathbf{J}_2\vec{\eta}_{j1} \tag{4.6.8}$$

$$\dot{\vec{\eta}}_{j2j}(t) = \mathbf{J}\vec{\eta}_{j2} + \Lambda^{(j)}\mathbf{J}_2\vec{\eta}_{j2} + \mathbf{J}_2\vec{\eta}_{j,1} \tag{4.6.9}$$

$$\vdots$$

$$\dot{\vec{\eta}}_{j,m_j}(t) = \mathbf{J}\vec{\eta}_{jm_j} + \Lambda^{(j)}\mathbf{J}_2\vec{\eta}_{jm_j} + \mathbf{J}_2\vec{\eta}_{jm_j-1} \tag{4.6.10}$$

To simplify the following analysis, we will assume to deal with a stationary reference solution $\vec{x}^*(t) = \vec{x}^*$, hence all the involved matrices are constant ones. Hence, the first Equation (4.6.8) is the analogous of Equation (4.2.6) (main text) and one can determine a condition on $\Lambda^{(j)}$ to make the projection $\vec{\eta}_{j1}$ unstable; in the case $d = 2$ this accounts to perform the analysis above presented, returning the condition (4.3.2), where $\hat{\alpha}$ is replaced by j.

Let us now consider the second Equation (4.6.9) and observe that it is composed by two terms: the first one involves the same matrix of the first equation, $\mathbf{J} + \Lambda^{(j)}\mathbf{J}_2$, while the second one depends on the projection $\vec{\eta}_{j,1}(t)$. If, for the choice of $\Lambda^{(j)}$ the matrix is unstable and thus $\vec{\eta}_{j1}(t)$ has an exponential growth, then the same is true for $\vec{\eta}_{j2}(t)$. By considering the remaining equations and by exploiting the peculiar shape of the system, this allows to prove that if the first Equation (4.6.8) returns an unstable solution, then all the solutions $\vec{\eta}_i^{(j)}(t)$ are unstable as well.

In conclusion, if the Laplace matrix $\mathscr{L}$ is defective, one can check the instability condition on the available eigenvalues and conclude on the emergence of patterns solely based on this information. Let us observe that this is a sufficient condition. Indeed, it can happen that the matrix $\mathbf{J} + \Lambda^{(j)}\mathbf{J}_2$ is stable, but the presence of Jordan blocks introduces a transient (polynomial) growth in the linear regime that results strong enough

to limit the validity of the linear approximation. Thus, the nonlinear system could exhibit orbits departing from the homogeneous reference solution and only infinitesimal perturbations will be attracted to the latter. Stated differently, the stability basin of the reference solution shrinks considerably in presence of defective Laplace matrix: the solution is thus stable but finite perturbations can be amplified, consistently with previous results [78].

4.7 SM 3: Analysis of the Brusselator model

Let us consider the two species Brusselator model, $\vec{F}(\vec{x}_i) = (1-(b+1)u_i + cu_i^2 v_i, bu_i - cu_i^2 v_i)$, where $\vec{x}_i = (u_i, v_i)$, and the non-local coupling given by

$$\vec{F}(\vec{x}_i, \vec{x}_j) = (1-(b+1)u_i + cu_i^2 v_i, bu_j - cu_i^2 v_i)$$

where $\vec{x}_j = (u_j, v_j)$. Equation (4.2.2) can thus be rewritten as

$$\begin{cases} \dot{u}_i &= \dfrac{1}{k_i^{(in)}} \displaystyle\sum_{j=1}^{n} A_{ij} \left(1-(b+1)u_i + cu_i^2 v_i\right) \\ \dot{v}_i &= \dfrac{1}{k_i^{(in)}} \displaystyle\sum_{j=1}^{n} A_{ij} \left(bu_j - cu_i^2 v_i\right) \end{cases} \qquad \forall i = 1, \dots, n$$

By recalling the definition of $k_i^{(in)} = \sum_j A_{ij}$ and observing that the first equation does not depend on the index j, it can be straightforwardly simplified to return

$$\dot{u}_i = 1-(b+1)u_i + cu_i^2 v_i \quad \forall i = 1, \dots, n$$

Let us now consider the second equation and isolate the terms not depending on the index j

$$\begin{aligned} \dot{v}_i &= -cu_i^2 v_i + \frac{b}{k_i^{(in)}} \sum_{j=1}^{n} A_{ij} u_j = \\ &= -cu_i^2 v_i + b \sum_{j=1}^{n} \left(\frac{A_{ij}}{k_i^{(in)}} - \delta_{ij} \right) u_j + bu_i = bu_i - cu_i^2 v_i + b \sum_{j=1}^{n} \mathscr{L}_{ij} u_j \end{aligned}$$

$\forall i = 1, \dots, n$.
In conclusion, we obtain

$$\begin{cases} \dot{u}_i &= 1-(b+1)u_i + cu_i^2 v_i \\ \dot{v}_i &= bu_i - cu_i^2 v_i + b \displaystyle\sum_{j=1}^{n} \mathscr{L}_{ij} u_j \end{cases} \qquad \forall i = 1, \dots, n$$

From the definitions of $\vec{F}(\vec{x}_i)$ and $\vec{F}(\vec{x}_i, \vec{x}_j)$, we can compute the associated Jacobian matrices

$$\mathbf{J}_{\text{Bxl}} = \begin{pmatrix} b-1 & c \\ -b & -c \end{pmatrix} \text{ and } \mathbf{J}_2 = \begin{pmatrix} 0 & 0 \\ b & 0 \end{pmatrix}$$

and thus, by using the formulae (4.6.3) and (4.6.4) for the coefficients $c_{1,i}$, $i = 0,1,2,3,4$, and $c_{2,i}$, $i = 0,1,2$, we obtain the polynomials S_1 and S_2:

$$S_1(\kappa) = c(b-c-1)^2(1-b\kappa) \text{ and } S_2(\kappa) = -b^2c^2$$

The condition that the complex eigenvalues $\Lambda^{(\alpha)}$ of $\mathscr{L}$ have to satisfy to induce an instability is eventually given by

$$(\mathscr{I}\Lambda^{(\alpha)})^2 \geq \frac{(b-c-1)^2}{cb^2}\left(1-b\mathscr{R}\Lambda^{(\alpha)}\right)$$

4.8 SM 4: Analysis of the Mimura-Murray model

Let us consider the Mimura-Murray model with reaction terms, $\vec{F}(\vec{x}_i) = \left(u_i\left(\frac{a+bu_i-u_i^2}{c} - v_i\right), v_i(u_i-(1+dv_i))\right)$, where $\vec{x}_i = (u_i, v_i)$. The chosen non-local coupling is

$$\vec{F}(\vec{x}_i,\vec{x}_j) = \left(u_i\left(\frac{a+bu_j-u_i^2}{c} - v_j\right), v_i(u_j-(1+dv_i))\right)$$

From Equation (4.2.2) we obtain

$$\begin{cases} \dot{u}_i &= \dfrac{1}{k_i^{(in)}}\displaystyle\sum_{j=1}^{n} A_{ij}u_i\left(\frac{a+bu_j-u_i^2}{c} - v_j\right) \\ \dot{v}_i &= \dfrac{1}{k_i^{(in)}}\displaystyle\sum_{j=1}^{n} A_{ij}v_i(u_j-(1+dv_i)) \end{cases} \quad \forall i = 1,\dots,n$$

By using again the definition of $k_i^{(in)}$ and isolating the terms independent from j

$$\begin{cases} \dot{u}_i &= u_i\dfrac{a-u_i^2}{c} + \dfrac{u_i}{k_i^{(in)}}\displaystyle\sum_{j=1}^{n} A_{ij}\left(\frac{u_j}{c} - v_j\right) \\ \dot{v}_i &= -v_i(1+dv_i) + \dfrac{v_i}{k_i^{(in)}}\displaystyle\sum_{j=1}^{n} A_{ij}u_j \end{cases} \quad \forall i = 1,\dots,n$$

By adding and removing suitable ,terms we eventually obtain

$$\begin{cases} \dot{u}_i &= u_i\left(\dfrac{a+bu_i-u_i^2}{c} - v_i\right) + \dfrac{b}{c}u_i\displaystyle\sum_{j=1}^{n}\mathscr{L}_{ij}u_j - u_i\sum_{j=1}^{n}\mathscr{L}_{ij}v_j \\ \dot{v}_i &= v_i(u_i-(1+dv_i)) + v_i\displaystyle\sum_{j=1}^{n}\mathscr{L}_{ij}u_j \end{cases} \quad \forall i = 1,\dots,n$$

The Jacobian matrices follow directly from the definitions of the functions $\vec{F}(\vec{x}_i)$ and $\vec{F}(\vec{x}_i,\vec{x}_j)$

$$\mathbf{J}_{\mathrm{MM}} = \begin{pmatrix} u^*\frac{b-2u^*}{c} & -u^* \\ v^* & -dv^* \end{pmatrix} \text{ and } \mathbf{J}_2 = \begin{pmatrix} \frac{b}{c}u^* & -u^* \\ v^* & 0 \end{pmatrix}$$

and, from the latter, one can compute the coefficients $c_{1,i}$, $i = 0,1,2,3,4$, and $c_{2,i}$, $i = 0,1,2$, and eventually the polynomials S_1 and S_2. In the present case the resulting expressions are rather unwieldy and not very explicative. However, they can be used to numerically determine the instability region in the complex plane.

4.9 SM 5: Analysis of the Volterra model

Let us study a set of n coupled Volterra models [174] that describes the interactions of preys and predators in an ecological setting, where they can interact via long-range connections modeled by

$$\begin{cases} \dot{x}_i = -dx_i + ac_1 y_i \dfrac{1}{k_i^{(in)}} \displaystyle\sum_{j=1}^{n} A_{ij} x_j + (1-a) c_1 x_i \dfrac{1}{k_i^{(in)}} \displaystyle\sum_{j=1}^{n} A_{ij} y_j \\ \dot{y}_i = r y_i - s y_i^2 - c_2 y_i \dfrac{1}{k_i^{(in)}} \displaystyle\sum_{j=1}^{n} A_{ij} x_j \end{cases}$$

By using the reactive Laplacian matrix (4.2.3), we can rewrite the previous equations as

$$\begin{cases} \dot{x}_i = -dx_i + c_1 y_i x_i + ac_1 y_i \displaystyle\sum_{j=1}^{n} \mathscr{L}_{ij} x_j + (1-a) c_1 x_i \displaystyle\sum_{j=1}^{n} \mathscr{L}_{ij} y_j \\ \dot{y}_i = r y_i - s y_i^2 - c_2 y_i x_i - c_2 y_i \displaystyle\sum_{j=1}^{n} \mathscr{L}_{ij} x_j \end{cases} \tag{4.9.1}$$

where one can easily recognize the in-node Volterra model (4.3.8) and the corrections stemming from non-local contributions. The Jacobian matrices are obtained as

$$\mathbf{J}_{\mathrm{V}} = \begin{pmatrix} 0 & c_1 x^* \\ -c_2 y^* & -s y^* \end{pmatrix} \text{ and } \mathbf{J}_2 = \begin{pmatrix} ac_1 y^* & (1-a) c_1 x^* \\ -c_2 y^* & 0 \end{pmatrix}$$

where (x^*, y^*) is the homogeneous equilibrium of the Volterra system.

By inserting the given expressions for $\mathbf{J}_{\mathrm{V}}$ and $\mathbf{J}_2$, in the general formulae (4.6.3) and (4.6.4), we obtain for the coefficients of $S_2(\kappa)$

$$\begin{aligned} c_{2,2} &= -(a-1)(c_1 r - ds)\left(4\frac{(a-1)(c_1 r - ds)}{c_1} + a^2 d\right) \\ c_{2,1} &= (c_1 r(a-2) + 2ds)\left(4\frac{(a-1)(c_1 r - ds)}{c_1} + a^2 d\right) \\ c_{2,0} &= -\frac{(c_1 r(a-2) + 2ds)^2}{c_1} + \left(\frac{c_1 r(a-2) + 2ds}{c_1}\right) ads + (a-1)(c_1 r - ds) a^2 d \end{aligned}$$

and $S_1(\kappa)$

$$\begin{aligned} c_{1,4} &= -(a-1)(c_1 r - ds) a^2 d \\ c_{1,3} &= ad\left(-(c_1 r(a-2) + 2ds)a + 2\frac{s(a-1)(c_1 r - ds)}{c_1}\right) \end{aligned}$$

$$
\begin{aligned}
c_{1,2} &= (c_1 r - ds)a^2 d + 2\frac{c_1 r(a-2)+2ds}{c_1} ads - \frac{(a-1)(c_1 r - ds)}{c_1^2} ds^2 \\
c_{1,1} &= -ds\left(2\frac{c_1 r - ds}{c_1} a + \frac{c_1 r(a-2)+2ds}{c_1}\frac{s}{c_1}\right) \\
c_{1,0} &= \frac{c_1 r - ds}{c_1^2} ds^2
\end{aligned}
$$

Given such polynomials, one can determine the (in)stability region as shown in Figure 4.4 (main text) or Figure 4.7 and thus conclude about the onset of the instability according to the position of the complex eigenvalues of the Laplace matrix $\mathscr{L}$. In Figure 4.7 we report the region of instability (gray) for a set of parameters values allowing for the emergence of patterns for both the reciprocal and non-reciprocal long-range interactions. We can observe that, contrary to the case shown in the main text, now the instability region has a non empty intersection with the real axis, where it lies the spectrum of the Laplace operator for reciprocal interactions (black dots). We can thus determine a web of symmetrical long-range interactions for which the Volterra model (4.3.8) (main text) exhibits an instability and eventually evolves toward a patchy solution (panel b) of Figure 4.7). A similar result holds true using non-reciprocal long-range interactions. Indeed, the complex spectrum of the associated Laplace matrix (white dots in panel a) of Figure 4.7) also lies in the instability region and thus the system converges to a spatially heterogeneous solution (panel c) of Figure 4.7). The underlying long-range coupling is a directed Erdős-Rényi network with $n = 50$ nodes and a probability for a directed link to exist between two nodes is $p = 0.5$.

In Figure 4.8, we provide a more global view of the parameters range associated to bifurcation diagram, showing the parameters values, d and c_1, for which the instability emerges in the case of both reciprocal interactions and non-reciprocal ones (black A region) and in the case of only non-reciprocal ones (white B region), once the remaining parameters have been fixed to some generic values. One can clearly appreciate how large is the latter compared to the former, and thus how more often one can find patterns due to non-reciprocal interactions instead of reciprocal ones.

4.10 SM 6: Analysis of the FitzHugh-Nagumo model

Let us consider the FitzHugh-Nagumo model, $\vec{F}(\vec{x}_i) = (\mu u_i - u_i^3 - v_i, \gamma(u_i - v_i))$, with $\vec{x}_i = (u_i, v_i)$, and the non-local coupling

$$\vec{F}(\vec{x}_i, \vec{x}_j) = (\mu u_i - u_i^3 - v_j, \gamma(u_j - v_i))$$

with $\vec{x}_j = (u_j, v_j)$. From Equation (4.2.2) we obtain

$$
\begin{cases}
\dot{u}_i &= \dfrac{1}{k_i^{(in)}} \displaystyle\sum_{j=1}^{n} A_{ij} \left(\mu u_i - u_i^3 - v_j\right) \\
\dot{v}_i &= \dfrac{1}{k_i^{(in)}} \displaystyle\sum_{j=1}^{n} A_{ij} \gamma(u_j - v_i)
\end{cases}
\qquad \forall i = 1, \ldots, n
$$

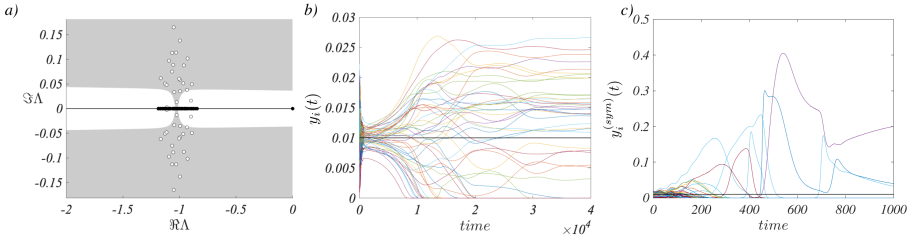

Figure 4.7: Instability region and patterns for the Volterra model. We report the region of the complex plane $(\mathscr{R}\Lambda, \mathscr{I}\Lambda)$ for which the instability condition is satisfied (gray), the instability is at play if at least one eigenvalue of $\mathscr{L}$ belongs to the region. The model parameters have been fixed to the values $c_1 = 2$, $c_2 = 13$, $r = 1$, $s = 1$, $d = 0.02$ and $a = 0.05$, and we can observe that the instability region intersects the real axis and thus both non-reciprocal (white dots) and reciprocal (black dots) interactions can exhibit eigenvalues entering into the instability region. This in turns implies the existence of an heterogeneous solution for both the reciprocal (see panel b) where we report the density of preys vs. time) and non-reciprocal (see panel c) where we report the density of preys vs. time) long-range interactions assumption. In both panels, the horizontal black line denotes the homogeneous equilibrium y^*.

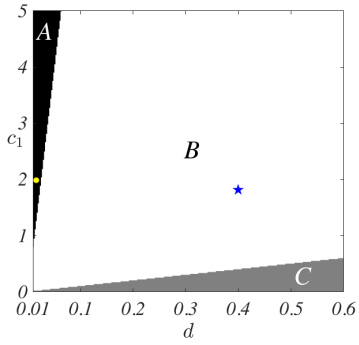

Figure 4.8: Bifurcation diagram for the Volterra model, reciprocal interactions. We fix the parameters values $c_2 = 13$, $r = 1$, $s = 1$ and $a = 0.05$, and we show the bifurcation region as a function of the remaining parameters d and c_1. The C region (gray) corresponds to an unstable homogeneous equilibrium that remains unstable even when the coupling is present, being the latter reciprocal or non-reciprocal one; patterns can develop but they are not due to the interactions. For parameters values in the A region (black), the stable homogeneous equilibrium is destabilized by the introduction of reciprocal coupling (as well by a non-reciprocal one); the patterns shown in panels b) and c) of Figure 4.7 associated to the values $c_1 = 2$ and $d = 0.02$ fall in this class (yellow dot). Finally in the large B region (white) the homogeneous equilibrium is stable for any reciprocal coupling, and thus no pattern can develop in this case, however the use of non-reciprocal interactions can drive the instability and thus the emergence of patterns. The patterns shown in the panel b) of Figure 4.4 (main text) correspond to the values $c_1 = 2$ and $d = 0.4$, clearly belonging to the B region (blue star).

By using again the definition of $k_i^{(in)} = \sum_j A_{ij}$, we get

$$\begin{cases} \dot{u}_i &= \mu u_i - u_i^3 - \dfrac{1}{k_i^{(in)}} \displaystyle\sum_{j=1}^{n} A_{ij} v_j \\ \dot{v}_i &= -\gamma v_i + \dfrac{\gamma}{k_i^{(in)}} \displaystyle\sum_{j=1}^{n} A_{ij} u_j \end{cases} \qquad \forall i = 1, \dots, n$$

hence

$$\begin{cases} \dot{u}_i &= \mu u_i - u_i^3 - v_i + \sum_{j=1}^{n} \mathscr{L}_{ij} v_j \\ \dot{v}_i &= \gamma(u_i - v_i) + \gamma \sum_{j=1}^{n} \mathscr{L}_{ij} u_j \end{cases} \qquad \forall i = 1, \dots, n$$

The Jacobian matrices can be obtained as follows

$$\mathbf{J}_{\text{FHN}} = \begin{pmatrix} \mu & -1 \\ \gamma & -\gamma \end{pmatrix} \text{ and } \mathbf{J}_2 = \begin{pmatrix} 0 & 1 \\ \gamma & 0 \end{pmatrix}$$

By using the formulae (4.6.3) and (4.6.4), we obtain the polynomials S_1 and S_2

$$S_1(\kappa) = \gamma(\mu - \gamma)^2 \left[(1+\kappa)^2 - \mu\right] \text{ and } S_2(\kappa) = -4\gamma^2(\kappa+1)^2 - \gamma(\mu-\gamma)^2$$

The instability is thus realized if the complex eigenvalues $\Lambda^{(\alpha)}$ of $\mathscr{L}$ satisfy the constraint

$$(\mathscr{I}\Lambda^{(\alpha)})^2 \geq \frac{(\mu-\gamma)^2}{4\gamma} \frac{(1+\mathscr{R}\Lambda^{(\alpha)})^2 - \mu}{(1+\mathscr{R}\Lambda^{(\alpha)})^2 + 1}$$

4.11 SM 7: Analysis of the Stuart-Landau model

We turn now our attention to the study of the paradigmatic model of nonlinear oscillators given by the Stuart-Landau system (SL) [177, 100]

$$\frac{dw}{dt} = \sigma w - \beta w |w|^2$$

where $\sigma = \sigma_{\mathscr{R}} + i\sigma_{\mathscr{I}}$ and $\beta = \beta_{\mathscr{R}} + i\beta_{\mathscr{I}}$ are complex model parameters. One can straightforwardly prove that $w_{LC}(t) = \sqrt{\sigma_{\mathscr{R}}/\beta_{\mathscr{R}}} e^{i\omega t}$, $\omega = \sigma_{\mathscr{I}} - \beta_{\mathscr{I}}\sigma_{\mathscr{R}}/\beta_{\mathscr{R}}$, is a limit cycle solution of the SL system and it is stable provided $\sigma_{\mathscr{R}} > 0$ and $\beta_{\mathscr{R}} > 0$.

We then assume to have n identical copies of the SL system coupled through non-reciprocal interactions and the hypothesis of mean field Equation (4.3.13) (main text), hereby reported

$$\dot{w}_j = \frac{\sigma}{k_j^{(in)}} \sum_\ell A_{j\ell} w_\ell - \beta w_j |w_j|^2 = \sigma w_j - \beta w_j |w_j|^2 + \sigma \sum_\ell \mathscr{L}_{j\ell} w_\ell$$

Because of the structure of the coupling, $w_{LC}(t)$ is also a solution of the latter equation. To inquire about its stability, we consider the perturbation given by $w_j(t) = w_{LC}(t)\,(1+u_j(t))\,e^{iv_j(t)}$, where $u_j(t)$ and $v_j(t)$ are real and small functions nodes dependent. We then insert the latter into (4.3.13) (main text) and we expand by retaining only the first order terms, obtaining

$$\frac{d}{dt}\begin{pmatrix} u_j \\ v_j \end{pmatrix} = \begin{pmatrix} -2\sigma_{\mathscr{R}} & 0 \\ -2\beta_{\mathscr{I}}\frac{\sigma_{\mathscr{R}}}{\beta_{\mathscr{R}}} & 0 \end{pmatrix} \begin{pmatrix} u_j \\ v_j \end{pmatrix} + \sum_\ell \mathscr{L}_{j\ell} \begin{pmatrix} \sigma_{\mathscr{R}} & -\sigma_{\mathscr{I}} \\ \sigma_{\mathscr{I}} & \sigma_{\mathscr{R}} \end{pmatrix} \begin{pmatrix} u_\ell \\ v_\ell \end{pmatrix} \quad (4.11.1)$$

We invoke once again the existence of an eigenbasis of the Laplace matrix, $\vec{\varphi}^{(\alpha)}$, $\Lambda^{(\alpha)}$, to decompose the perturbation u_j and v_j, and eventually get

$$\begin{aligned}\frac{d}{dt}\begin{pmatrix}u^\alpha\\ v^\alpha\end{pmatrix} &= \left[\begin{pmatrix}-2\sigma_{\mathscr{R}} & 0\\ -2\beta_{\mathscr{I}}\frac{\sigma_{\mathscr{R}}}{\beta_{\mathscr{R}}} & 0\end{pmatrix}+\Lambda^{(\alpha)}\begin{pmatrix}\sigma_{\mathscr{R}} & -\sigma_{\mathscr{I}}\\ \sigma_{\mathscr{I}} & \sigma_{\mathscr{R}}\end{pmatrix}\right]\begin{pmatrix}u^\alpha\\ v^\alpha\end{pmatrix}\\ &= \left(\mathbf{J}+\Lambda^{(\alpha)}\mathbf{J}_2\right)\begin{pmatrix}u^\alpha\\ v^\alpha\end{pmatrix} =: \mathbf{J}^{(\alpha)}\begin{pmatrix}u^\alpha\\ v^\alpha\end{pmatrix}\end{aligned} \tag{4.11.2}$$

By inserting the given expressions for $\mathbf{J}$ and $\mathbf{J}_2$, in the general formulae we obtain for the coefficients of $S_2(\kappa)$

$$\begin{aligned}c_{2,2} &= -\sigma_{\mathscr{I}}^2\left(\sigma_{\mathscr{R}}^2+\sigma_{\mathscr{I}}^2\right)\\ c_{2,1} &= 2\sigma_{\mathscr{I}}^2\sigma_{\mathscr{R}}\left(\beta_{\mathscr{R}}\sigma_{\mathscr{R}}+\beta_{\mathscr{I}}\sigma_{\mathscr{I}}\right)\frac{1}{\beta_{\mathscr{R}}}\\ c_{2,0} &= -\sigma_{\mathscr{I}}^2\sigma_{\mathscr{R}}^2\left(\beta_{\mathscr{R}}^2+\beta_{\mathscr{I}}^2\right)\frac{1}{\beta_{\mathscr{R}}^2}\end{aligned} \tag{4.11.3}$$

while for $S_1(\kappa)$

$$\begin{aligned}c_{1,4} &= \sigma_{\mathscr{R}}^2\left(\sigma_{\mathscr{R}}^2+\sigma_{\mathscr{I}}^2\right)\\ c_{1,3} &= -2\sigma_{\mathscr{R}}^2\left(2\beta_{\mathscr{R}}\sigma_{\mathscr{R}}^2+\beta_{\mathscr{I}}\sigma_{\mathscr{I}}\sigma_{\mathscr{R}}+\beta_{\mathscr{R}}\sigma_{\mathscr{I}}^2\right)\frac{1}{\beta_{\mathscr{R}}}\\ c_{1,2} &= \sigma_{\mathscr{R}}^2\left(5\beta_{\mathscr{R}}\sigma_{\mathscr{R}}^2+4\beta_{\mathscr{I}}\sigma_{\mathscr{I}}\sigma_{\mathscr{R}}+\beta_{\mathscr{R}}\sigma_{\mathscr{I}}^2\right)\frac{1}{\beta_{\mathscr{R}}}\\ c_{1,1} &= -2\sigma_{\mathscr{R}}^3\left(\beta_{\mathscr{R}}\sigma_{\mathscr{R}}+\beta_{\mathscr{I}}\sigma_{\mathscr{I}}\right)\frac{1}{\beta_{\mathscr{R}}}\\ c_{1,0} &= 0\end{aligned} \tag{4.11.4}$$

As previously done in the case of the Volterra model, the explicit knowledge of the polynomial S_1 and S_2 allows to compute the (in)stability region as shown in Figure 4.6 (main text) or Figure 4.9 in a setting where the instability condition can be realized for both a reciprocal and non-reciprocal coupling. The instability region (gray) is shown in the complex plane $(\mathscr{R}\Lambda, \mathscr{I}\Lambda)$ together with the spectrum of a reciprocal web of long-range interactions (black dots) as well with a non-reciprocal one (white dots): Because in both cases there are eigenvalues belonging to the instability region, the instability is possible and thus a spatio-temporal pattern emerges (see panel b) in the case of reciprocal interactions and panel c) for non-reciprocal ones). The numerical simulations have been perfumed using a 4-th order Runge-Kutta method starting from initial conditions δ-close to the homogeneous limit cycle solution $w_{LC}(t) = \sqrt{\sigma_{\mathscr{R}}/\beta_{\mathscr{R}}}e^{i\omega t}$. In both cases, the maximum of the dispersion relation λ_α is of order of the unity and thus a relatively small integration span is sufficient to reveal the wavy solution. The underlying coupling is a directed Erdős-Rényi network with $n = 40$ nodes and a probability for a directed link to exist between two nodes is $p = 0.08$. In Figure 4.10, we report the bifurcation diagram in the plane $\sigma_{\mathscr{I}}$ and $\beta_{\mathscr{I}}$, for $\sigma_{\mathscr{R}} = \beta_{\mathscr{R}} = 1$. Two regions can be observed: in region A (black), the instability can be initiated by both a reciprocal and non-reciprocal web of long-range interactions, while, in region B (white), only non-reciprocal interactions can determine an instability and the ensuing wavy solution.

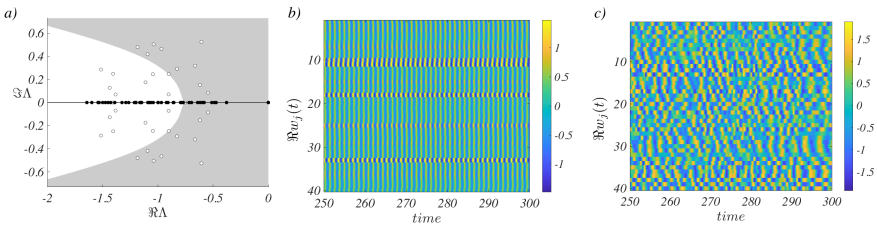

Figure 4.9: Instability region and patterns for the Stuart-Landau model. In panel a) we report the region of the complex plane $(\mathscr{R}\Lambda, \mathscr{I}\Lambda)$ for which the instability condition is satisfied (gray), for the parameters values $\sigma_{\mathscr{R}} = 1$, $\sigma_{\mathscr{I}} = 4.3$, $\beta_{\mathscr{R}} = 1$ and $\beta_{\mathscr{I}} = -2$. We can observe that the instability region intersects the real axis and thus any kind of coupling, being reciprocal (black dots) or non-reciprocal(white dots), can exhibit eigenvalues entering the instability region and thus allowing for an instability to set on, followed by a spatio-temporal patterns as shown in panel b), where we report the real part of the complex state variable w_i in the case of a reciprocal coupling, and panel c), for a non-reciprocal one.

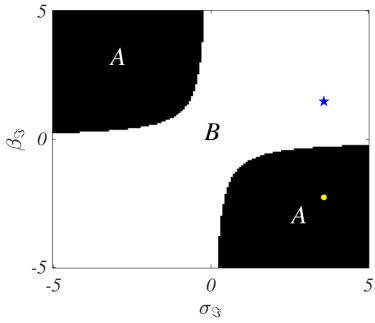

Figure 4.10: Bifurcation diagram for the Stuart-Landau model. For the set of parameters values $\sigma_{\mathscr{R}} = 1.0$ and $\beta_{\mathscr{R}} = 1.0$, we report the range of the remaining parameters $\sigma_{\mathscr{I}}$ and $\beta_{\mathscr{I}}$ for which the instability can emerge. In the A region (black), the homogeneous equilibrium is stable and it can be destabilized by a reciprocal coupling as well as a non-reciprocal one. On the other hand, in the B region (white), the homogeneous equilibrium is always stable and no pattern can develop using a symmetric coupling. On the contrary, one can found non-reciprocal couplings capable to destabilize the homogeneous equilibrium and thus the system to develop a wavy heterogeneous solution. The patterns shown in the panel b) of Figure 4.6 (main text) correspond to the values $\sigma_{\mathscr{I}} = 4$ and $\beta_{\mathscr{I}} = 1$ and clearly belong to the B region (blue star). The patterns presented in Figure 4.9 for parameters values $\sigma_{\mathscr{I}} = 4$ and $\beta_{\mathscr{I}} = -2$ correspond to the region A (yellow dot).

4.12 SM 8: Instability onset in the general d-dimensional case

Let us consider n copies of a generic d-dimensional system coupled through non-reciprocal interactions as in Equation (4.2.4), hereby recalled

$$\dot{\vec{x}}_i = \vec{F}(\vec{x}_i) + \sum_{j=1}^{n} \mathscr{L}_{ij} \vec{F}(\vec{x}_i, \vec{x}_j) \quad \forall i = 1, \dots, n$$

Assume that there exists a homogeneous solution $\vec{x}_i = \vec{x}^s$ for the decoupled system, that clearly results a solution also for the coupled one. To study its stability in the coupled

case, let us linearize the system about this reference solution to obtain Equation (4.2.5), which can be further analyzed by projecting it onto the Laplacian's eigenbasis to eventually get Equation (4.2.7).

The stability of the reference solution can be determined by studying the sign of the real part of the roots of the characteristic polynomial (4.3.14)

$$p_d(\lambda) := (-1)^d \left[a_0 \lambda^d + a_1 \lambda^{d-1} + a_2 \lambda^{d-2} + \cdots + a_d \right]$$

A straightforward computation, ultimately based on the expansion of the determinant defining the characteristic polynomial, allows to determine

$$\begin{aligned}
a_1 &= -\mathrm{tr}\left(\mathbf{J}_1 + \mathscr{R}\Lambda^{(\alpha)} \mathbf{J}_2 \right) - i\mathscr{I}\Lambda^{(\alpha)} \mathrm{tr}\mathbf{J}_2 \qquad (4.12.1)\\
a_2 &= \sum_{\ell=1}^{d} \sum_{j=\ell+1}^{d} \Big\{ (\mathbf{J}_1 + \mathscr{R}\Lambda^{(\alpha)} \mathbf{J}_2)_{\ell\ell} (\mathbf{J}_1 + \mathscr{R}\Lambda^{(\alpha)} \mathbf{J}_2)_{jj} + \\
&- (\mathbf{J}_1 + \mathscr{R}\Lambda^{(\alpha)} \mathbf{J}_2)_{\ell j} (\mathbf{J}_1 + \mathscr{R}\Lambda^{(\alpha)} \mathbf{J}_2)_{j\ell} + \\
&+ (\mathscr{I}\Lambda^{(\alpha)})^2 \left[(\mathbf{J}_2)_{j\ell} (\mathbf{J}_2)_{\ell j} - (\mathbf{J}_2)_{\ell\ell} (\mathbf{J}_2)_{jj} \right] \Big\} + \\
&+ i\mathscr{I}\Lambda^{(\alpha)} \sum_{\ell=1}^{d} \sum_{j=\ell+1}^{d} \Big\{ (\mathbf{J}_1 + \mathscr{R}\Lambda^{(\alpha)} \mathbf{J}_2)_{\ell\ell} (\mathbf{J}_2)_{jj} + (\mathbf{J}_1 + \mathscr{R}\Lambda^{(\alpha)} \mathbf{J}_2)_{jj} (\mathbf{J}_2)_{\ell\ell} + \\
&- (\mathbf{J}_1 + \mathscr{R}\Lambda^{(\alpha)} \mathbf{J}_2)_{\ell j} (\mathbf{J}_2)_{j\ell} - (\mathbf{J}_1 + \mathscr{R}\Lambda^{(\alpha)} \mathbf{J}_2)_{j\ell} (\mathbf{J}_2)_{\ell j} \Big\}
\end{aligned}$$

Assuming to deal with reciprocal interactions, we can show (see SM 4.5) that the spectrum is real even if the Laplace matrix is not symmetric. The previous equations simplify by imposing $\mathscr{I}\Lambda^{(\alpha)} = 0$, and in particular a_1 and a_2 are real numbers, that are assumed to be positive because of the assumption of stable equilibrium under symmetric interactions.

Let us now discuss the role of the auxiliary polynomial $q(\lambda)$. Let $P(z)$ by a generic polynomial with complex coefficients. Let us assume z_1 to be a simple complex root and, to simplify, let us also assume to be able to factorize $P(z) = (z - z_1)P_1(z)$, where $P_1(z)$ has real coefficients. Let us define $Q(z) = (z - \overline{z_1})P(z)$, then

$$Q(z) = (z - \overline{z_1})P(z) = (z - \overline{z_1})(z - z_1)P_1(z) = (z^2 - 2z\mathscr{R}z_1 + |z_1|^2)P_1(z)$$

from which it follows that $Q(z)$ has real coefficients and its roots have the same real part of the roots of $P(z)$ (computed twice in the case of z_1). The general strategy would be to factorize all the complex roots of $P(z)$ and build an auxiliary polynomial $Q(z)$ according to this recipe. In general, we do not know all such roots and thus we can simply assume to apply this process to all roots, even to the real ones, i.e., to the whole polynomial, thus defining $Q(z) = \overline{P(\overline{z})}P(z)$. The resulting polynomial will have a degree equal to the double of the degree of $P(z)$, all its coefficients will be real by construction and its roots will have the same real part of the roots of $P(z)$.

By applying such recipe to $p_d(\lambda) = \lambda^d + a_1\lambda^{d-1} + a_2\lambda^{d-2} + \cdots + a_d$, we obtain the polynomial $q(\lambda) = \lambda^{2d} + b_1\lambda^{2d-1} + b_2\lambda^{2d-2} + \cdots + b_{2d}$ defined in the main text.

A direct computation, consisting in equating coefficients of equal powers of λ in $q(z)$ and $\overline{p_d(\overline{z})}p_d(z)$, allows to determine

$$\begin{aligned} b_1 &= a_1 + \overline{a_1} = 2\mathscr{R}a_1 \\ b_2 &= a_2 + \overline{a_2} + a_1\overline{a_1} = 2\mathscr{R}a_2 + |a_1|^2 \end{aligned}$$

By using the previously obtained expression (4.12.1) for a_1, we attain

$$b_1 = -2\mathrm{tr}\left(\mathbf{J}_1 + \mathscr{R}\Lambda^{(\alpha)}\mathbf{J}_2\right)$$

and we can observe that it coincides (module a factor 2) with a_1 obtained once we impose $\mathscr{I}\Lambda^{(\alpha)} = 0$; hence b_1 results to be always positive, as a_1 does. The non-reciprocal interactions cannot thus change the sign of b_1. On the other hand, by using the expression for a_2 given in (4.12.2), we can obtain the conditions presented in the main text (4.3.15) and (4.3.16) ensuring $b_2 < 0$. Indeed, recalling (4.12.2) we can write

$$\begin{aligned} b_2 &= 2\mathscr{R}a_2 + |a_1|^2 = \left(2\mathscr{R}a_2 + |a_1|^2\right)_{\mathscr{I}\Lambda^{(\alpha)}=0} + \\ &+ 2(\mathscr{I}\Lambda^{(\alpha)})^2 \sum_{\ell=1}^{d}\sum_{j=\ell+1}^{d}\left\{\left[(\mathbf{J}_2)_{j\ell}(\mathbf{J}_2)_{\ell j} - (\mathbf{J}_2)_{\ell\ell}(\mathbf{J}_2)_{jj}\right]\right\} + (\mathscr{I}\Lambda^{(\alpha)})^2\,(\mathrm{tr}\mathbf{J}_2)^2 \end{aligned}$$

By observing that $\left(2\mathscr{R}a_2 + |a_1|^2\right)_{\mathscr{I}\Lambda^{(\alpha)}=0} > 0$, because of the assumption of stability of the system using symmetric interactions, we can conclude that b_2 can be negative if $(\mathscr{I}\Lambda^{(\alpha)})^2$ is large enough and

$$2\sum_{\ell=1}^{d}\sum_{j=\ell+1}^{d}\left\{\left[(\mathbf{J}_2)_{j\ell}(\mathbf{J}_2)_{\ell j} - (\mathbf{J}_2)_{\ell\ell}(\mathbf{J}_2)_{jj}\right]\right\} + (\mathrm{tr}\mathbf{J}_2)^2 < 0$$

After some algebraic manipulations, we can rewrite the term involving the double sum as

$$\sum_{\ell=1}^{d}\sum_{j=\ell+1}^{d}\left\{\left[(\mathbf{J}_2)_{j\ell}(\mathbf{J}_2)_{\ell j} - (\mathbf{J}_2)_{\ell\ell}(\mathbf{J}_2)_{jj}\right]\right\}\frac{\mathrm{tr}\mathbf{J}_2^2 - (\mathrm{tr}\mathbf{J}_2)^2}{2},$$

from which the condition (4.3.15) follows. This is a sufficient conditions for the destabilization of the equilibrium solution; if the latter does not hold true, one could in principle look for other conditions capable to change the sign of one of the remaining coefficients, b_j, of the polynomial $q(\lambda)$.

4.13 On the different Laplacian operators and their use

This section was not part of the original paper, but was added to further discuss the use of the Laplacian operator.

In the above Chapter, we have discussed a framework where non-reciprocal nonlocal interactions cause the formation of patterns through a mechanism closely related

to the Turing one, even if no diffusion takes place. Already during the work, which eventually lead to the paper, we have struggled to frame the kind of interactions between the nodes. For us, coming from the Turing framework, it is clear from Equation (4.2.2) that the interactions are long-range, because the reaction parts involve terms not limited to single node variables, and non-diffusive, because the coupling is not realized with a combinatorial Laplace matrix, as described in Figure 4.1. However, as already discussed in the introduction, in the literature long-range interactions are those occurring between nodes that are not adjacent, hence such adjective may have confused the reader. On the other hand, non-local couplings are widely used in the study of chimera patterns and they describe lattices where each node is coupled not only to its direct neighbors, but also to neighbors at distance greater than 1. Hence, to describe our setting, we opted for a compromise between the two terminologies and chose the term *non-local long-range* interactions.
The Laplacian we obtained to describe the interaction process, Equation (4.2.3), is called *consensus* or *reactive Laplacian* and it is a kind of normalized Laplacian, like the *random walk Laplacian* [179]. Let us however stress that the consensus Laplacian performs an average of the connected nodes while the random walk Laplacian does not. For scholars studying reaction-diffusion processes on networks, "true" diffusion is always modeled by the *combinatorial Laplacian* because, for a regular lattice, it is the equivalent of the Laplace operator on continuous support. Since the latter represents a diffusive phenomenon once we assume Fick's law, it is straightforward to use the former Laplacian to model diffusion on any network topology (see also Chapter 3, where we derive the diffusive process on a general network by using the incidence matrix). Let us observe that sometimes normalized Laplacians, and in particular the random walk one, are used to model diffusion. However, this is correct only in the case of regular networks, otherwise the total mass is not conserved and the process is not "true" diffusion.

Part II

Higher-order interactions

Chapter 5

From pairwise to many-body and higher-order interactions

Networks are a powerful tool in the modeling of complex systems. Then, why would we need to go beyond them? Their simple and effective formalism hides a big limitation: they capture only pairwise interactions among the elementary units. For instance, let us assume to have three oscillators coupled through a complete network, i.e., each oscillator is connected to the other two. However, a 3-body interaction may be of a different nature than a 2-body (pairwise) one. Indeed, there is increasing evidence that many natural and social systems exhibit *higher-order* (or *high-order*) interactions, rather than pairwise ones. For example, co-authorship networks are intrinsically higher-order, as they are made of group interactions, i.e., co-authoring a scientific publication, involving, in general, more than two authors [180]. In competitive ecological networks, it was found that the effect of one competitor on another one may be affected by the presence of a third species [181]. Further examples come from neuroscience, where it was observed that pairwise models are not enough in describing neuronal dynamics [182, 183]. Moreover, many-body interactions allow to explain several other phenomena, such as epileptic seizures in the brain [184], bi-stable visual perception [185], and critical mass phenomena in the emergence of social conventions [186]. Some of the examples mentioned above are not recent. Indeed, as it is common in research, it took a critical amount of piling up evidence, before the network community turned to this exciting framework. The mathematical tools were already there, namely hypergraphs [187] and simplicial complexes [188], and have been the backbone of the successive research, as much as graph theory had been for network science. Such structures have been used to review several dynamical processes, such as random walks [189, 190, 191], consensus [192, 193], epidemics [194] and social contagion [195, 196] and scholars have found that many-body interactions may dramatically affect the global behavior of the system, such as explosive (abrupt) transitions from one state to another [197], e.g., from synchronization to decoherence and vice versa [198].

Other popular emergent properties, such as pattern formation and synchronization, have been studied and revisited in light of higher-order interactions. Pattern formation has, however, attracted less attention and the work in this second part of the thesis is an attempt to fill the gap. For what concerns synchronization of chaotic and periodic oscillators on higher-order systems, a vast literature has developed from the end of the 2010s up to now, in particular for the Kuramoto model [43]. For example, it was shown that the latter exhibits abrupt desynchronization and multi-stability when 3-body interactions replace [199], or are added to [200], pairwise interactions in all-to-all configurations, i.e., when every oscillator is coupled to all the others. Moreover, still in the framework of the Kuramoto model, a general theory for any higher-order complex topology has been developed [201]. In the above works, the dynamics lie in the nodes, whilst the structure mediates the interactions (pairwise and higher-order) among them. However, the tools of algebraic topology allow to extend the framework and consider dynamics not only on the nodes, but also on the links and higher-order hyperedges. We, then, talk about topological signals, and it was observed that such higher-order dynamics yield explosive transitions to synchronization [202, 203], in analogy with many-body interactions. The framework of the Kuramoto model is, nonetheless, intrinsically different from ours. In fact, the former model does not require a homogeneous state, while that is a necessary condition for the development of our theory. As discussed in Chapter 1, complete synchronization of chaotic oscillators provides a formalism which, considered some *caveats*, fits also the Turing framework, and effects of many-body interactions on the stability of the synchronous solutions have been studied, for instance, in [204, 45]. The latter is the backbone of the work discussed in Chapter 6, while the theory of topological signals will be put to use for the paper of Chapter 7. The scope of this Chapter is to introduce aforementioned works, which are among the firsts of their kind, as Turing patterns have been studied on higher-order structures only in another previous work [205]. The basic mathematical tools of higher-order structures will be examined in the next section. Then, in Section 5.2, we will introduce a formalism to study the stability of the synchronous solution for systems with many-body interactions, while, in Section 5.3, topological signals on higher-order structures will be discussed.

5.1 Higher-order structures: simplicial complexes and hypergraphs

Pairwise interactions are encoded through the well-known adjacency matrix $\mathbf{A}$ [79]. For non-weighted networks[(1)], we have that, if there is a link between two nodes i and j, the entry $A_{ij} = 1$. When dealing with many-body interactions, we resort to *adjacency tensors*. A $(d+1)$-body interaction will be represented through the d-th order adjacency tensor $\mathbf{A}^{(d)}$: the entry $A^{(d)}_{ij_1\dots j_d} = 1$ if there is a $(d+1)$-body interaction between nodes $i, j_1, ..., j_d$. We say that the considered higher-order structure has a *hyperedge* between nodes $i, j_1, ..., j_d$. Such hyperedges, and thus the adjacency tensors, are symmetric. In

[(1)]The theory is, of course, more general and so it is for weighted higher-order structures [206]. Nonetheless, in the following, we will only address non-weighted hypergraphs and simplicial complexes, hence all the definitions will be for non-weighted structures.

light of this new definition, we can observe that the adjacency matrix is a 1-st order adjacency tensor, since it encodes the 2-body interactions, and can be referred as $\mathbf{A}^{(1)}$. We can also generalize the concept of degree, by defining the *d-degree* $k_i^{(d)}$ as

$$k_i^{(d)} = \frac{1}{d!} \sum_{j_1,\dots,j_d=1}^{N} A_{ij_1\dots j_d}^{(d)},$$

representing the number of hyperedges of order d of which node i is part of. In a simplicial complex, if a d-body interaction is present, then all other sub-interactions need to be present as well [207]. For example, if there exists a hyperedge between nodes i, j, k and l, i.e., the 4-body interaction $\{i,j,k,l\}$, then there exist also the hyperedges $\{i,j,k\}$, $\{i,j,l\}$, $\{i,k,l\}$ and $\{j,k,l\}$ (4 3-body interactions), $\{i,j\}$, $\{i,k\}$, $\{i,l\}$, $\{j,k\}$, $\{j,l\}$ and $\{k,l\}$ (6 2-body interactions). The definition of hypergraph is less restrictive and the presence of a d-body interaction does not reveal anything about the presence of other hyperedges. Their laxer definition makes them more appealing to model large real-world systems, where it is less likely to have all the sub-interactions active [208]. In order to highlight the distinction between the two higher-order structures, in Figure 5.1, we depict an example of hypergraph and simplicial complex with the same number of nodes and higher-order interactions. Such structural difference may affect the dynamics: for example, it has been recently suggested that synchronization is enhanced in the Kuramoto model on hypergraphs, respect to the same model on simplicial complexes [209].

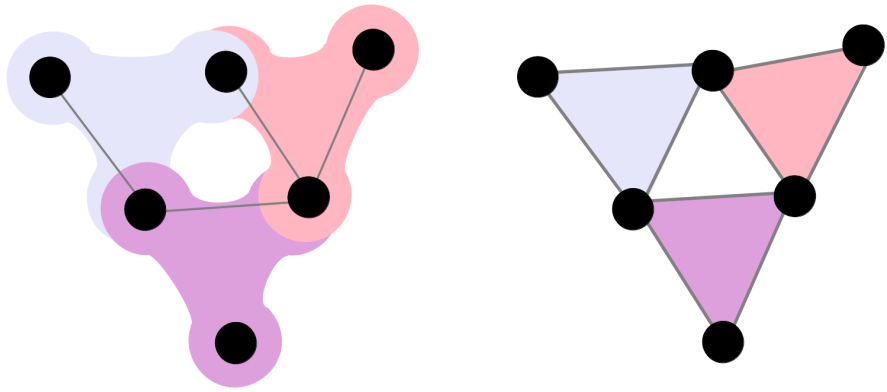

Figure 5.1: On the left, a hypergraph of 6 nodes, 4 links and 3 2-hyperedges; on the right a simplicial complex of 6 nodes, 9 links and 3 2-hyperedges (triangles). We can observe that, for every triangle, all the pairwise interactions are active in the simplicial complex, whilst the hypergraph does not have such closure relation.

In the literature, scholars tend to refer to higher-order interactions as *hyperedges*, when the support is a hypergraph, and *simplices*, when it is a simplicial complex. Moreover, a d-body interaction is called d-hyperedge or $(d-1)$-simplex, because in the theory of simplicial complex the nodes are 0-simplices, links (2-body) are 1-simplices, and so on. We find the latter nomenclature more rigorous, as it comes from algebraic

topology. Nonetheless, not all hyperedges are simplices, whilst the vice versa is true. For the following, we have chosen to use the more general, but rigorous, definition of $(d-1)$-hyperedge for a general d-body interaction.

In the first part of this work we have dealt with non-reciprocal pairwise interactions, which are modeled by asymmetric networks. One may wonder whether an analogous formalism is available also for higher-order structures. Indeed, computer scientists have been using directed hypergraphs to model the flow of information for over thirty years [210]. In order to study dynamics on top of them, a tensor formalism for a particular sub-class of directed hypergraph has been introduced in [211] (see also Summary of other coauthored papers, at the end of this thesis). The latter does not describe all possible forms of directed interactions, but allow to perform a semi-analytical study of the Master Stability Function. Another novel and interesting framework is that of *triadic interactions* [212], which will not be discussed further. The above description, both symmetric and non-reciprocal, falls within the paradigm of *many-body* interactions. In fact, the dynamical units are (in) the nodes and the hyperedges mediate the interactions among them. Simplicial complexes can thus be thought as a particular case of hypergraphs. However, the rigorous definition of simplicial complex and the tools of algebraic topology allow for a further extension of the framework, yielding what can be considered as *proper* higher-order interaction, as we will show at the end of this Chapter.

5.2 A formalism to study the stability of the homogeneous solution

In Chapter 1, we have discussed the stability of an ensemble of n identical units $\vec{x}_i$, perturbed in their homogeneous (synchronous) state. For every unit, the dynamics are described by the following equation

$$\dot{\vec{x}}_i = \vec{f}(\vec{x}_i) + \sigma \sum_{j=1}^{n} A_{ij} \vec{g}(\vec{x}_j, \vec{x}_i) \tag{5.2.1}$$

where A_{ij}, i.e., the adjacency matrix, determines the pairwise connections between the units. In this section we will perform an analogous analysis, extending the framework by considering systems with many-body interactions, following the formalism developed by Gambuzza et al. [45] for simplicial complexes. As we have discussed in the previous section, a simplicial complex may be thought as a hypergraph with a closure relation, as long as we consider the many-body framework. The aforementioned formalism was developed without considering such closure relation and it is more general than originally thought. In fact, it is suitable for any hypergraph. Let us start with the dynamical equations for an ensemble of n identical units $\vec{x}_i$ subject to many-body interactions up to an arbitrary order P ($P \leq n$)

$$\begin{aligned}\dot{\vec{x}}_i = \vec{f}(\vec{x}_i) + \sigma_1 \sum_{j_1=1}^{n} A^{(1)}_{ij_1} \vec{g}^{(1)}(\vec{x}_i, \vec{x}_{j_1}) + \sigma_2 \sum_{j_1,j_2=1}^{n} A^{(2)}_{ij_1j_2} \vec{g}^{(2)}(\vec{x}_i, \vec{x}_{j_1}, \vec{x}_{j_2}) + \\ + \cdots + \sigma_P \sum_{j_1,j_2,\ldots,j_P=1}^{n} A^{(P)}_{ij_1j_2\ldots j_P} \vec{g}^{(P)}(\vec{x}_i, \vec{x}_{j_1}, \vec{x}_{j_2}, \ldots, \vec{x}_{j_P})\end{aligned} \tag{5.2.2}$$

where $\vec{f} : \mathbb{R}^m \to \mathbb{R}^m$ describes the local (isolated) dynamics of each unit $\vec{x}_i$, σ_d are the coupling strengths for every order, $\vec{g}^{(d)} : \mathbb{R}^{m\times(d+1)} \to \mathbb{R}^m$ the coupling functions and $A^{(d)}$ the adjacency tensors, with $d \in \{1,\ldots,P\}$. Note that $A^{(1)}_{ij_1}$, σ_1 and $\vec{g}^{(1)}$ of the above equation are exactly A_{ij}, σ and $\vec{g}$ of Equation (5.2.1). To guarantee the existence of the synchronous solution $\vec{x}_1 = \cdots = \vec{x}_n \equiv \vec{x}^*$ [44], we need the coupling functions to be non-invasive, i.e., $\vec{g}^{(d)}(\vec{x},\ldots,\vec{x}) = 0$ at each order d. Let us remark that such hypothesis is necessary to proceed with a semi-analytical study of the global synchronization properties of an ensemble of identical oscillators. In other frameworks, for instance when dealing with the Kuramoto model, the above assumption is not needed, because in this case the oscillators have often different proper frequencies and the goal is not to determine a global (full) synchronization. Without loss of generality, let us assume the latter to be also diffusive-like, namely

$$\vec{g}^{(d)}(\vec{x}_i, \vec{x}_{j_1}, \vec{x}_{j_2}, \ldots, \vec{x}_{j_d}) = \vec{h}^{(d)}(\vec{x}_{j_1}, \ldots, \vec{x}_{j_d}) - \vec{h}^{(d)}(\vec{x}_i, \ldots, \vec{x}_i)$$

with

$$\vec{h}^{(d)} : \mathbb{R}^{m\times d} \to \mathbb{R}^m$$

Let us remark that , as long as the coupling is non-invasive, the following analysis could be more general and does not require diffusive-like coupling functions. However, through the "glasses" of Turing theory of pattern formation, the coupling is always diffusive-like. Hence, the choice. Additionally, we require the coupling functions to be nonlinear, in order to deal with a proper many-body dynamics. In fact, if those would be linear, the d-body interaction could be reduced to a 2-body one, only by rescaling the adjacency matrix, which would become weighted [192]. Then, Equation (5.2.2) turns into

$$\begin{aligned}\dot{\vec{x}}_i \quad &= \vec{f}(\vec{x}_i) + \sigma_1 \sum_{j_1=1}^{n} A^{(1)}_{ij_1} (\vec{h}^{(1)}(\vec{x}_{j_1}) - \vec{h}^{(1)}(\vec{x}_i)) + \\ &+ \sigma_2 \sum_{j_1,j_2=1}^{n} A^{(2)}_{ij_1j_2} (\vec{h}^{(2)}(\vec{x}_{j_1}, \vec{x}_{j_2}) - \vec{h}^{(2)}(\vec{x}_i, \vec{x}_i)) + \cdots + \\ &+ \sigma_P \sum_{j_1,j_2,\ldots,j_P=1}^{n} A^{(P)}_{ij_1j_2\ldots j_P} (\vec{h}^{(P)}(\vec{x}_{j_1}, \ldots, \vec{x}_{j_P}) - \vec{h}^{(P)}(\vec{x}_i, \ldots, \vec{x}_i))\end{aligned} \tag{5.2.3}$$

We know that a synchronous solution exists; let us now study its stability against small perturbations. Hence, let us perturb the solution $\vec{x}^*$ with a heterogeneous perturbation, i.e., $\vec{x}_i = \vec{x}^* + \delta\vec{x}_i$, $\forall\, i \in \{1,\ldots,n\}$. If we insert the latter into Equation (5.2.3) and expand up to the first order, we obtain the following expression

$$\delta\dot{\vec{x}}_i \quad = \quad \frac{\partial \vec{f}(\vec{x}_i)}{\partial \vec{x}_i}\Big|_{\vec{x}^*} \delta\vec{x}_i + \sigma_1 \sum_{j_1=1}^{n} \tau_{ij_1} \partial_1 \vec{h}^{(1)}(\vec{x}_{j_1})\Big|_{\vec{x}^*} \delta\vec{x}_{j_1} +$$

$$+\sigma_2 \sum_{j_1,j_2=1}^{n} \tau_{ij_1j_2}\Big(\partial_1\vec{h}^{(2)}(\vec{x}_{j_1},\vec{x}_{j_2})\Big|_{(\vec{x}^*,\vec{x}^*)}\delta\vec{x}_{j_1}+\partial_2\vec{h}^{(2)}(\vec{x}_{j_1},\vec{x}_{j_2})\Big|_{(\vec{x}^*,\vec{x}^*)}\delta\vec{x}_{j_2}\Big)+$$
$$+\cdots+\sigma_P \sum_{j_1,j_2,\dots,j_P=1}^{n} \tau_{ij_1j_2\dots j_P}\Big(\partial_1\vec{h}^{(P)}(\vec{x}_{j_1},\dots,\vec{x}_{j_P})\Big|_{(\vec{x}^*,\dots,\vec{x}^*)}\delta\vec{x}_{j_1}+\cdots+$$
$$+\partial_P\vec{h}^{(P)}(\vec{x}_{j_1},\dots,\vec{x}_{j_P})\Big|_{(\vec{x}^*,\dots,\vec{x}^*)}\delta\vec{x}_{j_P}\Big)$$

where ∂_i indicates[2] the derivative with respect to the i-th variable of functions $h^{(d)}$ and the tensors τ are given by

$$\tau_{ij_1}=A^{(1)}_{ij_1}-k^{(1)}_i\delta_{ij_1},\quad \dots\dots\ ,\ \tau_{ij_1j_2\dots j_P}=A^{(P)}_{ij_1j_2\dots j_P}-P!k^{(P)}_i\delta_{ij_1j_2\dots j_P}$$

$k^{(d)}_i$ is the *d-degree*, defined in the previous section, and $\delta_{ij_1\dots j_d}$ is the generalized Kronecker delta. By defining

$$k^{(d)}_{i,j}=\frac{1}{(d-1)!}\sum_{k_1,\dots,k_{d-1}}^{N}A^{(d)}_{ijk_1\dots k_{d-1}},$$

which represents the number of hyperedges of order d to which link $\{i,j\}$ is part and by observing that tensors $\tau_{ij_1j_2\dots j_d}$ are symmetric, we obtain

$$\begin{aligned}\delta\dot{\vec{x}}_i &= \frac{\partial\vec{f}(\vec{x}_i)}{\partial\vec{x}_i}\Big|_{\vec{x}^*}\delta\vec{x}_i+\sigma_1\sum_{j_1=1}^{n}L^{(1)}_{ij_1}\partial_1\vec{h}^{(1)}(\vec{x}_{j_1})\Big|_{\vec{x}^*}\delta\vec{x}_{j_1}+\cdots+\\ &+\sigma_P\Big(\sum_{j_1}^{n}L^{(P)}_{ij_1}\partial_1\vec{h}^{(P)}(\vec{x}_{j_1},\dots,\vec{x}_{j_P})\Big|_{(\vec{x}^*,\dots,\vec{x}^*)}\delta\vec{x}_{j_1}+\cdots+\\ &+\sum_{j_P}^{n}L^{(P)}_{ij_P}\partial_P\vec{h}^{(P)}(\vec{x}_{j_1},\dots,\vec{x}_{j_P})\Big|_{(\vec{x}^*,\dots,\vec{x}^*)}\delta\vec{x}_{j_P}\Big)\end{aligned}$$

where we have defined the generalized Laplacian matrix[3] for the interactions of order d as

$$L^{(d)}_{ij}=\begin{cases}-d!k^{(d)}_i & i=j\\ (d-1)!k^{(d)}_{i,j} & i\neq j\end{cases}. \tag{5.2.4}$$

Let us observe that, for each order d, the following relation stands

$$\sum_{j_1}^{n}L^{(d)}_{ij_1}\partial_1\vec{h}^{(d)}(\vec{x}_{j_1},\dots,\vec{x}_{j_d})\Big|_{(\vec{x}^*,\dots,\vec{x}^*)}\delta\vec{x}_{j_1}+\cdots+\sum_{j_d}^{n}L^{(d)}_{ij_d}\partial_d\vec{h}^{(d)}(\vec{x}_{j_1},\dots,\vec{x}_{j_d})\Big|_{(\vec{x}^*,\dots,\vec{x}^*)}\delta\vec{x}_{j_d}=$$

[2] Formally, it would be more correct to write $\partial\vec{h}^{(1)}(\vec{x}_{j_i})/\partial\vec{x}_{j_i}$ as done in [45, 211], however the latter form risks to be ambiguous with respect to the nodes' index.

[3] As discussed in Chapter 1, Laplacian matrices are usually defined as to be positive semi-definite in the framework of synchronization dynamics, while we prefer the negative semi-definite version in the case of Turing pattern formation. For this reason, the Laplacians used in this Chapter are all negative semi-definite, while in the original work, where this formalism was introduced, they are positive semi-definite [45].

$$= \sum_{j}^{n} L_{ij}^{(d)} \left(\partial_1 \vec{h}^{(d)}(\vec{x}_{j_1}, \ldots, \vec{x}_{j_d}) \Big|_{(\vec{x}^*, \ldots, \vec{x}^*)} \delta\vec{x}_{j_1} + \cdots + \partial_d \vec{h}^{(d)}(\vec{x}_{j_1}, \ldots, \vec{x}_{j_d}) \Big|_{(\vec{x}^*, \ldots, \vec{x}^*)} \delta\vec{x}_{j_d} \right)$$

If, moreover, we define the matrix

$$\mathbf{J}_h^{(d)} = \partial_1 \vec{h}^{(d)}(\vec{x}_{j_1}, \ldots, \vec{x}_{j_d}) \Big|_{(\vec{x}^*, \ldots, \vec{x}^*)} + \cdots + \partial_d \vec{h}^{(d)}(\vec{x}_{j_1}, \ldots, \vec{x}_{j_d}) \Big|_{(\vec{x}^*, \ldots, \vec{x}^*)}$$

and the nm-dimensional perturbation vector $\vec{\zeta} = [\delta\vec{x}_1^\top, \ldots, \delta\vec{x}_n^\top]^\top$, Equation (5.2.3) can be rewritten in a compact form

$$\dot{\vec{\zeta}} = \left[\mathbb{I}_n \otimes \mathbf{J}_f + \sigma_1 \mathbf{L}^{(1)} \otimes \mathbf{J}_h^{(1)} + \sigma_2 \mathbf{L}^{(2)} \otimes \mathbf{J}_h^{(2)} + \cdots + \sigma_P \mathbf{L}^{(P)} \otimes \mathbf{J}_h^{(P)} \right] \vec{\zeta} \tag{5.2.5}$$

The above equation describes the perturbation about the synchronous solution $\vec{x}^*$, but, in order to study its stability, we need to decompose the potential instability modes, i.e., we must diagonalize the system. We know that the generalized Laplacians are symmetric and zero-row-sum matrices, diagonalizable and with a real negative semi-definite spectrum, to which corresponds an orthonormal basis. However, this does not mean that all the generalized Laplacians are diagonalizable on the same basis and, in general, it is not true. In order to decompose the modes, the authors of [45] considered the hypothesis of natural coupling, namely $\forall \vec{x} \in \mathbb{R}^m$

$$\vec{h}^{(P)}(\vec{x}, \ldots, \vec{x}) = \cdots = \vec{h}^{(2)}(\vec{x}, \vec{x}) = \vec{h}^{(1)}(\vec{x})$$

This assumption means that all coupling functions have the same effect, when the whole system lies in a homogeneous state. The latter leads to

$$\mathbf{J}_h^{(P)} = \cdots = \mathbf{J}_h^{(2)} = \mathbf{J}_h^{(1)}$$

Hence, Equation (5.2.5) becomes

$$\dot{\vec{\zeta}} = \left[\mathbb{I}_n \otimes \mathbf{J}_f + (\sigma_1 \mathbf{L}^{(1)} + \cdots + \sigma_P \mathbf{L}^{(P)}) \otimes \mathbf{J}_h^{(P)} \right] \vec{\zeta}$$

If we define the matrix

$$\mathbf{M} = \sigma_1 \mathbf{L}^{(1)} + \ldots + \sigma_D \mathbf{L}^{(D)}$$

we can write the following Master Stability Equation describing the dynamics of the perturbation

$$\dot{\vec{\zeta}} = \left[\mathbb{I}_n \otimes \mathbf{J}_f + \mathbf{M} \otimes \mathbf{J}_h \right] \vec{\zeta} \tag{5.2.6}$$

which is analogous to Equation (1.2.2). Let $\vec{v}_1, \ldots, \vec{v}_n$ be the orthonormal basis of the matrix $\mathbf{M}$. By defining the new variable $\vec{\xi} = (V \otimes \mathbb{I}_m)\vec{\zeta}$, where $V = [\vec{v}_1, \ldots, \vec{v}_n]$, we can decouple the modes and rewrite, for $\alpha = 1, \ldots, n$, Equation (5.2.6) as

$$\dot{\vec{\xi}}_\alpha = [\mathbf{J}_f + \Lambda^{(\alpha)} \mathbf{J}_h] \vec{\xi}_\alpha \tag{5.2.7}$$

where $\Lambda^{(1)}, \ldots, \Lambda^{(n)}$ are the eigenvalues of the matrix $\mathbf{M}$. As for the pairwise case, the equation for the largest eigenvalue, $\Lambda^{(1)} = 0$, corresponds to the isolated system. In the

synchronization literature, it is said that the latter describes the linearized motion along the synchronous solution, while all the other equations describe the motion transverse to it. In both frameworks, Turing pattern formation and synchronization, only the transverse perturbation can drive the system unstable.

As we will show in the next Chapter, the formalism and techniques discussed above are ductile and powerful and the reformulation of reaction-diffusion equations is more general than a previous study of pattern formation in higher-order systems [205]. Nonetheless, the fact of projecting the interactions of all orders onto a matrix (**M**), which gives us the stability properties of the global system, may lead to the loss of certain local synchronization patterns, such as cluster synchronization [213].

5.3 From many-body to higher-order and topological signals

When the dynamics lie on the nodes of the higher-order structure, in the literature we talk about higher-order interactions. However, the hyperedges mediate concurrent interactions between the units, which remain interactions among 0-simplices (i.e., nodes); for this reason it would be more correct, in our opinion, to call them *many-body* interactions. In fact, they cannot model interactions between higher dimensions (simplices), nor one could move between different orders. Through the tools of algebraic topology, and in particular the boundary operators, we can attain such objective: in fact, this framework allows to study signals on each simplex, and to project them in the lower and upper dimensions. Such signals could, hence, interact with signals of different dimensions. Already by considering 0- and 1-simplices (i.e., nodes and links), this formalism appears extremely versatile and, besides bringing new and exciting perspectives, it could be use to revisit some already developed frameworks. For instance, the currents vector $\vec{\chi}$ seen in Chapter 3, modeling the currents entering and exiting the nodes, could be rethought as a topological signal on the links. Or, as another example, some aspects of the theory of temporal networks [214] could be extended by considering this new framework[(4)]. Interactions regarding topological signals are what, in our opinion, should be considered as *proper* higher-order interactions. This last statement stands in spite of our own works, in which we have dealt with many-body interactions, but called them higher-order [211, 215]. The first reason for this was that such distinction has been made clear by Bianconi only recently [207] and most of the community is not yet familiar with it. The other reason is that such distinction was not completely clear to us selves and it became clearer while we were working in both frameworks, i.e., many-body interactions (Chapter 6) and topological signals (Chapter 7). Let us consider a symmetric network of n nodes and m links. In Chapter 3, we defined the Laplacian matrix as $\mathbf{L} = -\mathbf{B}\mathbf{B}^\top$, where $\mathbf{B} \in \mathbb{R}^{n\times m}$ is the incidence matrix, obtained by choosing an orientation for the links. The first important remark is that such orienta-

[(4)] One significant difference between the framework of temporal networks and that of topological signal is that in the latter links are always present, despite the signal being zero, while in the former links can disappear. Nonetheless, one could consider, for example, the network of all possible interactions among the nodes and the topological signals on the links as the dynamical variable.

tion does not mean that the network becomes directed. The network is and remains symmetric, whilst defining an orientation on the links is equivalent to choosing a basis in a vector space. Indeed, different orientations yield different incidence matrices and the choice of the matrix $\mathbf{B}$, i.e., the base of the system of coordinates, sets the spatial coordinates. The Laplacian matrix $\mathbf{L}$ is, instead, orientation-independent, and it reflects the structure of the space.

It turns out that the matrix $\mathbf{B}$ is known in algebraic topology as the *boundary operator* $\mathbf{B}_1$. Leaving a detailed discussion for Chapter 7, let us say that $\mathbf{B}_1$ maps elements from the space of the 1-simplices (links) to the space of the 0-simplices (nodes). Its transposed, $\mathbf{B}_1^\top$, is known as *co-boundary operator* and performs the opposite action, i.e., from 0- to 1-simplices. Using this formalism, we can consider a signal on the nodes, $\vec{u} \in \mathbb{R}^n$, and, by means of the co-boundary operator, project it in the space of the links, namely $\mathbf{B}_1^\top \vec{u} \in \mathbb{R}^m$. Vice versa, we can project a signal on the links, $\vec{v} \in \mathbb{R}^m$, onto the space of the nodes, namely $\mathbf{B}_1 \vec{v} \in \mathbb{R}^n$. The boundary and co-boundary operators can be seen as analogous to the divergence and gradient in vector calculus: the former lowers the rank of a tensor, while the latter increases it[(5)]. The network Laplacian obtained from the boundary and co-boundary operators is known as *Hodge Laplacian* $\mathbf{L}_0$ and describes the propagation of the signal on the nodes through the links [216]. Indeed, $\mathbf{L}_0$ is exactly the symmetric network Laplacian we have used in Chapter 1 to develop Turing theory on networks. However, this bridge between network theory and algebraic topology allows us to go further, as Hodge Laplacians do not stop at the first order. In fact, with an analogous reasoning, we can model the propagation of the signal on the links through the nodes, yielding $\mathbf{L}_1 = -\mathbf{B}_1^\top \mathbf{B}_1$. The above discussion can be generalized for simplices of any dimensions d. The general formula of the Hodge Laplacians is the following

$$\mathbf{L}_d = \mathbf{L}_d^{down} + \mathbf{L}_d^{up} \tag{5.3.1}$$

where $\mathbf{L}_d^{down} = -\mathbf{B}_d^\top \mathbf{B}_d$ is the diffusion of the topological signals between d-simplices through the lower order $(d-1)$-simplices, and $\mathbf{L}_d^{up} = -\mathbf{B}_{d+1}\mathbf{B}_{d+1}^\top$ is the diffusion of the d-simplices' signals through the higher order $(d+1)$-simplices. Hodge Laplacians at every order are negative semi-definite. Coming back of the simple higher-order extension of a network (signals in the nodes and in the links), we obtain that $\mathbf{L}_0 = \mathbf{L}_0^{up} = -\mathbf{B}_1\mathbf{B}_1^\top$, because 0-simplices are not the boundary of a lower order structure and the operator $\mathbf{B}_0$ does not exist, hence the signals on the nodes can only propagate through the links. On the other hand, $\mathbf{L}_1 = \mathbf{L}_1^{down} = -\mathbf{B}_1^\top \mathbf{B}_1$; in fact, given the absence of 2-simplices, the signals on the links propagates only through the nodes.

The distinction between many-body and higher-order interactions can be further clarified by comparing the expression of the Hodge Laplacians 5.3.1, with the definitions of the generalized Laplacians 5.2.4 in the previous section. While the latter encode the many-body interactions, it is only with Hodge Laplacian that we can *properly* move to higher orders.

[(5)] To further stress the analogy with $\mathbf{L}$, one may as well observe that the vector calculus Laplacian operator ∇^2 is defined in vector calculus as the divergence of the gradient.

5.4 Discussion

Many-body interactions and topological signals are both usually called *higher-order interactions* (or also higher-order), even though they are very different in what they represent. They are considered close topics and are generally discussed together [208, 217, 218]. However, dynamical systems on higher-order structures is a rather young topic, even for today's standards, where aging happens quicker than ever; it is possible that, in the near future, the two frameworks will drift apart and will develop their own course. Before that, we believe that the community needs to stress the fundamental differences between the two formalisms. To the best of our knowledge, such distinction rarely emerges in the literature [207]. Most examples of higher-order systems are, indeed, many-body ones, for example, as co-authorship networks [180], epidemics [195] and ecological [181] processes, while examples of topological signals can be found, for instance, in brain dynamics [219] and power-grids [220]. More clarity in their distinction would certainly facilitate the development of the two theories, especially for what concerns applications.

In Chapter 7, Turing theory is developed for topological signals on higher-order structures. In the Supplementary Materials, section 7.6, the reader may find a compendium of algebraic topology and Hodge theory, which we have only briefly introduced in this Section. It is important to note that the Laplacians of Chapter 7 are all positive semi-definite, being defined in the following way: $\mathbf{L}_n^{down} = \mathbf{B}_n^\top \mathbf{B}_n$ and $\mathbf{L}_n^{up} = \mathbf{B}_{n+1}\mathbf{B}_{n+1}^\top$. Hence, the diffusive coupling in the reaction-diffusion equations comes with a minus sign.

Chapter 6

Turing patterns in systems with higher-order interactions

In the Introduction, we have seen that one limitation of classical Turing theory is the difference in magnitude between the diffusivities of the two species, which is difficult to obtain (and observe) experimentally. The above fact motivates most of the research done in the past years on the subject, i.e., to relax the conditions yielding Turing patterns by adding realistic hypotheses to the original ideal setting, such as a finite propagation (see Chapter 3), noise [221], etc. Can we take a step back and modify the starting framework *tout court* without any other additional hypothesis? As a matter of fact yes, and this is what we pursued in the work discussed in this Chapter, where we reformulated the problem originally studied by Turing within the framework of higher-order (many-body) interactions. Our starting point was the elegant formalism developed by Gambuzza et al. in [45] for synchronization dynamics on simplicial complexes and its comparison with a previous extension of Turing theory on hypergraphs [205]. First, we realized that the former is more ductile and works very well also for hypergraphs (more, even for directed hypergraphs [211]); then, we proved that it extends the latter, which results to be a particular case of the former for a specific coupling. This last point is proven in the appendix of the paper. By reformulating reaction-diffusion equations on hypergraphs through this new formalism, we observed that higher-order terms could reverse the behavior that would be observed in the pairwise setting. In fact, one could be dealing with diffusion coefficients which would allow (or not) the formation of Turing patterns, but different diffusivities for higher-order terms may, instead, yield stability (or instability). Our theoretical setting would turn out particularly useful in applications where the model parameters are fixed, but different interactions at higher-orders can process the desired final state.

My contribution This work was conducted with another PhD student, Luca Gallo, and it is part of his thesis. Together with Luca we worked on two papers in parallel, one on synchronization [211] and this one on Turing patterns. We jointly developed

the mathematical formalism, built upon a previous work on synchronization [45]. My additional contribution to this work was to develop the codes and perform the numerical simulations.

R. Muolo, L. Gallo, V. Latora, M. Frasca & T. Carletti. Chaos, Solitons & Fractals, 166, 112912 (2023) [215]
This article is not open access, but it is freely available as a pre-print.

Abstract

Turing theory of pattern formation is among the most popular theoretical means to account for the variety of spatio-temporal structures observed in nature and, for this reason, finds applications in many different fields. While Turing patterns have been thoroughly investigated on continuous support and on networks, only a few attempts have been made toward their characterization in systems with higher-order interactions. In this paper, we propose a way to include group interactions in reaction–diffusion systems, and we study their effects on the formation of Turing patterns. To achieve this goal, we rewrite the problem originally studied by Turing in a general form that accounts for a microscopic description of interactions of any order in the form of a hypergraph, and we prove that the interplay between the different orders of interaction may either enhance or repress the emergence of Turing patterns. Our results shed light on the mechanisms of pattern-formation in systems with many-body interactions and pave the way for further extensions of Turing original framework.

6.1 Introduction

Many natural and engineered systems exhibit collective behaviors, manifesting themselves as spatio-temporal ordered motifs, whose emergence can be explained utterly by considering the interactions within the system [1]. One of the most elegant and popular theories for the emergence of self-organized patterns is due to the British mathematician Alan Turing, who proposed, in the context of morphogenesis, a mechanism of pattern-formation rooted on a diffusion-driven instability, which now bears his name [4]. In a nutshell, the Turing instability results from the combined action of two processes, (local) reaction and (long-range) diffusion, involving an activator and an inhibitor species [5, 108]. While each process considered separately would drive the system to a spatially homogeneous state, there can be conditions on the models and on the interactions such that any heterogeneous, arbitrarily small, perturbation of the homogeneous state is amplified and eventually returns a macroscopic patchy (non-homogeneous) solution, i.e., a Turing pattern. The diffusive terms being the destabilizing factors, the above mechanism is also known in the literature as diffusion-driven instability.

Despite its generality, the framework requires the involved species to diffuse with quite different rates, a condition that is not often naturally realized without introducing

additional mechanisms, such as convection, electromagnetic fields, differential adherence. Indeed experimental evidence of the existence of Turing patterns was obtained almost half a century later in chemical reactions [6, 7] and in Cellular Neural Networks [222, 223]. Without adding unnecessary mechanisms and still looking for simple models, scholars have proposed several variants to the original Turing scheme to facilitate the emergence of patterns. For example, noise [10] or an upper bound to the signal propagation [16, 49] can be added to the picture.

In many relevant applications by their very definition, the local reactions involve very close species, that can thus be considered spatially separated from other groups. Starting from this observation, Turing's idea has been extended to discrete systems: species occupy spatially limited zones, i.e., nodes, and diffuse across links connecting different zones. Initially, the theory has been developed as to include regular $1D$ and $2D$ lattices [25], and then extended on complex networks [31, 109].

The latter framework has proven particularly fruitful for Turing patterns, especially for the introduction of asymmetric displacements [40], as in the case of directed networks [38] or non-normal ones [70], where it was shown that the Turing mechanism is enhanced. In particular, such framework is very general and allows to study the Turing instability on discrete topologies which are not trivially embedded on continuous domains, as it is the case for regular lattices. Nevertheless, certain dynamics escape the network framework, as the interactions between the elementary units are not only pairwise, but can involve several agents at the same time: we are thus in presence of many-body interactions. Let us here stress that we do not (only) refer to processes that introduce, possibly small, corrections to the first order model, i.e., the pairwise coupling, but we overcome this setting and consider cases where higher-order interactions are the main driver. Think of systems where the group interactions of humans or other social animals determine the dynamics, for example the spreading of viruses [195, 224]. Or consider processes where crowding is a key factor, as for the case of random walks [225, 226] or chemical systems [227, 228]. Let us observe that nonlinear terms introduced with the higher-order interaction can be associated to nonlinear diffusion processes already studied in the literature. Our results differentiate however from the latter because of the many-body assumption. One thus needs to resort to more sophisticated mathematical structures, such as hypergraphs or simplicial complexes, which are an extension of networks, beyond the framework of pairwise interactions [208, 217]. Dynamical systems on higher-order topologies have been recently studied [205, 45], but a general theory of Turing pattern formation on top of such structures is still lacking. Let us observe that a similar framework has been used to study synchronization of higher-order coupled oscillators [201]. Reaction-diffusion systems have been recently studied in the frameworks of topological signals [229], which differs from the problem we are studying, as in the former species lie in nodes and links, while in the latter only in nodes. The aim of this paper is to take one step further by proposing an extension of Turing instability on higher-order topologies. For this scope, we will employ the formalism developed by Gambuzza et al. [45] in the context of synchronization.

By performing a linear stability analysis involving a higher-order Laplace matrix and the Jacobian matrices of the reaction and coupling parts, we will show that the joint action of higher-order structures and nonlinear interactions is the key feature in driving

the systems unstable. Then, considering suitable choices of couplings and higher-order topologies, we will analytically determine the conditions for the instability to occur by focusing on the role of the diffusion coefficients at every order. As we will show, having different orders of diffusivity allows either to enhance or to reduce the formation of Turing patterns with respect to the case of systems with only-pairwise interactions, by tuning the parameters of the higher-order couplings.

The paper is organized as follows. In Section 6.2 we will set the theoretical ground, by extending the reaction–diffusion equations originally studied by Turing to the case of systems coupled through higher-order interactions. In Section 6.3, we will choose a particular type of nonlinear coupling, namely the diffusive-like cubic one, and we will analyze the emergence of patterns in the case of systems with only-pairwise interactions. In Section 6.4, we will study the effects of higher-order interactions on Turing instability. We will first restrict to the particular case of the so-called natural coupling, which allows for a fully analytical treatment, showing how this is a generalization of some previous attempts to tackle the problem. We will then relax the natural coupling hypothesis, and examine an intermediate case with some specific structure, that we call regular topologies, which also allow an analytical treatment. Lastly, we will consider the case of the most general higher-order coupling topologies, where only a numerical study is possible. Finally, in the last section, we will discuss further lines of investigation and possible applications.

6.2 Reaction–Diffusion systems on higher-order structures

Let us consider a dynamical system composed by N identical units subject to some (local) nonlinear reaction dynamics. Assume moreover that many-body interactions, i.e., interactions in groups of more than two units, are allowed.

Let the state of the i-th unit to be described by the vector $\vec{x}_i(t) \in \mathbb{R}^m$. Then, under the mentioned assumptions, the evolution rate of the state vector of the i-th unit is governed by the following equation:

$$\dot{\vec{x}}_i = \vec{f}(\vec{x}_i) + \sum_{d=1}^{P} \sigma_d \sum_{j_1=1}^{N} \cdots \sum_{j_d=1}^{N} A^{(d)}_{i j_1 j_2 \dots j_d} \vec{g}^{(d)}(\vec{x}_i, \vec{x}_{j_1}, \vec{x}_{j_2}, \dots, \vec{x}_{j_d}) \tag{6.2.1}$$

with $i = 1, \dots, N$, where $\vec{f} : \mathbb{R}^m \to \mathbb{R}^m$ describes the local nonlinear dynamics. Let $P+1$ denote the size of the largest group of interacting units; then, $\vec{g}^{(d)} : \mathbb{R}^{m \times (d+1)} \to \mathbb{R}^m$, $d \in \{1, \dots, P\}$, are the nonlinear coupling functions ruling the $(d+1)$-body interactions, encoded into the adjacency tensors $A^{(d)}$, with $A^{(d)}_{i j_1 \dots j_d} = 1$ if and only if the $d+1$ units $\{i, j_1, \dots, j_d\}$ interact together, i.e., they are connected by a hyperedge with the convention that repeated indexes yield a 0 entry. We denote by $\sigma_d > 0$ the coupling strengths. Let us assume the nonlinear couplings to be diffusive-like, hence for every d there exists a function $\vec{h}^{(d)} : \mathbb{R}^{m \times d} \to \mathbb{R}^m$ such that $\vec{g}^{(d)}$ can be written as:

$$\vec{g}^{(d)}(\vec{x}_i, \vec{x}_{j_1}, \dots, \vec{x}_{j_d}) = \vec{h}^{(d)}(\vec{x}_{j_1}, \dots, \vec{x}_{j_d}) - \vec{h}^{(d)}(\vec{x}_i, \dots, \vec{x}_i) \tag{6.2.2}$$

This definition of $\vec{g}^{(d)}$ guarantees that the coupling vanishes when all units have the same state vector, namely $\vec{g}^{(d)}(\vec{x}_i,\vec{x}_i,\dots,\vec{x}_i)=0$. This could be intuitively considered as a generalization of Fickean diffusion on networks, which tends to homogenize local differences, hence to vanish in the case of equal system states. In addition, we assume the existence of $\vec{x}^*\in\mathbb{R}^m$ such that $\vec{f}(\vec{x}^*)=0$, meaning that a solution of the N isolated systems exists. By setting $\vec{x}_i=\vec{x}^*$, for all $i=1,\dots,N$, and assuming Equation (6.2.2) to hold true, then $(\vec{x}_1,\dots,\vec{x}_N)^\top=(\vec{x}^*,\dots,\vec{x}^*)^\top$ results to be a spatially independent solution of Equation (6.2.1). This condition is a prerequisite for Turing instability that, as mentioned above, is based on the existence of a homogeneous stable equilibrium eventually destabilized by the diffusion. Notice that the diffusion terms are determined by the topology of the connections as well as by the parameters entering in the diffusive couplings, so that all these factors concurrently contribute to the mechanism of Turing pattern formation in the general model, Equation (6.2.1).

The standard framework to study Turing instability consists of two species reaction–diffusion systems, thus, even if the proposed framework is quite general, we preferred in the following to limit our analysis to a 2-dimensional case. Let us thus set $m=2$ and denote the two components of the state vector $\vec{x}_i$ by (u_i,v_i). Then, by defining

$$\vec{f}(\vec{x})=(f_1(u,v),f_2(u,v))$$

and

$$\vec{h}^{(d)}(\vec{x}_1,\dots,\vec{x}_d)=(h_1^{(d)}(u_1,\dots,u_d,v_1,\dots,v_d),h_2^{(d)}(u_1,\dots,u_d,v_1,\dots,v_d))\quad\forall d=1,\dots,P$$

we can rewrite Equation (6.2.1) as

$$\begin{cases}\dot{u}_i=f_1(u_i,v_i)+\displaystyle\sum_{d=1}^{P}\sigma_d\sum_{j_1=1}^{N}\cdots\sum_{j_d=1}^{N}A^{(d)}_{i,j_1,\dots,j_d}\Big[h_1^{(d)}(u_{j_1},\dots,u_{j_d},v_{j_1},\dots,v_{j_d})\\ \qquad\qquad -h_1^{(d)}(u_i,\dots,u_i,v_i,\dots,v_i)\Big]\\ \dot{v}_i=f_2(u_i,v_i)+\displaystyle\sum_{d=1}^{P}\sigma_d\sum_{j_1=1}^{N}\cdots\sum_{j_d=1}^{N}A^{(d)}_{i,j_1,\dots,j_d}\Big[h_2^{(d)}(u_{j_1},\dots,u_{j_d},v_{j_1},\dots,v_{j_d})\\ \qquad\qquad -h_2^{(d)}(u_i,\dots,u_i,v_i,\dots,v_i)\Big]\end{cases}\tag{6.2.3}$$

where we have taken into account condition (6.2.2). To focus on the role of higher-order interactions, we can further simplify the model by assuming that the nonlinear diffusion does not contain any cross-diffusion term, namely for all $d\in\{1,\dots,P\}$ the function $h_1^{(d)}$ (resp. $h_2^{(d)}$) depends only on $\{u_{j_1},\dots,u_{j_d}\}$ (resp. $\{v_{j_1},\dots,v_{j_d}\}$). A throughout analysis of the general case goes beyond the scope of this work and it could be consider in a

forthcoming study. Under this hypothesis, the examined system is for all $i = 1, \dots, N$

$$\begin{cases} \dot{u}_i = f_1(u_i, v_i) + \sum_{d=1}^{P} \sigma_d \sum_{j_1=1}^{N} \cdots \sum_{j_d=1}^{N} A^{(d)}_{i,j_1,\dots,j_d} \left[h_1^{(d)}(u_{j_1}, \dots, u_{j_d}) - h_1^{(d)}(u_i, \dots, u_i) \right] \\ \dot{v}_i = f_2(u_i, v_i) + \sum_{d=1}^{P} \sigma_d \sum_{j_1=1}^{N} \cdots \sum_{j_d=1}^{N} A^{(d)}_{i,j_1,\dots,j_d} \left[h_2^{(d)}(v_{j_1}, \dots, v_{j_d}) - h_2^{(d)}(v_i, \dots, v_i) \right] \end{cases} \tag{6.2.4}$$

In the next sections, we will study the conditions for the emergence of Turing patterns in systems of the form (6.2.4) focusing, one-by-one, on the two novel aspects of our model. First, we will deal with the study of Turing patterns in the standard case when only two-body interactions are present (i.e., the model with $P = 1$), but the diffusive coupling is nonlinear, in Section 6.3. Then, we will investigate the model in presence of many-body nonlinear diffusive coupling in Section 6.4.

6.3 Turing theory with nonlinear diffusive-like coupling

Let us start with the analysis of the conditions on the fixed point for the isolated system, that we here indicate as (u^*, v^*). This means to only consider local reaction and silence the interactions among the different units. The fixed point satisfies the equations

$$f_1(u^*, v^*) = f_2(u^*, v^*) = 0$$

and should be stable, a condition that can be obtained by imposing

$$\mathrm{tr}\mathbf{J}_0 < 0 \text{ and } \det \mathbf{J}_0 > 0 \tag{6.3.1}$$

where $\mathbf{J}_0 = \begin{pmatrix} \partial_u f_1 & \partial_v f_1 \\ \partial_u f_2 & \partial_v f_2 \end{pmatrix}$ is the Jacobian matrix of the reaction function, being $\partial_a f_\ell = \frac{\partial f_\ell}{\partial a}(u^*, v^*)$, with $\ell \in \{1, 2\}$ and $a \in \{u, v\}$. We remark that with the notation $\partial_a f_\ell = \frac{\partial f_\ell}{\partial a}(u^*, v^*)$ we indicate that all the derivatives in the Jacobian matrix are evaluated at the equilibrium point (u^*, v^*).

Before studying the effects of higher-order terms on the emergence of Turing patterns in the most general system in Equation (6.2.4), let us first analyze the effect of a nonlinear diffusive coupling in a system with pairwise interactions only, i.e., when $P = 1$. This corresponds thus to consider a reactive system where nonlinear diffusion is present and interactions occur among units that are mapped as the nodes of a complex network. Let us observe that the problem of Turing instability with nonlinear diffusion has already been studied, but on a continuous support for the dynamics [230, 231, 232]. The main purpose of the following sections is to extend this analysis to the case of networked systems and to introduce the reader to the framework of Turing theory on networks.

For sake of definitiveness, we will present our results by using a cubic diffusion term. We adopt the same assumption even in the case of higher-order interactions, so that it will be easier to examine the effects of the latter on the dynamical behavior of the system.

6.3.1 Turing patterns in networked systems with nonlinear diffusion

By setting $P = 1$ in Equation (6.2.4) we obtain

$$\begin{cases} \dot{u}_i = f_1(u_i, v_i) + \sigma_1 \sum_{j=1}^{N} A_{ij}^{(1)} \left(h_1^{(1)}(u_j) - h_1^{(1)}(u_i) \right) \\ \dot{v}_i = f_2(u_i, v_i) + \sigma_1 \sum_{j=1}^{N} A_{ij}^{(1)} \left(h_2^{(1)}(v_j) - h_2^{(1)}(v_i) \right) \end{cases} \quad \forall i = 1, \ldots, N \tag{6.3.2}$$

These equations can be linearized around the equilibrium point (u^*, v^*), by giving

$$\begin{cases} \delta\dot{u}_i = \partial_u f_1(u^*, v^*)\delta u_i + \partial_v f_1(u^*, v^*)\delta v_i + \sigma_1 \sum_{j=1}^{N} A_{ij}^{(1)} \partial_u h_1^{(1)}(u^*)(\delta u_j - \delta u_i) \\ \delta\dot{v}_i = \partial_u f_2(u^*, v^*)\delta u_i + \partial_v f_2(u^*, v^*)\delta v_i + \sigma_1 \sum_{j=1}^{N} A_{ij}^{(1)} \partial_v h_2^{(1)}(v^*)(\delta v_j - \delta v_i) \end{cases} \tag{6.3.3}$$

where $\delta u_i = u_i - u^*$, $\delta v_i = v_i - v^*$ and $i = 1, 2, \ldots, N$. Let $L_{ij}^{(1)} = A_{ij}^{(1)} - k_i^{(1)} \delta_{ij}$ be the i, j element of the network Laplacian matrix[(1)], where $k_i^{(1)} = \sum_j A_{ij}^{(1)}$ is the node degree. We can rewrite the latter equation in compact form to emphasize the 2-dimensional nature of the problem as

$$\frac{d}{dt} \begin{pmatrix} \delta u_i \\ \delta v_i \end{pmatrix} = \mathbf{J}_0 \begin{pmatrix} \delta u_i \\ \delta v_i \end{pmatrix} + \sigma_1 \sum_{j=1}^{N} L_{ij}^{(1)} \mathbf{J}_{H^{(1)}} \begin{pmatrix} \delta u_j \\ \delta v_j \end{pmatrix} \quad \forall i = 1, \ldots, N \tag{6.3.4}$$

where $\mathbf{J}_{H^{(1)}} = \begin{pmatrix} \partial_u h_1^{(1)}(u^*) & 0 \\ 0 & \partial_v h_2^{(1)}(v^*) \end{pmatrix}$. Let us observe that matrix $\mathbf{J}_{H^{(1)}}$ is diagonal, as there are no off-diagonal terms, due to the assumption of no cross-diffusion terms. By defining as $\vec{\zeta} = (\delta u_1, \delta v_1, \ldots, \delta u_N, \delta v_N)^\top$, we can eventually rewrite the last equation in a compact form

$$\dot{\vec{\zeta}} = \left(\mathbb{I}_N \otimes \mathbf{J}_0 + \sigma_1 \mathbf{L}^{(1)} \otimes \mathbf{J}_{H^{(1)}} \right) \vec{\zeta} \tag{6.3.5}$$

where $\mathbb{I}_N$ is the $N \times N$ identity matrix and $\otimes$ is the Kronecker product.

The eigenvalues of the $2N \times 2N$ linear system (6.3.5) determine the stability of the solution $\vec{x^*} = 0$, which corresponds to $(u_i, v_i) = (u^*, v^*)$ for all i. Being $\mathbf{L}^{(1)}$ a symmetric matrix, one can find a set of orthonormal eigenvectors $\vec{\varphi}^{(\alpha)}$ associated to eigenvalues $\Lambda^{(\alpha)}$, $\alpha = 1, \ldots, N$. We can then make one step further by projecting Equation (6.3.5)

[(1)] Let us observe that such matrix has a non positive spectrum and it is the discrete analogous of the continuous diffusion operator ∇^2 once the underlying network is a regular lattice; for this reason, the network Laplacian matrix plays a relevant role in the context of Turing pattern formation. However, we would like to point out that in the literature, e.g., consensus and synchronization, it is common to find the Laplacian matrix defined as $L_{ij}^{(1)} = k_i^{(1)} \delta_{ij} - A_{ij}^{(1)}$ (e.g., [86, 45]), having thus a non negative spectrum. In such cases the coupling term will exhibit a negative sign.

onto this basis, and thus obtaining N linear and decoupled 2×2 systems, each one depending on a single eigenvalue, namely

$$\frac{d}{dt}\begin{pmatrix}\delta\hat{u}_\alpha\\ \delta\hat{v}_\alpha\end{pmatrix} = \left[\mathbf{J}_0 + \sigma_1\Lambda^{(\alpha)}\mathbf{J}_{H^{(1)}}\right]\begin{pmatrix}\delta\hat{u}_\alpha\\ \delta\hat{v}_\alpha\end{pmatrix} :- \mathbf{J}^{(\alpha)}\begin{pmatrix}\delta\hat{u}_\alpha\\ \delta\hat{v}_\alpha\end{pmatrix} \quad \forall\alpha = 1,\dots,N \tag{6.3.6}$$

Here $\delta\hat{u}_\alpha = \sum_i \delta u_i \varphi_i^{(\alpha)}$ and $\delta\hat{v}_\alpha = \sum_i \delta v_i \varphi_i^{(\alpha)}$, are the projection respectively of δu_i and δv_i on such eigenbasis, and the last equality defines the matrix $\mathbf{J}^{(\alpha)}$. Its eigenvalues can be obtained by solving

$$\det\left(\mathbf{J}^{(\alpha)} - \lambda\mathbb{I}_2\right) = 0$$

that is

$$\lambda^2 - 2\mathrm{tr}\,\mathbf{J}^{(\alpha)}\lambda + \det\mathbf{J}^{(\alpha)} = 0$$

The root with the largest real part, considered as a function of $\Lambda_\alpha^{(1)}$, is named dispersion relation, $\lambda_\alpha = \max\lambda\left(\Lambda_\alpha^{(1)}\right)$. If there exists $\hat{\alpha}$ such that $\lambda_{\hat{\alpha}} > 0$, then the equilibrium solution $(u_i, v_i) = (u^*, v^*)$ is unstable and a Turing instability is observed, the system drives away from the homogeneous equilibrium to eventually reach a new, possibly heterogeneous, solution.

Let us observe that $\mathrm{tr}\,\mathbf{J}^{(\alpha)} = \mathrm{tr}\,\mathbf{J}_0 + \Lambda_\alpha^{(1)}\mathrm{tr}\,\mathbf{J}_H$. Because h_1 and h_2 encode a diffusive coupling, one can safely assume that $\partial_u h_1(u^*) > 0$ and $\partial_v h_2(v^*) > 0$. Moreover being $\Lambda_\alpha^{(1)} \leq 0$ and $\mathrm{tr}\mathbf{J}_0 < 0$, one can infer that $\mathrm{tr}\mathbf{J}^{(\alpha)} < 0$ for all α. In conclusion, a sufficient condition to have $\lambda_{\hat{\alpha}} > 0$ results to be

$$\det\mathbf{J}^{(\hat{\alpha})} < 0 \tag{6.3.7}$$

for some $\hat{\alpha} > 1$.

6.3.2 The Brusselator model with cubic diffusion

For sake of simplicity and without loss of generality, let us illustrate the above results using as a reaction part the Brusselator model [95, 96], an extensively adopted dynamical system, when it comes to study the emergence of self-organized patterns. In addition, let us consider a cubic diffusion term. This accounts to set

$$\begin{aligned} f_1(u,v) &= 1 - (b+1)u + cu^2v \\ f_2(u,v) &= bu - cu^2v \end{aligned} \tag{6.3.8}$$

and

$$\begin{aligned} h_1^{(1)}(u) &= D_u^{(1)}u^3 \\ h_2^{(1)}(u) &= D_v^{(1)}v^3 \end{aligned} \tag{6.3.9}$$

where b and $c > 0$ are model parameters, and $D_u^{(1)} > 0$ and $D_v^{(1)} > 0$ are generalized diffusion coefficients. Hence, the system under investigation reads

$$\begin{cases} \dot{u}_i = 1 - (b+1)u_i + cu_i^2 v_i + \sigma_1 D_u^{(1)} \sum_{j_1=1}^{N} A_{ij_1}^{(1)} (u_{j_1}^3 - u_i^3) \\ \dot{v}_i = bu_i - cu_i^2 v_i + \sigma_1 D_v^{(1)} \sum_{j_1=1}^{N} A_{ij_1}^{(1)} (v_{j_1}^3 - v_i^3) \end{cases} \tag{6.3.10}$$

for which it is straightforward to show the existence of a unique fixed point $(u^*, v^*) = (1, b/c)$. Correspondingly, the matrices $\mathbf{J}_0$ and $\mathbf{J}_{H^{(1)}}$ are

$$\mathbf{J}_0 = \begin{bmatrix} b-1 & c \\ -b & -c \end{bmatrix} \quad \text{and} \quad \mathbf{J}_{H^{(1)}} = 3 \begin{bmatrix} (u^*)^2 D_u^{(1)} & 0 \\ 0 & (v^*)^2 D_v^{(1)} \end{bmatrix} \tag{6.3.11}$$

Thus, the equilibrium (u^*, v^*) is stable provided that $\mathrm{tr}\mathbf{J}_0 = b - c - 1 < 0$ and $\det \mathbf{J}_0 = c > 0$. The conditions (6.3.7) for the onset of the instability are given by

$$\begin{cases} -c^3 D_u^{(1)} + (b-1) b^2 D_v^{(1)} > 0 \\ 4b^2 c^3 D_u^{(1)} D_v^{(1)} - \left(-c^3 D_u^{(1)} + (b-1) b^2 D_v^{(1)} \right)^2 < 0 \end{cases} \tag{6.3.12}$$

Let us observe that the above conditions do not depend on σ_1. As in the case of Turing instability resulting from linear diffusion, the relevant parameter is the ratio between the diffusive coefficients.

In Figure 6.1, we compare the Turing instability regions (i.e., the set of parameters for which Turing patterns can emerge) obtained in the case of a linear diffusion term and in the case of a cubic one. By fixing in both cases the diffusion coefficients $D_u^{(1)} = 0.1$ and $D_v^{(1)} = 1$, and the coupling strength $\sigma_1 = 1$, we can observe the following behavior in the plane (b, c). The instability region is wider in the case of linear coupling than in the cubic one for large values of the parameters, while the instability region shrinks to zero more slowly in the case of cubic coupling for small values of the parameters. This implies that there is a region for large enough values of b and c where the linear diffusion allows the emergence of Turing patterns, while in the case of cubic diffusion any initial perturbation about the homogeneous equilibrium fades out. On the contrary, if b and c are small enough, Turing patterns can emerge under the assumption of cubic diffusion but not if diffusion is linear. These considerations are confirmed by the dispersion relation as reported in the left panels of Figure 6.1: the reader can clearly identify the existence of eigenmodes associated to a positive dispersion relation for the cubic diffusion case (upper panel), while under the assumption of linear diffusion the dispersion relation is always negative, or the opposite case (bottom panel), where the dispersion curve associated to nonlinear diffusion is always negative. Let us remark that the spectrum of the Laplacian $\Lambda^{(\alpha)}$ is discrete; however, in order to help the reader to better visualize the results, the dispersion relations are plotted also as continuous curves.

Let us conclude this section by observing that the standard Turing framework of linear Fickean diffusion, operating both with networks or continuous supports, requires

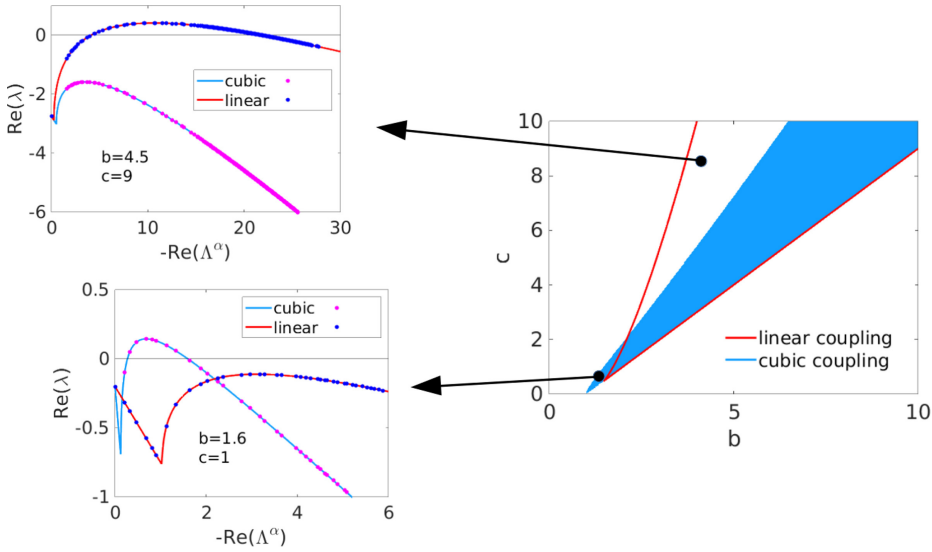

Figure 6.1: Turing instability in networks with nonlinear diffusion. Right panel: Turing instability regions for the Brusselator model with $D_u^{(1)} = 0.1$, $D_v^{(1)} = 1$ and $\sigma_1 = 1$. The analytical red curves indicate the boundary of the instability regions for the linear coupling, while the blue region is for the cubic coupling, as obtained numerically. We can observe that, for lower values of the parameters (b,c) the cubic coupling allows for pattern formation, where the linear one does not, while for greater values we find the opposite situation. This can be visualized through the dispersion relations reported in the left panels: on the bottom left for lower values of the parameter (only the system subject to cubic coupling can go unstable), while on the upper left for greater values of the parameter (only the linear case yields patterns).

the activator species to diffuse faster than the inhibitor one [5], i.e., $D_v^{(1)} > D_u^{(1)}$. With the introduction of nonlinear diffusion, such condition can be relaxed, as the system can yield patterns even with equal diffusivities or with faster activator [230]. This claim follows directly from conditions (6.3.12) for the specific case of the Brusselator model. However, it is important to note that if one considers the entries of $J_{H^{(1)}}$ as the "effective" diffusion coefficients, one finds a generalization of the Turing condition $D_v^{(1)} > D_u^{(1)}$, which is

$$(v^*)^2 D_v^{(1)} > (u^*)^2 D_u^{(1)} \tag{6.3.13}$$

for the cubic case. In fact, conditions (6.3.1) and (6.3.7) imply that $\partial_u f_1 < \partial_v f_2$, from which we obtain

$$\begin{aligned} &\partial_u f_1 (v^*)^2 D_v^{(1)} > \partial_v f_2 (u^*)^2 D_u^{(1)} \Rightarrow \\ &\partial_u f_1 (v^*)^2 D_v^{(1)} > \partial_v f_2 (u^*)^2 D_u^{(1)} > \partial_u f_1 (u^*)^2 D_u^{(1)} \end{aligned}$$

hence the new condition $(v^*)^2 D_v^{(1)} > (u^*)^2 D_u^{(1)}$.

Let us remark that the above condition is necessary but not sufficient for Turing patterns. This means that if conditions (6.3.12) are verified, then we have condition (6.3.13), but the vice versa is not true.

In the following, we will make use of the above results and focus our attention on the impact of higher-order terms on the onset of the instability. The nonlinear coupling

is necessary to make such many-body interactions meaningful, as pointed out in [192]: in fact, if the higher-order coupling is linear, higher-order interactions are nothing more than the sum of pairwise ones. Moreover, nonlinear couplings are of particular physical interest, as they can be associated to anomalous diffusion [232].

6.4 Higher-order interactions

Let us now consider the most general case of Equation (6.2.4) with higher-order interactions. For simplicity and without loss of generality, we will limit ourselves to consider only first and second order interactions, i.e., $P = 1$ and $P = 2$. Nevertheless, the theory goes beyond the exposed examples and can be straightforwardly generalized as to include higher P. The system we are thus interested in is given by

$$\begin{cases} \dot{u}_i = f_1(u_i, v_i) + \sigma_1 D_u^{(1)} \sum_{j_1=1}^{N} A_{ij_1}^{(1)} (h_1^{(1)}(u_{j_1}) - h_1^{(1)}(u_i)) \\ \qquad\qquad + \sigma_2 D_u^{(2)} \sum_{j_1=1}^{N} \sum_{j_2=1}^{N} A_{ij_1j_2}^{(2)} (h_1^{(2)}(u_{j_1}, u_{j_2}) - h_1^{(2)}(u_i, u_i)) \\ \dot{v}_i = f_2(u_i, v_i) + \sigma_1 D_v^{(1)} \sum_{j_1=1}^{N} A_{ij_1}^{(1)} (h_2^{(1)}(v_{j_1}) - h_2^{(1)}(v_i)) \\ \qquad\qquad + \sigma_2 D_v^{(2)} \sum_{j_1=1}^{N} \sum_{j_2=1}^{N} A_{ij_1j_2}^{(2)} (h_2^{(2)}(v_{j_1}, v_{j_2}) - h_2^{(2)}(v_i, v_i)) \end{cases} \tag{6.4.1}$$

where $h_1^{(1)}(u)$ and $h_2^{(1)}(v)$ encode the first order interaction, while $h_1^{(2)}(u_1, u_2)$ and $h_2^{(2)}(v_1, v_2)$ model the second order coupling. We again assume the existence of a homogeneous solution $(u_i, v_i) = (u^*, v^*)$ and for it to be stable once we silence both the pairwise coupling, $P = 1$, and the higher-order one, $P > 1$. To study its stability under spatially dependent perturbations, we can follow the derivation presented in the previous section (see also [45]), that ultimately relies on the computation of a Master Stability Function [44] in a setting involving a stationary equilibrium and higher-order coupling.

Let us introduce again the perturbation vector $\vec{\zeta} = (\delta u_1, \delta v_1, \dots, \delta u_N, \delta v_N)^\top$, where $\delta u_i = u_i - u^*$ and $\delta v_i = v_i - v^*$, then one can straightforwardly show that it evolves according to

$$\dot{\vec{\zeta}} = \left(\mathbb{I}_N \otimes \mathbf{J}_0 + \sigma_1 \mathbf{L}^{(1)} \otimes \mathbf{J}_{H^{(1)}} + \sigma_2 \mathbf{L}^{(2)} \otimes \mathbf{J}_{H^{(2)}} \right) \vec{\zeta} \tag{6.4.2}$$

where $\mathbf{J}_{H^{(2)}} = \begin{pmatrix} \partial_{u_1} h_1^{(2)}(u^*,u^*) + \partial_{u_2} h_1^{(2)}(u^*,u^*) & 0 \\ 0 & \partial_{v_1} h_2^{(2)}(v^*,v^*) + \partial_{v_2} h_2^{(2)}(v^*,v^*) \end{pmatrix}$ and $\mathbf{L}^{(2)}$ represents a generalized Laplacian matrix [45] accounting for the 3-body interactions, whose elements are given by

$$\mathbf{L}_{ij}^{(2)} = \begin{cases} -\sum_{j,k=1}^{N} A_{ijk}^{(2)} & \text{for } i = j \\ \sum_{k=1}^{N} A_{ijk}^{(2)} & \text{for } i \neq j \end{cases} \tag{6.4.3}$$

In the following, we will examine different cases of coupling: first, in Section 6.4.1, the so called natural coupling [45, 154], which allows an analytical treatment of the

problem, but does not permit to fully unveil the potential of higher-order terms. The latter will be fully exploited in Section 6.4.2, where we will present two special cases of higher-order structures in which, despite the general form of the coupling functions, a complete analytical study can be performed. Finally, in Section 6.4.3 the scenario where both the coupling and the topology are general will be dealt with.

6.4.1 Natural coupling

A largely used assumption on the coupling terms $\vec{h}^{(d)}$ is that, once they are evaluated on the homogeneous state[(2)], they return the same value given by $\vec{h}^{(1)}$, more precisely

$$\vec{h}^{(d)}(\vec{x},\dots,\vec{x}) = \cdots = \vec{h}^{(2)}(\vec{x},\vec{x}) = \vec{h}^{(1)}(\vec{x})$$

Such condition is known in the literature as *natural coupling* [45]. In the present framework, this implies that

$$h_1^{(2)}(u,u) = h_1^{(1)}(u) \text{ and } h_2^{(2)}(v,v) = h_2^{(1)}(v)$$

To compare the case $P > 1$ with the one presented for $P = 1$, we consider nonlinearities based on polynomials and product of variables with total power equal to three, both in the first and in the second order terms. In particular, we set $h_1^{(1)}(u) = D_u^{(1)} u^3$ and $h_2^{(1)}(v) = D_v^{(1)} v^3$ for the 2-body coupling, while we take $h_1^{(2)}(u_1,u_2) = D_u^{(2)} u_1^2 u_2$ and $h_2^{(2)}(v_1,v_2) = D_v^{(2)} v_1^2 v_2$, for the 3-body interaction. Note that this choice for the coupling functions satisfies the condition of natural coupling as long as

$$D_u^{(1)} = D_u^{(2)} \text{ and } D_v^{(1)} = D_v^{(2)} \tag{6.4.4}$$

Given these coupling functions, we can rewrite Equation (6.4.1) as

$$\begin{cases} \dot{u}_i = f_1(u_i,v_i) + \sigma_1 D_u^{(1)} \displaystyle\sum_{j_1=1}^{N} A_{ij_1}^{(1)} (u_{j_1}^3 - u_i^3) \\ \qquad\quad + \sigma_2 D_u^{(2)} \displaystyle\sum_{j_1=1}^{N}\sum_{j_2=1}^{N} A_{ij_1j_2}^{(2)} (u_{j_1}^2 u_{j_2} - u_i^3) \\ \dot{v}_i = f_2(u_i,v_i) + \sigma_1 D_v^{(1)} \displaystyle\sum_{j_1=1}^{N} A_{ij_1}^{(1)} (v_{j_1}^3 - v_i^3) \\ \qquad\quad + \sigma_2 D_v^{(2)} \displaystyle\sum_{j_1=1}^{N}\sum_{j_2=1}^{N} A_{ij_1j_2}^{(2)} (v_{j_1}^2 v_{j_2} - v_i^3) \end{cases} \tag{6.4.5}$$

Again, to study the stability of the homogeneous solution $(u_i,v_i) = (u^*,v^*)$, we linearize Equation (6.4.5). By resorting to the natural coupling assumption, we can conclude that $\mathbf{J}_{H^{(1)}} = \mathbf{J}_{H^{(2)}}$ and thus rewrite Equation (6.4.2) as follows

$$\dot{\vec{\zeta}} = \left[\mathbb{I}_N \otimes \mathbf{J}_0 + \left(\sigma_1 \mathbf{L}^{(1)} + \sigma_2 \mathbf{L}^{(2)} \right) \otimes \mathbf{J}_{H^{(1)}} \right] \vec{\zeta} \tag{6.4.6}$$

[(2)] In the framework of synchronization dynamics, when all units are in the same state we talk about synchronous solution.

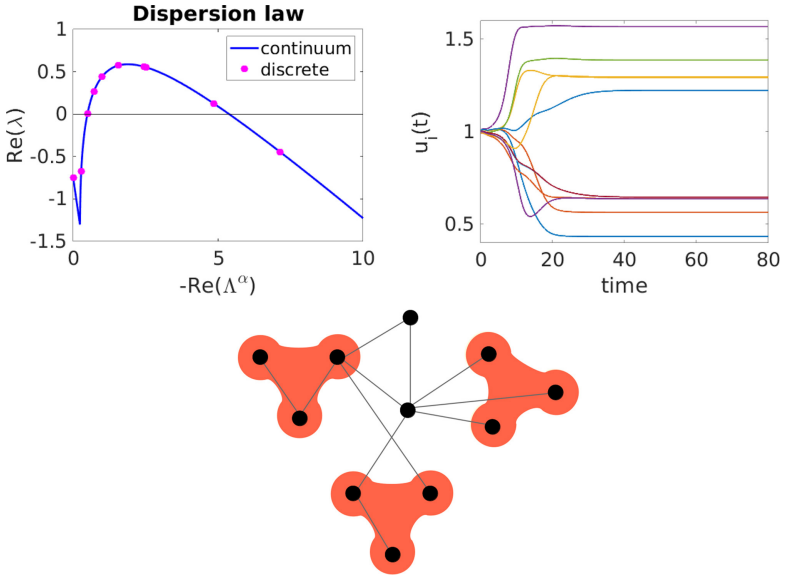

Figure 6.2: Turing instability with nonlinear diffusion in higher-order structures. Brusselator model with $b = 3$, $c = 3.5$, $D_u^{(1,2)} = 0.1$, $D_v^{(1,2)} = 2$, $\sigma_{1,2} = 1$; the initial perturbation is $\sim 10^{-2}$. On the upper left panel, the dispersion law: the blue line is the continuous one, while the magenta dots indicate the discrete counterpart. On the upper right panel, Turing patterns for the u species. On the bottom panel, the hypergraph on which the system has been simulated: 11 nodes, 11 links and 3 2-hyperedges (i.e., triangles).

where

$$\mathbf{J}_{H^{(1)}} = 3 \begin{bmatrix} (u^*)^2 D_u^{(1)} & 0 \\ 0 & (v^*)^2 D_v^{(1)} \end{bmatrix}$$

and $\vec{\zeta} = (\delta u_1, \delta v_1, \ldots, \delta u_N, \delta v_N)^\top$, with $\delta u_i = u_i - u^*$ and $\delta v_i = v_i - v^*$. Let us observe that Equation (6.4.6) recalls the similar result obtained in [205]. However, the mathematical framework here proposed is more general, because it allows to study a broader class of higher-order couplings (see Section 6.6 for more details).

The natural coupling assumption allowed us to introduce an "effective" Laplacian that encodes the higher-order structure into a weighted network, whose weights are self-consistently determined, $\mathbf{M} = \sigma_1 \mathbf{L}^{(1)} + \sigma_2 \mathbf{L}^{(2)}$. Resorting to the eigenbasis for $\mathbf{M}$, one can make one step further and project the $2N \times 2N$ linear system onto N linear systems of size 2×2 depending each one on a single eigenvalue, $\Lambda^{(\alpha)}$, of $\mathbf{M}$, more precisely

$$\frac{d}{dt} \begin{pmatrix} \delta \hat{u}_\alpha \\ \delta \hat{v}_\alpha \end{pmatrix} = \left[\mathbf{J}_0 + \Lambda^{(\alpha)} \mathbf{J}_{H^{(1)}} \right] \begin{pmatrix} \delta \hat{u}_\alpha \\ \delta \hat{v}_\alpha \end{pmatrix} := \mathbf{J}^{(\alpha)} \begin{pmatrix} \delta \hat{u}_\alpha \\ \delta \hat{v}_\alpha \end{pmatrix} \quad \forall \alpha = 1, \ldots, N \tag{6.4.7}$$

where again $\delta \hat{u}_\alpha = \sum_i \delta u_i \varphi_i^{(\alpha)}$, resp. $\delta \hat{v}_\alpha = \sum_i \delta v_i \varphi_i^{(\alpha)}$, is the projection of δu_i, resp. δv_i, on the eigenvector $\vec{\varphi}_\alpha$.

Let us observe that the latter equation is formally the same as the one obtained in the case of pairwise interactions (6.3.6) and thus the same analysis follows, except that now the eigenvalues depend on the coupling strengths. In Fig, 6.2, we show the

dispersion relation and an example of Turing patterns for the Brusselator model (Equations (6.3.8)). Let us notice that the blue curve (top left panel of Figure 6.2) has been computed by replacing $\Lambda^{(\alpha)}$ with a continuous variable, corresponding thus to the dispersion relation for a system defined on a continuous support with periodic boundary conditions. Having fixed the topology of binary interactions and the higher-order ones, hence the matrices $\mathbf{L}^{(1)}$ and $\mathbf{L}^{(2)}$, we can vary the coupling strengths σ_1 and σ_2, and thus letting $\Lambda^{(\alpha)}$ "slide" along this curve (cyan dots). Stated differently, the Turing instability can be obtained (or repressed) by simply changing the coupling and keeping the remaining parts of the model unchanged.

6.4.2 Regular topologies

Let us now relax the natural coupling assumption by setting different diffusion coefficients at the different considered order, i.e., $D_u^{(1)} \neq D_u^{(2)}$ and $D_v^{(1)} \neq D_v^{(2)}$, but keeping the same form for the coupling functions. Namely we take $h_1^{(1)}(u) = D_u^{(1)} u^3$ and $h_2^{(1)}(v) = D_v^{(1)} v^3$ for the 2-body coupling, while we take $h_1^{(2)}(u_1, u_2) = D_u^{(2)} u_1^2 u_2$ and $h_2^{(2)}(v_1, v_2) = D_v^{(2)} v_1^2 v_2$ for the 3-body coupling. It would also be possible to adopt different coupling functional forms for each order, but, as it will be clear in the following, it is more interesting to focus on the diffusion coefficients, the latter having a key role in the Turing mechanism of pattern formation. Nevertheless, the following analysis could be easily extended to a setting in which coupling functions have different form, as long as they remain diffusive-like.

The starting point for the linear stability analysis is, again, Equation (6.4.2); however, because $\mathbf{J}_{H^{(1)}} \neq \mathbf{J}_{H^{(2)}}$, one cannot simplify the latter equation to obtain the analogous of Equation (6.4.6). In the same spirit of simplifying the stability equation, we can observe that in general the two Laplacians do not commute, thus, they cannot be simultaneously diagonalized. In conclusion, one cannot determine a single equation, depending on the spectrum of the involved Laplacian matrices, and proceed with the analysis as done in the case of the Master Stability Function. The numerical computation of the eigenvalues of the $2N \times 2N$ linear system would not allow a clear understanding of the role of the involved parameters.

There are however some higher-order structures allowing for a complete analytical description: this is the case whenever the higher-order Laplacian matrix is a multiple of the network Laplacian one. We will call topologies with the above property *regular topologies*. Tetrahedra or icosaedra are examples of regular topologies as well as the *triangular lattice with periodic boundary conditions*, i.e., a 2-torus paved with triangles, that we hereby analyze in details. Let us observe that we assume the nodes forming a triangle (of first order interactions) to be also part of a 3-body interaction; for this reason we will call it triangular 2-lattice. In this case, each node interacts with its six neighbors through six 2-body interactions and six 3-body interactions

Let us consider a triangular 2-lattice of N nodes, where each node i has 6 incident links. Its first order Laplacian will then be

$$\mathbf{L}_{ij}^{(1)} = \begin{cases} -6 & \text{if } i = j \\ A_{ij}^{(1)} & \text{otherwise} \end{cases}$$

If now each node will also have 6 incident triangles, we have that

$$\sum_{j,k=1}^{N} A^{(2)}_{ijk} = 2 \cdot 6 = 12 \quad \text{and} \quad \sum_{k=1}^{N} A^{(2)}_{ijk} = 2A^{(1)}_{ij}$$

From the definition of the second order Laplacian, Equation (6.4.3), we obtain the relation

$$\mathbf{L}^{(2)} = 2\mathbf{L}^{(1)} \tag{6.4.8}$$

hence, the two Laplacians can be both diagonalized through the eigenvectors of $\mathbf{L}^{(1)}$.

Equation (6.4.2) now takes the form

$$\dot{\vec{\zeta}} = \left(\mathbb{I}_N \otimes \mathbf{J}_0 + \mathbf{L}^{(1)} \otimes (\sigma_1 \mathbf{J}_{H^{(1)}} + 2\sigma_2 \mathbf{J}_{H^{(2)}}) \right) \vec{\zeta} \tag{6.4.9}$$

We can then proceed in projecting on the eigenvectors of $\mathbf{L}^{(1)}$, by obtaining

$$\frac{d}{dt} \begin{pmatrix} \delta\hat{u}_\alpha \\ \delta\hat{v}_\alpha \end{pmatrix} = \left[\mathbf{J}_0 + \Lambda^{(\alpha)} (\sigma_1 \mathbf{J}_{H^{(1)}} + 2\sigma_2 \mathbf{J}_{H^{(2)}}) \right] \begin{pmatrix} \delta\hat{u}_\alpha \\ \delta\hat{v}_\alpha \end{pmatrix} \quad \forall \alpha = 1, \dots, N \tag{6.4.10}$$

which is analogous to Equation (6.4.7), due to the properties of the topology. The Laplacian's eigenvalues $\Lambda^{(\alpha)}$ can be effectively replaced by a continuous parameter, which is the continuous spectrum of the corresponding diffusion operator, allowing us to have an analytical expression of the dispersion law. The above result can be straightforwardly generalized to all regular topologies.

Let us point out that the assumption of $\mathbf{L}^{(2)}$ to be proportional to $\mathbf{L}^{(1)}$ allows to emphasize the effects of higher-order interactions, which would not be possible to fully appreciate under the natural coupling assumption. In fact, one can deal with sets of parameters which do not allow the formation of patterns by considering the sole pairwise interactions, i.e., condition (6.3.13) would not be satisfied, $(v^*)^2 D_v^{(1)} < (u^*)^2 D_u^{(1)}$, and thus patterns could not develop, but the appropriate values of the second order couplings would make possible the Turing instability. This is the case shown in Figure 6.3, where we can observe the dispersion law and an example of a pattern obtained with the Brusselator model on a triangular 2-lattice of 16 nodes; we notice that, while the pairwise case (red curve) never allows instability, the higher-order one yields Turing patterns. Let us remark that the dispersion law is a function of the spectrum of the Laplacian $\mathbf{L}^{(1)}$.

Let us stress that it is also possible to find the opposite case, in which pairwise interactions would normally give rise to Turing patterns, but the presence of higher-order ones annihilates them and stabilizes the system, as exemplified in Figure 6.4.

The interplay between nonlinear diffusion and regular topologies could be better highlighted by rewriting (6.4.10). Under our working assumptions, we have

$$\mathbf{J}_{H^{(1)}} = 3 \begin{bmatrix} D_u^{(1)} & 0 \\ 0 & \left(\frac{b}{c}\right)^2 D_v^{(1)} \end{bmatrix} \quad \text{and} \quad \mathbf{J}_{H^{(2)}} = 3 \begin{bmatrix} D_u^{(2)} & 0 \\ 0 & \left(\frac{b}{c}\right)^2 D_v^{(2)} \end{bmatrix} \tag{6.4.11}$$

We can hence define the effective diffusion coefficients

$$\mathscr{D}_u^{eff} = \sigma_1 D_u^{(1)} + \sigma_2 D_u^{(2)} \quad \text{and} \quad \mathscr{D}_v^{eff} = \sigma_1 D_v^{(1)} + \sigma_2 D_v^{(2)} \tag{6.4.12}$$

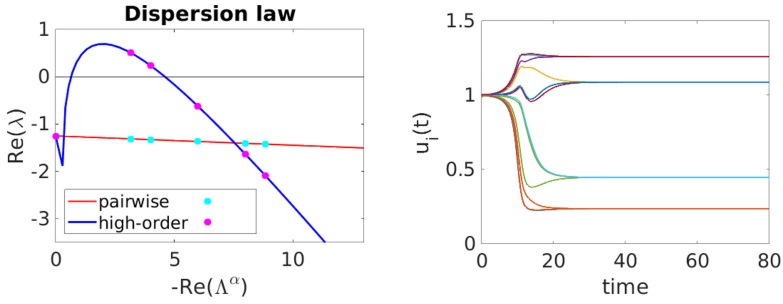

Figure 6.3: Triangular 2-lattice of 16 nodes with periodic boundary conditions; Brusselator model with $b = 5.5$, $c = 7$, $D_u^{(1)} = 1$, $D_v^{(1)} = 0.5$, $D_u^{(2)} = 0.1$, $D_v^{(2)} = 1$, $\sigma_1 = 0.01$ and $\sigma_2 = 1$; the initial perturbation is $\sim 10^{-2}$. In the left panel, the dispersion law for the higher-order case (blue line and magenta dots) compared with the case where only pairwise interactions are present (red line and cyan dots). In the right panel, an example of a Turing pattern for the u species.

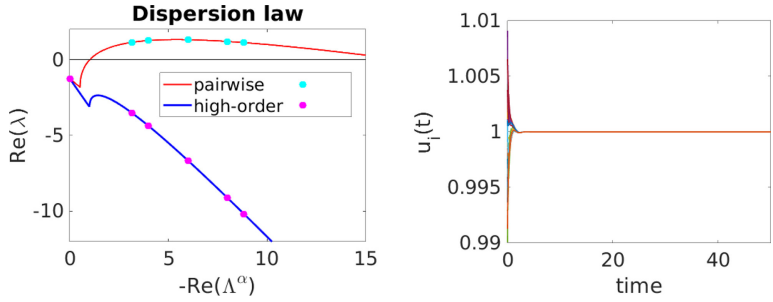

Figure 6.4: Triangular 2-lattice of 16 nodes with periodic boundary conditions; Brusselator model with $b = 5.5$, $c = 7$, $D_u^{(1)} = 0.1$, $D_v^{(1)} = 1.5$, $D_u^{(2)} = 1$, $D_v^{(2)} = 0.5$, $\sigma_1 = 0.7$ and $\sigma_2 = 0.2$; the initial perturbation is $\sim 10^{-2}$. In the left panel, the dispersion law for the higher-order case (blue line and magenta dots) compared with the case where only pairwise interactions are present (red line and cyan dots). As the higher-order dispersion law is always negative, there is no emergence of Turing patterns, as also shown in the right panel for the u species.

so that we can cast (6.4.9) in the following way

$$\dot{\vec{\zeta}} = \left(\mathbb{I}_N \otimes \mathbf{J}_0 + \mathbf{L}^{(1)} \otimes \mathbf{J}_{\mathscr{H}}^{eff}\right) \vec{\zeta} \tag{6.4.13}$$

where

$$\mathbf{J}_{\mathscr{H}}^{eff} = 3 \begin{bmatrix} \mathscr{D}_u^{eff} & 0 \\ 0 & \left(\frac{b}{c}\right)^2 \mathscr{D}_v^{eff} \end{bmatrix} \tag{6.4.14}$$

By projecting on the eigenvectors of $\mathbf{L}^{(1)}$, we obtain a new form of Equation (6.4.10), namely

$$\frac{d}{dt}\begin{pmatrix} \delta\hat{u}_\alpha \\ \delta\hat{v}_\alpha \end{pmatrix} = \left[\mathbf{J}_0 + \Lambda^{(\alpha)} \mathbf{J}_{\mathscr{H}}^{eff}\right] \begin{pmatrix} \delta\hat{u}_\alpha \\ \delta\hat{v}_\alpha \end{pmatrix} \quad \forall \alpha = 1, \ldots, N \tag{6.4.15}$$

Following the steps presented above to determine the onset of Turing instability, we can

now obtain

$$\begin{cases} -c^3\mathscr{D}_u^{eff} + (b-1)b^2\mathscr{D}_v^{eff} > 0 \\ 4b^2c^3\mathscr{D}_u^{eff}\mathscr{D}_v^{eff} - \left(-c^3\mathscr{D}_u^{eff} + (b-1)b^2\mathscr{D}_v^{eff}\right)^2 < 0 \end{cases} \tag{6.4.16}$$

From the latter relations it emerges that Turing patterns are the result of the interplay not only between the model parameters and the diffusion coefficients, but also with the strength of the interactions at every order.

In the next section, we will study the general case where, in absence of specific assumptions on the coupling or on the structure, an analytical study cannot be performed, and we thus have to resort to numerical simulations. But before that, let us examine a particular case of regular topology, where the Laplacians of all orders can be diagonalized simultaneously: the *all-to-all coupling*, where every possible d-body interaction is active. When dealing with such coupling, the analysis is not restricted to some orders of interactions, but can be extended to all of them. Nonetheless, without further ado, let us again restrict the analysis to first- and second-order interactions. For N interconnected systems, we have $\mathbf{L}^{(2)} = (N-2)\mathbf{L}^{(1)}$ (see [45] for a detailed analysis); let us observe that this is again a case where $\mathbf{L}^{(2)}$ is proportional to $\mathbf{L}^{(1))}$. However, here the proportionality constant depends on the system's size. Based on the above, Equation (6.4.2) can be rewritten as

$$\dot{\vec{\zeta}} = \left(\mathbb{I}_N \otimes \mathbf{J}_0 + \sigma_1\mathbf{L}^{(1)} \otimes \left(\mathbf{J}_{H^{(1)}} + \frac{\sigma_2}{\sigma_1}(N-2)\mathbf{J}_{H^{(2)}}\right)\right)\vec{\zeta} \tag{6.4.17}$$

Projecting again on the eigenvectors of $\mathbf{L}^{(1)}$ we obtain

$$\frac{d}{dt}\begin{pmatrix}\delta\hat{u}_\alpha \\ \delta\hat{v}_\alpha\end{pmatrix} = \left[\mathbf{J}_0 + \sigma_1\Lambda^{(\alpha)}\left(\mathbf{J}_{H^{(1)}} + \frac{\sigma_2}{\sigma_1}(N-2)\mathbf{J}_{H^{(2)}}\right)\right]\begin{pmatrix}\delta\hat{u}_\alpha \\ \delta\hat{v}_\alpha\end{pmatrix}$$
$$\forall\alpha = 1,\dots,N$$

Let us observe that $\Lambda^{(\alpha)} \in \{0,N\}$, hence the dispersion law depends on the number of nodes. The above equation indicates that it is possible to decompose the instability modes. For a given value of N, having fixed the ratio σ_2/σ_1, we can vary the value of σ_1, thus generating a continuous curve. Observe that such a curve allows us to check for the onset of Turing instability on the "all-to-all" configuration. Indeed, when the curve is negative Turing instability cannot occur for any value of σ_1, while Turing patterns can emerge in the opposite case. Hence, the continuous curve, as function of a parameter $\gamma = \sigma_1\Lambda_\alpha$, can be subsumed in the framework of the Master Stability Function approach [44].

To provide a numerical example, let us consider an ensemble of N Brusselator systems interacting in the all-to-all configuration, with $h_1^{(1)} = D_u^{(1)}u^3$, $h_2^{(1)} = D_v^{(1)}v^3$, $h_1^{(2)}(u_1,u_2) = D_u^{(2)}u_1^2u_2$ and $h_2^{(2)}(v_1,v_2) = D_v^{(2)}v_1^2v_2$, and with the values of the diffusion coefficients set such that the coupling functions do not satisfiy the natural coupling condition. In Section 6.5, we report a case analogous to that displayed in Section 6.3, namely, patterns emerge due to higher-order interaction. Also in this case, with the appropriate coupling functions we can obtain the opposite situation, i.e., higher-order interactions annihilate patterns, which would otherwise emerge with the sole pairwise ones.

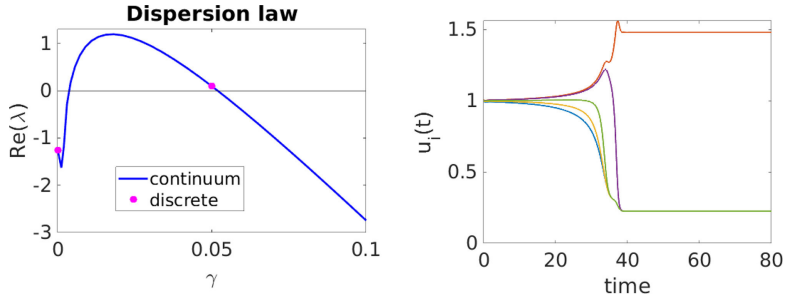

Figure 6.5: All-to-all 2-hypergraph of 5 nodes; Brusselator model with $b = 5.5$, $c = 7$, $D_u^{(1)} = 1$, $D_v^{(1)} = 0.1$, $D_u^{(2)} = 0.07$, $D_v^{(2)} = 1$, $\sigma_1 = 0.01$ and $\sigma_2 = 1$; the initial perturbation is $\sim 10^{-2}$. On the left panel, the discrete dispersion law; note that the continuous curve is a fictitious dispersion law, but it is a Master Stability Function, as explained in the text. For this reason, the continuous curve can be thought as a function of a parameter γ. On the right panel, an example of a Turing pattern for the u species.

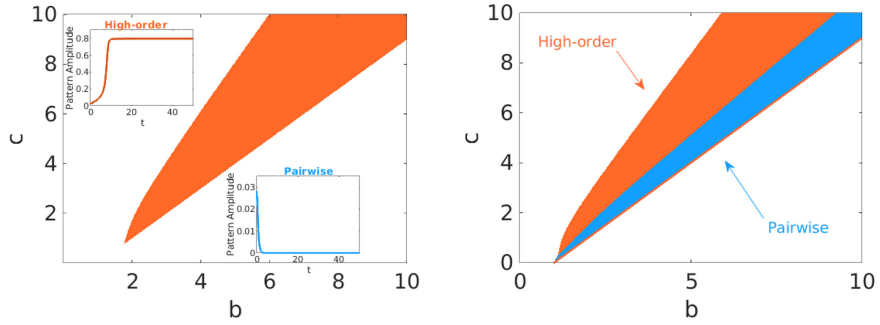

Figure 6.6: Left panel: Brusselator model with $D_u^{(1)} = 1$, $D_v^{(1)} = 0.5$, $D_u^{(2)} = 0.1$, $D_v^{(2)} = 2$, $\sigma_1 = 0.1$ and $\sigma_2 = 1$. The setting does not allow for Turing patterns when only pairwise interaction are considered, hence to obtain the instability region we need to include also higher-order (3-body) interactions (the region of parameters where patterns are obtained is shown in orange). Numerical simulations of the system with $b = 5.5$ and $c = 7$ without (resp. with) higher-order terms show that Turing patterns are not obtained (resp. are obtained) as confirmed by the total pattern amplitude [31] in blue (resp. orange) on the lower (resp. upper) inset. Right panel: Brusselator model with $D_u^{(1)} = 0.1$, $D_v^{(1)} = 0.5$, $D_u^{(2)} = 0.01$, $D_u^{(2)} = 1$, $\sigma_1 = 0.2$ and $\sigma_2 = 1$. The instability region when only pairwise interactions are considered is depicted in blue, while in orange the one obtained when also higher-order ones are active; note that the blue region is a subset of the orange one. For both panels, the initial perturbation is $\sim 10^{-2}$ and the hypergraph is that of in Figure 6.2.

6.4.3 General topologies

Let us now focus on the most general case, in which arbitrary higher-order topologies are considered and the coupling is not restricted to the natural coupling form. Following the same reasoning of the previous section, we use different diffusion coefficients, while the coupling functions remain of the same form. In such setting, we cannot have a semi-analytical form of the dispersion law, because the Laplacian matrices cannot be diagonalized simultaneously. Hence, we will resort to numerical simulations to determine the onset of the Turing instability. Based on the above discussion, we thus performed a dedicated numerical analysis of this scenario that allows us to fully exploit the pres-

ence of higher-order terms. The results are reported in Figure 6.6 where we show the parameters region associated to a Turing instability in the case of the Brusselator model in Equation (6.4.5) for two different sets of values of the weights σ_i. On the left panel, the first order diffusion coefficients (i.e., pairwise) do not allow Turing instability (since $(v^*)^2 D_v^{(1)} > (u^*)^2 D_u^{(1)}$), on the other hand the presence of higher-order diffusion with a suitable choice of the weights σ_i allows the formation of patterns. On the right panel, instead, Turing instability arises even in the pairwise setting, but many-body interactions are still beneficial as they yield a larger region of parameters for which patterns can be obtained.

Let us conclude by remarking that, in analogy with the setting studied in the previous section (i.e., regular topologies), it is also possible to find couplings such that higher-order interactions hamper the formation of Turing patterns, which would normally arise when the interactions are limited to be pairwise.

6.5 Discussion

In this work, we have formulated a general theory to study the emergence of Turing patterns for dynamical systems where many-body interactions are taken into account, modeled by using higher-order interactions. Our framework goes beyond the one recently proposed [205] that, as shown in the SM (Section 6.6), can be recovered as a special case of the theory hereby developed. Our framework is inspired by the work of [45] dealing with synchronization in higher-order structures and allows to obtain Turing patterns in settings where it would be otherwise impossible, e.g., by restricting to pairwise interactions. At the same time, it also permits to suppress the instability which would occur with only pairwise interactions, depending on the desired applications. We have shown that including diffusion terms from higher-order interactions may either widen the region of parameters where patterns occur, or, on the contrary, reduce its extension. This can be achieved acting solely on the diffusion coefficients, but also using different coupling functions. The detailed analytical study we performed provided us a clear understanding of the role of the model parameters, as well as of the higher-order topology in the pattern emergence. This further flexibility in the choice of the parameters can shed light on the fine tuning problem [135] and benefit the field of optimal control of patterns [233, 234, 235]. In fact, one could choose the appropriate coupling functions and/or diffusion coefficients in order to obtain the desired inhomogeneous state.

A natural extension of our framework would be to study Turing-like instability emerging from a limit cycle: in fact, it has been shown that a similar instability mechanism can occur also when the homogeneous stable state is a limit cycle [46, 78]. In many applications, where it is important to control the emergence of synchronization, such as neuroscience, our theory could provide to be extremely useful. Moreover, exploring the onset of Turing patterns in the newly developed framework of M-directed hypergraphs [211] could provide another interesting direction where to focus the attention in future works.

6.6 SM 1: Formalism mapping

In this SM, we show how the formalism introduced in [205] to study the formation of Turing patterns on hypergraphs can be recovered from the mathematical framework developed in [45] for the analysis of synchronization of chaotic oscillators in simplicial complexes. Note that the latter also applies to the case of hypergraphs, as discussed in [211].

We start from the dynamical system (6.2.1). First, we assume the coupling functions $\vec{g}^{(d)}$ to be of the form

$$\begin{aligned}\vec{g}^{(d)}(\vec{x}_i,\vec{x}_{j_1},\vec{x}_{j_2},\ldots,\vec{x}_{j_d}) &= \vartheta(d+1)[\gamma(\vec{x}_{j_1})-\gamma(\vec{x}_i)+\cdots+\gamma(\vec{x}_{j_d})-\gamma(\vec{x}_i)] \\ &= \vartheta(d+1)\left[\sum_{n=1}^{d}\gamma(\vec{x}_{j_n})-d\gamma(\vec{x}_i)\right]\end{aligned} \tag{6.6.1}$$

where $\vartheta:\mathbb{R}\longrightarrow\mathbb{R}$ is a generic function of the number of nodes involved in the higher-order interaction, i.e., the size of the hyperedge or of the simplex, while $\gamma:\mathbb{R}^m\longrightarrow\mathbb{R}^m$ is a generic function encoding the contribution of the node state vectors to the coupling. Note that, given the form in Equation (6.6.1), all the coupling functions are non-invasive. Equation (6.2.1) can be hence rewritten as

$$\begin{aligned}\dot{\vec{x}}_i = \vec{f}(\vec{x}_i)&+\sigma_1\sum_{j_1=1}^{N}A^{(1)}_{ij_1}\vartheta(2)[\gamma(\vec{x}_{j_1})-\gamma(\vec{x}_i)]+ \\ &+\sigma_2\sum_{j_1=1}^{N}\sum_{j_2=1}^{N}A^{(2)}_{ij_1j_2}\vartheta(3)[\gamma(\vec{x}_{j_1})+\gamma(\vec{x}_{j_2})-2\gamma(\vec{x}_i)]+\cdots \\ &+\sigma_P\sum_{j_1=1}^{N}\cdots\sum_{j_P=1}^{N}A^{(P)}_{ij_1j_2\ldots j_P}\vartheta(P+1)\left[\sum_{n=1}^{P}\gamma(\vec{x}_{j_n})-P\gamma(\vec{x}_i)\right]\end{aligned} \tag{6.6.2}$$

Noticing that each adjacency tensor $A^{(d)}$ is symmetric with respect to its $d+1$ indices, i.e., $A^{(d)}_{ij_1j_2\ldots j_d}=A^{(d)}_{\pi(ij_1j_2\ldots j_d)}$, where π is a generic permutation of the indices, we can simplify the coupling terms, thus writing Equation (6.6.2) as

$$\begin{aligned}\dot{\vec{x}}_i = \vec{f}(\vec{x}_i)&+\sigma_1\sum_{j_1=1}^{N}A^{(1)}_{ij_1}\vartheta(2)[\gamma(\vec{x}_{j_1})-\gamma(\vec{x}_i)]+ \\ &+2\sigma_2\sum_{j_1=1}^{N}\vartheta(3)[\gamma(\vec{x}_{j_1})-\gamma(\vec{x}_i)]\sum_{j_1=1}^{N}A^{(2)}_{ij_1j_2}+\cdots \\ &+P\sigma_P\sum_{j_1=1}^{N}\vartheta(P+1)[\gamma(\vec{x}_{j_1})-\gamma(\vec{x}_i)]\sum_{j_2=1}^{N}\cdots\sum_{j_P=1}^{N}A^{(P)}_{ij_1j_2\ldots j_P}\end{aligned} \tag{6.6.3}$$

By recalling the definition [45] of the generalized d-degree, $k^{(d)}_{ij}$, of a link (i,j), which represents the number of d-order structures the link (i,j) is part of

$$(d-1)!k^{(d)}_{ij}=\sum_{l_2=1}^{N}\cdots\sum_{l_d=1}^{N}A^{(d)}_{il_1l_2\ldots l_d} \tag{6.6.4}$$

and by noticing that $k_{ij}^{(1)} = A_{ij}^{(1)}$, we can write the equations governing the dynamics of the system as

$$\begin{aligned}\dot{\vec{x}}_i \;=\; & \vec{f}(\vec{x}_i) + \sigma_1 \sum_{j=1}^{N} k_{ij}^{(1)} \vartheta(2)\Delta_j + 2\sigma_2 \sum_{j=1}^{N} k_{ij}^{(2)} \vartheta(3)\Delta_j + \cdots \\ & + P(P-1)!\sigma_P \sum_{j=1}^{N} k_{ij}^{(P)} \vartheta(P+1)\Delta_j\end{aligned} \tag{6.6.5}$$

where we have relabeled index j_1 as j, and where we have defined $\Delta_j = \gamma(\vec{x}_j) - \gamma(\vec{x}_i)$.

By considering the higher-order incidence matrix [205], $e_{i\alpha}$, defined as

$$e_{i\alpha} = \begin{cases} 1 & v_i \in E_\alpha \\ 0 & \text{otherwise} \end{cases} \tag{6.6.6}$$

where E_α can represent either a hyperedge or a simplex, we can now write Equation (6.6.5) as

$$\begin{aligned}\dot{\vec{x}}_i \;=\; & \vec{f}(\vec{x}_i) + \sigma_1 \sum_{j=1}^{N} \sum_{\alpha:E_\alpha=2} e_{i\alpha} e_{j\alpha} \vartheta(2)\Delta_j + 2\sigma_2 \sum_{j=1}^{N} \sum_{\alpha:E_\alpha=3} e_{i\alpha} e_{j\alpha} \vartheta(3)\Delta_j \\ & + \cdots + P!\sigma_P \sum_{j=1}^{N} \sum_{\alpha:E_\alpha=P+1} e_{i\alpha} e_{j\alpha} \vartheta(P+1)\Delta_j\end{aligned} \tag{6.6.7}$$

In fact, as for each order d of the higher-order interactions, the factor $e_{i\alpha}e_{j\alpha}$ is equal to one when both nodes i and j belong to E_α, by summing over all $j \neq i$, each summation has exactly $k_{ij}^{(d)}$ non-zero terms.

Lastly, by assuming the d-th coupling strength to be $\sigma_d = \varepsilon/d!$, we finally obtain

$$\dot{\vec{x}}_i = \vec{f}(\vec{x}_i) + \varepsilon \sum_{j=1}^{N} \sum_{\alpha} e_{i\alpha} e_{j\alpha} \vartheta(E_\alpha)[\gamma(\vec{x}_j) - \gamma(\vec{x}_i)] \tag{6.6.8}$$

which recovers the dynamical system analyzed in [205] as we set $\vartheta(E_\alpha) = E_\alpha - 1$. Hence, the mathematical framework here considered permits to extend the analysis of Turing pattern formation on hypergraphs, as it allows to consider more general coupling functions.

Chapter 7

Diffusion-driven instability of topological signals coupled by the Dirac operator

In the previous Chapter, we have seen a higher-order extension of Turing theory, from the many-body perspective. Despite the novelty of the work, the setting resembles the pairwise one and what changes is the possibility of having many-body interactions, possibly with different diffusivities, affecting thus the final state of the system. In fact, both species have the node as a support and, instead of diffusing through links, they diffuse through hyperedges. In this work, we enter the actual higher-order setting, a new framework mathematically and conceptually, whose possibilities are yet to be fully exploited. By using the tools of algebraic topology, we are able to further push the boundaries of the Turing framework and couple species lying in different manifolds, namely on the nodes and on the links. In such context, it is more appropriate to talk about topological signals, rather than species, as the latter is tied to the framework where all the interacting units are of the same nature. Topological signals have been studied in the framework of synchronization dynamics and, in particular, for the Kuramoto model [202], but never to investigate the emergence of Turing patterns. The main difference between the two frameworks is that the former deals with non-identical units, hence, in general, there does not exist a homogeneous solution of the whole coupled system, which always exists in the latter, the oscillators being identical. In the framework of Turing patterns, when the manifold where the dynamics take place is restricted to the nodes, a homogeneous state can always be achieved for connected networks and a diffusive-like coupling. On the other hand, when also signals on links are considered, a homogeneous state exists if and only if the network is Eulerian, i.e., every node has an even degree, as we prove in the next pages. Such constraint may seem limiting, but is the price to pay if we want to consider higher-order signals. On the other hand, this allows us to relax the strict condition on the diffusion coefficients, as Turing patterns can be obtained

even with equal diffusivities for the signals on the nodes and on the links. Nonetheless, the perspective can be reversed to transform constraint on the nodes' degrees in an opportunity: if the application requires inhomogeneity, one can consider simplicial structures that do not allow a homogeneous state due to their topological conformation. This becomes particularly relevant in the case of synchronization, where the goal of certain applications is not to achieve it [236]. Another relevant aspect of Turing instability for topological signals is that we lose the activator-inhibitor dichotomy, as patterns are obtained only when both signals are inhibitors.

Note Until this point, all Laplacians encountered throughout this thesis are negative semi-definite. For this reason, in the brief introduction to higher-order dynamics given in Section 5.3 of Chapter 5, we have reformulated and defined the Hodge Laplacians as negative semi-definite matrices. In this paper the notation and some definitions are a bit different from those used in the rest of the work and, whilst we tried as much as possible to uniform the manuscript, some changes would have altered too much the original work or made the notation extremely heavy. This is why, for example, the Laplacians encountered in this Chapter are positive semi-definite, or the vectors do not have the $\vec{\cdot}$ symbol.

My contribution This work was conducted with two PhD students, Lorenzo Giambagli and M. Lucille Calmon, and it may result in part of their theses. Lorenzo and M. Lucille mainly developed the theoretical framework, while my contribution mainly regards the development of Turing theory and the numerical study.

L. Giambagli, M.L. Calmon, R. Muolo, T. Carletti & G. Bianconi, Physical Review E, 106, 064314 (2022) [229]
This article is not open access, but it is freely available as a pre-print.

Note During the revision of this thesis, we realized that Figure 7.7a) had a mistake in the values of the color scale. In the following Chapter it has been fixed, but in the original paper we could not, as it was already published.

Abstract

The study of reaction-diffusion systems on networks is of paramount relevance for the understanding of nonlinear processes in systems where the topology is intrinsically discrete, such as the brain. Until now, reaction-diffusion systems have been studied only when species are defined on the nodes of a network. However, in a number of real systems including, e.g., the brain and the climate, dynamical variables are not only defined on nodes but also on links, faces and higher-dimensional cells of simplicial or cell complexes, leading to *topological signals*. In this work, we study reaction-diffusion processes of topological signals coupled through the Dirac operator. The Dirac operator allows topological signals of different dimension to interact or cross-diffuse as it

projects the topological signals defined on simplices or cells of a given dimension to simplices or cells of one dimension up or one dimension down. By focusing on the framework involving nodes and links, we establish the conditions for the emergence of Turing patterns and we show that the latter are never localized only on nodes or only on links of the network. Moreover when the topological signals display a Turing pattern their projection does as well. We validate the theory hereby developed on a benchmark network model and on square lattices with periodic boundary conditions.

7.1 Introduction

Nature is a blossoming of patterns, namely spatially heterogeneous structures, spontaneously emerging from the web of nonlinear interactions existing among the many basic units constituting the system under scrutiny [95, 42]. Scholars have developed theories capable of dealing with both stationary patterns [4, 31, 109] and time-varying ones [43, 237, 41, 238, 24]. Such research has been developed in the framework of network science [155, 86, 239, 240] relying on the assumption that system interactions can be sufficiently well described by using a pairwise representation: the basic units composing the system exhibit their own dynamics, i.e., a local evolution law associated with each node of the network, and then they interact by diffusing or via non-local (long-range) interactions, by using the available links.

Networks, however, only capture pairwise interactions while higher-order interactions [207, 208, 241, 242, 243, 244, 245, 218] are crucial to describe several empirical systems in physics, biology, neuroscience, or social sciences. Interestingly, recent research taking into account higher-order interactions is rapidly changing our understanding of the relation between the structure and function of complex systems [207, 217, 246].

Simplicial complexes are higher-order networks that come with extremely rich and useful structures inherited from discrete topology [207, 247, 216]. Roughly speaking, a simplicial complex is a topological structure that, in addition to nodes and links, also contains triangles, i.e., 3-body interactions, tetrahedra (i.e., 4-body interactions) and so on. Even more generally cell complexes [248] also include the other convex polytopes, i.e., not only triangles and tetrahedra but also squares, pentagons, etc., and hypercubes, orthoplexes etc. One can thus consider topological signals defined on nodes and links, but also on higher-order structures [207]. Examples of topological signals occur, for instance, in Figure 7.1: We schematically represent the dynamical state of a simplicial complex encoded by the vector neuronal networks, where the interaction between two neurons is mediated by the synaptic signal [249]. Recent scientific literature points out the relevance of edge signals also in large-scale brain networks [250, 251], and in biological transportation networks [252, 253]. Edge signals occur also in power-grids [220] or in traffic on a road network [254, 255, 256, 257]. Moreover, edge signals might also represent a number of climate data such as currents in the ocean and velocity of wind that can be projected on a suitable triangulation of the Earth's surface [256, 257]. Topological signals can undergo higher-order simplicial synchronization [202, 258, 259, 260, 203, 261, 262, 263, 264], and higher-order diffusion [260, 265, 266]. Moreover, datasets of topological signals can be treated with topological signal processing [254, 189, 257]

and with topological machine-learning tools [267, 268, 269, 270]. Note that this increasing interest in topological signals occurs while the entire field of dynamical processes on simplicial complexes and hypergraphs is bursting with significant research activity [199, 271, 45, 272, 273, 274, 190, 201, 275, 276, 277, 278].

Topological signals of a given dimension can be coupled by higher-order Laplacians, also called Hodge-Laplacians or combinatorial Laplacians [207, 279, 216]. However, the Dirac operator [280, 281, 282, 283] is necessary to couple topological signals of different dimension such as interacting signals defined on nodes and links of a network. For instance, the dynamics of neuronal networks can be modeled by using two different topological signals: one defined on the nodes (the activity of each neuron) and the other defined on the edges (the neurotransmitter current across each synapse). Interestingly, the Dirac synchronization, which stems from the adoption of the Dirac operator to couple topological signals of different dimension, provides a topological and local pathway toward explosive synchronization and rhythmic phases [261, 262].

In this paper, we propose a framework to reveal Turing patterns of reacting species described by topological signals defined on the cells of different dimensions (nodes, links, triangles, squares) coupled through the Dirac operator. Our main goal is to consider reaction-diffusion systems [108] and extend the Turing theory developed so far on networked systems [31] to the framework of simplicial and cell complexes.

Turing's original framework involved two reacting species whose stable homogeneous equilibrium can turn out to be unstable once the species are allowed to diffuse and suitable conditions of the species diffusion coefficients are assumed [4]. Gierer and Meinhardt later emphasized that for the Turing instability to set up, one of the two species needs to be an activator while the other should be an inhibitor, and moreover the latter needs to diffuse much faster than the former [5]. The theory was successively extended to regular lattices by Othmer and Scriven [25] and finally to complex networks by Nakao and Mikhailov [31]. Let us emphasize that network patterns are equilibrium states of the system with a dependence on the node. The latter framework has been further expanded considering directed networks [38], multiplex [34], temporal networks [115], and non-normal networks [70], just to mention a few. In all the above settings, the two species react in each node while diffusing through the links. For signals defined exclusively on the nodes, cross-diffusion terms have been introduced in Refs. [15, 284]. Turing patterns on higher-order structures have been recently studied in Refs. [205, 215]. Note however that our approach is different because in those works the dynamics are restricted to nodes, while links and higher-order structures support the generalized diffusion.

In this paper we provide a general theory describing reaction-diffusion systems of topological signals of different dimension (i.e., defined on nodes, links, triangles, squares, etc.) coupled with the Dirac operator. In particular, we consider two different settings. In the first case, we assume the reaction term to be solely responsible for the coupling of signals of different dimension, and the diffusion term is modeled by the Hodge-Laplacians. In the second case, we assume the diffusion also to include cross-diffusion terms coupling the dynamics of signals in different dimension. For sake of simplicity, in this work, we will focus our analysis on the case of coupled nodes and links signals, which is arguably also the most relevant to applications. Indeed, it is a common scenario to have localized reactions and quantities produced in the nodes,

to flow across links connecting couples of node; in some cases, links themselves are dynamical entities, whose behavior influences the local reactions but can also be in turn influenced by the latter. We derive the conditions under which stable Turing patterns can be observed, and we highlight the differences between the dynamics with and without cross-diffusion terms. The analytical results derived in general are presented with applications to square lattices with periodic boundary conditions and validated by numerical simulations on a benchmark network.

The paper is structured as follows. In Section II we outline a general theoretical framework for investigating Turing patterns of topological signals, and we distinguish the case in which there is only a Dirac reaction term while diffusion is dictated by Hodge-Laplacians and the case in which we introduce also Dirac cross-diffusion terms describing diffusion processes among signals defined on different dimensions. In Secs. III and IV we focus on topological signals defined on nodes and links of the network, and we define the conditions for the onset of the Turing instability when only a Dirac reaction term is considered (Section III) and when additionally Dirac cross-diffusion terms are introduced (SectionIV). The theoretical insights gained in Section III and IV are tested and validated on a benchmark model. Finally, in Section V we provide the concluding remarks. The paper is enriched with a few Appendixes (Supplementary Materials) providing background information on algebraic topology, some details of the derivations discussed in the main body of the work, and simulations results on Turing patterns of topological signals defined on nodes and links of a square lattice with periodic boundary conditions.

7.2 Turing theory for topological signals

We are interested in studying reaction-diffusion systems defined on simplicial and cell complexes (for an introduction to such topological structures and their main properties see SM 7.6). This entails defining appropriate reaction and diffusion terms. In a network, the reaction term is localized on nodes, where the interacting species can be found. When the interacting species are associated with simplices of different dimension, a Dirac reaction term that uses the Dirac operator is required to allow topological signals of different dimension to interact. In a network, concentrations can flow from one node to one of its neighbors, passing through links, namely the structure one dimension above. A similar idea can be applied in simplicial complexes: quantities defined on links can flow among links by using the faces they share, hence again the structures one dimension above. There is, however, a second possibility: they can use structures one dimension below, i.e., nodes, to communicate. Such processes can be described by introducing the Hodge-Laplacian operator, which describes uncoupled diffusion of topological signals of any given dimension. However, Hodge-Laplacians describe diffusion terms that act on topological signals of any given dimension separately. Requiring a diffusive coupling of topological signals of different dimension can only be achieved by considering Dirac cross-diffusion terms which involve odd powers of the Dirac operator. Specifically, this includes cross-diffusion terms that are linear or cubic in the Dirac operator.

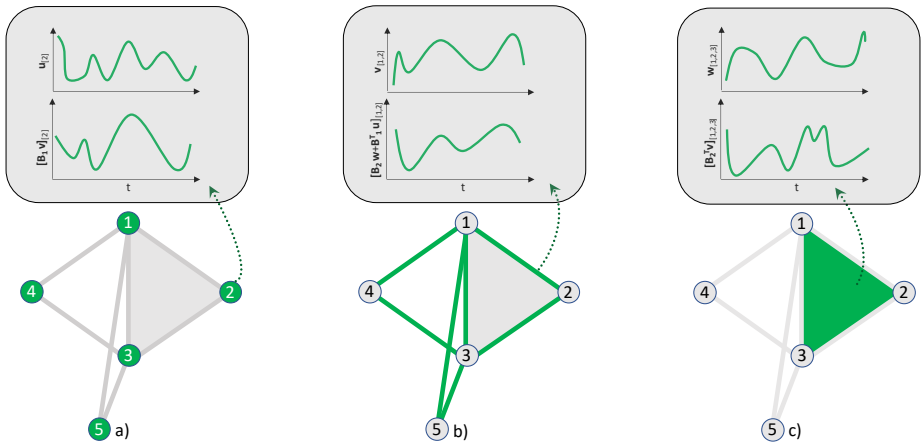

Figure 7.1: We schematically represent the dynamical state of a simplicial complex encoded by the vector $\mathbf{\Phi} = (u, v, w)^\top$ and the vector $\mathbf{\Psi} = \mathscr{D}\mathbf{\Phi} = (\hat{u}, \hat{v}, \hat{w})^\top$. In particular we represent topological signals and projected topological signals supported on 0, 1 and 2-simplices respectively in panels a), b), and c). The Dirac operator $\mathscr{D}$ projects the topological signals of each dimension either one dimension up or one dimension down, and it leads to projected components defined on nodes ($\hat{u} = \mathbf{B}_1 v$, links $\hat{v} = \mathbf{B}_2 w + \mathbf{B}_1^\top v$, and triangles $\hat{w} = \mathbf{B}_2^\top v$). Here $\hat{u} = \mathbf{B}_1 v$ describes the link signals projected on the nodes; $\mathbf{B}_1^\top u$ indicates the irrotational component of $\hat{v}$ and describes the projection of the node signals on the links; $\mathbf{B}_2 w$ indicates the solenoidal component of $\hat{v}$ and describes the projection of the triangle signals on the links; and finally $\mathbf{B}_2^\top v$ describes the projection of the link signals on the triangles.

Here we propose a theory of Turing instability for topological signals and to this end we consider simplicial complexes and cell complexes of dimension d and species living on nodes, links, triangles, etc. In the present terminology, the concentration of the species living on nodes is a 0-topological signal, while the concentration of the species defined on links is a 1-topological signal, etc. The dynamical state of the structures we are considering is described by a vector Φ, which is the direct sum of all topological signals defined on the simplicial or cell complex. For example, in a $(d = 2)$-dimensional cell complex with N_0 nodes, N_1 links, and N_2 2-dimensional cells (such as triangles, squares, pentagons, etc.), we have

$$\Phi = \begin{pmatrix} u \\ v \\ w \end{pmatrix} \tag{7.2.1}$$

where $u \in \mathbb{R}^{N_0}, v \in \mathbb{R}^{N_1}, w \in \mathbb{R}^{N_2}$ are the vectors of concentration of species defined on nodes, links and 2-dimensional cells respectively. These signals can only interact with each other when we consider their projection to simplices of one dimension up or one dimension down. This projection is performed by applying the Dirac operator $\mathscr{D}$ to Φ obtaining new (projected) signals (for the definition of the Dirac operator see SM 7.6), i.e.,

$$\Psi = \mathscr{D}\Phi = \begin{pmatrix} \hat{u} \\ \hat{v} \\ \hat{w} \end{pmatrix} \tag{7.2.2}$$

where $\hat{u} \in \mathbb{R}^{N_0}, \hat{v} \in \mathbb{R}^{N_1}, \hat{w} \in \mathbb{R}^{N_2}$ are defined on nodes, links and 2-dimensional cells respectively. In a general cell complex of dimension $d = 2$, the Dirac operator $\mathscr{D}$ is a $M \times M$ matrix with $M = N_0 + N_1 + N_2$ which can be expressed in terms of the incidence matrices $\mathbf{B}_1, \mathbf{B}_2$ (defined in SM 7.6) and their transpose as

$$\mathscr{D} = \begin{pmatrix} 0 & \mathbf{B}_1 & 0 \\ \mathbf{B}_1^\top & 0 & \mathbf{B}_2 \\ 0 & \mathbf{B}_2^\top & 0 \end{pmatrix} \tag{7.2.3}$$

We therefore obtain that the projected signal Ψ is given by

$$\Psi = \mathscr{D}\Phi = \begin{pmatrix} \hat{u} \\ \hat{v} \\ \hat{w} \end{pmatrix} = \begin{pmatrix} \mathbf{B}_1 v \\ \mathbf{B}_1^\top u + \mathbf{B}_2 w \\ \mathbf{B}_2^\top v \end{pmatrix} \tag{7.2.4}$$

where $\mathbf{B}_1^\top u$ and $\mathbf{B}_2 w$ describe the irrotational part and the solenoidal part of the link signal $\hat{v}$ respectively. Therefore, the dynamical state of the cell complex comprises both the topological signals Φ and their projections $\Psi = \mathscr{D}\Phi$ (see Figure 7.1 for a schematic illustration). Note that the Dirac operator can be seen as the "square root" of the higher-order or Hodge-Laplacian operator $\mathscr{L}$ as

$$\mathscr{L} = \mathscr{D}^2 = \begin{pmatrix} \mathbf{L}_0 & 0 & 0 \\ 0 & \mathbf{L}_1 & 0 \\ 0 & 0 & \mathbf{L}_2 \end{pmatrix} \tag{7.2.5}$$

where $\mathbf{L}_0 = \mathbf{B}_1\mathbf{B}_1^\top, \mathbf{L}_1 = \mathbf{B}_1^\top\mathbf{B}_1 + \mathbf{B}_2\mathbf{B}_2^\top$ and $\mathbf{L}_2 = \mathbf{B}_2^\top\mathbf{B}_2$ are the Hodge-Laplacians acting on topological signals of dimension zero, one, and two respectively, and describing higher-order diffusion (for details see SM 7.6) [260, 265, 266]. In particular, in the case of a simplicial complex we have that $\mathbf{L}_0$ describes diffusion from nodes to nodes through links, $\mathbf{L}_1$ describes diffusion from links to links either through nodes or through triangles and, $\mathbf{L}_2$ describes diffusion from triangles to triangles through links. Here we propose a Turing instability theory for topological signals where the topological signals $\mathbf{\Phi}$ can be coupled to the projected topological signals Ψ either through a Dirac reaction term or through a Dirac diffusion term or both. In the presence of a Dirac reaction term and a Laplacian diffusion term, the reaction-diffusion process of a topological signal is defined as

$$\dot{\Phi} = F(\Phi, \mathscr{D}\Phi) - \gamma\mathscr{L}\Phi \tag{7.2.6}$$

where $F(\Phi, \mathscr{D}\Phi)$ is the Dirac reaction term coupling each topological signal of dimension n with the nearby topological signals of dimension $n+1$ or $n-1$ projected to dimension n. In particular $F(\Phi, \mathscr{D}\Phi)$ here indicates a generic nonlinear function, assumed to be applied component-wise on the vectors. For instance for $d = 2$ we have

$$F(\Phi, \mathscr{D}\Phi) = \begin{pmatrix} f_0(u, \mathbf{B}_1 v) \\ f_1(v, \mathbf{B}_1^\top u + \mathbf{B}_2 w) \\ f_2(w, \mathbf{B}_2^\top v). \end{pmatrix} \tag{7.2.7}$$

where $f_n(x,y)$ are nonlinear functions, such that
$f_1(u, \mathbf{B}_1 v) = (f_1(u_1, (\mathbf{B}_1 v)_1), \ldots, f_1(u_{N_0}, (\mathbf{B}_1 v))_{N_0})$ etc. The matrix γ in Equation (7.2.6)

is a diagonal matrix,

$$\gamma = \begin{pmatrix} D_0 & 0 & 0 \\ 0 & D_1 & 0 \\ 0 & 0 & D_2 \end{pmatrix} \tag{7.2.8}$$

where D_n is the diffusion constant acting on topological signals of order n. Therefore, Equation (7.2.6) describes topological signals defined on the cells of the cell complex that react with the projection of the topological signals defined in different dimension while undergoing higher-order diffusion.

Note that from the dynamical system given by Equation (7.2.6), one can derive the dynamics of the projected signal $\Psi = \mathscr{D}\Phi$ which is given by

$$\dot{\Psi} = \hat{F}(\Phi, \Psi) - \mathscr{D}\gamma\mathscr{D}\Psi \tag{7.2.9}$$

where $\hat{F}(\Phi, \Psi) = \mathscr{D}F(\Phi, \Psi)$. In the case of diffusion constants independent on the order of the simplices, i.e., for $D_k = D$ for all $k = 0, 1, 2$, this equation reduces to

$$\dot{\Psi} = \hat{F}(\Phi, \Psi) - \gamma\mathscr{L}\Psi \tag{7.2.10}$$

Therefore, in this case the dynamics of the projected signal is the same as the dynamics of the signal Φ (Equation (7.2.6)) provided that $F(\Psi, \Phi) = \hat{F}(\Phi, \Psi) = \mathscr{D}F(\Phi, \Psi)$ as for instance in the case of square lattices with periodic boundary conditions.

We now consider Dirac cross-diffusion terms enforcing diffusion of signals across different dimensions. In particular, we consider including a linear or a cubic Dirac cross-diffusion term, which are proportional to a linear or cubic power of the Dirac operator, respectively. Let us observe that this is a natural choice, since as already observed, the second power of the Dirac operator is a diagonal matrix containing Hodge-Laplacians on its diagonal. In the case of a linear Dirac cross-diffusion term, the reaction-diffusion dynamics take the form

$$\dot{\Phi} = F(\Phi, \mathscr{D}\Phi) - \tilde{\gamma}\mathscr{D}\Phi - \gamma\mathscr{L}\Phi \tag{7.2.11}$$

where $\tilde{\gamma}$ is the diagonal matrix of cross-diffusion constants $\tilde{D}_n$,

$$\tilde{\gamma} = \begin{pmatrix} \tilde{D}_0 & 0 & 0 \\ 0 & \tilde{D}_1 & 0 \\ 0 & 0 & \tilde{D}_2 \end{pmatrix} \tag{7.2.12}$$

In this case, the corresponding projected signals $\Psi = \mathscr{D}\Phi$ obey the dynamical system of equations

$$\dot{\Psi} = \hat{F}(\Phi, \Psi) - \mathscr{D}\tilde{\gamma}\Psi - \mathscr{D}\gamma\mathscr{D}\Psi \tag{7.2.13}$$

If the diffusion and cross-diffusion constants are the same and γ and $\tilde{\gamma}$ are proportional to the identity matrix, then we have that both γ and $\tilde{\gamma}$ commute with the Dirac operator $\mathscr{D}$ and the dynamics of projected signals becomes

$$\dot{\Psi} = \hat{F}(\Phi, \Psi) - \tilde{\gamma}\mathscr{D}\Psi - \gamma\mathscr{L}\Psi \tag{7.2.14}$$

Therefore, in this case too, as long as $\hat{F}(\Phi, \psi) = \mathscr{D}F(\Phi, \Psi)$ can be written as the reaction term $F(\Phi, \Psi)$ (as happens for square lattices with periodic boundary conditions, for

example), the equation for the signal is equal to the equation for the projected signals. In the case of a cubic Dirac cross-diffusion term, we have instead that

$$\dot{\Phi} = F(\Phi, \mathscr{D}\Phi) - \gamma\mathscr{L}\Phi - \tilde{\gamma}\mathscr{D}^3\Phi \tag{7.2.15}$$

The corresponding projected dynamics read,

$$\dot{\Psi} = \hat{F}(\Phi, \Psi) - \mathscr{D}\gamma\mathscr{D}\Psi - \mathscr{D}\tilde{\gamma}\mathscr{L}\Psi \tag{7.2.16}$$

which reduces to

$$\dot{\Psi} = \hat{F}(\Phi, \Psi) - \gamma\mathscr{L}\Psi - \tilde{\gamma}\mathscr{D}^3\Psi \tag{7.2.17}$$

when, again, both γ and $\tilde{\gamma}$ are proportional to the identity matrix.

In all the considered cases, the Turing mechanism requires the presence of a stable homogeneous equilibrium once the diffusion part is silenced. Such a state turns out to be unstable for suitable values of the diffusion coefficients and conditions on the underlying topology. Eventually, arbitrarily small initial perturbations around the homogeneous state will grow exponentially and ultimately return a pattern, i.e., a spatially heterogeneous solution.

When dealing with topological signals, a necessary condition is that the homogeneous state vector $h = (1, \dots, 1)^\top$ is in the kernel of the Dirac operator $h \in \ker(\mathscr{D})$ or, equivalently,

$$\mathscr{D}h = 0 \tag{7.2.18}$$

In the conventional node-to-node diffusion case, in which only the node signal is considered, such a condition is always satisfied for a connected network. However, when the state vector includes both nodes and links signals, Equation (7.2.18)then requires

$$\mathbf{B}_1 h = 0 \text{ and } \mathbf{B}_2^\top h = 0 \tag{7.2.19}$$

where $h = (1, 1 \dots, 1)^\top$ is a homogeneous N_1-dimensional column vector defined on the links of the network.

By assuming to have a 1-simplicial complex, (i.e., a network) we discard the presence of 2-dimensional cells (such as triangles, squares, pentagons,etc.). In that case $\mathbf{B}_2 = 0$, and the second of the conditions in Equation (7.2.19) is trivially satisfied. Let us now focus on the remaining condition. Tackling this problem becomes much easier by noticing that the i-th row of the boundary operator is equal to minus the divergence of node i. Such equivalence, proven in [216], can be exploited to construct a simplicial complex with the wanted property.

By requiring that every node has an equal amount of in-coming and out-going links, we thus ensure that a homogeneous signal, namely an edge-flow directed as indicated by the links orientation[(1)], has zero divergence. To sum up, the following analysis grounded on the conditions given in Equation (7.2.19), holds for every network (1-dimensional cell complex) whose nodes have an even number of connected edges. Notable examples of these networks are square lattices with periodic boundary conditions.

[(1)]Let us stress that we are dealing with undirected network and thus the incoming / outgoing edges are defined with respect to the ordering of the simplicial or cell complex.

Note that the analogous condition applying to 2-dimensional cell complexes is much more demanding. In particular no 2-dimensional simplicial complex admits a homogeneous eigenvector in the kernel of the Dirac operator. However it was recently shown [258] that 2-dimensional cell complexes built from square lattices with periodic boundary conditions obey this property. More generally it is possible to show that d-dimensional cell complexes built from d-dimensional square lattices obey this property for any dimension d.

7.3 Interacting topological signals of nodes and links with Dirac reaction term

7.3.1 Conditions for the onset of the Turing instability

In this section we focus on reaction-diffusion systems involving topological signals defined on the nodes and on the links of a network. Our goal is to derive the dispersion relation, roughly speaking the largest Lyapunov exponent of the homogeneous state considered as a function of the model parameters and of the topological structure. This allows us to determine the conditions for the Turing instability onset in the presence exclusively of a Dirac reaction term that couples the two topological signals of different dimension, while the diffusion part is modeled with the relevant Hodge-Laplacians , i.e., driven by Equation(7.2.6) which we rewrite here for convenience

$$\dot{\Phi} = F(\Phi, \mathscr{D}\Phi) - \gamma \mathscr{L} \Phi \tag{7.3.1}$$

In a network we have $\Phi = (u,v)^\top$ and $F(\Phi, \mathscr{D}\Phi) = \left(f(u, \mathbf{B}_1 v), g(v, \mathbf{B}_1^\top u)\right)^\top$ where f and g are two generic nonlinear functions, assumed to be applied component-wise on the vectors, i.e., $f(u, \mathbf{B}_1 v) = (f(u_1, (\mathbf{B}_1 v)_1), \ldots, f(u_{N_0}, (\mathbf{B}_1 v))_{N_0})$. Here γ reduces to the $(N_0 + N_1) \times (N_0 + N_1)$ block diagonal matrix with structure

$$\gamma = \begin{pmatrix} D_0 \mathbf{I}_{N_0} & 0 \\ 0 & D_1 \mathbf{I}_{N_1} \end{pmatrix} \tag{7.3.2}$$

where D_0 and D_1 indicate the diffusion constants of the species defined on nodes and links respectively and $\mathbf{I}_{N_a}$ indicates the $N_a \times N_a$ identity matrix, $a = 0, 1$. The Dirac operator $\mathscr{D}$ and the Hodge-Laplacian operator $\mathscr{L}$ are defined as the $(N_0 + N_1) \times (N_0 + N_1)$ matrices with block structure

$$\mathscr{D} = \begin{pmatrix} 0 & \mathbf{B}_1 \\ \mathbf{B}_1^\top & 0 \end{pmatrix}, \quad \mathscr{L} = \mathscr{D}^2 = \begin{pmatrix} \mathbf{L}_0 & 0 \\ 0 & \mathbf{L}_1 \end{pmatrix} \tag{7.3.3}$$

If follows that the dynamics driven by Equation (7.3.1) can be rewritten explicitly as

$$\begin{aligned} \dot{u} &= f(u, \mathbf{B}_1 v) - D_0 \mathbf{L}_0 u \\ \dot{v} &= g\left(v, \mathbf{B}_1^\top u\right) - D_1 \mathbf{L}_1 v \end{aligned} \tag{7.3.4}$$

where $D_0 > 0$ (resp. $D_1 > 0$) is the diffusive coefficient of species u (resp. v). For instance, resuming the biological example from the introduction where neurotransmitters concentration and neuronal activity are schematized by topological signals, we can

think of v as the synaptic signal, and of u as a neuron signal. In this setting the Dirac operator is capable of properly connecting the lower and higher dimensional signals, by acting as an effective and simple dynamical operator. In the spirit of Turing theory, let us silence the diffusive terms and look for a homogeneous solutions, i.e., the existence of $u^* = u_0 h$ and $v^* = v_0 h$, for some constants u_0 and v_0. Because of the assumption on the underlying simplex, we have $\mathbf{B}_1 v^* = 0$ and $\mathbf{B}_1^\top u^* = 0$. The existence of a homogeneous fixed point reverberates on the structure of f, g such that

$$0 = f(u^*, 0) \text{ and } 0 = g(v^*, 0) \tag{7.3.5}$$

which in turn yields that u_0 and v_0 are solutions of $f(u_0, 0) = g(v_0, 0) = 0$.

To study the stability feature of the homogeneous equilibrium, we consider a homogeneous perturbation about the latter, $\delta u = u - u^*$ and $\delta v = v - v^*$. Hence by linearizing (7.3.4), we obtain

$$\begin{aligned} \delta \dot{u} &= \partial_u f(u^*, 0) \delta u \\ \delta \dot{u} &= \partial_v g(v^*, 0) \delta v \end{aligned} \tag{7.3.6}$$

where we used again the conditions $h = (1, \dots, 1)^\top \in \ker \mathbf{B}_1$ and $h \in \ker \mathbf{B}_1^\top$ to remove some terms in the previous equation. The condition for the stability is thus

$$\partial_u f(u^*, 0) < 0 \text{ and } \partial_v g(v^*, 0) < 0 \tag{7.3.7}$$

Let us observe that Equation (7.3.7) implies that both species are self inhibitors, this is the result of the peculiar form of Equation (7.3.4), and of the assumption $\mathbf{B}_1 v^* = 0$ and $\mathbf{B}_1^\top u^* = 0$ which ultimately decouples the dynamics of the two species in the linear regime. This is at odd with the classical Turing instability where patterns can never emerge in the inhibitor-inhibitor setting, unless some additional assumptions are made [49].

We now focus on the stability of such equilibrium once subjected to heterogeneous perturbations, hence not in the kernels of $\mathbf{L}_0$ and $\mathbf{L}_1$. Let us linearize Equation (7.3.4) about the equilibrium solution, by obtaining

$$\begin{aligned} \delta \dot{u} &= (\partial_u f)\, \delta u + (\partial_{\mathbf{B}_1 v} f)\, \mathbf{B}_1 \delta v - D_0\, \mathbf{L}_0\, \delta u \\ \delta \dot{v} &= (\partial_{\mathbf{B}_1^\top u} g) \mathbf{B}_1^\top \delta u + (\partial_v g) \delta v - D_1\, \mathbf{L}_1\, \delta v \end{aligned} \tag{7.3.8}$$

where $\partial_{\mathbf{B}_1 v} f$ and $\partial_{\mathbf{B}_1 v} f$ denote the scalars indicating the derivative of f, g with respect to their second argument, (i.e., the projected higher and lower dimensional signal respectively) calculated at the homogeneous stationary solution.

We now note that the network Laplacians $\mathbf{L}_0 = \mathbf{B}_1 \mathbf{B}_1^\top$ and $\mathbf{L}_1 = \mathbf{B}_1^\top \mathbf{B}_1$ are isospectral, i.e., they have the same non-zero spectrum. The $\hat{N}$ non-zero eigenvalues Λ_0^k with $1 \le k \le \hat{N}$ of $\mathbf{L}_0$ and $\mathbf{L}_1$ can be expressed as the square of the singular values b_k of $\mathbf{B}_1$, i.e., $\Lambda_0^k = b_k^2$. The eigenvectors ψ_0^m and ψ_1^m of $\mathbf{L}_0$ and $\mathbf{L}_1$ can be adopted as a basis to perform the singular value decomposition of $\mathbf{B}_1$. On a connected network these eigenvectors include the eigenvectors ψ_0^k and ψ_1^k corresponding to the non-zero eigenvalue $\Lambda_0^k = \Lambda_1^k = b_k^2$, the eigenvector $\phi_0^h = (1, \dots, 1)^\top$ of $\mathbf{L}_0$ associated to the zero eigenvalue $\Lambda_0 = 0$ and the eigenvectors ψ_1^l associated with the zero eigenvalues $\Lambda_1^l = 0$ of $\mathbf{L}_1$. Interestingly the eigenvectors ψ_0^k and ψ_1^k associated to the eigenvalue $\Lambda_0^k = \Lambda_1^k = b_k^2 > 0$

obey

$$\mathbf{B}_1 \psi_1^k = b_k \psi_0^k \quad \mathbf{B}_1^\top \psi_0^k = b_k \psi_1^k \tag{7.3.9}$$

Using these results, the signals δu and δv, as well as the projected signals $\delta \hat{u} = \mathbf{B}_1 \delta v$ and $\delta \hat{v} = \mathbf{B}_1^\top \delta u$, can be projected onto the basis of the eigenvectors ψ_n^m of $\mathbf{L}_n$ (with $n = 0, 1$ for the analyzed case) corresponding to the non-zero eigenvalues $\Lambda_0^k = b_k^2$. We obtain

$$\langle \psi_0^k, \delta u \rangle = \delta \hat{u}_k \qquad \langle \psi_1^k, \delta v \rangle = \delta \hat{v}_k \tag{7.3.10}$$

$$\langle \psi_0^k, \mathbf{B}_1 \delta v \rangle = b_k \delta \hat{v}_k \qquad \langle \psi_1^k, \mathbf{B}_1^\top \delta u \rangle = b_k \delta \hat{u}_k \tag{7.3.11}$$

where $\langle \cdot, \cdot \rangle$ denotes the scalar product. By using Equation (7.3.10) and Equation (7.3.11), we can project in Equation (7.3.8) the equations for δu onto ${\psi_0^k}^\top$ and the ones for δv on ${\psi_1^k}^\top$, with k such that $\Lambda_0^k = \Lambda_1^k = b_k^2 \neq 0$, to eventually obtain:

$$\begin{aligned} \frac{d\delta \hat{u}_k}{dt} &= (\partial_u f)\, \delta \hat{u}_k + (\partial_{\mathbf{B}_1 v} f)\, b_k \delta \hat{v}_k - D_0 b_k^2 \delta \hat{u}_k \\ \frac{d\delta \hat{v}_k}{dt} &= (\partial_v g)\, \delta \hat{v}_k + \left(\partial_{\mathbf{B}_1^\top u} g\right) b_k \delta \hat{u}_k - D_1 b_k^2 \delta \hat{v}_k \end{aligned} \tag{7.3.12}$$

It is interesting to notice that the leftover modes are those associated to the eigenvectors spanning the kernel space of both $\mathbf{L}_0$ and $\mathbf{L}_1$. Since in the relevant case of a connected network, the eigenvector associated to the zero eigenvalue is the homogeneous one, i.e it is aligned to the stationary state u^* of the nodes, it follows that δu will never have a component along this eigenvector. However, we need to consider the projection of δv onto the eigenvectors ψ_1^l associated with the zero eigenvalues of $\mathbf{L}_1$, by obtaining

$$\frac{d\delta \hat{v}_l}{dt} = (\partial_v g)\, \delta \hat{v}_l \tag{7.3.13}$$

Hence these modes are always stable due to the second condition in Equation (7.3.7).

The instability is realized if the linear system (7.3.12) admits at least one unstable mode; more precisely we have to compute the eigenvalues of the matrix

$$\mathbf{J}_k = \begin{pmatrix} \partial_u f - D_0 b_k^2 & b_k \partial_{\mathbf{B}_1 v} f \\ b_k \partial_{\mathbf{B}_1^\top u} g & \partial_v g - D_1 b_k^2 \end{pmatrix} \tag{7.3.14}$$

and determine if there is k for which the associated eigenvalue, $\lambda(b_k)$, has a positive real part. Let us notice that the latter is usually named dispersion relation in the literature. The eigenvalues of $\mathbf{J}_k$ can be obtained by solving

$$\lambda^2 + \lambda \Gamma_1\left(b_k^2\right) + \Gamma_2\left(b_k^2\right) = 0 \tag{7.3.15}$$

where $\Gamma_1\left(b_k^2\right)$ and $\Gamma_2\left(b_k^2\right)$ are given by

$$\Gamma_1\left(b_k^2\right) = b_k^2(D_1 + D_0) - (\partial_v g + \partial_u f) \tag{7.3.16}$$

$$\Gamma_2\left(b_k^2\right) = a_2 b_k^4 + a_1 b_k^2 + a_0 \tag{7.3.17}$$

with

$$\begin{aligned} a_2 &= D_0 D_1 \\ a_1 &= -\left(D_1 \partial_u f + D_0 \partial_v g + \partial_{\mathbf{B}_1^\top u} g \; \partial_{\mathbf{B}_1 v} f\right) \\ a_0 &= \partial_u f \; \partial_v g \end{aligned} \tag{7.3.18}$$

Since both the leading coefficient of Equation (7.3.15) and $\Gamma_1(b_k^2)$ are positive, the existence of a solution with a positive real part requires that $\Gamma_2(b_k^2) < 0$ for some k. Let us observe that $\Gamma_2(b_k^2)$ given by Equation (7.3.17) is a parabola in b_k^2 with positive concavity, $a_2 = D_0 D_1 > 0$, and positive constant term, $a_0 = \partial_u f \; \partial_v g > 0$. Therefore, to satisfy the condition $\Gamma_2(b_k) < 0$ with a real b_k, a necessary condition is

$$D_0 \partial_v g + D_1 \partial_u f + \partial_{\mathbf{B}_1^\top u} g \; \partial_{\mathbf{B}_1 v} f > 0 \tag{7.3.19}$$

By using these conditions we can guarantee that $\Gamma_2(b_k^2) < 0$ if the minimum of the parabola is negative. A straightforward computation returns the condition

$$\left(D_0 \partial_v g + D_1 \partial_u f + \partial_{\mathbf{B}_1^\top u} g \partial_{\mathbf{B}_1 v} f\right)^2 > 4 D_0 D_1 \partial_u f \partial_v g \tag{7.3.20}$$

Let us observe that differently from the classical Turing framework, such condition depends on the diffusive coefficients separately and not on their ratio.

In conclusion, we have hence found the conditions for the onset of Turing instability for topological signals whose dynamics are described by Equation (7.3.4), namely the stability of the homogeneous solution given by Equation (7.3.7) and the existence of at least one unstable mode according to Equations (7.3.19) and (7.3.20). Moreover the roots of Equation (7.3.15) are given by $\lambda_{1,2} = -\Gamma_1 \pm \sqrt{\Gamma_1^2 - 4\Gamma_2}$, but $\Gamma_1 > 0$ and $\Gamma_2 < 0$, and thus $\lambda_{1,2}$ are real numbers. Consequently, the corresponding patterns are stationary.

Let us now note that as expected, when the topological signals on nodes and links are not coupled by the Dirac reaction term, i.e., when

$$F(\Phi, \mathscr{D}\Phi) = F(\Phi) = \begin{pmatrix} f(u) \\ g(v) \end{pmatrix} \tag{7.3.21}$$

we can never have Turing patterns. In fact in this case we would have $\partial_{\mathbf{B}_1^\top u} g = 0, \partial_{\mathbf{B}_1 v} f = 0$ and Equation (7.3.19) cannot be satisfied together with Equation (7.3.7). A major result of this study is that the Turing instability of the topological signals of a network will never be localized only on nodes or only on links but will always involve both nodes and links signals. Moreover, we also obtain that if the original signals $\Phi = (u, v)^\top$ display a Turing pattern, the projected dynamics of $\mathscr{D}\Phi = (\mathbf{B}_1 v, \mathbf{B}_1^\top u)^\top$ also do.

7.3.2 Numerical results on a benchmark network

The aim of this section is to validate the above results with a numerical study. To focus on the novelty of the framework and to remove unnecessary complicated features, we will build a toy model with cubic nonlinearities to test our theory (see SM 7.7

for additional results on topological Turing patterns on the square lattice with periodic boundary conditions). By keeping the same notation as before, i.e., u is the signal on the nodes and v that on the links, the equations of our model read

$$\begin{aligned} \dot{u} &= -au - bu^3 + c\mathbf{B}_1 v - D_0 \mathbf{L}_0 u \\ \dot{v} &= -\alpha v - \beta v^3 + \gamma \mathbf{B}_1^\top u - D_1 \mathbf{L}_1 v \end{aligned} \tag{7.3.22}$$

where $a, b, c, \alpha, \beta, \gamma$ are non-negative real parameters.

System (7.3.22) admits $(u_0, v_0) = (0,0)$ as equilibrium point. By computing the Jacobian of the system evaluated at this point, we get

$$\mathbf{J}_0 = \begin{pmatrix} \partial_u f & \partial_{\mathbf{B}_1 v} f \\ \partial_{\mathbf{B}_1^\top u} g & \partial_v g \end{pmatrix} = \begin{pmatrix} -a & c \\ \gamma & -\alpha \end{pmatrix}$$

The system exhibits a Turing instability if the above parameters satisfy the conditions (7.3.7), (7.3.19) and (7.3.20), that we now rewrite

$$a > 0 \quad \alpha > 0, \quad c\gamma > \alpha D_0 + a D_1 \tag{7.3.23}$$

$$(c\gamma - \alpha D_0 - a D_1)^2 > 4 D_0 D_1 a \alpha \tag{7.3.24}$$

and the simplicial complex is such that $h \in \ker \mathbf{L}_1$.

A simple example of a 1-dimensional simplicial complex satisfying the latter condition is provided by a network of 12 nodes and 16 links, whose nodes degrees are even and with closed loops. Note that the latter is chosen to be a subset of a square lattice. In Figure 7.2 we report the result of numerical simulation clearly showing the emergence of Turing patterns, namely stationary equilibria where the concentrations vary across nodes and links. Moreover, the system state is far from the homogeneous solution $(u_0, v_0) = (0,0)$. In Figure 7.2.*a* the nodes and links are colored according to the asymptotic concentration of respectively u and v and we can thus have a geometrical view of the emerging pattern. On the other hand a dynamical view is presented in Figure 7.2.$b-c$ where we report the nodes concentration, $u_i(t)$, and links concentration, $v_i(t)$, as a function of time, and we can observe the deviation from the homogeneous solution and the stationary asymptotic behavior of the solution. From this figure one can clearly appreciate the onset of the instability at short time because of the Turing condition, namely the positive dispersion relation (see Figure 7.3), pushing the initial conditions far from the equilibrium state $(u_0, v_0) = (0,0)$. Interestingly we observe that the projected dynamics also display a Turing pattern (see Figure7.2.d and Figure7.2.e).

To have a global view, we report in Figure 7.3 the Turing region in the plane (c, γ), i.e., the pairs for which the Turing instability is realized. In the main panel (B) we show the maximum of the real part of the dispersion relation as a function of c and γ by using a color code, white corresponding to the impossibility of Turing instability while red to yellow are associated with the onset of the instability. The left panels, (A1), (A2) and (A3), correspond to a choice for which Turing patterns cannot emerge as confirmed by the negativity of the dispersion relation (A1) and the vanishing of the node and link amplitude (A2 and A3). The latter is defined by $A_{\text{node}}(t) = \sqrt{\sum_{i=1}^{N_0} (u_i(t) - u_0)^2}$ for the nodes and $A_{\text{link}}(t) = \sqrt{\sum_{j=1}^{N_1} (v_j(t) - v_0)^2}$ for the links, where u_0 (resp. v_0) is the

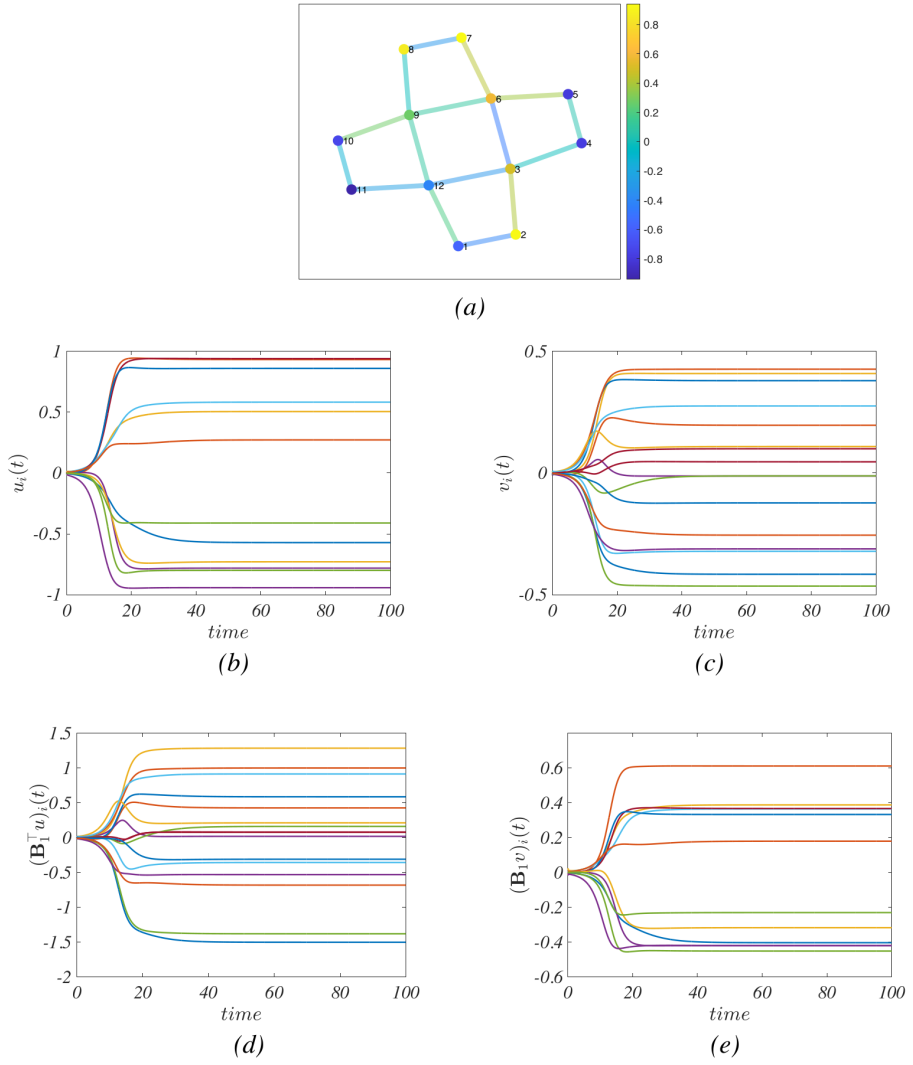

Figure 7.2: *a*) Turing patterns for species defined on nodes and on links described by model (7.3.22) on a network satisfying the conditions for the existence of a homogeneous equilibrium. In panels *b*) and *c*) we depict time series of the two species u and v on the nodes and the links, respectively, while panels *d*) and *e*) show the time series of the projection of the two species with the action of the boundary operator $\mathbf{B}_1$. The parameters are $a = \alpha = b = \beta = \gamma = D_0 = D_1 = 1$ and $c = 6$. The perturbation defining the initial condition, is $\sim 10^{-2}$.

nodes (resp. links), homogeneous equilibrium value. The right panels are associated with parameters inside the Turing region, and indeed the dispersion relation assumes positive values (C1) and the node and link amplitude are strictly positive (C2 and C3). Let us observe that the amplitude can be thus considered as an order parameter capable

of distinguishing between the presence or the absence of patterns.

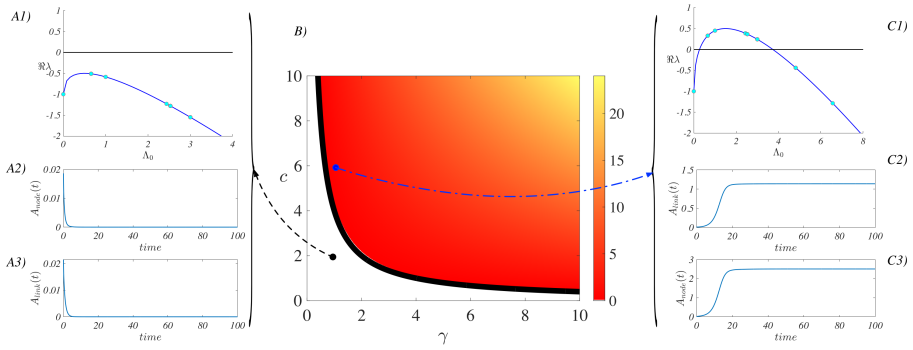

Figure 7.3: Turing region in the parameters space (c,γ). In the main panel (B), we report the region of parameters for which the Turing instability emerges; having fixed $a=\alpha=b=\beta=D_0=D_1=1$ we show the maximum of the real part of dispersion relation as a function of c and γ, by using a color code (yellow corresponding to large values, red to small but positive ones and white to negative ones). The black solid curves is given by $c\gamma=\sqrt{4D_0D_1a\alpha}+\alpha D_0+aD_1$ (see Equation (7.3.24)). Panels A1), A2) and A3) correspond to the choice $(c,\gamma)=(2,2)$ that lies outside the Turing region; one can observe that the dispersion relation (panel A1) is negative and indeed patterns cannot develop as shown by the node (resp. link) amplitude (panel A2) resp. A3) decaying to 0. Panels C1, C2 and C3) show similar results but for $(c,\gamma)=(6,2)$ inside the Turing region; the dispersion relation (C1) reaches positive values and the node (resp. link) amplitude stabilizes far from zero (see panels C2 and C3).

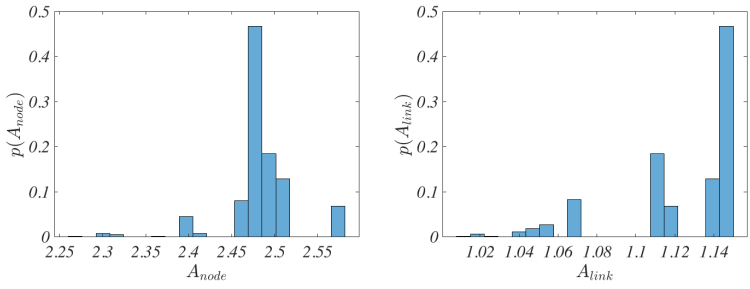

Figure 7.4: We report the distribution of the node (a) and link (b) amplitude of the Turing patterns obtained by numerically simulating 5000 times system (7.3.22) with the parameters used in Figure 7.2 and by changing the initial conditions.

Having fixed the topology of the support and the model parameters, nodes and links amplitudes depend on the initial conditions and the peculiar dynamical path followed by the system to settle into the pattern. In Figure 7.4 we report the distribution of A_{node} and A_{link} once we repeat several times the numerical simulations by changing the initial conditions. We can observe that both distributions are peaked at some value and the dispersion is relatively small, however let us stress that the link amplitude distribution is very skewed.

7.4 Interacting topological signals of nodes and links with Dirac cross-diffusion term

We now consider the dynamics including the Dirac cross-diffusion terms. In particular we first cover the linear cross-diffusion case and leave the analysis of the cubic cross-diffusion term to a next section.

7.4.1 Cross-diffusion term linear in the Dirac operator

Topological signals on nodes and links can be coupled by a linear cross-diffusion term, leading to the reaction-diffusion dynamics

$$\dot{\Phi} = F(\Phi, \mathscr{D}\Phi) - \tilde{\gamma}\mathscr{D}\Phi - \gamma\mathscr{L}\Phi \tag{7.4.1}$$

where the dynamical state of the network is captured by the vector $\Phi = (u,v)^\top$. The diagonal $(N_0+N_1)\times(N_0+N_1)$ matrix $\tilde{\gamma}$ of cross-diffusion constants is here chosen to have block structure

$$\tilde{\gamma} = \begin{pmatrix} D_{01}\mathbf{I}_{N_0} & 0 \\ 0 & D_{10}\mathbf{I}_{N_1} \end{pmatrix} \tag{7.4.2}$$

In particular the coupled dynamics of the topological signals u and v can be re-written as

$$\begin{aligned} \dot{u} &= f(u, \mathbf{B}_1 v) - D_{01}\mathbf{B}_1 v - D_0 \mathbf{L}_0 u \\ \dot{v} &= g\left(v, \mathbf{B}_1^\top u\right) - D_{10}\mathbf{B}_1^\top u - D_1 \mathbf{L}_1 v \end{aligned} \tag{7.4.3}$$

In SM 7.8 we prove that system (7.4.1) can be mapped onto (7.3.1) and thus results from the previous section can be used to derive the conditions under which the reaction-diffusion dynamics with the linear cross-diffusion term display Turing patterns. These conditions are the stability of the homogeneous solution (7.3.7) and the existence of at least one unstable mode that is guaranteed by the following two conditions to hold true:

$$\begin{aligned} A &= D_0\partial_v g + D_1\partial_u f + (\partial_{\mathbf{B}_1^\top u} g - D_{01})(\partial_{\mathbf{B}_1 v} f - D_{10}) > 0 \\ A^2 &> 4D_0 D_1 \partial_u f \partial_v g \end{aligned} \tag{7.4.4}$$

Let us stress a major consequence of these conditions, i.e., the cross-diffusion term is the driver for the instability. Indeed the cross-diffusion term enforced through the Dirac operator allows the onset of Turing patterns also in situations where patterns can never emerge if we silence cross-diffusion. In particular, we can observe Turing patterns in the presence of Dirac-type crossed-diffusion patterns, also when the reaction term only depends on Φ but not on $\mathscr{D}\Phi$, i.e.,

$$F(\Phi, \mathscr{D}\Phi) = F(\Phi) = \begin{pmatrix} f(u) \\ g(v) \end{pmatrix} \tag{7.4.5}$$

as long as Equation (7.3.7) and Equations (7.4.4) hold which can occur as long as $D_{01}D_{10} > 0$. Let us recall that, as discussed in the previous section, under the latter assumption (7.4.5), Turing patterns cannot develop in absence of linear cross-diffusion

terms. Indeed if $D_{01} = D_{10} = 0$, the variables u_i and v_i in system (7.4.3) become decoupled and thus, because of condition (7.3.7) and the non-positivity of the spectra of $\mathbf{L}_0$ and $\mathbf{L}_1$, the homogeneous equilibrium is stable also with respect to heterogeneous perturbations.

Let us conclude this section by observing that Turing instability can also emerge for systems where the coupling is realized solely with the Dirac operator, i.e., there is no need to include the two Hodge-Laplacian matrices, $\mathbf{L}_0$ and $\mathbf{L}_1$ in Equation (7.4.3). This claim can be proven by simply setting $D_0 = D_1 = 0$ into Equation (7.4.4) and requiring thus

$$(\partial_{\mathbf{B}_1^\top u} g - D_{01})(\partial_{\mathbf{B}_1 v} f - D_{10}) > 0$$

the second relation in (7.4.4) being automatically satisfied.

7.4.2 Cross-diffusion term cubic in the Dirac operator

Cross-diffusion terms for topological signals can be also implemented with a cubic Dirac operator in the reaction-diffusion dynamics

$$\dot{\Phi} = F(\Phi, \mathscr{D}\Phi) - \mathscr{L}(\gamma\Phi + \tilde{\gamma}\mathscr{D}\Phi) \tag{7.4.6}$$

which can also be written in terms of the signals u of the nodes and the signals v of the links as

$$\begin{aligned} \dot{u} &= \tilde{f}(u, \mathbf{B}_1 v) - \mathbf{L}_0(D_0 u + D_{01}\mathbf{B}_1 v) \\ \dot{v} &= \tilde{g}\left(v, \mathbf{B}_1^\top u\right) - \mathbf{L}_1(D_1 v + D_{10}\mathbf{B}_1^\top u) \end{aligned} \tag{7.4.7}$$

Starting from the existence of a homogeneous equilibrium (u^*, v^*) that we assume to be stable with respect to homogeneous perturbations, we can determine the conditions for the onset of Turing instability. We thus consider perturbations about such equilibrium, $\delta u = u - u^*$, $\delta v = v - v^*$, whose evolution is given by the linearized system

$$\begin{aligned} \delta\dot{u} &= (\partial_u f)\,\delta u + (\partial_{\mathbf{B}_1 v} f)\,\mathbf{B}_1\delta v - \mathbf{L}_0(D_0\delta u + D_{01}\mathbf{B}_1\delta v) \\ \delta\dot{v} &= (\partial_{\mathbf{B}_1^\top u} g)\mathbf{B}_1^\top\delta u + (\partial_v g)\delta v - \mathbf{L}_1(D_1\delta v + D_{10}\mathbf{B}_1^\top\delta u) \end{aligned} \tag{7.4.8}$$

Considering the stability of perturbations within the kernel of the Laplacians leads to the stability conditions given by Equation (7.3.7), because of the assumption $\mathbf{B}_1 h = \mathbf{B}_1^\top h = 0$ where $h = (1, ..., 1)^\top$.

On the other hand, by considering a generic perturbation and projecting it on the Laplacian eigenbasis, we obtain a new Jacobian matrix, $\mathscr{J}_k$

$$\mathscr{J}_k = \begin{pmatrix} \partial_u f - D_0 b_k^2 & b_k\partial_{\mathbf{B}_1 v} f - D_{01} b_k^3 \\ b_k\partial_{\mathbf{B}_1^\top u} g - D_{10} b_k^3 & \partial_v g - D_1 b_k^2 \end{pmatrix} \tag{7.4.9}$$

whose spectrum determines the stability of the heterogeneous perturbation and thus the possible onset of the instability.

The eigenvalues of $\mathscr{J}_k$ are determined by solving

$$\det\begin{pmatrix} \partial_u f - D_0 b_k^2 - \lambda & b_k\partial_{\mathbf{B}_1 v} f - D_{01} b_k^3 \\ b_k\partial_{\mathbf{B}_1^\top u} g - D_{10} b_k^3 & \partial_v g - D_1 b_k^2 - \lambda \end{pmatrix} = 0 \tag{7.4.10}$$

which can be rewritten as

$$\lambda^2 + \lambda\tilde{\Gamma}_1\left(b_k^2\right) + \tilde{\Gamma}_2\left(b_k^2\right) = 0 \tag{7.4.11}$$

where $\tilde{\Gamma}_1(b_k^2) = \Gamma_1(b_k^2)$ is given by Equation (7.3.16) and is then always positive if the homogeneous equilibrium is stable. In this scenario $\tilde{\Gamma}_2(b_k^2)$ is a cubic polynomial in b_k^2, given by

$$\tilde{\Gamma}_2(b_k^2) = \tilde{a}_3 b_k^6 + \tilde{a}_2 b_k^4 + \tilde{a}_1 b_k^2 + \tilde{a}_0 \tag{7.4.12}$$

with

$$\begin{aligned} \tilde{a}_3 &= -D_{01}D_{10}, & (7.4.13)\\ \tilde{a}_2 &= (D_0D_1 + D_{01}\partial_{\mathbf{B}_1^\top u}g + D_{10}\partial_{\mathbf{B}_1 v}f) & (7.4.14) \end{aligned}$$

and $\tilde{a}_1 = a_1, \tilde{a}_0 = a_0$. As for the case without cross-diffusion, also in this setting, only stationary Turing patterns can be observed.

We consider exclusively the situation in which we have $D_{01}D_{10} < 0$ which enforces the stability of modes corresponding to large values of Λ_0. In this case, the conditions to observe stationary Turing patterns are, in addition to (7.3.7), that one of the two following inequalities needs to be satisfied

$$\begin{aligned} \tilde{a}_2 &= D_0D_1 + D_{01}\partial_{\mathbf{B}_1^\top u}g + D_{10}\partial_{\mathbf{B}_1 v}f < 0\\ \tilde{a}_1 &= -\left(D_1\partial_u f + D_0\partial_v g + \partial_{\mathbf{B}_1^\top u}g\ \partial_{\mathbf{B}_1 v}f\right) < 0 \end{aligned} \tag{7.4.15}$$

together with

$$2D_0D_1K_+ + D_0^2D_1^2 + K_-^2 > 0 \tag{7.4.16}$$

where $K_\pm$ is given by

$$K_\pm = D_{01}\partial_{\mathbf{B}_1^\top u}g \pm D_{10}\partial_{\mathbf{B}_1 v}f \tag{7.4.17}$$

(see SM 7.9 for the derivation of these results).

Interestingly, from this study it emerges that for a cubic Dirac cross-diffusion term, as long as $D_{01}D_{10} < 0$ we cannot observe the onset of the Turing instability for a reaction term of the type $F(\Phi, \mathscr{D}\Phi) = F(\Phi)$. Indeed in this case we have $\partial_{\mathbf{B}_1^\top u}g = 0$ and $\partial_{\mathbf{B}_1 v}f = 0$ and hence neither one of the conditions (7.4.15) can be satisfied when the stability condition (7.3.7) holds.

7.4.3 Numerical results with a cubic Dirac cross-diffusion term

Let us now numerically validate the above analysis of the reaction-diffusion system with cubic Dirac cross-diffusion terms. By considering the benchmark model (7.3.22) with the addition of cubic Dirac cross-diffusion terms, we obtain

$$\begin{aligned} \dot{u} &= -au - bu^3 + c\mathbf{B}_1 v - \mathbf{L}_0(D_0 u + D_{01}\mathbf{B}_1 v)\\ \dot{v} &= -\alpha v - \beta v^3 + \gamma\mathbf{B}_1^\top u - \mathbf{L}_1(D_1 v + D_{10}\mathbf{B}_1^\top u) \end{aligned} \tag{7.4.18}$$

Let us assume conditions (7.3.7), (7.4.15) and (7.4.16) to hold true, and, to be concrete, let us consider the case $D_{01} < 0$ and $D_{10} > 0$. Assuming once again to work with

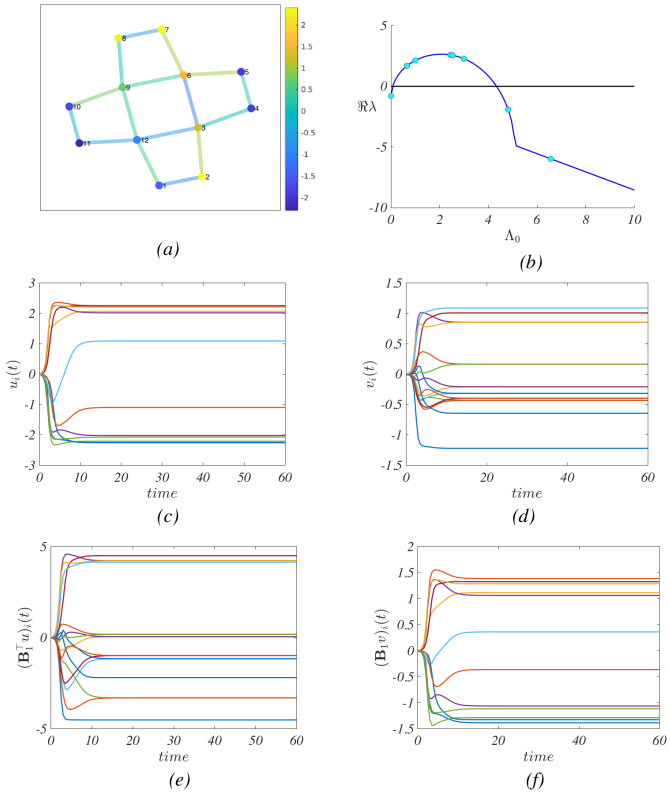

Figure 7.5: *a*) Turing patterns for the species on the nodes and on the links described by model (7.4.18) on a network satisfying the conditions for the homogeneous equilibrium; *b*) dispersion relation: in blue we depict the continuous curve, computed by replacing the discrete parameter b_k^2 with a continuous variable, while the cyan dots are the actual dispersion relation, where now the onset of the Turing instability is a function of the (real) spectrum of $\mathbf{L}_0$, i.e., computed by using the discrete values of b_k^2. In panels *c*) and *d*) we depict time series of the two species u and v on the nodes and the links, respectively, while panels *e*) and *f*) show the time series of the projection of the two species with the action of the boundary operator B_1. The parameters are $a = 0.8$, $\alpha = 1.3$, $b = 1$, $\beta = 0.5$, $c = 8$, $\gamma = 2$, $D_0 = 0.5$, $D_1 = 1$, $D_{01} = -1.5$ and $D_{10} = 0.4$; the initial perturbation is $\sim 10^{-2}$.

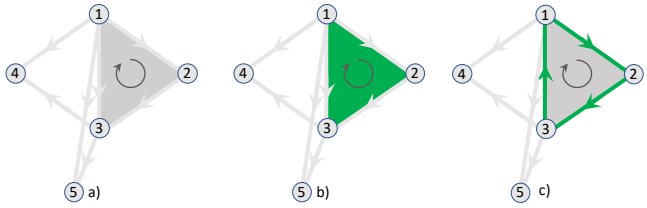

Figure 7.6: Panel a) shows a simplicial complex of dimension 2, with simplicial orientation induced by a labeling of the nodes. The boundary of the 2-simplex $[1,2,3]$ highlighted in panel Panel b) is shown in panel c)

the simplicial complex used in the previous section, then Turing patterns can emerge as shown in Figure 7.5.*a*, where nodes and links, colored according to the asymptotic values of u_i and v_i, clearly show a dependence of the solution on the latter ones. In Figure 7.5.$c-e$ we report the temporal evolution of $u_i(t)$, $v_i(t)$ and one can clearly appreciate how far from the homogeneous state they are; a similar result can be observed for their projections $\mathbf{B}_1^\top u$ and $\mathbf{B}_1 v$. Finally, the dispersion relation is presented in Figure 7.5.*b* to support the claim of short time instability.

7.5 Conclusions

In this paper we have formulated reaction-diffusion dynamics of topological signals defined on nodes, links, and higher-order simplices of simplicial complexes or cells of cell complexes. In this framework, each species of reactants lives on simplices or cells of a given dimension, for instance in a simplicial complex of dimension $d = 2$ one would consider three kind of species living on nodes, links and triangles. Species associated to simplices of different dimension can be coupled thanks to the Dirac operator which projects a signal defined on n-dimensional simplices either one dimension up or one dimension down. In the proposed reaction-diffusion dynamics, the coupling can then be enforced either by a Dirac reaction term or/and Dirac cross-diffusion terms. After discussing the general framework valid for simplicial and cell complexes of arbitrary dimension, we focus on the reaction-diffusion dynamics of topological signals defined on networks, i.e., coupling the dynamics between links and nodes, and we establish conditions for the onset of the Turing instability. The latter conditions are derived when signals of different dimension are only coupled with the Dirac reaction term, as well as when they are also coupled by a linear or a cubic Dirac cross-diffusion term.

We have found that the Turing patterns arising from the reaction-diffusion dynamics of topological signals are never localized only on nodes or links of the network. Instead they always involve both node and link signals. Moreover, the projection of the link signals on the nodes, and the projection of the node signals onto the links are shown to also display a Turing pattern.

We also observe that when the reaction term does not depend on the projected signal, the Turing pattern can be observed only in presence of a linear Dirac cross-diffusion term.

Our results are validated on a small toy model for the reaction-diffusion of topological signal on a network, and on simulations of square lattices with periodic boundary conditions.

7.6 SM 1: Basics properties of algebraic topology

Simplicial and cell complexes, the boundary and co-boundary operators

A d-dimensional cell complex $\mathscr{S}$ is a collection of cells whose dimension n is smaller or equal to d which is closed under the inclusion of the cells' faces. The n-dimensional cells are convex polytopes of dimension n, i.e., for $n = 0$ they are nodes, for $n = 1$ they are links, for $n = 2$ they are triangles, squares, pentagons etc. and for $n = 3$ they

are tetrahedra, hypercubes, orthoplexes etc. The faces of an n-cell are the $(n-1)$-dimensional cells at its boundary. A special case of cell complex is a simplicial complex which is only formed by simplices, i.e., cells whose underlying network structure is a clique, such as nodes, links, triangles, tetrahedra and so on. The cells of a cell complex are *oriented* and typically for simplicial complexes the orientation of the simplicial complex induced by the nodes label is used, for instance a link $[i,j]$ is positively oriented if $i<j$ and similarly a triangle $[i,j,k]$ and all the triangles obtained by a cyclic permutation of the indices are positively oriented if $i<j<k$. For more information about simplicial and cell complexes see Refs.[207, 218, 285].

The topology of cell complexes can be investigated using methods coming from algebraic topology. Let us indicate with N_m the number of m-dimensional cells present in the considered cell complex. In algebraic topology the cells $\mu_n^{(m)}$ of dimension n of a simplicial complex define the basis of a vector space C_n of *n-chains*. Therefore, a n-chain $\mathbf{c}\in C_n$ is a finite linear combination of the n-cells $\mu_n^{(m)}$ with $1\leq m\leq N_n$ with coefficients c_i

$$\mathbf{c}=\sum_{m=1}^{N_n} c_i\mu_n^{(m)} \tag{7.6.1}$$

The boundary of a chain can be obtained from a chain by applying to it the *boundary operator* $\partial_n : C_n \to C_{n-1}$ which is represented by the boundary matrix $\mathbf{B}_n$.

The boundary matrix $\mathbf{B}_n$ is a $N_{n-1}\times N_n$ rectangular matrix of elements $[B_n]_{\mu,\mu'}=+1$ if μ is a $(n-1)$-dimensional face of the n-cell μ with coherent orientation, $[B_n]_{\mu,\mu'}=-1$ if the orientation is not coherent, and $[B_n]_{\mu,\mu'}=0$ if μ is not a face of μ'. In the particular case of $\mathbf{B}_1$, we have for instance

$$[B_1]_{i\ell}=\begin{cases} 1 & \text{if } \ell=[j,i] \text{ and } j<i \\ -1 & \text{if } \ell=[i,j] \text{ and } i<j \\ 0 & \text{otherwise} \end{cases} \tag{7.6.2}$$

once we assume the orientation to be induced by the nodes labels. As an example, the matrix $\mathbf{B}_1$ and $\mathbf{B}_2$ of the simplicial complex shown in Figure 7.6 are given by

$$\mathbf{B}_1 = \begin{array}{c} \\ [1] \\ [2] \\ [3] \\ [4] \\ [5] \end{array} \begin{array}{c} \begin{array}{ccccccc} [1,2] & [1,3] & [1,4] & [1,5] & [2,3] & [3,4] & [3,5] \end{array} \\ \begin{bmatrix} -1 & -1 & -1 & -1 & 0 & 0 & 0 \\ 1 & 0 & 0 & 0 & -1 & 0 & 0 \\ 0 & 1 & 0 & 0 & 1 & -1 & -1 \\ 0 & 0 & 1 & 0 & 0 & 1 & 0 \\ 0 & 0 & 0 & 1 & 0 & 0 & 1 \end{bmatrix} \end{array}$$

and

$$\mathbf{B}_2 = \begin{array}{c} \\ [1,2] \\ [1,3] \\ [1,4] \\ [1,5] \\ [2,3] \\ [3,4] \\ [3,5] \end{array} \begin{array}{c} [1,2,3] \\ \left[\begin{array}{c} 1 \\ -1 \\ 0 \\ 0 \\ 1 \\ 0 \\ 0 \end{array}\right. \end{array}$$

The set of all the boundary matrices $\mathbf{B}_n$ with $0 \leq n \leq d$ of a simplicial complex fully encodes the topology of the simplicial complex. The adjoint of the boundary operator or *co-boundary operator* is represented by the matrix $\mathbf{B}_n^\top$.

The Hodge-Laplacians and the Dirac operator of a cell complex

Starting from the boundary and the co-boundary operators, we define the higher-order Laplacians and the Dirac operator.

The Laplace operator [279, 216, 207] of order n, also called n-Hodge-Laplacian, describes higher-order diffusion from n-cells to n-cells and are $N_n \times N_n$ matrices defined as

$$\mathbf{L}_n = \mathbf{B}_n^\top \mathbf{B}_n + \mathbf{B}_{n+1}\mathbf{B}_{n+1}^\top = \mathbf{L}_n^{down} + \mathbf{L}_n^{up} \tag{7.6.3}$$

for $1 \leq n < d$. For $n = 0$ and $n = d$, the Hodge-Laplacians $\mathbf{L}_0$ and $\mathbf{L}_d$ are respectively given by $\mathbf{L}_0 = \mathbf{L}_0^{up} = \mathbf{B}_1\mathbf{B}_1^\top$ and $\mathbf{L}_d = \mathbf{L}_d^{down} = \mathbf{B}_d^\top \mathbf{B}_d$.

The action of the Hodge-Laplacian can be interpreted as follows. The term $\mathbf{L}_n^{up}$ represents the diffusion between n-cells through shared $(n+1)$-dimensional cells. In the case of a network, as previously noticed, this is the combinatorial Laplacian, where concentrations on nodes diffuse through incident links. The term $\mathbf{L}_n^{down}$ represents diffusion between n-cells through shared $(n-1)$-cells, i.e., incident $(n-1)$-faces. For instance in a network (i.e., a 1-simplicial complex) $\mathbf{L}_1 = \mathbf{L}_1^{down}$ determines diffusion from links to links through nodes. From this definition, it is clear that the Hodge-Laplacian of order n only acts on topological signals of dimension n. Therefore, the n-Hodge-Laplacian cannot couple signals of different dimension. In order to couple signal of different dimension, we require the Dirac operator [280, 281, 282, 283], $\mathscr{D}$, which is encoded by an $M \times M$ matrix where $M = \sum_{n=0}^{d} N_n$ and has elements

$$\mathscr{D}_{\mu,\mu'} = \begin{cases} [B_n]_{\mu,\mu'} & \text{if} \quad |\mu'| = |\mu| + 1 = n \\ [B_n^\top]_{\mu,\mu'} & \text{if} \quad |\mu| = |\mu'| + 1 = n \end{cases} \tag{7.6.4}$$

where with $|\mu|$ we indicate the dimension of the cell μ. It follows that in a two dimensional cell complex, the Dirac operator has the block structure

$$\mathscr{D} = \begin{pmatrix} 0 & \mathbf{B}_1 & 0 \\ \mathbf{B}_1^\top & 0 & \mathbf{B}_2 \\ 0 & \mathbf{B}_2^\top & 0 \end{pmatrix} \tag{7.6.5}$$

while in a network the Dirac operator is given by

$$\mathscr{D} = \begin{pmatrix} 0 & \mathbf{B}_1 \\ \mathbf{B}_1^\top & 0 \end{pmatrix} \tag{7.6.6}$$

It follows that the Dirac operator, differently from the Hodge-Laplacian, can couple topological signals of different dimension. In particular the Dirac operator can be used to project a topological signal of any dimension n onto simplices of dimension $n+1$ and $n-1$. One of the most significant properties of the Dirac operator is that it can be considered the "square root" of the Laplacian. In fact we have

$$\mathscr{D}^2 = \mathscr{L} = \mathbf{L}_0 \oplus \mathbf{L}_1 \oplus \ldots \oplus \mathbf{L}_d \tag{7.6.7}$$

For instance, for a simplicial complex of dimension $d = 2$ we have

$$\mathscr{D}^2 = \mathscr{L} = \begin{pmatrix} \mathbf{L}_0 & 0 & 0 \\ 0 & \mathbf{L}_1 & 0 \\ 0 & 0 & \mathbf{L}_2 \end{pmatrix} \tag{7.6.8}$$

and for a network

$$\mathscr{D}^2 = \mathscr{L} = \begin{pmatrix} \mathbf{L}_0 & 0 \\ 0 & \mathbf{L}_1 \end{pmatrix} \tag{7.6.9}$$

Interestingly, both the Hodge-Laplacians and the Dirac operator can be extended to treat weighted simplicial complexes (see for instance [206]).

Major Spectral properties of the boundary operators, the Hodge-Laplacians and the Dirac operator

The n-order Hodge-Laplacian [279, 216, 207] is a semi-definite positive operator whose kernel has dimension equal to the n-th Betti number β_n, i.e., the degeneracy of its null eigenvalue is equal to the Betti number β_n. In addition to this, the Hodge-Laplacians obey the Hodge decomposition which implies that the space of n-chains can be decomposed as

$$C_n = \mathrm{im}(\mathbf{B}_n^\top) \oplus \ker(\mathbf{L}_n) \oplus \mathrm{im}(\mathbf{B}_{n+1}) \tag{7.6.10}$$

where the kernel of the Hodge-Laplacians are given by

$$\ker(\mathbf{L}_0) = \ker(\mathbf{B}_1^\top) \quad \ker(\mathbf{L}_n) = \ker(\mathbf{B}_n) \cap \ker(\mathbf{B}_{n+1}^\top) \tag{7.6.11}$$

The Dirac operator [280] has a kernel given by the direct sum of the kernels of the Laplacians,

$$\ker(\mathscr{D}) = \ker(\mathscr{L}) = \ker(\mathbf{L}_0) \oplus \ker(\mathbf{L}_1) \oplus \ldots \oplus \ker(\mathbf{L}_d) \tag{7.6.12}$$

The non-zero spectrum of the Dirac operator is formed by the concatenation of the spectra of the Hodge-Laplacians taken with positive and negative sign. Let us now focus on the spectrum of the Hodge-Laplacians $\mathbf{L}_0$ and $\mathbf{L}_1$ defined on a network, and reveal the relation between their spectra and the singular values of the boundary operator $\mathbf{B}_1$. Since $\mathbf{L}_0 = \mathbf{B}_1\mathbf{B}_1^\top$ and $\mathbf{L}_1 = \mathbf{B}_1^\top\mathbf{B}_1$ it follows that $\mathbf{L}_0$ and $\mathbf{L}_1$ are isospectral, i.e., they

have the same non-zero eigenvalues and any eigenvalue Λ_0^k of $\mathbf{L}_0$ can be written as $\Lambda_0^k = b_k^2$ where b_k indicates the non-zero singular eigenvalues of the boundary matrix $\mathbf{B}_1$. We note however that the degeneracy of the zero eigenvalue $\Lambda_a^1 = 0$, $a = 0,1$ is different for $\mathbf{L}_0$ and $\mathbf{L}_1$. Indeed, for $\mathbf{L}_0$ the degeneracy of the zero eigenvalue is β_0, i.e., the number of connected components of the network, while for $\mathbf{L}_1$ it is given by β_1, i.e., the number of independent cycles of the network. Therefore, for a network that has the topology of a linear chain with periodic boundary conditions when $N_0 = N_1$, we have $\beta_0 = \beta_1 = 1$, for a tree when we have $N_1 = N_0 - 1$ we have $\beta_0 = 1$ and $\beta_1 = 0$ and in general for a connected network we have $\beta_0 = 1$, $\beta_1 = N_1 - N_0 + 1$. Let us denote by ψ_a^k the eigenvector of $\mathbf{L}_a$ associated to the non-zero eigenvalue Λ_a^k, for $a = 0,1$, namely $\mathbf{L}_a \psi_a^k = \Lambda_a^k \psi_a^k$, then we have by the properties of the singular value decomposition applied to $\mathbf{B}_1$ that

$$\mathbf{B}_1 \psi_1^k = b_k \psi_0^k, \quad \mathbf{B}_1^\top \psi_0^k = b_k \psi_1^k \tag{7.6.13}$$

7.7 SM 2: Square Lattice with periodic boundary conditions

For this case of interest, where the cell complex is a d-dimensional square lattice with periodic boundary conditions (p.b.c.), interesting phenomena occur. For a rectangular portion of a d-dimensional square lattice with linear size L_m in the direction m, the eigenvalues and the eigenvectors of the graph Laplacians $\mathbf{L}_0$ and $\mathbf{L}_1$ can be easily computed [207]. Indeed the eigenvectors of $\mathbf{L}_0$ are the Fourier modes of the lattice associated with wave number $\mathbf{q} = (q_1, q_2, \ldots, q_m, \ldots, q_d)$ and the eigenvalues of $\mathbf{L}_0$ can be expressed as

$$\Lambda_0(\mathbf{q}) = 4 \sum_{m=1}^{d} \sin^2(q_m/2) \tag{7.7.1}$$

The periodic boundary conditions impose

$$q_m = \frac{2\pi}{L_m} \hat{n}_m \quad \hat{n}_m = 0, 1, 2 \ldots L_m - 1 \tag{7.7.2}$$

The analysis that has been carried out for the case presented in the main text will let us to conclude that as soon as an eigenvalue returns a positive dispersion law, i.e., $\lambda(b_k^2) > 0$, the corresponding eigenspace will be constituted by one periodic eigenvector that spans the nodes and one, again periodic, that spans the links. Consequently, as in the general case, the arising instability cannot be confined to the space of nodes or links, here too. To be concrete, we have numerically analyzed the dynamical system (7.3.22) defined on a 4×4 2-dimensional lattice with p.b.c.. The results are depicted in Figure 7.7: on the left column, panels a), c) and e), refer to the case where there is single unstable mode, while on the right column (panels b), d) and f)), multiple unstable modes are allowed. Let us first observe that the critical mode, i.e., the one associated to the largest value of the dispersion relation, is the same for both parameter configurations; we also remark that to each mode, except for the 0-th one, there are associated several linearly independent eigenvectors, four vectors in the case of a 4×4 lattice with p.b.c. When only one mode is unstable (see panel c) in Figure 7.7), we observe that

the signal on the nodes exhibits a (horizontal) striped-like pattern and the signals on the links are non-zero only when the link connects nodes with different signals values (Figure 7.7*a*). Such ordered structure is destroyed when multiple modes are unstable (Figure 7.7*b*,*d*). When there is a single unstable mode, the stationary pattern is a linear combination of the 4 eigenvectors associated to such mode (Figure 7.7*e*); remarkably this continues to be true when more than one mode is unstable (Figure 7.7*f*). Let us conclude by observing that the former result is a slight generalization of the one we can found in [31], where authors showed that in the case of a unique unstable and non-degenerate mode, the patterns can be described by such eigenvector, despite the fact that they are the reflex of a nonlinear process. Here we have shown that the same result holds true if the unique critical eigenvalue possesses a high-dimensional subspace spanned by several eigenvectors and even in the case of multiple unstable modes.

7.8 SM 3: Turing patterns with a linear Dirac term

In this SM our goal is to derive the condition for the onset of the Turing instability for the reaction-diffusion dynamics with linear Dirac cross-diffusion term which we rewrite here for convenience,

$$\dot{\Phi} = F(\Phi, \mathscr{D}\Phi) - \tilde{\gamma}\mathscr{D}\Phi - \gamma\mathscr{L}\Phi \tag{7.8.1}$$

We notice that by putting

$$F(\Phi, \mathscr{D}\Phi) - \tilde{\gamma}\mathscr{D}\Phi = \tilde{F}(\Phi, \mathscr{D}\Phi) \tag{7.8.2}$$

Equation (7.8.1) reduces to Equation (7.3.1) with Dirac reaction term given by $\tilde{F}(\Phi, \mathscr{D}\Phi)$, i.e. it reduces to

$$\dot{\Phi} = \tilde{F}(\Phi, \mathscr{D}\Phi) - \gamma\mathscr{L}\Phi \tag{7.8.3}$$

It follows that the conditions for the onset of the Turing instability can be obtained directly from Equation (7.3.19) and Equation (7.3.20) by making the substitutions

$$\partial_{\mathbf{B}_1 v} f \to \partial_{\mathbf{B}_1 v} f - D_{01} \quad \partial_{\mathbf{B}_1^\top u} g \to \partial_{\mathbf{B}_1^\top u} g - D_{10} \tag{7.8.4}$$

This allows us to obtain that in the case with linear Dirac cross-diffusion terms we can observe the onset of the Turing instability when in addition to Equation (7.3.7), the following two conditions are satisfied:

$$\begin{aligned} A &= D_0\partial_v g + D_1\partial_u f + (\partial_{\mathbf{B}_1 v} f - D_{01})(\partial_{\mathbf{B}_1^\top u} g - D_{10}) > 0 \\ A^2 &> 4D_0 D_1 \partial_u f \; \partial_v g \end{aligned} \tag{7.8.5}$$

7.9 SM 4: Turing patterns with a cubic Dirac term

In this SM we derive the condition for the onset of the Turing instability in presence of a cubic Dirac cross-diffusion term. The Turing instability is observed when the eigenvalue λ satisfying (7.4.11) is positive. Let us note that the second order equation (7.4.11) has both leading coefficients positive. According to Descartes' rule of

signs, this equation only admits a positive root if $\tilde{\Gamma}_2(b_k^2) < 0$. Consequently, a positive dispersion on a finite number of modes can be guaranteed by requiring that $\tilde{\Gamma}_2(b_k^2) < 0$ on a finite range of b_k^2. First of all, we need to ensure that Equation (7.4.11) admits no positive root in the limit $b_k^2 \to \infty$ to avoid long wavelength instability. This can only be guaranteed if we impose that $D_{01}D_{10} < 0$. This ensures that there is a $\bar{b}_k^2$ such that $\tilde{\Gamma}_2(b_k^2) > 0$ for all $b_k^2 > \bar{b}_k^2$. Note that D_{01}, D_{10} are not diffusion coefficients but cross-diffusion coefficients. Indeed they are coupling each signal with the projection of the signal defined on a different dimension. For this reason we do not need to limit the values of D_{01} and D_{10} to be positive and we can allow negative values while still retaining their physical meaning. Requiring the existence of positive roots in λ over a finite range of $b_k^2 < \bar{b}_k^2$ can be done again by studying the roots of $\tilde{\Gamma}_2$ using *Descartes' rule of sign*, remembering that the leading and the last coefficients of $\tilde{\Gamma}_2(b_k^2)$ are positive $(+)$. As $\tilde{\Gamma}_2(b_k^2) > 0$ in the limit $b_k^2 \to \infty$, we require that $\tilde{\Gamma}_2(b_k^2)$ admits a positive root in b_k^2 to ensure that the system obeys all conditions required for the existence of Turing patterns. A change in sign in the coefficients of $\tilde{\Gamma}_2(b_k^2)$ is a necessary condition to guarantee this, which leads to patterns of signs $(+--+)$, $(+-++)$, $(++-+)$. All these have two sign changes. Hence, applying the rule of sign, $\tilde{\Gamma}_2(b_k^2)$ can admit either 2 or 0 real positive roots. We now need to find a condition to exclude the case of 0 positive roots. To do so, we start by using the rule of sign for the polynomial of opposite sign, $\tilde{\Gamma}_2(-b_k^2)$, which yields the number of negative rules of $\tilde{\Gamma}_2(b_k^2)$. The possible sign patterns $(+--+)$, $(+-++)$, $(++-+)$ respectively become $(--++)$, $(---+)$, $(-+++)$. These all have a single sign change. Hence, by the rule of sign, $\tilde{\Gamma}_2(-b_k^2)$ has exactly one positive root. Consequently, $\tilde{\Gamma}_2(b_k^2)$ has exactly one negative root, provided the coefficients fall into one of the cases $(+--+)$, $(+-++)$, $(++-+)$. The last condition can be obtained using the cubic discriminant of $\tilde{\Gamma}_2(b_k^2)$. Indeed, in the above three possible cases, we are guaranteed to have a single negative root. There can be 0 or two positive roots. Guaranteeing two positive roots can be done by imposing that all roots are distinct, and this can be achieved by setting the discriminant of $\tilde{\Gamma}_2(b_k^2)$ to be positive. Mathematically, this corresponds to first imposing that one of the following two conditions is satisfied

$$D_0 D_1 + D_{01}\partial_{\mathbf{B}_1^\top u} g + D_{10}\partial_{\mathbf{B}_1 v} f < 0 \tag{7.9.1}$$

$$D_1 \partial_u f + D_0 \partial_v g + \partial_{\mathbf{B}_1{}_1^\top u} g \; \partial_{\mathbf{B}_1 v} f < 0 \tag{7.9.2}$$

which constrain the polynomial to one of the above sign patterns, and ensures and the presence of one negative root and either one or two positive roots. By imposing that the three roots are distinct mathematically through the discriminant of $\tilde{\Gamma}_2(b_k^2)$ leads to the condition

$$2D_0 D_1 K_+ + D_0^2 D_1^2 + K_-^2 > 0 \tag{7.9.3}$$

where $K_\pm$ is given by

$$K_\pm = D_{01}\partial_{\mathbf{B}_1^\top u} g \pm D_{10}\partial_{\mathbf{B}_1 v} f \tag{7.9.4}$$

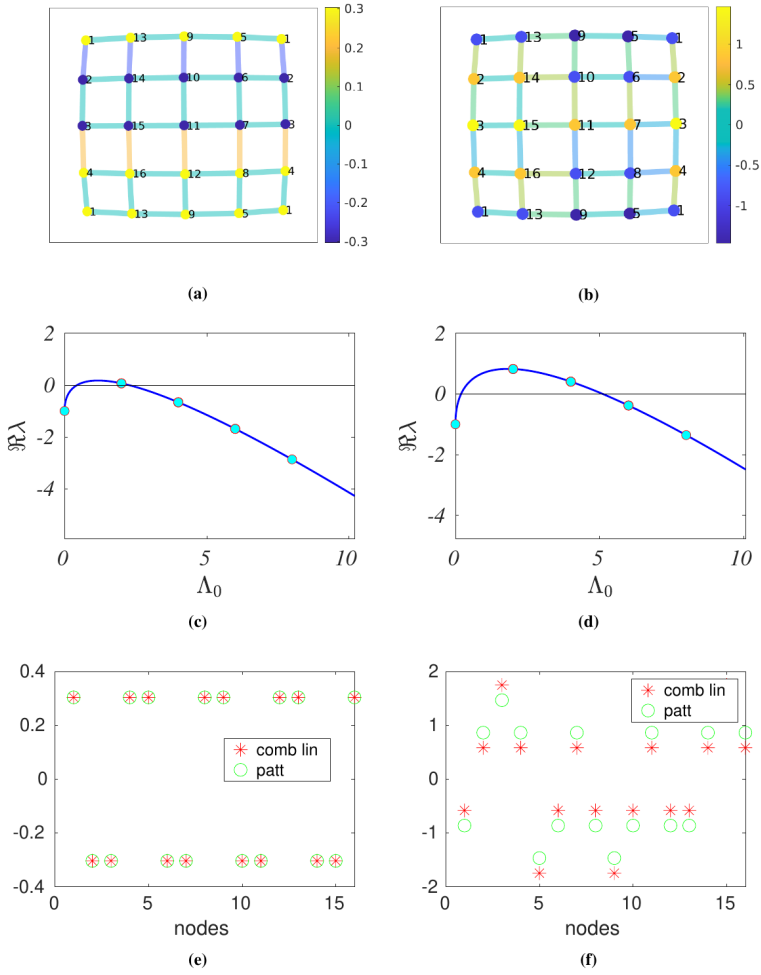

Figure 7.7: Model (7.3.22) on a 4×4 2-dimensional lattice with p.b.c. The periodicity of lattice, shown in panels a) and b), is represented by adding one column and one row, so that the displayed nodes are 25, but effectively they are 16. Panels on the left show the case where only one mode contributes to the instability, while those on the right where multiple modes are unstable, as shown by the dispersion laws in panels c) and d), respectively. When only one mode is unstable, the nodes' pattern is striped-like, while the signal on the links is non-zero only when the given link connects two nodes with different signals, as shown in panel a); on the other hand, when multiple modes are unstable, such regular structure is lost, as we can see in panel b). Panels e) and f) show a comparison of the nodes' pattern with a linear combination of the eigenvector associated to the critical mode(s), showing a good accordance. The model parameters are $a = \alpha = b = \beta = \gamma = D_0 = D_1 = 1$; $c = 4.7$ for panels a), c), e), while $c = 7.3$ for panels b), d), f); the initial perturbation is $\sim 10^{-2}$.

Part III

Conclusions and perspectives

Conclusions and future directions

"We can only see a short distance ahead,
but we can see plenty there that needs to be done."
Alan Turing

In this thesis we have explored some extensions of Turing theory of pattern formation, both in the pairwise setting and in the new and exciting framework of higher-order interactions. Besides extending the theory, our main goal was to relax the conditions under which patterns arising from a symmetry breaking mechanism could be inscribed in a Turing mechanism. We have shown that a discrete topology offers several possibilities of instability and reinterpretations of the phenomenon: we can have patterns even when a linear stability analysis predicts otherwise, or without relying on diffusion. Moreover, when considering higher-order topologies and the mathematical tools developed in that framework, we can even consider signals on the links, which become not simply the connectors between the nodes, but part of the support where the dynamics take place. As for any research, we conclude this journey with more questions than answers and with further research ideas. In the following, we will discuss some further developments of the research presented above, some of which are already in the process of being developed; some others are, for now, only planned.

For what concerns non-normality, we have two interesting ongoing projects that, hopefully, will see the light in the coming months. The first one, in collaboration with Doctor Malbor Asllani of Florida State University and Professor James Gleeson of University of Limerick, is about synchronization patterns on real-world networks. Within the same framework of Chapter 2, i.e., Turing-like instability for oscillatory systems, we studied what happens when the support is a real-world network, which is known to be strongly non-normal [39]. We analyzed a data-set of empirical networks, from food-webs to biochemical ones, and we noticed that, after a symmetry breaking of the homogeneous synchronized state, some nodes continued to oscillate about the attractor of the isolated system, while a part was oscillating with the same frequency but different amplitude. We realized that the observed patterns were indeed Amplitude Chimeras, i.e., chimeras with respect to the amplitude rather than the phase [286]. We understood that such behavior is due to the structure of the eigenvectors, which are strongly local-

ized for non-normal networks, and that leader nodes, i.e., nodes with only either in- or out-going links [287], have a pivotal role in the formation of the chimera state. The next step will be to extend the considered data-set, in order to prove the universality of the phenomenon. The second work is currently undertaken by a Master Student we are supervising, Marie Dorchain, who is studying Turing patterns on non-diagonalizable networks. The goal of this Master project is to determine if and how the generalized eigenvectors contribute to the formation of the asymptotic pattern and to provide a characterization of the latter.

When studying inertia-driven patterns, we have investigated the phenomenon on symmetric support. The network framework facilitates a deeper understanding of the phenomenon and allows for a reinterpretation, but, as we have shown in Chapters 2 and 4, one great advantage of considering a discrete topology is the straightforward extension to a directed one. We have started exploring the possibility to extend the theory of inertia-driven patterns developed in Chapter 3 to directed networks. We have preliminary numerical results showing that, as expected, both the diffusion- and the inertia-driven regions of pattern formation are enhanced when the underlying network is directed. Now, the challenge is to tackle the problem analytically: for this we could either apply a generalization of the Routh-Hurwitz criterion for complex polynomials, or extend the method developed in Chapter 4 to study the onset of instability for systems of any dimension.

In the introduction of Chapter 4, we discussed the perspective of testing experimentally our claim that non-reciprocal interactions enhance the possibility of pattern-formation. This is certainly the work toward which we have more expectations and we are more excited to develop. Having our theory tested would be extremely pleasant and rewarding. With the same purpose, we discussed with our colleagues at University of Catania, Doctor Valentina Gambuzza and Professor Mattia Frasca, the possibility of experimentally testing the effects of higher-order interactions. However, while their experimental apparatus is perfectly suited for the pairwise non-local coupling discussed in Chapter 4, how to build integrated circuits representing higher-order coupling is still an open question and needs to be further investigated. It would be, of course, very exciting *per se* to achieve such a task and there are already in line several theoretical works to be tested. Nonetheless, we hope that one day the theory we developed on Turing patterns with higher-order interactions, presented in Chapter 6, could be tested. In particular, it would be extremely interesting to tune the emergence of patterns with the strength of higher-order interactions; this way it would be possible to obtain the desired state without having to change the model parameters. Within the same framework, another interesting study to pursue in the future would be the emergence of Turing patterns in systems with many-body interactions, when the latter are directed. Such non-reciprocal higher-order structures have been studied in the context of synchronization dynamics [211], hence an extension toward the Turing framework would be straightforward.

Also the theory of topological signals provides a fertile ground for applications in neuroscience. In fact, there is increasing evidence that neuronal networks should not be modeled having signals merely in the nodes, but signals (at least) on the links should be considered. The latter are called *edge signals* [219]. Together with Lorenzo Giambagli and Professor Ginestra Bianconi of Queen Mary University of London, we are extending the model studied in Chapter 7 to settings in which two species lie in the nodes

and one in the links, coupled through a nonlinear version of the Dirac operator. This way, we can obtain Turing oscillatory patterns even in models which would not exhibit such behavior, as it is not allowed for only two interacting species [8]. In the coming future, we plan to focus on models that are studied in neuroscience and check whether our extension is able to reproduce the behaviors observed experimentally.
The tools of algebraic topology may as well allow us to rigorously define directed networks. In fact, while diffusion on symmetric networks is defined by the boundary operator $\mathbf{B}_1$ (see Chapter 7), which gives the coordinates of the considered space, it is not known how to analogously define a directed Laplacian matrix. We know that diffusion on a directed network is equivalent to isotropic diffusion with a differential flow, but this can be easily proven only for a 1-dimensional lattice ring with periodic boundary conditions and a general theory is missing. Together with Professor Juan Ignacio Perotti, of National University of Córdoba, we are studying the problem from the perspective of simplicial complexes, trying to formulate a general theory of directed networks using higher-order vector fields. Such theory would open the way for a generalization of directed networks in higher-order structures, i.e., directed simplicial complexes. Once the ground is built, it would be exciting to extend Turing theory on such directed higher-order structures.
Lastly, and not related to Turing patterns, with Professor Stefanella Boatto, of Federal University of Rio de Janeiro, we are studying a SIR-network model with time-varying infectivity parameters. During this work, currently in preparation, we observed the impact of the flow of individuals, tourists and climate in the occurrence and in the intensity of the epidemic. Moreover, we extended the model for non-constant populations and for time-varying chaotic infectivity parameters. The last part of this work will be to fit the data of infected individuals of Dengue fever in the city of Rio de Janeiro for the epidemics 2007-2008 and confront our results with previous models.

Turing theory of pattern formation is often considered a niche topic, more suited for chemistry or developmental biology journals, rather than network ones. However, during our work we have been able to show that the network reformulation of the theory relies on a formalism similar to what is commonly used to study synchronization dynamics. Indeed, we have been able to communicate and collaborate with scholars of networks and dynamics on network, and the goal for the future is to also reach the community originally studying Turing patterns for PDEs systems. The main challenge will be to make a bridge between these two communities and to join the longstanding expertise on Turing patterns of the latter with the knowledge and tools of networks and higher-order interactions of the former.

Before concluding, we would like to emphasize how remarkable is that the original theory branched in such various lines of research. It gives us a feeling of the power of Turing's intuition that, more than 70 years after its conception, continues to amaze us.

Summary of other coauthored papers

The common message of constraint-based optimization approaches: overflow metabolism is caused by two growth-limiting constraints

Mathematicians have always tried to find common features and similarities of the models they study. French mathematician Henri Poincaré used to say that "*Mathematics is the art of giving the same name to different things*". However, not all disciplines bear the same philosophy, for example biology. My friend and colleague Daan, a mathematician who moved to theoretical biology, noticed that a certain phenomenon, consisting in an inefficient usage of resources by cells and called *overflow metabolism*, was reproduced by different modeling approaches, which appeared, at first sight, rather different. We hence analyzed 14 of them, among the most popular and cited papers in the field, from a mathematical point of view. We realized that all the models could be reformulated as a linear programming problem and the system would show overflow metabolism when two constraints were active at the same time. 14 approaches, with 14 different names, were in the end the same model.

D.H. de Groot, J. Lischke, R. Muolo, R. Planqué, F.J. Bruggeman & B. Teusink. Cellular and Molecular Life Sciences, 77 (3), 441-453 (2020) [288]
This article is open access.

Abstract

Living cells can express different metabolic pathways that support growth. The criteria that determine which pathways are selected in which environment remain unclear. One recurrent selection is overflow metabolism: the simultaneous usage of an ATP-efficient

and -inefficient pathway, shown for example in *Escherichia coli*, *Saccharomyces cerevisiae* and cancer cells. Many models, based on different assumptions, can reproduce this observation. Therefore, they provide no conclusive evidence which mechanism is causing overflow metabolism. We compare the mathematical structure of these models. Although ranging from flux balance analyses to self-fabricating metabolism and expression models, we can rewrite all models into one standard form. We conclude that all models predict overflow metabolism when two, model-specific, growth-limiting constraints are hit. This is consistent with recent theory. Thus, identifying these two constraints is essential for understanding overflow metabolism. We list all imposed constraints by these models, so that they can hopefully be tested in future experiments.

Synchronization induced by directed higher-order interactions

higher-order interactions allow to capture certain features that escape a pairwise (network) description. However, there are many systems in which higher-order interactions are present but they are non-reciprocal: for example, bullying is a group interaction directed toward one, or more, individuals; or some chemical reactions need more than two reactants at the same time and there is a privileged direction given by thermodynamics. Directed hypergraphs existed in the literature, but were mainly used in computer science to model the flow of information and could not be used to study dynamics on top of them. Together with our colleagues from Università di Catania, we were able to develop a formalism allowing to overcome this problem. We defined a class of hypergraphs where the interactions are directed toward a fixed number of nodes. Our tensor formalism enables a semi-analytical study of the Master Stability Function and allows to investigate the stability of the synchronous solution when the system has a directed hypergraph as a support. Not all types of directed higher-order interactions can be modeled through our formalism, but our study was the first of this kind and it opens the way for future works in this direction.

L. Gallo, R. Muolo, L.V. Gambuzza, V. Latora, M. Frasca & T. Carletti. Communications Physics, 5, 263 (2022) [211]

Abstract

Non-reciprocal interactions play a crucial role in many social and biological complex systems. While directionality has been thoroughly accounted for in networks with pairwise interactions, its effects in systems with higher-order interactions have not yet been explored as deserved. Here, we introduce the concept of M-directed hypergraphs, a general class of directed higher-order structures, which allows to investigate dynamical systems coupled through directed group interactions. As an application we study the synchronization of nonlinear oscillators on 1-directed hypergraphs, finding that directed higher-order interactions can destroy synchronization, but also stabilize otherwise unstable synchronized states.

Publications

* equal contributions

- R.M., M. Asllani, D. Fanelli, P.K. Maini & T. Carletti, *Patterns of non-normality in networked systems*, Journal of Theoretical Biology, Volume 480, Pages 81-91 (2019) → link to the paper;
- D.H. de Groot, J. Lischke*, R.M.*, R. Planqué, F.J. Bruggeman & B. Teusink, *The common message of constraint-based optimization approaches: overflow metabolism is caused by two growth-limiting constraints*, Cellular and Molecular Life Sciences, Volume 77, 3, Pages 441-453 (2020) → link to the paper;
- R.M., T. Carletti, J.P. Gleeson & M. Asllani, *Synchronization dynamics in non-normal networks: the trade-off for optimality*, Entropy, Volume 23(1), 36, Pages 1-12 (2021) → link to the paper;
- T. Carletti* & R.M.*, *Finite propagation enhances Turing patterns in reaction-diffusion networked systems*, Journal of Physics: Complexity, Volume 2(4), 045004 (2021) → link to the paper;
- R.M., T. Carletti, J.P. Gleeson & M. Asllani, *Reply to "Comment on Synchronization dynamics in non-normal networks: the trade-off for optimality"*, Accepted in Entropy, (2022) → link to the paper;
- T. Carletti & R.M., *Non-reciprocal interactions enhance heterogeneity*, Chaos, Solitons & Fractals, Volume 164, 112638 (2022) → link to the paper;
- L. Gallo*, R.M.*, L.V. Gambuzza, V. Latora, M. Frasca & T. Carletti, *Synchronization induced by directed higher-order interactions*, Communications Physics, Volume 5, 263 (2022) → link to the paper;
- L. Giambagli, M.L. Calmon*, R.M.*, T. Carletti & G. Bianconi, *Diffusion-driven instability of topological signals coupled by the Dirac operator*, Physical Reveiw E, Volume 106, 064314 (2022) → link to the paper;

- R.M.*, L. Gallo*, V. Latora, M. Frasca & T. Carletti, *Turing patterns in systems with high-order interactions*, Chaos, Solitons & Fractals, Volume 166, 112912 (2022) → link to the paper.

Acknowledgements

There is only one person who deserves to be thanked for first and that is **Teo**. Thank you for believing in me, even after a first failed attempt on a PhD, for the support to all ideas and propositions, the freedom to organize my time, your calm and zen temper in any situation and your teachings, which go well beyond science. I was very lucky to have a supervisor who was always present while giving me time and space to let myself develop at my own pace. I am also very grateful to **Mattia**, for the many encouragements and feedback, for the wise advise which helped me grow and see things from different perspectives and for the always positive and enthusiast looks at our projects. A huge thanks also to the other members of the Jury **Ginestra Bianconi**, **Francesca Di Patti**, **Anne-Sophie Libert** and **Hiroya Nakao** for taking the time to read this thesis, for the many constructive feedback and positive words. I had the incredible chance to work with many Professors and Researchers who, despite their busy schedule, always found the time to clarify my doubts and give me some advice. With some of them I interacted via Skype or at conferences, some others kindly hosted me in their groups for short and long visits, a few were here in Namur and we chatted over coffee. Not all of them are (yet) coauthors, but this work is also a result of the interactions we had and I would like to thank them all: **Malbor Asllani**, **Stefanella Boatto**, **Hilda Cerdeira**, **Valentina Gambuzza**, **James Gleeson**, **Vito Latora**, **Alexandre Mauroy** and **Juan Ignacio Perotti**. A big thanks also to **Duccio Fanelli** and **Peter De Maesschalck** for being in my *comité d'accompagnement* and all the help in the application process and to **Bob Planqué** for his support and advise. There is one person who, above all others, encouraged me to study mathematics. Now he is a teacher and I envy his students: thanks **Giulione**. Among my tutors, I would also like to include my **Genitore 1**, for sharing with me her love for books and knowledge, and my **grandparents**.

One of the greatest experiences I had in this journey was to collaborate with my peers. It was very nice working with **Lorena** and **Thierry** and I look forward to see the final products of our work. It is even greater when friends and colleagues become mentors. First of all, **Daan**, who guided me through the vast biological literature and helped me deal with the legendary Dutch directedness. It was fun proving that so many models, in the end, were all the same. Then, I want to thank **Giamba**, master of top-

-ology and *Wizard of Hodge* and **Luca**, amazing scientist and part-time *heartbreaker*. Working with you two and hanging out with also **Matteo**, the most *indefesso* of us, was the best part of my PhD. It has been great to go to work happy and be around amazing people: *la cuchilla* **Carolina**, who always made me look at things from a different perspective, *mein Lieblingsarbeitsführer* and office-mate **Anthony**, **Jérôme**, with whom I shared an empty department for many months, my little *Dobby* **Martin**, my favorite French teacher **Candy**, **Cédric**, **Jean-François**, **Julien**, **Pascal** and all the others. Coffees and (especially) beers have been good, but the best part was to be with you at the table. Thanks to **Paulito** for his wisdom and caring advice and to **Andrea** *il Maestro* and **Matteo** for turning my last months in Amsterdam in something to remember and for always watching my back. I also want to thank **Bram**, **Age** and **Marie**. Supervising you and your feedback helped to improve as researcher and as a person. Lastly, to all my friends in Namur, who made these years pass by in a heartbeat: **José**, **Fede**, **Jan**, **Sofia**, **Carmen**, **Raul**, **Nacho** and **Carlos**.

I am thankful to all the **members of the Math Department** and **naXys**, for creating such a nice and cozy work environment. In particular, thanks to **Pascale**, **Alice** and **Juan**, always so helpful and available. The department would not work as good without you. I am also grateful to **University of Limerick**, **Università di Catania**, **Università degli Studi di Firenze**, **Universidade Federal do Rio de Janeiro** and **Universidad Nacional de Córdoba** for their hospitality and all researchers there who welcomed me and with whom I interacted, and also to **Xavier Leoncini** and **Viola Priesemann** for their kind invitations to their research centers.

None of this would have been possible without the amazing funding opportunities that I have had the luck to obtain. First of all, the **FNRS**, for believing in my project, and to the **Erasmus+** for funding my training abroad, but also the **yrCSS**, the **EDT Complex** and the **Royal Academy of Belgium**, for allowing me to interact with many researchers and to present our work in other institutes. We tend to underestimate the luck we have to live in countries where education is public and affordable to everyone. It is hard to feel too proud of one's achievements when looking at the immense privilege that is given only by being born in the "right" side of the world and the huge inequalities regarding the access to education, funding, obtaining visas, etc. Not to talk about discrimination based on gender and race. I wish that every kid, independently on where they are born, had the same opportunities I had.

Bibliography

[1] P.W. Anderson. More is different. broken symmetries and the nature of hierarchical structure of science. *Phys. Rev. Lett.*, 177(4047), 1972.

[2] J. Buck and E. Buck. Mechanism of rhythmic synchronous flashing of fireflies: Fireflies of southeast asia may use anticipatory time-measuring in synchronizing their flashing. *Science*, 159(3821):1319–1327, 1968.

[3] A. Cavagna, A. Cimarelli, I. Giardina, G. Parisi, R. Santagati, F. Stefanini, and M. Viale. Scale-free correlations in starling flocks. *Proc. Natl. Acad. Sci. U.S.A.*, 107(26):11865–11870, 2010.

[4] A.M. Turing. The chemical basis of morphogenesis. *Phil. Trans. R. Soc. Lond. B*, 237:37, 1952.

[5] A. Gierer and H. Meinhardt. A theory of biological pattern formation. *Kybernetik*, 12:30, 1972.

[6] V. Castets, E. Dulos, J. Boissonade, and P. De Kepper. Experimental evidence of a sustained standing turing-type nonequilibrium chemical pattern. *Phys. Rev. Lett.*, 64:2953, 1990.

[7] P. De Kepper, V. Castets, E. Dulos, and J. Boissonade. Turing-type chemical patterns in the chlorite–iodide–malonic acid reaction. *Physica D*, 49, 1991.

[8] S. Hata, H. Nakao, and A.S. Mikhailov. Sufficient conditions for wave instability in three-component reaction–diffusion systems. *Prog. Theor. Exp. Phys.*, 1(013A01), 2014.

[9] A.M Zhabotinsky, M. Dolnik, and I.R. Epstein. Pattern formation arising from wave instability in a simple reaction-diffusion system. *J. Chem. Phys.*, 103(10306), 1995.

[10] T. Biancalani, F. Di Patti, and D. Fanelli. Stochastic turing patterns in the brusselator model. *Phys. Rev. E*, 4(81):046215, 2010.

[11] T E Woolley, R E Baker, and Ph K Maini. Turing's theory of morphogenesis: Where we started, where we are and where we want to go. In *The Incomputable. Theory and Applications of Computability*. Springer, 2017.

[12] A.L. Krause, E.A. Gaffney, P.K. Maini, and V. Klika. A modern perspectives on near-equilibrium analysis of turing systems. *Proc. R. Soc. A*, 379:2213, 2021.

[13] A.B. Rovinsky and M. Menzinger. Chemical instability induced by a differential flow. *Phys. Rev. Lett.*, 69(8), 1992.

[14] A.B. Rovinsky and M. Menzinger. Self-organization induced by the differential flow of activator and inhibitor. *Phys. Rev. Lett.*, 70(6), 1993.

[15] D. Fanelli, C. Cianci, and F. Di Patti. Turing instabilities in reaction-diffusion systems with cross diffusion. *Eur. Phys. J. B*, 86:142, 2013.

[16] E.P. Zemskov and W. Horsthemke. Diffusive instabilities in hyperbolic reaction-diffusion equations. *Phys. Rev. E*, 93:032211, 2016.

[17] Y. Kato and H. Nakao. Turing instability in quantum activator–inhibitor systems. *Sci. Rep.*, 12 (1)(1-17), 2022.

[18] Y. Fuseya, H. Katsuno, K. Behnia, and A. Kapitulnik. Nanoscale turing patterns in a bismuth monolayer. *Nat. Phys.*, 17(1031–1036), 2021.

[19] F. Di Patti, L. Lavacchi, R. Arbel-Goren, L. Schein-Lubomirsky, D. Fanelli, and J. Stavans. Robust stochastic turing patterns in the development of a one-dimensional cyanobacterial organism. *PLoS Biol.*, 16(5):e2004877, 2018.

[20] A. Anma, K. Sakamoto, and T. Yoneda. Unstable subsystems cause turing instability. *Kodai Math. J.*, 35 (2)(215 - 247), 2012.

[21] A. Currò and G. Valenti. Pattern formation in hyperbolic models with cross-diffusion: Theory and applications. *Physica D*, 418:132846, 2021.

[22] J. Ritchie, A.L. Krause, and R.A. Van Gorder. Turing and wave instabilities in hyperbolic reaction-diffusion systems: The role of second-order time derivatives and cross-diffusion terms on pattern formation. *Ann. Phys.*, 444(169033), 2022.

[23] D. Ghosh, M. Frasca, A. Rizzo, S. Majhi, S. Rakshit, K. Alfaro-Bittner, and S. Boccaletti. The synchronized dynamics of time-varying networks. *Phys. Rep.*, 949:1–63, 2022.

[24] T. Carletti and D. Fanelli. Theory of synchronisation and pattern formation on time varying networks. *Chaos Solit. Fractals*, 159:112180, 2022.

[25] H.G. Othmer and L.E. Scriven. Instability and dynamic pattern in cellular networks. *J. Theor. Biol.*, 32:507, 1971.

[26] H.G. Othmer and L.E. Scriven. Non-linear aspects of dynamic pattern in cellular networks. *J. Theor. Biol.*, 43(1):83–112, 1974.

[27] R. Albert and A.L. Barabási. Statistical mechanics of complex networks. *Rev. Mod. Phys.*, 74(1):47, 2002.

[28] M.E.J. Newman. Spread of epidemic disease on networks. *Phys. Rev. E*, 66(1):016128, 2002.

[29] S.H. Strogatz. Exploring complex networks. *Nature*, 410(6825):268, 2001.

[30] R. Pastor-Satorras and A. Vespignani. Epidemic spreading in scale-free networks. *Phys. Rev. Lett.*, 86(14), 2001.

[31] H. Nakao and A.S. Mikhailov. Turing patterns in network-organized activator-inhibitor systems. *Nat. Phys.*, 6:544, 2010.

[32] R. Lambiotte and M.T. Schaub. *Modularity and Dynamics on Complex Networks*. Cambridge University Press, 2021.

[33] R.G. Plaza, F. Sánchez-Garduño, P. Padilla, R.A. Barrio, and P.K. Maini. The effect of growth and curvature on pattern formation. *J. Dyn. Differ. Equ.*, 16:1093, 2004.

[34] M. Asllani, D.M. Busiello, T. Carletti, D. Fanelli, and G. Planchon. Turing patterns in multiplex networks. *Phys. Rev. E*, 90:042814, 2014.

[35] N.E. Kouvaris, S. Hata, and A. Diaz-Guilera. Pattern formation in multiplex networks. *Scientific Reports*, 5:10840, 2015.

[36] M. Asllani, T. Carletti, and D. Fanelli. Tune the topology to create or destroy patterns. *Eur. Phys. J. B*, page 89, 2016.

[37] M. Boguñá, I. Bonamassa, M. De Domenico, S. Havlin, D. Krioukov, and M.A. Serrano. The physics of spreading processes in multilayer networks. *Nature Rev. Phys.*, 3:114–135, 2021.

[38] M. Asllani, J.D. Challenger, F.S. Pavone, L. Sacconi, and D. Fanelli. The theory of pattern formation on directed networks. *Nature Communication*, 5(4517), 2014.

[39] M. Asllani, R. Lambiotte, and T. Carletti. Structure and dynamical behavior of non-normal networks. *Sci. Adv.*, 4:Eaau9403, 2018.

[40] M. Asllani, T. Carletti, D. Fanelli, and P.K. Maini. A universal route to pattern formation in multicellular systems. *The European Physics Journal B*, 93(153), 2020.

[41] A. Arenas, A. Díaz-Guilera, J. Kurths, Y. Moreno, and C. Zhou. Synchronization in complex networks. *Phys. Rep.*, 469(3):93–153, 2008.

[42] A. Pikovsky, M. Rosenblum, and J. Kurths. *Synchronization. A universal concept in nonlinear sciences*. Cambridge University Press, Cambridge, UK, 2001.

[43] Y. Kuramoto. Self-entrainment of a population of coupled non-linear oscillators. In Huzihiro Araki, editor, *International Symposium on Mathematical Problems in Theoretical Physics*, pages 420–422, Berlin, Heidelberg, 1975. Springer Berlin Heidelberg.

[44] L.M. Pecora and T.L. Carroll. Master stability functions for synchronized coupled systems. *Phys. Rev. Lett.*, 80(10):2109, 1998.

[45] L.V Gambuzza, F. Di Patti, L. Gallo, S. Lepri, M. Romance, R. Criado, M. Frasca, V. Latora, and S. Boccaletti. Stability of synchronization in simplicial complexes. *Nat. Comm.*, 12(1):1–13, 2021.

[46] J. Challenger, R. Burioni, and D. Fanelli. Turing-like instabilities from a limit cycle. *Phys. Rev. E*, 92:022818, 2015.

[47] S.H. Strogatz. *Nonlinear Dynamics and Chaos*. Avalon Publishing, 2014.

[48] F. Di Patti, D. Fanelli, F. Miele, and T. Carletti. Ginzburg-landau approximation for self-sustained oscillators weakly coupled on complex directed graphs. *Commun. Nonlinear Sci. Numer. Simul.*, 56:447 – 456, 2018.

[49] T. Carletti and R. Muolo. Finite propagation enhances Turing patterns in reaction–diffusion networked systems. *J. phys. Complex.*, 2(4):045004, 2021.

[50] K. Kaneko. Clustering, coding, switching, hierarchical ordering, and control in a network of chaotic elements. *Physica D*, 41:137–172, 1990.

[51] D. Domínguez and H.A. Cerdeira. Order and turbulence in rf-driven josephson junction series arrays. *Phys. Rev. Lett.*, 71(20), 1993.

[52] Y. Kuramoto. Scaling behavior of turbulent oscillators with non-local interaction. *Prog. Theor. Phy.*, 94(321), 1995.

[53] Y. Kuramoto and H. Nakao. Origin of power-law spatial correlations in distributed oscillators and maps with nonlocal coupling. *Phys. Rev. Lett.*, 76(4352), 1996.

[54] Y. Kuramoto and H. Nakao. Power-law spatial correlations and the onset of individual motions in self-oscillatory media with non-local coupling. *Physica D*, 103(294), 1997.

[55] Y. Kuramoto, D. Battogtokh, and H. Nakao. Multiaffine chemical turbulence. *Phys. Rev. Lett.*, 81(3543), 1998.

[56] Y. Kuramoto, H. Nakao, and D. Battogtokh. Multi-scaled turbulence in large populations of oscillators in a diffusive medium. *Physica A*, 288(244), 2000.

[57] Y. Kuramoto and D. Battogtokh. Coexistence of coherence and incoherence in nonlocally coupled phase oscillators. *Nonlinear Phenom. Complex Syst.*, 5(380), 2002.

[58] D.M. Abrams and S.H. Strogatz. Chimera states for coupled oscillators. *Phys. Rev. Lett.*, 93(17):174102, 2004.

[59] A.B. Rovinsky and M. Menzinger. Interaction of turing and hopf bifurcations in chemical systems. *Phys. Rev. A*, 46(10), 1993.

[60] M. Meixner, A. De Wit, S. Bose, and E. Schöll. Generic spatiotemporal dynamics near codimension-two turing-hopf bifurcations. *Phys. Rev. E*, 55(6), 1997.

[61] K. Gizynski and J. Gorecki. Chemical memory with states coded in light controlled oscillations of interacting belousov-zhabotinsky droplets. *Phys. Chem. Chem. Phys*, 19:6519, 2017.

[62] V. Voorsluijs, I.G. Kevrekidis, and Y. De Decker. Nonlinear behavior and fluctuation-induced dynamics in the photosensitive belousov-zhabotinsky reaction. *Phys. Chem. Chem. Phys.*, 19:22528, 2017.

[63] J.M. Parrilla-Gutierrez, A. Sharma, S. Tsuda, G.J.T. Cooper, G. Aragon-Camarasa, K. Donkers, and L. Cronin. A programmable chemical computer with memory and pattern recognition. *Nat. Comm.*, (1):1442.

[64] B.N. Belintsev, M.A. Livshits, and M.V. Volkenstein. Pattern formation in systems with nonlocal interactions. *Z. Phys. B*, 44:345–351, 1981.

[65] J. Furter and M. Grinfeld. Local vs. non-local interactions in population dynamics. *J. Math. Biol.*, 27:65–80, 1989.

[66] G. Cencetti, F. Battiston, D. Fanelli, and V. Latora. Reactive random walkers on complex networks. *Phys. Rev. E*, 98(5):052302, 2018.

[67] E. Estrada, L.V. Gambuzza, and M. Frasca. Long-range interactions and network synchronization. *SIAM J. Appl. Dyn. Syst.*, 17, 2018.

[68] G. Abramson, C.A. Trejo Soto, and L. Oña. The role of asymmetric interactions on the effect of habitat destruction in mutualistic networks. *PLoS ONE*, 6:e21028, 2011.

[69] M. Fruchart, R. Hanai, P.B. Littlewood, and V. Vitelli. Non-reciprocal phase transitions. *Nature*, 592:363–369, 2021.

[70] R. Muolo, M. Asllani, D. Fanelli, P.K. Maini, and T. Carletti. Patterns of non-normality in networked systems. *J. Theor. Biol.*, 480:81, 2019.

[71] R. Muolo. *Effects of Nonnormality on Turing-like pattern formation*. Master Thesis, Università di Firenze, 2018.

[72] T. Nishikawa, A.E. Motter, and L.M. Pecora. Comment on "synchronization dynamics in non-normal networks: the trade-off for optimality". *arxiv preprint https://arxiv.org/abs/2110.14069*, 2022.

[73] R. Muolo, T. Carletti, J.P. Gleeson, and M. Asllani. Reply to "comment on synchronization dynamics in non-normal networks: the trade-off for optimality". *Accepted - Entropy*, 2022.

[74] T. Nishikawa and A.E. Motter. Synchronization is optimal in nondiagonalizable networks. *Phys. Rev. E*, 73:065106(R), 2006.

[75] F. Sorrentino and C. Nathe. Comment on "synchronization dynamics in non-normal networks: the trade-off for optimality". *preprint https://arxiv.org/abs/2201.09872*, 2022.

[76] J. Fish and E.M. Bollt. Non-normality, optimality and synchronization. *preprint https://arxiv.org/abs/2202.00156*, 2022.

[77] L.N. Trefethen and M. Embree. *Spectra and Pseudospectra: The Behavior of Nonnormal Matrices and Operators*. Princeton Univ. Press, 2005.

[78] R. Muolo, T. Carletti, J.P. Gleeson, and M. Asllani. Synchronization dynamics in non-normal networks: the trade-off for optimality. *Entropy*, 23:36, 2021.

[79] M.E.J. Newman. *Networks: An Introduction. Second Edition*. Oxford University Press, Oxford, 2018.

[80] S.H. Strogatz. From kuramoto to crawford: exploring the onset of synchronization in populations of coupled oscillators. *Physica D*, 143:1–21, 2000.

[81] P.S. Skardal, D. Taylor, and J. Sun. Optimal synchronization of directed complex networks. *Chaos*, 26:094807, 2016.

[82] P.S. Skardal, R. Sevilla-Escoboza, V.P. Vera-Ávila, and J.M. Buldú. Optimal phase synchronization in networks of phase-coherent chaotic oscillators. *Chaos*, 27:013111, 2017.

[83] T. Nishikawa and A.E. Motter. Maximum performance at minimum cost in network synchronization. *Physica D*, 224:77–89, 2006.

[84] M. Barahona and L.M. Pecora. Synchronization in small-world systems. *Phys. Rev. Lett.*, 89(5):054101, 2002.

[85] L. Marrec and S. Jalan. Analysing degeneracies in networks spectra. *Europhys. Lett.*, 117, 2017.

[86] M.E.J. Newman. *Networks: An Introduction*. Oxford University Press, Oxford, 2010.

[87] M. Asllani and T. Carletti. Topological resilience in non-normal networked systems. *Phys. Rev. E*, 97, 2018.

[88] S. Nicoletti, N. Zagli, D. Fanelli, R. Livi, T. Carletti, and G. Innocenti. Non-normal amplification of stochastic quasicycles. *Phys. Rev. E*, 98, 2018.

[89] S. Nicoletti, D. Fanelli, N. Zagli, M. Asllani, G. Battistelli, T. Carletti, L. Chisci, G. Innocenti, and R. Livi. Resilience for stochastic systems interacting via a quasi-degenerate network. *Chaos*, 29:083123, 2019.

[90] G. Baggio, V. Rutten, G. Hennequin, and Zampieri S. Efficient communication over complex dynamical networks: The role of matrix non-normality. *Sci. Adv.*, 6(22):eaba2282, 2020.

[91] L.N. Trefethen, A.E. Trefethen, S.C. Reddy, and T.A. Driscoll. Hydrodynamic stability without eigenvalues. *Science*, 261:578–584, 1993.

[92] M.G. Neubert and H. Caswell. Alternatives to resilience for measuring the responses of ecological systems to perturbations. *Math. Biosci.*, 78:653–665, 1997.

[93] M.G. Neubert, H. Caswell, and J.D. Murray. Transient dynamics and pattern formation: Reactivity is necessary for turing instabilities. *Math. Biosci.*, 175(1):1–11, 2002.

[94] Z.G. Nicolaou, T. Nishikawa, S.B. Nicholson, J.R. Green, and A.E. Motter. Non-normality and non-monotonic dynamics in complex reaction networks. *Phys. Rev. Res.*, 2:043059, 2020.

[95] I. Prigogine and G. Nicolis. Symmetry breaking instabilities in dissipative systems. *J. Chem. Phys.*, 46:3542, 1967.

[96] R.P. Boland, T. Galla, and A.J. McKane. How limit cycles and quasi-cycles are related in a system with intrinsic noise. *J. Stat. Mech.*, page P09001, 2008.

[97] J.A. Sanders, F. Verhulst, and J. Murdock. *Averaging Methods in Nonlinear Dynamical Systems. Second Edition, Applied Mathematical Sciences vol. 59*. Springer-Verlag, 2007.

[98] P.J. Davis. *Circulant Matrices: Second Edition*. AMS Chelsea Publishing, 1994.

[99] R. Brown and N.F. Rulkov. Synchronization of chaotic systems: Transverse stability of trajectories in invariant manifolds. *Chaos*, 7, 1997.

[100] Y. Kuramoto. *Chemical oscillations, waves, and turbulence*. Springer-Verlag, New York, 1984.

[101] J. Gao, B. Barzel, and A.-L. Barabási. Universal resilience patterns in complex networks. *Nature*, 530:307–312, 2016.

[102] T.G. Wright. *MATLAB® ToolBox*. 2002.

[103] P. Erdős and A. Rényi. On random graphs. *Publ. Math.*, 6:290–297, 1959.

[104] P.J. Menck, J. Heitzig, N. Marwan, and J. Kurths. How basin stability complements the linear-stability paradigm. *Nat. Phys.*, 9:89–92, 2013.

[105] C. Cattaneo. Sulla conduzione del calore. *Atti. Sem. Mat. Fis. Univ. Modena*, 3:83, 1948.

[106] R.M. Pringle and C.E. Tarnita. Spatial self-organization of ecosystems: Integrating multiple mechanisms of regular-pattern formation. *Annu. Rev. Entomol.*, 62:359–377, 2017.

[107] G. Nicolis and I. Prigogine. *Self-organization in nonequiibrium systems: From dissipative structures to order through fluctuations*. J. Wiley and Sons, 1977.

[108] J.D. Murray. *Mathematical biology II: Spatial models and biomedical applications*. Springer-Verlag, 2001.

[109] R. Pastor-Satorras and A. Vespignani. Patterns of complexity. *Nat. Phys.*, 6:480, 2010.

[110] N. Tompkins, N. Li, C. Girabawe, M. Heymann, G.B. Ermentrout, I.R. Epstein, and S. Fraden. Testing turing's theory of morphogenesis in chemical cells theory of morphogenesis in chemical cells. *Proc. Natl. Acad. Sci. U.S.A.*, 111(12):4397, 2014.

[111] L.M. Pecora, T.L. Carroll, G.A. Johnson, D.J. Mar, and J.F. Heagy. Fundamentals of synchronization in chaotic systems, concepts, and applications. *Chaos*, 7(4):520, 1997.

[112] L.M. Pismen. *Patterns and interfaces in dissipative dynamics*. Springer Science & Business Media, 2006.

[113] E.J. Crampin, E.A. Gaffney, and P.K. Maini. Reaction and diffusion on growing domains: scenarios for robust pattern formation. *Bull. Math. Biol.*, 61:1093, 1999.

[114] R.A. Van Gorder. Turing and benjamin-feir instability mechanisms in non-autonomous systems. *Proc. R. Soc. A*, 476:20200003, 2020.

[115] J. Petit, B. Lauwens, D. Fanelli, and T. Carletti. Theory of turing patterns on time varying networks. *Phys. Rev. Lett.*, 119:148301, 2017.

[116] R.A. Van Gorder. A theory of pattern formation for reaction-diffusion systems on temporal networks. *Proc. R. Soc. A*, 477:20200753, 2021.

[117] C. Cattaneo. Sur une forme de l'équation de la chaleur éliminant le paradoxe d'une propagation instantanée. *C. R. Acad. Sci.*, 247:431, 1958.

[118] J. Casas-Vázquez, D. Jou, and G. Lebon. *Extended IReversible Thermodynamics*. Springer, Berlin, 1996.

[119] V. Méndez, S. Fedotov, and W. Horsthemke. *Reaction-Transport Systems*. Springer-Verlag Berlin Heidelberg, 2010.

[120] J.A. López Molina, M.J. Rivera, and E. Berjano. Fourier, hyperbolic and relativistic heat transfer equations: a comparative analytical study. *Proc. R. Soc. A*, 470:20140547, 2014.

[121] J. Masoliver and G.H. Weiss. Finite-velocity diffusion. *Eur. J. Phys.*, 17(190), 1996.

[122] I. Müller and T. Ruggeri. *Rational Extended Thermodynamics*. Springer-Verlag, New York, 2013.

[123] E.J. Routh. *Stability of a given state of motion*. MacMillan and Co, London, 1877.

[124] A. Hurwitz. Ueber die bedingungen, unter welchen eine gleichung nur wurzeln mit negativen reellen theilen besitzt. *Math. Ann.*, 46:273, 1895.

[125] S. Barnett. *Polynomials and Linear Control Systems*. Dekker, New York, 1983.

[126] R. FitzHugh. Impulses and physiological states in theoretical models of nerve membrane. *Biophys. J.*, 1:445, 1961.

[127] J. Nagumo, S. Arimoto, and S. Yoshizawa. An active pulse transmission line simulating nerve axon. *Proc. IRE*, 50:2061, 1962.

[128] J. Rinzel and J.B. Keller. Traveling wave solutions of a nerve conduction equation. *Biophys. J.*, 13:1313, 1973.

[129] T. Ohta. Decay of metastable rest state in excitable reaction-diffusion system. *Prog. Theoret. Phys. Suppl.*, 99:425, 1989.

[130] H. Shoji, K. Yamada, D. Ueyama, and T. Ohta. Turing patterns in three dimensions. *Phys. Rev. E*, 75:046212, 2007.

[131] T. Carletti and H. Nakao. Turing patterns in a network-reduced Fitzhugh-Nagumo model. *Phys. Rev. E*, 101:022203, 2020.

[132] B.A. Siebert, C.L. Hall, J.P. Gleeson, and M. Asllani. Role of modularity in self-organization dynamics in biological networks. *Phys. Rev. E*, 102:052306, 2020.

[133] I. Vragovic, E. Louis, and A. Díaz-Guilera. Performance of excitable small-world networks of bonhoeffer-van der pol-fitzhugh-nagumo oscillators. *Europhys. Lett.*, 76:780, 2006.

[134] M. Aqil, K.-S. Hong, and M.-Y. Jeong. Synchronization of coupled chaotic fitzhugh-nagumo systems. *Commun. Nonlinear Sci. Numer. Simul.*, 17(4):1615, 2012.

[135] P.A. Haas and R.E. Goldstein. Turing's diffusive threshold in random reaction-diffusion systems. *Phys. Rev. Lett.*, 126:238101, 2021.

[136] X. Diego, L. Marcon, P. Muller, and J. Sharpe. Key features of turing systems are determined purely by network topology. *Phys. Rev. X*, 8(2):21071, 2018.

[137] S. Mimar, M.M. Juane, J. Park, A.P. Munuzuri, and G. Ghoshal. Turing patterns mediated by network topology in homogeneous active systems. *Phys. Rev. E*, 99(6):062303, 2019.

[138] L. Szili and J. Tóth. Necessary condition of the turing instability. *Phys. Rev. E*, 48:183, 1993.

[139] V. Hárs and J. Tóth. n the inverse problem of reaction kinetics. *Colloq. Math. Soc. János Bolyai*, page 363, 1981.

[140] P. Erdős and A. Rényi. On the evolution of random graphs. *Publications of the Mathematical Institute of the Hungarian Academy of Sciences*, 5:17, 1960.

[141] MATLAB. *Version: 9.10.0.1602886 (R2021a)*. The MathWorks Inc., Natick, Massachusetts, 2021.

[142] S. Subramanian and S.M. Murray. Pattern selection in reaction diffusion systems. *Phys. Rev. E*, 103:012215, 2021.

[143] A.J. Lotka. Undamped oscillations derived from the law of mass action. *J. Am. Chem. Soc.*, 42(1595), 1920.

[144] V. Volterra. Variazionie fluttuazioni del numero d'individui in specie animali conviventi. *Mem. Acad. Lincei*, 2(31), 1926.

[145] C.C. Bissell. Stodola, hurwitz and the genesis of the stability criterion. *Int. J. Control*, 50(2313), 1989.

[146] C.M. Bender and S.A. Orszag. *Advanced Mathematical Methods for Scientists and Engineers I. Asymptotic Methods and Perturbation Theory*. Springer-Verlag New York, 1999.

[147] G.H. Golub and C.F. Van Loan. *Matrix Computations*. Baltimore: Johns Hopkins University Press, 1996.

[148] A. Nakamasu, G. Takahashi, A. Kanbe, and S. Kondo. Interactions between zebrafish pigment cells responsible for the generation of turing patterns. *Proc. Natl. Acad. Sci. U.S.A.*, 106:8429, 2009.

[149] D. Bullara and Y. De Decker. Pigment cell movement is not required for generation of turing patterns in zebrafish skin. *Nat. Comm.*, 6:6971, 2015.

[150] C.T. Lee, M.F. Hoopes, J. Diehl, W. Gilliland, G. Huxel, E.V. Leavier, K. McCann, J. Umbanhowar, and A. Mogilner. Non-local concepts and models in biology. *J. Theor. Biol.*, 210:201–219, 2001.

[151] B.L. Segal, V.A. Volpert, and A. Bayliss. Pattern formation in a model of competing populations with nonlocal interactions. *Physica D*, 253:12–22, 2013.

[152] C. Tian, L. Zhi, and L. Zhang. Nonlocal interaction driven pattern formation in a prey–predator model. *Appl. Math. Comput.*, 308:73–83, 2017.

[153] B. Karakaya, L. Minati, L.V. Gambuzza, and M. Frasca. Fading of remote synchronization in tree networks of stuart-landau oscillators. *Phys. Rev. E*, 99:052301, 2019.

[154] T. Carletti and R. Muolo. Non-reciprocal interactions enhance heterogeneity. *Chaos Solit. Fractals*, 164:112638, 2022.

[155] A.-L. Barabási. *Network science*. Cambridge university press, 2016.

[156] P.C. Bressloff, Cowan J.D., Golubitsky M., Thomas P.J., and Wiener M.C. Geometric visual hallucinations, euclidean symmetry and the functional architecture of striate cortex. *Phil. Trans. R. Soc. Lond. B*, 356:299, 2001.

[157] P.C. Bressloff and Cowan J.D. The functional geometry of local and horizontal connections in a model of $v1$. *J. of Physiology Paris*, 97:221, 2003.

[158] S.H. Strogatz. *Sync : The Emerging Science of Spontaneous Order*. Hyperion, 2003.

[159] G. Cencetti, F. Battiston, T. Carletti, and D. Fanelli. Generalized patterns from local and non local reactions. *Chaos Solit. Fractals*, 134:109707, 2020.

[160] J. Bascompte, P. Jordano, C.J. Melián, and J.M. Olesen. The nested assembly of plant-animal mutualistic networks. *Proc. Natl. Acad. Sci. U.S.A.*, 100(16):9383, 2003.

[161] E. Hollingdale, F.J. Pérez-Barbería, and D. McPetrie Walker. Inferring symmetric and asymmetric interactions between animals and groups from positional data. *PLoS ONE*, 13:e0208202, 2018.

[162] Y. Zhang, T.K. Tsang, E.A. Bushong, L.-A. Chu, A.-S. Chiang, M.H. Ellisman, J. Reingruber, and C.-Y. Su. Asymmetric ephaptic inhibition between compartmentalized olfactory receptor neurons. *Nat. Comm.*, 10(1):1560, 2019.

[163] R. Ghosh, S.-H. Teng, K. Lerman, and X. Yan. The interplay between dynamics and networks: centrality, communities, and cheeger inequality. In *Proceedings of the 20th ACM SIGKDD international conference on Knowledge discovery and data mining*, pages 1406–1415. ACM, 2014.

[164] R. Lambiotte, R. Sinatra, J.-C. Delvenne, T.S. Evans, M. Barahona, and V. Latora. Flow graphs: Interweaving dynamics and structure. *Phys. Rev. E*, 84(1):017102, 2011.

[165] R. Olfati-Saber, J.A. Fax, and R.M. Murray. Consensus and cooperation in networked multi-agent systems. *Proc. IEEE*, 95(1):215–233, 2007.

[166] U. Krause. Compromise, consensus, and the iteration of means. *Elem. Math.*, 64(1):1–8, 2009.

[167] S. Geršgorin. über die abgrenzung der eigenwerte einer matrix. *Izvestiya Rossiiskoi Akademii Nauk. Seriya Matematicheskaya*, page 749, 1931.

[168] L. Huang, Q. Chen, Y.-C. Lai, and L.M. Pecora. Generic behavior of master-stability functions in coupled nonlinear dynamical systems. *Phys. Rev. E*, 80:036204, 2009.

[169] I. Prigogine and R. Lefever. Symmetry breaking instabilities in dissipative systems. ii. *J. Chem. Phys.*, 48:1695, 1968.

[170] A. Koseska, E. Volkov, and J. Kurths. Oscillation quenching mechanisms: Amplitude vs. oscillation death. *Phys. Rep.*, 531:173, 2013.

[171] M. Lucas, D. Fanelli, T. Carletti, and J. Petit. Desynchronization induced by time-varying network. *EPL*, 121:58008, 2018.

[172] M. Mimura and J.D. Murray. Diffusive prey-predator model which exhibits patchiness. *J. Theor. Biol.*, 75:249, 1978.

[173] M. Asllani, D.M. Busiello, T. Carletti, D. Fanelli, and G. Planchon. Turing instabilities on cartesian product networks. *Scientific Reports*, 5:12927, 2015.

[174] A.J. McKane and T.J. Newman. Predator-prey cycles from resonant amplification of demographic stochasticity. *Phys. Rev. Lett.*, 94(21):218102, 2005.

[175] G.C. Layek and N.C. Pati. Organized structures of two bidirectionally coupled logistic maps. *Chaos*, 29:093104, 2019.

[176] N.C. Pati, G.C. Layek, and N. Pal. Bifurcations and organized structures in a predator-prey model with hunting cooperation. *Chaos Solit. Fractals*, 140:110184, 2020.

[177] J.T. Stuart and R.C. DiPrima. The eckhaus and benjamin-feir resonance mechanisms. *Proc. R. Soc. A*, 362:27, 1978.

[178] S. Nicoletti, T. Carletti, D. Fanelli, G. Battistelli, and L. Chisci. Generating directed networks with prescribed laplacian spectra. *J. Phys. Complex.*, 2, 2021.

[179] Naoki Masuda, Mason A Porter, and Renaud Lambiotte. Random walks and diffusion on networks. *Phys. Rep.*, 2017.

[180] A. Patania, G. Petri, and F. Vaccarino. The shape of collaborations. *EPJ Data Sci.*, 6(1):18, 2017.

[181] J. Grilli, G. Barabás, M.J. Michalska-Smith, and S. Allesina. Higher-order interactions stabilize dynamics in competitive network models. *Nature*, 548:210–213, 2017.

[182] G. Petri, P. Expert, F. Turkheimer, R. Carhart-Harris, D. Nutt, P.J. Hellyer, and F. Vaccarino. Homological scaffolds of brain functional networks. *J. Royal Soc. Interface*, 11(101):20140873, 2014.

[183] A.E. Sizemore, C. Giusti, A. Kahn, J.M. Vettel, R.F. Betzel, and D.S. Bassett. Cliques and cavities in the human connectome. *J. Comp. Neurosci.*, 44(1):115–145, 2018.

[184] R.D. Andrew, M. Fagan, B.A. Ballyk, and A.S. Rosen. Seizure susceptibility and the osmotic state. *Brain Res.*, 498:175–180, 2021.

[185] M. Wang, D. Arteaga, and B.j. He. Brain mechanisms for simple perception and bistable perception. *Proc. Natl. Acad. Sci. U.S.A.*, 110(35):E3350–E3359, 2013.

[186] D. Centola, J. Becker, D. Brackbill, and A. Baronchelli. Experimental evidence for tipping points in social convention. *Science*, 360(6393):1116–1119, 2018.

[187] C. Berge. *Graphs and hypergraphs*. North-Holl Math. Libr. North-Holland, Amsterdam, 1973.

[188] P.S. Aleksandrov. *Combinatorial topology*, volume 1. Courier Corporation, 1998.

[189] M.T. Schaub, A.R. Benson, P. Horn, G. Lippner, and A. Jadbabaie. Random walks on simplicial complexes and the normalized Hodge 1-Laplacian. *SIAM Rev.*, 62(2):353–391, 2020.

[190] T. Carletti, F. Battiston, G. Cencetti, and D. Fanelli. Random walks on hypergraphs. *Phys. Rev. E*, 101(2):022308, 2020.

[191] T. Carletti, D. Fanelli, and R. Lambiotte. Random walks and community detection in hypergraphs. *J. phys. Complex.*, 2(1):015011, 2021.

[192] L. Neuhäuser, A.W. Mellor, and R. Lambiotte. Multibody interactions and nonlinear consensus dynamics on networked systems. *Phys. Rev. E*, 101(3):032310, 2020.

[193] L. Neuhäuser, R. Lambiotte, and M.T. Schaub. Consensus dynamics on temporal hypergraphs. *Phys. Rev. E*, 104(6):064305, 2021.

[194] G. St-Onge, H. Sun, A. Allard, L. Hébert-Dufresne, and G. Bianconi. Universal nonlinear infection kernel from heterogeneous exposure on higher-order networks. *Phys. Rev. Lett.*, 127:158301, Oct 2021.

[195] I. Iacopini, G. Petri, A. Barrat, and V. Latora. Simplicial models of social contagion. *Nat. Comm.*, 10(1):2485, 2019.

[196] G.F. de Arruda, G. Petri, and Y. Moreno. Social contagion models on hypergraphs. *Phys. Rev. Res.*, 2:023032, 2020.

[197] C. Kuehn and C. Bick. A universal route to explosive phenomena. *Sci. Adv.*, 7:eabe3824, 2021.

[198] P.S. Skardal and A. Arenas. Higher-order interactions in complex networks of phase oscillators promote abrupt synchronization switching. *Comm. Phys.*, 3(218), 2020.

[199] P.S. Skardal and A. Arenas. Abrupt desynchronization and extensive multistability in globally coupled oscillator simplexes. *Phys. Rev. Lett.*, 122(24):248301, 2019.

[200] T. Tanaka and T. Aoyagi. Multistable attractors in a network of phase oscillators with three-body interactions. *Phys. Rev. Lett.*, 106(22):224101, 2011.

[201] M. Lucas, G. Cencetti, and F. Battiston. Multiorder laplacian for synchronization in higher-order networks. *Phys Rev. Res.*, 2(3):033410, 2020.

[202] A.P. Millán, J.J. Torres, and G. Bianconi. Explosive higher-order Kuramoto dynamics on simplicial complexes. *Phys. Rev. Lett.*, 124(21):218301, 2020.

[203] R. Ghorbanchian, J.G. Restrepo, J.J. Torres, and G. Bianconi. Higher-order simplicial synchronization of coupled topological signals. *Comm. Phy.*, 4(1):1–13, 2021.

[204] A. Krawiecki. Chaotic synchronization on complex hypergraphs. *Chaos Solit. Fractals*, 65:44–50, 2014.

[205] T. Carletti, D. Fanelli, and S. Nicoletti. Dynamical systems on hypergraphs. *J. phys. Complex.*, 1(3):035006, 2020.

[206] F. Baccini, F. Geraci, and G. Bianconi. Weighted simplicial complexes and their representation power of higher-order network data and topology. *Phsy. Rev. E*, 106(3):034319, 2022.

[207] G. Bianconi. *Higher-Order Networks:An introduction to simplicial complexes*. Cambridge University Press, 2021.

[208] F. Battiston, G. Cencetti, I. Iacopini, V. Latora, M. Lucas, A. Patania, J.-G. Young, and G. Petri. Networks beyond pairwise interactions: structure and dynamics. *Phys. Rep.*, 2020.

[209] Y. Zhang, M. Lucas, and F. Battiston. Higher-order interactions shape collective dynamics differently in hypergraphs and simplicial complexes. *Nat. Comm.*, 14(1605), 2023.

[210] G. Gallo, G. Longo, S. Pallottino, and S. Nguyen. Directed hypergraphs and applications. *Discret. Appl. Math.*, 42(2-3):177–201, 1993.

[211] L. Gallo, R. Muolo, L.V. Gambuzza, V. Latora, M. Frasca, and T. Carletti. Synchronization induced by directed higher-order interactions. *Comm. Phys., volume=5, number=236, year=2022, publisher=Nature*.

[212] H. Sun, F. Radicchi, J. Kurths, and G. Bianconi. Triadic interactions induce blinking and chaos in the connectivity of higher-order networks. *arXiv preprint https://arxiv.org/abs/2204.13067*, 2022.

[213] A. Salova and R.M. D'Souza. Cluster synchronization on hypergraphs. *arXiv preprint https://arxiv.org/abs/2101.05464*, 2021.

[214] P. Holme and J. Saramäki. Temporal networks. *Phys. Rep.*, 519:97–125, 2012.

[215] R. Muolo, L. Gallo, V. Latora, M. Frasca, and T. Carletti. Turing patterns in systems with high-order interaction. *Chaos Solit. Fractals*, 166:112912, 2023.

[216] L. Lek-Heng. Hodge laplacians on graphs. *SIAM Review*, 62(3):685–715, January 2020.

[217] Battiston F. and et al. The physics of higher-order interactions in complex systems. *Nat. Phys.*, 17:1093–1098, 2021.

[218] F. Battiston and G. Petri. Higher-order systems, 2022.

[219] J. Faskowitz, R.F. Betzel, and O. Sporns. Edges in brain networks: Contributions to models of structure and function. *Netw. Neurosci.*, 6(1):1–28, 2022.

[220] D. Witthaut, F. Hellmann, J. Kurths, S. Kettemann, H. Meyer-Ortmanns, and M. Timme. Collective nonlinear dynamics and self-organization in decentralized power grids. *Rev. Mod. Phys.*, 94(1):015005, 2022.

[221] M. Asllani, F. Di Patti, and D. Fanelli. Stochastic turing patterns on a network. *Phys. Rev. E*, 86(4):046105, 2012.

[222] L. Goras and L.O. Chua. Turing patterns in cnns. ii. equations and behaviors. *IEEE Trans. Circuits Syst. I Fund. T. App.*, 42(10):612–626, 1995.

[223] A. Buscarino, L. Corradino, L. Fortuna, M. Frasca, and L.O. Chua. Turing patterns in memristive cellular nonlinear networks. *IEEE Trans. Circuits Syst. I Regul. Pap.*, 63(8):1222–1230, 2016.

[224] A. Barrat, G.F. de Arruda, I. Iacopini, and Y. Moreno. Social contagion on higher-order structures. In *Higher-Order Systems*, pages 329–346. Springer, 2022.

[225] M. Asllani, T. Carletti, F. Di Patti, D. Fanelli, and F. Piazza. Hopping in the crowd to unveil network topology. *Phys. Rev. Lett.*, 120(15):158301, 2018.

[226] T. Carletti, M. Asllani, D. Fanelli, and V. Latora. Nonlinear walkers and efficient exploration of congested networks. *Phys. Rev. Res.*, 2(033012), 2020.

[227] D. Fanelli and A. McKane. Diffusion in a crowded environment. *Phys. Rev. E*, 82:021113, 2010.

[228] D. Fanelli, A.J. McKane, G. Pompili, B. Tiribilli, M. Vassalli, and D. Biancalani. Diffusion of two molecular species in a crowded environment: theory and experiments. *Phys. Biol.*, 10(4):045008, 2013.

[229] L. Giambagli, M.L. Calmon, R. Muolo, T. Carletti, and G. Bianconi. Diffusion-driven instability of topological signals coupled by the dirac operator. *Phys. Rev. E*, 106, 2022.

[230] N. Kumar and W. Horsthemke. Turing bifurcation in a reaction-diffusion system with density-dependent dispersal. *Physica A*, 389:1812–1818, 2010.

[231] F. Gambino, M.C. Lombardo, M. Sammartino, and V. Sciacca. Turing pattern formation in the brusselator system with nonlinear diffusion. *Phys. Rev. E*, 88:042925, 2013.

[232] A. Sadighi and D.D. Ganji. Exact solutions of nonlinear diffusion equations by variational iteration method. *Comp. Math. Appl.*, 54:1112–1121, 2007.

[233] S. Hata, H. Nakao, and A.S. Mikhailov. Global feedback control of turing patterns in network-organized activator-inhibitor systems. *Eur. Phys. Lett.*, 98:64004, 2012.

[234] A. Buscarino, C. Corradino, L. Fortuna, and M. Frasca. Turing patterns via pinning control in the simplest memristive cellular nonlinear networks. *Chaos*, 29:103145, 2019.

[235] S. Gao, L. Chang, I. Romić, Z. Wang, M. Jusup, and P. Holme. Optimal control of networked reaction–diffusion systems. *J. R. Soc. Interface*, 19(188):20210739, 2022.

[236] M. Asllani, P. Expert, and T. Carletti. A minimally invasive neurostimulation method for controlling abnormal synchronisation in the neuronal activity. *PLoS Comput. Biol.*, 14:e1006296, 2018.

[237] S.H. Strogatz. From Kuramoto to crawford: exploring the onset of synchronization in populations of coupled oscillators. *Physica D*, 143(1-4):1–20, 2000.

[238] S. Boccaletti, A. N. Pisarchik, C.I. Del Genio, and A. Amann. *Synchronization: from coupled systems to complex networks*. Cambridge University Press, 2018.

[239] V. Latora, V. Nicosia, and G. Russo. *Complex Networks: Principles, Methods and Applications*. Cambridge University Press, 2017.

[240] S. Boccaletti, V. Latora, Y. Moreno, M. Chavez, and D.-U. Hwang. Complex networks: Structure and dynamics. *Phys. Rep.*, 424(4-5):175–308, 2006.

[241] L. Torres, A.S. Blevins, D. Bassett, and T. Eliassi-Rad. The why, how, and when of representations for complex systems. *SIAM Rev.*, 63(3):435–485, 2021.

[242] C. Bick, E. Gross, H.A. Harrington, and M.T. Schaub. What are higher-order networks? *arXiv preprint arXiv:2104.11329*, 2021.

[243] C. Giusti, R. Ghrist, and D.S. Bassett. Two's company, three (or more) is a simplex. *J. Comput. Neurosci.*, 41(1):1–14, 2016.

[244] V. Salnikov, D. Cassese, and R. Lambiotte. Simplicial complexes and complex systems. *Eur. J. Phys.*, 40(1):014001, 2018.

[245] N. Otter, M. A Porter, U. Tillmann, P. Grindrod, and He.A. Harrington. A roadmap for the computation of persistent homology. *EPJ Data Science*, 6:1–38, 2017.

[246] S. Majhi, M. Perc, and D. Ghosh. Dynamics on higher-order networks: A review. *J. R. Soc. Interface*, 19(188):20220043, 2022.

[247] M. Nakahara. *Geometry, topology and physics*. CRC Press, 2003.

[248] D. Mulder and G. Bianconi. Network geometry and complexity. *J. Stat. Phys.*, 173(3):783–805, 2018.

[249] M.-L. Linne, J. Aćimović, A. Saudargiene, and T. Manninen. Neuron-glia interactions and brain circuits. In *Computational Modelling of the Brain*, pages 87–103. Springer, 2022.

[250] J. Faskowitz, R.F. Betzel, and O. Sporns. Edges in brain networks: Contributions to models of structure and function. *Netw. Neurosci.*, 6(1):1–28, 2022.

[251] A. Santoro, F. Battiston, G. Petri, and E. Amico. Unveiling the higher-order organization of multivariate time series. *arXiv preprint arXiv:2203.10702*, 2022.

[252] E. Katifori, G.J. Szöllősi, and M.O. Magnasco. Damage and fluctuations induce loops in optimal transport networks. *Phys. Rev. Lett.*, 104(4):048704, 2010.

[253] J.W. Rocks, A.J. Liu, and E. Katifori. Hidden topological structure of flow network functionality. *Phys. Rev. Lett.*, 126(2):028102, 2021.

[254] S. Barbarossa and S. Sardellitti. Topological signal processing over simplicial complexes. *IEEE Trans. Signal Process.*, 68:2992–3007, 2020.

[255] S. Sardellitti and S. Barbarossa. Topological signal representation and processing over cell complexes. pages 1558–1562, 2021.

[256] M.T. Schaub and S. Segarra. Flow smoothing and denoising: Graph signal processing in the edge-space. In *2018 IEEE Global Conference on Signal and Information Processing (GlobalSIP)*, pages 735–739. IEEE, 2018.

[257] M.T. Schaub, Y. Zhu, J.-B. Seby, T.M. Roddenberry, and S. Segarra. Signal processing on higher-order networks: Livin'on the edge... and beyond. *Signal Process.*, 187:108149, 2021.

[258] T. Carletti, L. Giambagli, and G. Bianconi. Global topological synchronization on simplicial and cell complexes. *arXiv preprint arXiv:2208.14783*, 2022.

[259] A.P. Millán, J.G. Restrepo, J.J. Torres, and G. Bianconi. Geometry, topology and simplicial synchronization. In *Higher-Order Systems*, pages 269–299. Springer, 2022.

[260] J.J. Torres and G. Bianconi. Simplicial complexes: higher-order spectral dimension and dynamics. *J. phys. Complex.*, 1(1):015002, 2020.

[261] M.L. Calmon, J.G. Restrepo, J.J. Torres, and G. Bianconi. Dirac synchronization is rhythmic and explosive. *Comm. Phys.*, 5:1–17, 2022.

[262] M.L. Calmon and G. Bianconi. Local dirac synchronization on networks. *arXiv preprint arXiv:2210.16124*, 2022.

[263] A. Arnaudon, R.L. Peach, G. Petri, and P. Expert. Connecting Hodge and Sakaguchi-Kuramoto through a mathematical framework for coupled oscillators on simplicial complexes. *Comm. Phys.*, 5(1):1–12, 2022.

[264] L. DeVille. Consensus on simplicial complexes: Results on stability and synchronization. *Chaos*, 31(2):023137, 2021.

[265] M. Reitz and G. Bianconi. The higher-order spectrum of simplicial complexes: a renormalization group approach. *J. Phys. A*, 53(29):295001, 2020.

[266] C. Ziegler, P.S. Skardal, H. Dutta, and D. Taylor. Balanced Hodge Laplacians optimize consensus dynamics over simplicial complexes. *Chaos*, 32(2):023128, 2022.

[267] C. Bodnar, F. Frasca, Y.G. Wang, N. Otter, G. Montúfar, P. Lio, and M. Bronstein. Weisfeiler and Lehman go topological: Message passing simplicial networks. *arXiv preprint arXiv:2103.03212*, 2021.

[268] S. Ebli, M. Defferrard, and G. Spreemann. Simplicial neural networks. *arXiv preprint https://arxiv.org/abs/2010.03633*, 2020.

[269] T.M. Roddenberry and S. Segarra. Hodgenet: Graph neural networks for edge data. In *2019 53rd Asilomar Conference on Signals, Systems, and Computers*, pages 220–224. IEEE, 2019.

[270] M. Hajij, K. Istvan, and G. Zamzmi. Cell complex neural networks. *arXiv preprint arXiv:2010.00743*, 2020.

[271] P.S. Skardal and A. Arenas. Higher order interactions in complex networks of phase oscillators promote abrupt synchronization switching. *Comm. Phys.*, 3(1):1–6, 2020.

[272] K. Kovalenko, X. Dai, K. Alfaro-Bittner, A.M. Raigorodskii, M. Perc, and S. Boccaletti. Contrarians synchronize beyond the limit of pairwise interactions. *Phys. Rev. Lett.*, 127(25):258301, 2021.

[273] U. Alvarez-Rodriguez, F. Battiston, G.F. de Arruda, Y. Moreno, M. Perc, and V. Latora. Evolutionary dynamics of higher-order interactions in social networks. *Nature Human Behaviour*, 5(5):586–595, 2021.

[274] Y. Lee, J. Lee, S.M. Oh, D. Lee, and B. Kahng. Homological percolation transitions in growing simplicial complexes. *Chaos*, 31(4):041102, 2021.

[275] Y. Tang, D. Shi, and L. Lü. Optimizing higher-order network topology for synchronization of coupled phase oscillators. *Comm. Phys.*, 5(1):1–12, 2022.

[276] Y. Zhang, V. Latora, and A.E. Motter. Unified treatment of synchronization patterns in generalized networks with higher-order, multilayer, and temporal interactions. *Comm. Phys.*, 4(1):1–9, 2021.

[277] M. Chutani, B. Tadić, and N. Gupte. Hysteresis and synchronization processes of kuramoto oscillators on high-dimensional simplicial complexes with competing simplex-encoded couplings. *Phys. Rev. E*, 104(3):034206, 2021.

[278] R. Mulas, C. Kuehn, and J. Jost. Coupled dynamics on hypergraphs: Master stability of steady states and synchronization. *Phys. Rev. E*, 101(6):062313, 2020.

[279] D. Horak and J. Jost. Spectra of combinatorial Laplace operators on simplicial complexes. *Advances in Mathematics*, 244:303–336, 2013.

[280] G. Bianconi. The topological Dirac equation of networks and simplicial complexes. *J. phys. Complex.*, 2(3):035022, 2021.

[281] S. Lloyd, S. Garnerone, and P. Zanardi. Quantum algorithms for topological and geometric analysis of data. *Nat. Comm.*, 7(1):1–7, 2016.

[282] B. Ameneyro, V. Maroulas, and G. Siopsis. Quantum persistent homology. *arXiv preprint arXiv:2202.12965*, 2022.

[283] O. Post. First order approach and index theorems for discrete and metric graphs. In *Annales Henri Poincaré*, volume 10, pages 823–866. Springer, 2009.

[284] D.M. Busiello, G. Planchon, M. Asllani, T. Carletti, and D. Fanelli. Pattern formation for reactive species undergoing anisotropic diffusion. *Eur. Phys. J. B*, 88:222, 2015.

[285] A. Hatcher. *Algebraic topology*. 2002.

[286] A. Zakharova. *Chimera Patterns in Networks. Interplay between Dynamics, Structure, Noise, and Delay*. Springer, 2020.

[287] J.D. O'Brien, K.A. Oliveira, J.P. Gleeson, and M. Asllani. Hierarchical route to the emergence of leader nodes in real-world networks. *Phys. Rev. Res.*, 3:023117, 2021.

[288] D. de Groot, J. Lischke, R. Muolo, R. Planqué, F.J. Bruggeman, and B. Teusink. The common message of constraint-based optimization approaches: overflow metabolism is caused by two growth-limiting constraints. *Cell. Mol. Life Sciences*, 77:441–453, 2020.